

**COMPOSITIONAL DEPENDENCE OF  
POTASSIUM-ARGON AGES AND  
HYDROGEN AND OXYGEN STABLE ISOTOPES  
IN HORNBLENDES FROM CONNEMARA,  
WESTERN IRELAND.**

by

**TREVOR GEORGE JAPPY.**

B.Sc. (Honours), University of Aberdeen.

M.Sc. (Research), University of Aberdeen.

A thesis submitted to the  
University of Glasgow for the  
Degree of Doctor of Philosophy.

Department of Geology and Applied Geology,  
University of Glasgow,  
Scotland,  
April, 1998.

ProQuest Number: 13815590

All rights reserved

INFORMATION TO ALL USERS

The quality of this reproduction is dependent upon the quality of the copy submitted.

In the unlikely event that the author did not send a complete manuscript and there are missing pages, these will be noted. Also, if material had to be removed, a note will indicate the deletion.



ProQuest 13815590

Published by ProQuest LLC (2018). Copyright of the Dissertation is held by the Author.

All rights reserved.

This work is protected against unauthorized copying under Title 17, United States Code  
Microform Edition © ProQuest LLC.

ProQuest LLC.  
789 East Eisenhower Parkway  
P.O. Box 1346  
Ann Arbor, MI 48106 – 1346

GLASGOW UNIVERSITY  
LIBRARY

11310 (copy 1)

This thesis is dedicated to my parents; John Albert and Jessie Jappy.

## **PREFACE.**

This thesis is submitted to the University of Glasgow for the degree of Doctor of Philosophy. The research work was carried out in the Department of Geology and Applied Geology, University of Glasgow, Scotland and at the Scottish Universities Research and Reactor Centre (SURRC), East Kilbride, Scotland between 1<sup>ST</sup> October, 1994 and 30<sup>TH</sup> September, 1997. It has not been submitted for any previous degree or award and consists of original work by the author except where otherwise stated.

Trevor. G. Jappy.

## ACKNOWLEDGEMENTS.

I would like to express my thanks and gratitude to Professor B.E. Leake in his role as supervisor for this project and for his guidance and help throughout the work.

I would also like to thank Professor A. E. Fallick for the use of equipment provided at the Scottish Universities Research and Reactor Centre (SURRC), East Kilbride and his help and advice in the interpretation of isotope studies.

I would also like to thank the Natural Environment Research Council (NERC) for providing the funding which made this project possible.

I also wish to express my gratitude to the following individuals in the Department of Geology and Applied Geology, University of Glasgow for their guidance and advice in experimental procedures and training in the use of necessary equipment:

Bill Higgison for help and instruction in the use of mineral separation techniques (magnetic and heavy liquid), chemical analysis techniques (atomic absorption spectrophotometry, flame emission spectrophotometry,  $\text{Fe}^{2+}$  determination by titration), determination of  $\text{CO}_2$  and  $\text{H}_2\text{O}$  by a gravimetric absorption technique and for advice for working with dangerous chemicals such as hydrofluoric acid and 1,1,2,2-tetrabromoethane.

Murdo MacLeod for purity checks by X-ray diffraction of mineral separates.

Dugie Turner for advice on mineral separation chemical analysis techniques.

Jim Gallagher for the use of rock crushing equipment, advice on preparation of glass beads for major element analysis by X-ray fluorescence and for running these sample beads on the X-ray fluorescence spectrophotometer.

Jon Gilleece for the preparation of polished rock sections for analysis by electron microprobe.

Robert MacDonald for instruction and advice in the use of the electron microprobe.

Pete Ainsworth and Dr T.J. Dempster for help in the use of the scanning electron microscope and obtaining backscatter electron images.

Roddy Morrison for general advice and help around the department.

Dr. C. M. Farrow for advice in mineral chemistry.

Dr. J. Harris for instruction and help in the use of the photomicroscope.

Douglas MacLean for the processing of the photomicrographs.

I also wish to express my gratitude to the following individuals at the SURRC, East Kilbride for their guidance and advice in experimental procedures and training in the use of necessary equipment:

Terry Donnelly for instruction and help in the use of equipment for hydrogen and oxygen stable isotope analyses and running the samples through the mass spectrometer.

Jim Imlach for instruction and help in the use of equipment for K-Ar dating and running the samples through the relevant mass spectrometer.

Chris Taylor for instruction and help in the use of equipment for hydrogen and oxygen stable isotope analyses.

Elsbeth Tweedie for instruction and help in the use of equipment for hydrogen stable isotope analysis and running the samples through the mass spectrometer.

Andrew Tait for instruction and help in the use of equipment for oxygen stable isotope analysis and running the samples through the mass spectrometer.

Julie Dougans for instruction and help in the use of equipment for oxygen stable isotope analyses and running the samples through the mass spectrometer.

## ABBREVIATIONS.

The following abbreviations have been used throughout this thesis.

XRD:	X-ray diffraction.
XRF:	X-ray fluorescence spectrometry.
EMPA:	electron microprobe analysis.
SEM:	scanning electron microscopy.
TEM:	transmitting electron microscopy.
AAS:	atomic absorption spectroscopy.
FES:	flame emission spectroscopy.
DDDW:	deionised, double distilled water.
RGF:	Retrogressive fluid at ~400Ma.
MGS:	Metagabbro Gneiss Complex (Suite).

## ABSTRACT.

The work of this thesis set out to investigate the relationship between K-Ar age, hydrogen isotope values, oxygen isotope values and mineral composition in samples collected from the Dalradian rocks of the Connemara region of western Ireland.

Previous studies by Elias et al. (1988) and Miller et al. (1991) found no evidence for a connection between hornblende K-Ar ages and compositions on hornblendes ranging from ~490Ma to ~390Ma. The hornblendes are believed to have cooled through their  $^{40}\text{Ar}^*$  closure temperature between 490Ma and 463Ma (Cliff et al., 1994; Friedrich et al., 1997), therefore the younger ages are not explainable by conventional understanding of  $^{40}\text{Ar}^*$  loss. Miller et al. (1991) found a relationship of increasing hornblende  $\delta\text{D}$  values (from -75‰ to -61‰) with decreasing age and excess water contents in hornblendes. This was interpreted as being due to the hornblende being infiltrated by a retrogressive, convecting meteoric fluid (RGF) at sub- $^{40}\text{Ar}^*$  closure temperatures (~275°C) of  $\delta\text{D}$  ~18‰ associated with the intrusion of the Galway Granite and its associated plutons at ~400Ma. It was suggested that OH<sup>-</sup> disturbed the K-Ar ages by displacing the  $^{40}\text{Ar}^*$  during re-equilibration of hornblende hydrogen isotopes. Microstructural defects observed in samples investigated by TEM were considered to be contributing to the hydrogen isotopic exchange and escape of  $^{40}\text{Ar}^*$ . A similar effect was also postulated for observations of muscovite and biotite.

Due to the more extensive examination of rock and mineral chemistry, this present study has shown that there is a compositional factor controlling the measured isotopic values. From a dataset of 30 hornblende samples it was found that Si-, Mg-rich hornblendes were more retentive of  $^{40}\text{Ar}^*$  and retained their  $\delta\text{D}$  values better than the Al-, Ti-, Fe-, Na-, K-rich varieties.

It was not confirmed that the presence of excess water (up to ~2.7wt.%) in hornblendes indicated a reduction in K-Ar age or increased  $\delta\text{D}$  value (Miller et al., 1991). In fact, the water contents are related to the composition of each sample and follow the trend as expected by whether a sample is Mg-rich (water = ~2.2wt.%) or Fe-rich (water =

~1.8wt.%). It is possible that the excess water contents observed by Miller et al. (1991) were due to chlorite or biotite alteration in cleavages of separated hornblende grains.

It was observed by EMPA that chemical variation on a scale of  $\mu\text{m}$  was present in samples collected in the northern part of the Dalradian inlier (lower metamorphic grade). These rocks also appeared to have relic grains of hornblende (discordant inclusion trails) which were larger than the surrounding foliation fabric. Two populations of hornblende compositions were observed within single grains in these samples: Si-, Mg-rich compositions co-existing with Al-, Ti-, Fe-, Na-, K-rich compositions.

The conclusions drawn from this study are that the hornblende K-Ar ages were set at the end of the main metamorphic (D2) event, ~490-463Ma (Leake, 1989; Friedrich et al., 1997), by cooling below their  $^{40}\text{Ar}^*$  temperatures; ~578-490°C (Harrison, 1981). The accumulated  $^{40}\text{Ar}^*$  in the hornblende structure was disrupted by the hydrogen isotope exchange mechanism (at 270-340°C) associated with the aggressively convecting retrogressive fluid at ~400Ma (Jenkin et al., 1997; O'Reilly et al., 1997). Intermediate K-Ar ages represent intermediate  $^{40}\text{Ar}^*$  retention between almost complete resistance to  $^{40}\text{Ar}^*$  loss (Mg-rich hornblendes) to complete  $^{40}\text{Ar}^*$  loss and renewed  $^{40}\text{Ar}^*$  accumulation from ~400Ma (Fe-rich hornblendes), the RGF  $\delta\text{D}$  signature being imprinted on the minerals in the process. The calculated fluid  $\delta\text{D}$  values (from hornblende  $\delta\text{D}$  values) shifting from metamorphic waters ( $\delta\text{D} = \sim -40 \pm 1.5\text{‰}$ ) to the meteoric water RGF ( $\delta\text{D} = \sim -16 \pm 1.5\text{‰}$ ). These effects combined with the observation of submicroscopic phyllosilicate alteration in hornblendes (Onstott and Peacock, 1987; Miller, 1990) may be considered as the very early stages of hornblende hydrothermal retrogressive alteration, the convecting RGF having lasted for only  $\sim 10^4$  years (Jenkin et al., 1992), not long enough to extensively alter the hornblendes.

Four hornblende samples gave K-Ar ages 510-556Ma. These may represent K-Ar ages surviving from the earlier D1 metamorphic event or be due to excess Ar affecting the K-Ar date estimation.

It is proposed that a finer scale study using TEM and  $^{40}\text{Ar}^*$ - $^{39}\text{Ar}$  laser probe techniques be employed to investigate the relationships between composition,  $^{40}\text{Ar}^*$  retention and microstructure of amphibolite derived hornblendes from Connemara.

A recent publication by Siebel et al. (1998) has confirmed the greater ability of Mg-rich hornblende to retain  $^{40}\text{Ar}^*$  than Fe-rich hornblende occurring in the same crystal. This study was in samples from Bavaria, Germany.

## CONTENTS.

	Page Number.
<b>CHAPTER 1. INTRODUCTION.</b>	1
<b>1.1 The Geology of Connemara.</b>	1
1.1.1 The Northern Metamorphic Belt.	6
1.1.2 The Southern Metamorphic Belt.	6
1.1.3 Geological Structure of Connemara.	7
1.1.4 Metamorphism of Connemara.	8
1.1.5 Post-Tectonic Intrusions.	9
<b>1.2 Previous Dating Studies.</b>	10
1.2.1 The Findings of Elias et al. (1988).	11
1.2.2 The Findings of Miller et al. (1991).	12
<b>1.3 Composition and Structure of Hornblende.</b>	14
<b>1.4 Diffusivity in Hornblende.</b>	21
1.4.1 Closure Temperatures in Amphiboles and Micas.	21
1.4.2 Diffusion Mechanisms in Minerals.	24
<b>CHAPTER 2. AIMS.</b>	25

<b>CHAPTER 3.</b>	<b>SAMPLE COLLECTION AND PREPARATION.</b>	<b>27</b>
<b>3.1</b>	<b>Sample Collection.</b>	<b>27</b>
3.1.1	Dalradian Supergroup.	27
3.1.2	Silurian Rocks.	35
3.1.3	Connemara Metagabbro Gneiss Complex.	35
<b>3.2</b>	<b>Sample Selection.</b>	<b>35</b>
3.2.1	Dalradian Supergroup.	36
3.2.2	Silurian Rocks.	36
3.2.3	Connemara Metagabbro Gneiss Complex.	36
<b>3.3</b>	<b>Sample Preparation.</b>	<b>43</b>
<b>CHAPTER 4.</b>	<b>ANALYTICAL WORK.</b>	<b>47</b>
<b>4.1</b>	<b>X-Ray Diffraction.</b>	<b>47</b>
<b>4.2</b>	<b>X-Ray Fluorescence.</b>	<b>48</b>
<b>4.3</b>	<b>Wet Chemical Analysis.</b>	<b>49</b>
4.3.1	Flame Emission and Atomic Absorption Spectrophotometry.	49
4.3.2	Ferrous Iron Analysis.	50
4.3.3	Water and Carbon Dioxide Analysis.	51
<b>4.4</b>	<b>Electron Microprobe Analysis.</b>	<b>52</b>
<b>4.5</b>	<b>Scanning Electron Microscope Imaging.</b>	<b>52</b>

<b>4.6</b>	<b>K-Ar Dating.</b>	<b>53</b>
4.6.1	Potassium Analysis.	53
4.6.2	Argon Analysis.	54
<b>4.7</b>	<b>Hydrogen Isotope Analysis.</b>	<b>54</b>
<b>4.8</b>	<b>Oxygen Isotope Analysis.</b>	<b>55</b>
<b>CHAPTER 5.</b>	<b>RESULTS.</b>	<b>57</b>
<b>5.1</b>	<b>Rock and Mineral Chemistry.</b>	<b>58</b>
5.1.1	Rock Chemistry.	58
5.1.2	Mineral Chemistry.	59
<b>5.2</b>	<b>Hornblende K-Ar Ages.</b>	<b>70</b>
5.2.1	K-Ar Ages - Rock XRF.	71
5.2.2	K-Ar Ages - Wet Chemical Analysis of Hornblendes.	72
5.2.3	K-Ar Ages - Hornblende EMPA.	73
5.2.4	Summary of K-Ar Ages - Rock and Bulk Hornblende Compositions.	74
<b>5.3</b>	<b>Hornblende <math>\delta D</math> Values.</b>	<b>87</b>
5.3.1	$\delta D$ Values - Water Contents and K-Ar Ages.	87
5.3.2	$\delta D$ Values - Rock XRF.	88
5.3.3	$\delta D$ Values - Wet Chemical Analysis of Hornblendes.	89
5.3.4	$\delta D$ Values - Hornblende EMPA.	89
5.3.5	Summary of $\delta D$ Values - Rock and Bulk Hornblende Compositions.	90

<b>5.4</b>	<b>Hornblende <math>\delta^{18}\text{O}</math> Values.</b>	102
5.4.1	$\delta^{18}\text{O}$ Values - K-Ar Ages and Fluid $\delta\text{D}$ Values.	102
5.4.2	$\delta^{18}\text{O}$ Values - Rock XRF.	104
5.4.3	$\delta^{18}\text{O}$ Values - Wet Chemical Analysis of Hornblendes.	104
5.4.4	$\delta^{18}\text{O}$ Values - Hornblende EMPA.	104
<b>5.5</b>	<b>Significance of Data.</b>	115
<b>CHAPTER 6.</b>	<b>DISCUSSION.</b>	117
<b>6.1</b>	<b>Hornblende Composition Related to K-Ar Age and Stable Isotopes.</b>	117
6.1.1	Consideration of Results.	117
6.1.2	Compositional Relationships with Stable Isotopes.	118
6.1.3	Evaluation with Previous Studies in Connemara.	119
6.1.4	Evaluation with Previous Studies in Other Areas.	122
<b>6.2</b>	<b>Ionic Porosity Related to K-Ar Age and Stable Isotopes.</b>	125
<b>6.3</b>	<b>Origins of Hydrothermal Fluid.</b>	131
6.3.1	Hydrothermal Palaeo-Fluids Active in Connemara.	132
6.3.2	Structural Water in Hornblendes.	136
6.3.3	Relationships with $\delta^{18}\text{O}$ .	139
<b>6.4</b>	<b>Relevance to Geological Synthesis in Connemara.</b>	141
<b>6.5</b>	<b>Future Study.</b>	143

<b>CHAPTER 7.</b>	<b>CONCLUSIONS.</b>	<b>147</b>
<b>7.1</b>	<b>Conclusions: K-Ar Dating, Composition and Stable Isotope Studies of Hornblendes.</b>	<b>147</b>
<b>7.2</b>	<b>Results in Relation to Geology.</b>	<b>148</b>
<b>7.3</b>	<b>Future Work.</b>	<b>151</b>
<b>APPENDIX 1.</b>	<b>SAMPLE LOCATIONS AND ROCK TYPES.</b>	<b>154</b>
<b>APPENDIX 2.</b>	<b>ELECTRON MICROPROBE SECTION DESCRIPTIONS.</b>	<b>164</b>
<b>APPENDIX 3.</b>	<b>ROCK X-RAY FLUORESCENCE ANALYSES.</b>	<b>174</b>
<b>APPENDIX 3A.</b>	<b>ROCK CIPW NORM RESULTS.</b>	<b>179</b>
<b>APPENDIX 4.</b>	<b>MINERAL SEPARATES CHEMICAL ANALYSES.</b>	<b>182</b>
<b>APPENDIX 5.</b>	<b>ELECTRON MICROPROBE ANALYSIS RESULTS. (estimated bulk analyses).</b>	<b>185</b>
<b>APPENDIX 5A.</b>	<b>ELECTRON MICROPROBE ANALYSIS RESULTS. (dual hornblende analyses).</b>	<b>191</b>
<b>APPENDIX 6.</b>	<b>ELECTRON MICROPROBE MINERAL FORMULAE. (from bulk EMPA results).</b>	<b>196</b>

<b>APPENDIX 6A.</b>	<b>ELECTRON MICROPROBE MINERAL FORMULAE. (from dual hornblende analyses).</b>	<b>199</b>
<b>APPENDIX 7.</b>	<b>MINERAL NAMES. (from bulk mineral formulae).</b>	<b>204</b>
<b>APPENDIX 7A.</b>	<b>MINERAL NAMES. (from dual hornblende formulae).</b>	<b>206</b>
<b>APPENDIX 8.</b>	<b>IONIC POROSITIES OF HORNBLENDES.</b>	<b>208</b>
<b>APPENDIX 9.</b>	<b>K-Ar AGE ISOTOPE DATA.</b>	<b>212</b>
<b>APPENDIX 10.</b>	<b>HYDROGEN ISOTOPE DATA.</b>	<b>215</b>
<b>APPENDIX 11.</b>	<b>OXYGEN ISOTOPE DATA.</b>	<b>219</b>
<b>APPENDIX 12.</b>	<b>K-Ar AGES AND <math>\delta D</math> VALUES FROM PREVIOUS STUDIES.</b>	<b>222</b>
<b>APPENDIX 13.</b>	<b>IONIC POROSITIES FROM PREVIOUS STUDY.</b>	<b>225</b>
<b>APPENDIX 14.</b>	<b>DATA FOR AGE-<math>\delta D</math>-Z DIAGRAM.</b>	<b>228</b>
<b>APPENDIX 15.</b>	<b>DATA FOR <math>\delta^{18}O</math>-<math>\delta D</math>-Z DIAGRAM.</b>	<b>230</b>
<b>REFERENCES.</b>		<b>232-243</b>

<b>LIST OF FIGURES:</b>	<b>Page Number.</b>
<b>FIGURE 1.1</b> Geological setting of Connemara.	2
<b>FIGURE 1.2</b> Structural features of Connemara.	4
<b>FIGURE 1.3</b> Distribution of metamorphic facies in Connemara.	5
<b>FIGURE 1.4</b> The findings of Miller et al. (1991): Hornblende $\delta D$ against K-Ar age, A-site occupancy and structural water contents.	13
<b>FIGURE 1.5</b> Cation site location in an amphibole.	15
<b>FIGURE 1.6</b> Crystal structure of an amphibole.	16
<b>FIGURE 1.7</b> Classification diagram of the calcic amphiboles.	19
<b>FIGURE 3.1</b> Sample location map.	28
<b>FIGURE 3.2</b> Photomicrograph of <b>TJ-7D</b> (from north of area): Relic hornblende grain with inclusion trails.	41
<b>FIGURE 3.3</b> Photomicrograph of <b>TJ-7D</b> (from north of area): Relic hornblende grain displaying zoning.	41
<b>FIGURE 3.4</b> Photomicrograph of <b>TJ-44</b> (from south of area): Pronounced cleavage traces in hornblende.	42
<b>FIGURE 3.5</b> Photomicrograph of <b>TJ-44</b> (from south of area): Biotite alteration in hornblende cleavage (close-up).	42
<b>FIGURE 5.1A</b> BSE image of <b>TJ-7D</b> : Fe-rich and Mg-rich hornblende. Patchy distribution.	61
<b>FIGURE 5.1B</b> BSE image of <b>TJ-7D</b> : Fe-rich and Mg-rich hornblende. Larger areas.	61
<b>FIGURE 5.1C</b> BSE image of <b>TJ-7D</b> : Fe-rich and Mg-rich hornblende. Displaying zoning.	62
<b>FIGURE 5.1D</b> BSE image of <b>TJ-44</b> : Uniform hornblende composition. Biotite and chlorite alteration along cleavages.	62

<b>FIGURE 5.1E</b>	BSE image of <b>TJ-44</b> : Uniform hornblende composition. Biotite and chlorite alteration along cleavages (close-up).	63
<b>FIGURE 5.1F</b>	BSE image of <b>TJ-45</b> : Uniform hornblende composition. Much less alteration than <b>TJ-44</b> .	63
<b>FIGURE 5.1G</b>	BSE element X-ray distribution map.	64
<b>FIGURE 5.1H</b>	Hornblende EMPA SiO <sub>2</sub> versus hornblende EMPA FeO/(FeO+MgO).	67
<b>FIGURE 5.1I</b>	Hornblende EMPA Al <sub>2</sub> O <sub>3</sub> versus hornblende EMPA FeO/(FeO+MgO).	67
<b>FIGURE 5.1J</b>	Hornblende EMPA FeO/(FeO+MgO) versus rock XRF FeO/(FeO+MgO).	68
<b>FIGURE 5.1K</b>	Diagram of hornblende bulk compositions.	69
<b>FIGURE 5.2</b>	Mineral separate K-Ar ages on map of Connemara.	77
<b>FIGURE 5.3</b>	<sup>40</sup> Ar/ <sup>36</sup> Ar - K/ <sup>36</sup> Ar isochron.	78
<b>FIGURE 5.4</b>	Hornblende separate FES K versus hornblende K-Ar age.	78
<b>FIGURE 5.5</b>	Rock XRF MgO versus hornblende K-Ar age.	80
<b>FIGURE 5.6</b>	Rock XRF FeO/(FeO+MgO) versus hornblende K-Ar age.	80
<b>FIGURE 5.7</b>	Hornblende separate AAS MgO versus hornblende K-Ar age.	82
<b>FIGURE 5.8</b>	Hornblende separate FES K <sub>2</sub> O versus hornblende K-Ar age.	82
<b>FIGURE 5.9</b>	Hornblende EMPA FeO versus hornblende K-Ar age.	84
<b>FIGURE 5.10</b>	Hornblende EMPA MgO versus hornblende K-Ar age.	84
<b>FIGURE 5.11</b>	Hornblende EMPA K <sub>2</sub> O versus hornblende K-Ar age.	85
<b>FIGURE 5.12</b>	Hornblende EMPA FeO/(FeO+MgO) versus hornblende K-Ar age.	85
<b>FIGURE 5.13</b>	Hornblende EMPA Mg# versus hornblende K-Ar age.	86
<b>FIGURE 5.14</b>	Hornblende EMPA ionic porosity versus hornblende K-Ar age.	86
<b>FIGURE 5.15</b>	Mineral separate δD values on map of Connemara.	92
<b>FIGURE 5.16</b>	Hornblende δD versus hornblende H <sub>2</sub> O content.	93
<b>FIGURE 5.17</b>	Hornblende δD versus hornblende K-Ar age.	93

<b>FIGURE 5.18</b>	Hornblende $\delta D$ versus rock XRF MgO.	95
<b>FIGURE 5.19</b>	Hornblende $\delta D$ versus rock XRF FeO/(FeO+MgO).	95
<b>FIGURE 5.20</b>	Hornblende $\delta D$ versus hornblende separate AAS MgO.	97
<b>FIGURE 5.21</b>	Hornblende $\delta D$ versus hornblende separate AAS FeO/(FeO+MgO).	97
<b>FIGURE 5.22</b>	Hornblende $\delta D$ versus hornblende EMPA FeO.	99
<b>FIGURE 5.23</b>	Hornblende $\delta D$ versus hornblende EMPA MgO.	99
<b>FIGURE 5.24</b>	Hornblende $\delta D$ versus hornblende EMPA FeO/(FeO+MgO).	100
<b>FIGURE 5.25</b>	Hornblende $\delta D$ versus hornblende EMPA Mg#.	100
<b>FIGURE 5.26</b>	Hornblende $\delta D$ versus hornblende EMPA derived Z.	101
<b>FIGURE 5.27</b>	Mineral separate $\delta^{18}O$ values on map of Connemara.	107
<b>FIGURE 5.28</b>	Hornblende $\delta^{18}O$ versus hornblende K-Ar age.	108
<b>FIGURE 5.29</b>	Hornblende $\delta D$ and fluid $\delta D$ versus hornblende $\delta^{18}O$ .	108
<b>FIGURE 5.30</b>	Fluid $\delta D$ versus fluid/hornblende $\delta^{18}O$ .	109
<b>FIGURE 5.31</b>	Hornblende EMPA FeO versus hornblende $\delta^{18}O$ .	113
<b>FIGURE 5.32</b>	Hornblende EMPA Na <sub>2</sub> O versus hornblende $\delta^{18}O$ .	113
<b>FIGURE 5.33</b>	Hornblende EMPA derived A-site occupancy versus hornblende $\delta^{18}O$ .	114
<b>FIGURE 5.34</b>	Hornblende EMPA ionic porosity versus hornblende $\delta^{18}O$ .	114
<b>FIGURE 6.1</b>	Comparison of hornblende separate FES K <sub>2</sub> O with hornblende K-Ar age between Elias (1985), Miller (1990) and Jappy (1998).	120
<b>FIGURE 6.2</b>	Hornblende EMPA Mg#, A-site occupancy and EMPA ionic porosity versus hornblende K-Ar age from Miller (1990).	121
<b>FIGURE 6.3</b>	Comparison of hornblende ionic porosity and $\delta D$ values with hornblende K-Ar age.	129
<b>FIGURE 6.4</b>	[Age- $\delta D$ -Z] diagram.	130

<b>FIGURE 6.5</b>	Comparison of hornblende K-Ar age, FES K <sub>2</sub> O and δD values with hornblende structural water contents.	137
<b>FIGURE 6.6</b>	Comparison of hornblende EMPA Mg#, ionic porosity and δ <sup>18</sup> O values with hornblende structural water contents.	138
<b>FIGURE 6.7</b>	[δ <sup>18</sup> O-δD-Z] diagram.	140

**LIST OF TABLES:**

Page Number.

<b>TABLE 1.1</b>	Names and formulae of calcic amphibole end-members.	20
<b>TABLE 3.1</b>	Rock descriptions and locations.	29
<b>TABLE 3.2</b>	Mineralogy of hornblende containing rocks.	38
<b>TABLE 3.3</b>	Mineralogy of mica containing rocks.	40
<b>TABLE 5.1</b>	Mineral K-contents and K-Ar ages.	76
<b>TABLE 5.2</b>	Correlation coefficients of hornblende K-Ar ages against rock XRF analysis and rock FeO, H <sub>2</sub> O and CO <sub>2</sub> .	79
<b>TABLE 5.3</b>	Correlation coefficients of hornblende K-Ar ages against hornblende mineral separate wet chemical analyses.	81
<b>TABLE 5.4</b>	Correlation coefficients of hornblende K-Ar ages against in-situ hornblende EMPA analyses.	83
<b>TABLE 5.5</b>	Mineral $\delta$ D values.	91
<b>TABLE 5.6</b>	Correlation coefficients of hornblende $\delta$ D values against rock XRF analysis and rock FeO, H <sub>2</sub> O and CO <sub>2</sub> .	94
<b>TABLE 5.7</b>	Correlation coefficients of hornblende $\delta$ D values against hornblende mineral separate wet chemical analyses.	96
<b>TABLE 5.8</b>	Correlation coefficients of hornblende $\delta$ D values against in-situ hornblende EMPA analyses.	98
<b>TABLE 5.9</b>	Mineral $\delta^{18}$ O values.	106
<b>TABLE 5.10</b>	Correlation coefficients of hornblende $\delta^{18}$ O values against rock XRF analysis and rock FeO, H <sub>2</sub> O and CO <sub>2</sub> .	110
<b>TABLE 5.11</b>	Correlation coefficients of hornblende $\delta^{18}$ O values against hornblende mineral separate wet chemical analyses.	111
<b>TABLE 5.12</b>	Correlation coefficients of hornblende $\delta^{18}$ O values against in-situ hornblende EMPA analyses.	112

## CHAPTER 1.

### INTRODUCTION.

This thesis is segmented into seven chapters; Introduction, Aims, Sample Collection and Preparation, Analytical Work, Results, Discussion, Conclusions. In addition to this the Results chapter is augmented by an extensive Appendix, giving details of experimental data.

The Introduction chapter is divided into four sections, dealing with; The Geology of Connemara, Previous Dating Studies, Composition and Structure of Hornblende, Diffusivity in Hornblende. Details of the K-Ar dating and stable isotope ( $\delta D$  and  $\delta^{18}O$ ) techniques are covered extensively in the literature and are not described in this work.

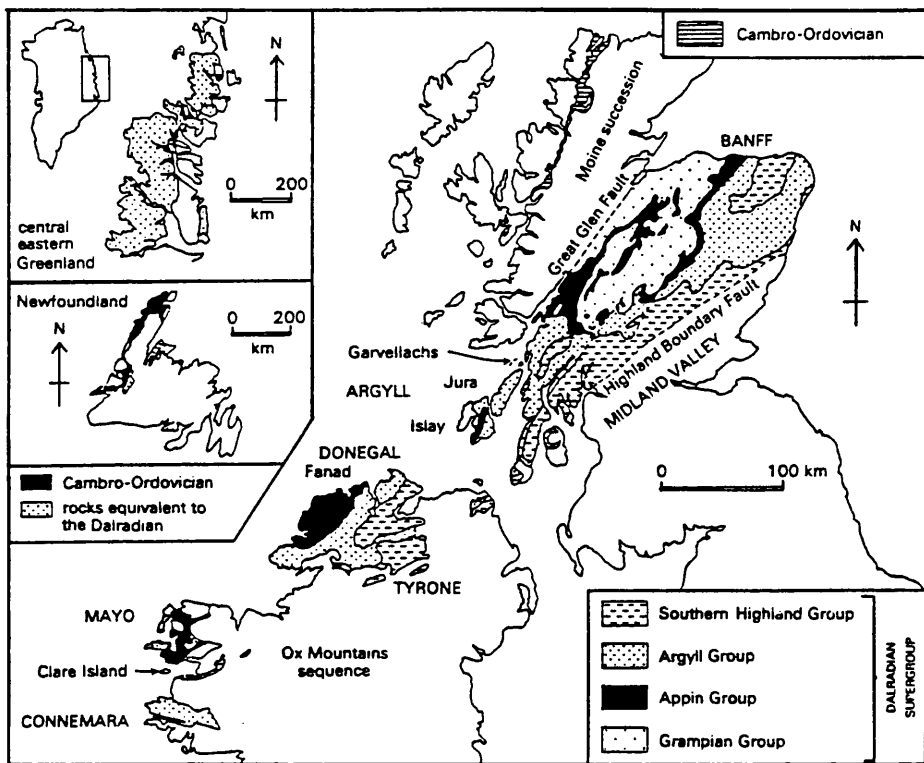
#### 1.1 The Geology of Connemara.

The geology of Connemara is reviewed in the Royal Irish Academy publication by Leake and Tanner (1994) which accompanies the 1:63,360 geological map of Connemara.

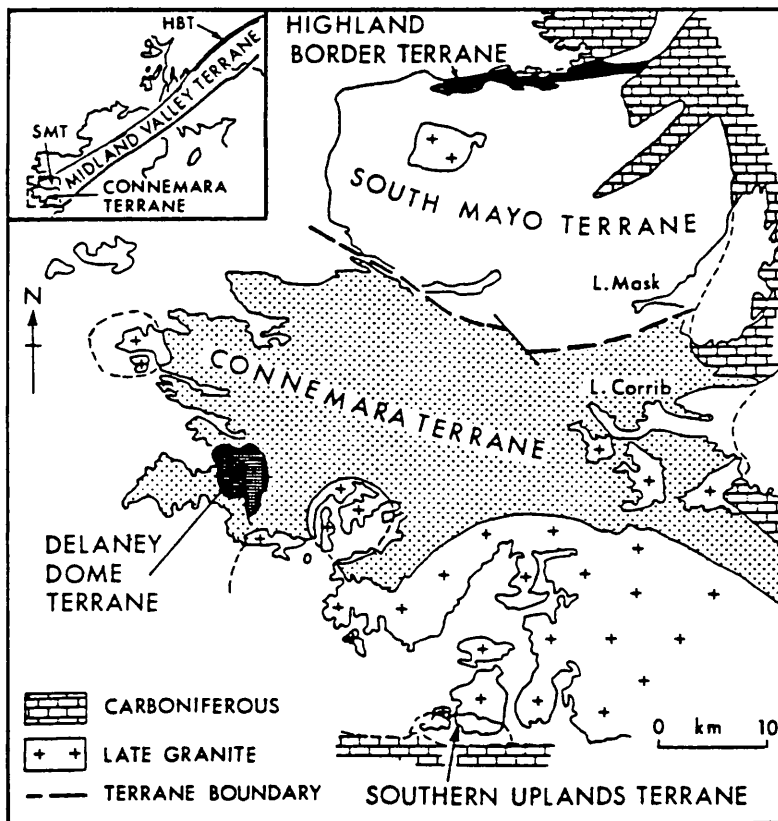
The Dalradian rocks of Connemara, western Ireland, belong to the Appalachian - Caledonide orogenic belt, extending from Scandinavia, across the British Isles, Greenland, Newfoundland and the Appalachian mountains of the eastern United States of America (Anderton et al., 1983; Leake, 1989; Cliff et al., 1996). Figure 1.1 shows the location of the Connemara metamorphic complex relative to the Caledonides in Britain and Ireland.

The Connemara metamorphic complex is a region of southwardly thrust and eastwardly strike-slip faulted metamorphosed sedimentary and igneous rocks in the southwest of County Galway, western Ireland. These metamorphosed rocks occupy an area 70km long (east-west) by 25km wide (north-south) and form an inlier, unconformably overlain by Silurian strata on the northern margin, truncated at the southern margin by the intruded batholiths and associated plutons of the Galway Granite, overlain by Carboniferous sediments to the east and obscured by the Atlantic Ocean to the west.

The Connemara metamorphic complex consists of two east-west trending and interlocking metamorphic belts. The northern belt is essentially metasedimentary while the



(a)



(b)

**FIGURE 1.1** (a) Connemara in relation to other outcrops of rocks of the Dalradian Supergroup in the British Isles. Diagram from Anderton et al. (1983). (b) The Connemara inlier in relation to the unconformably overlying Silurian of the South Mayo Trough to the north, the unconformably overlying Carboniferous limestones to the east, the intruded Galway Granite and its associated plutons to the south and the Atlantic Ocean to the west. Diagram from Leake and Tanner (1994).

southern belt is mainly meta-igneous (Figure 1.2). These are described in more detail in Sections 1.1.1 and 1.1.2 respectively.

The Silurian rocks of the South Mayo Trough are described extensively by Graham et al. (1989) and are thought to be of Upper Llandovery age in the north of Connemara. They consist of basal breccias and conglomerates which unconformably overlie the Dalradian metasediments, passing up into graded turbidites, mudstones, sandstones and interbedded volcanic diorites in the area just north of the Connemara metamorphic complex.

The Carboniferous sedimentary rocks are almost horizontal and unconformably overlie the Connemara Dalradian rocks, the Oughterard and Galway Granites and the Silurian rocks. They are believed to be of Viséan or possibly Courceyan age and consist of basal coarse grits and conglomerates, overlain by Carboniferous limestone to the east.

Post-tectonic igneous intrusions are mostly granite plutons with associated dyke swarms which cut the foliation in the metasediments and the metagabbro-gneiss (MGS) complex. They comprise an older suite of intrusions known collectively as the Oughterard Granite (dated at  $459 \pm 7$  Ma from K-feldspar-muscovite-whole-rock Rb-Sr isochron dating by Leggo et al., 1966 and at  $\sim 473$  Ma from Rb-Sr dating of muscovite by Tanner et al., 1997) and the main Caledonian Granite at  $\sim 400$  Ma (dated at  $398 \pm 10$  Ma from K-feldspar-muscovite-whole-rock Rb-Sr isochron dating by Leggo et al., 1966 and at  $412 \pm 15$  Ma from U-Pb dating of zircons by Pidgeon, 1969) which includes the Galway Granite and its satellite plutons. There are also minor dolerite intrusions and dykes of Carboniferous and Tertiary age.

The interpretation of the geology of Connemara is that it represents the roots of a magmatic arc at a continental margin above a subduction zone (Leake, 1989) of the Caledonian orogenic belt with the MGS complex of the southern belt being the eroded roots of a calc-alkaline intrusive complex. Subsequent strike-slip faulting (Dewey and Shackleton, 1984; Hutton and Dewey, 1986; Soper and Hutton, 1984; Soper, 1986; Hutton, 1987) laterally displaced parts of the MGS complex in a similar fashion to present day strike faults along the west coast of North America.

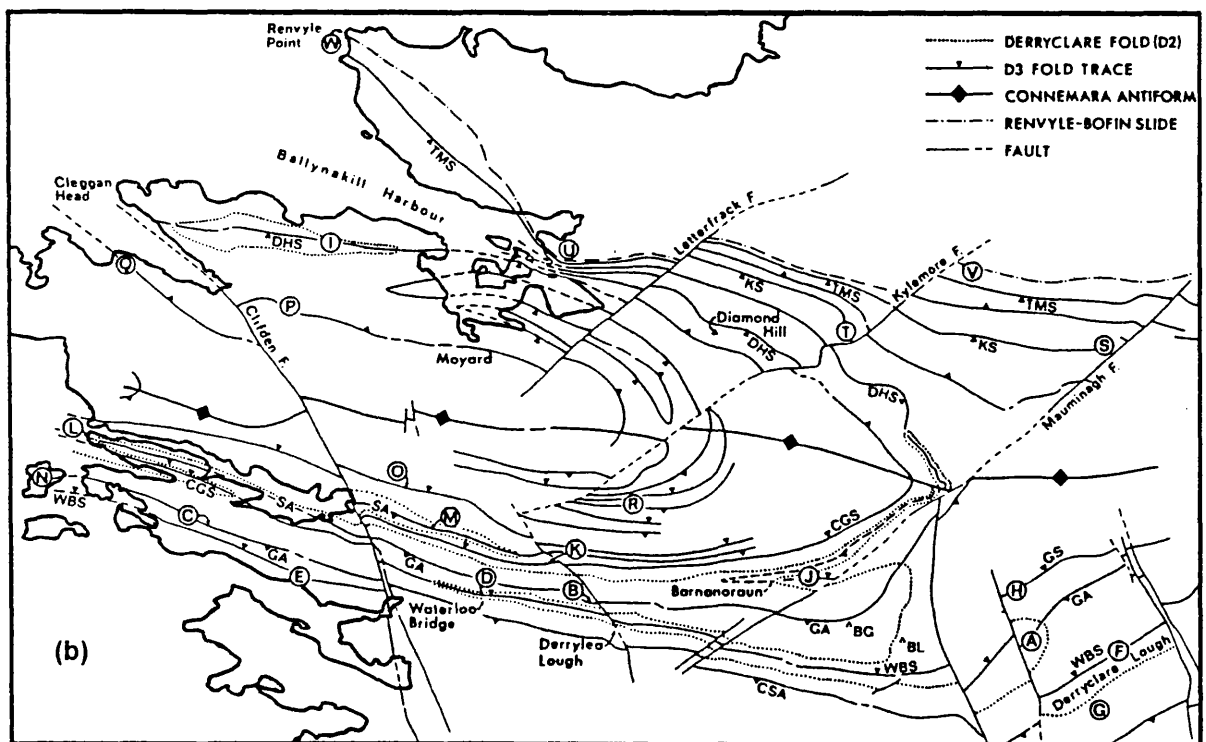
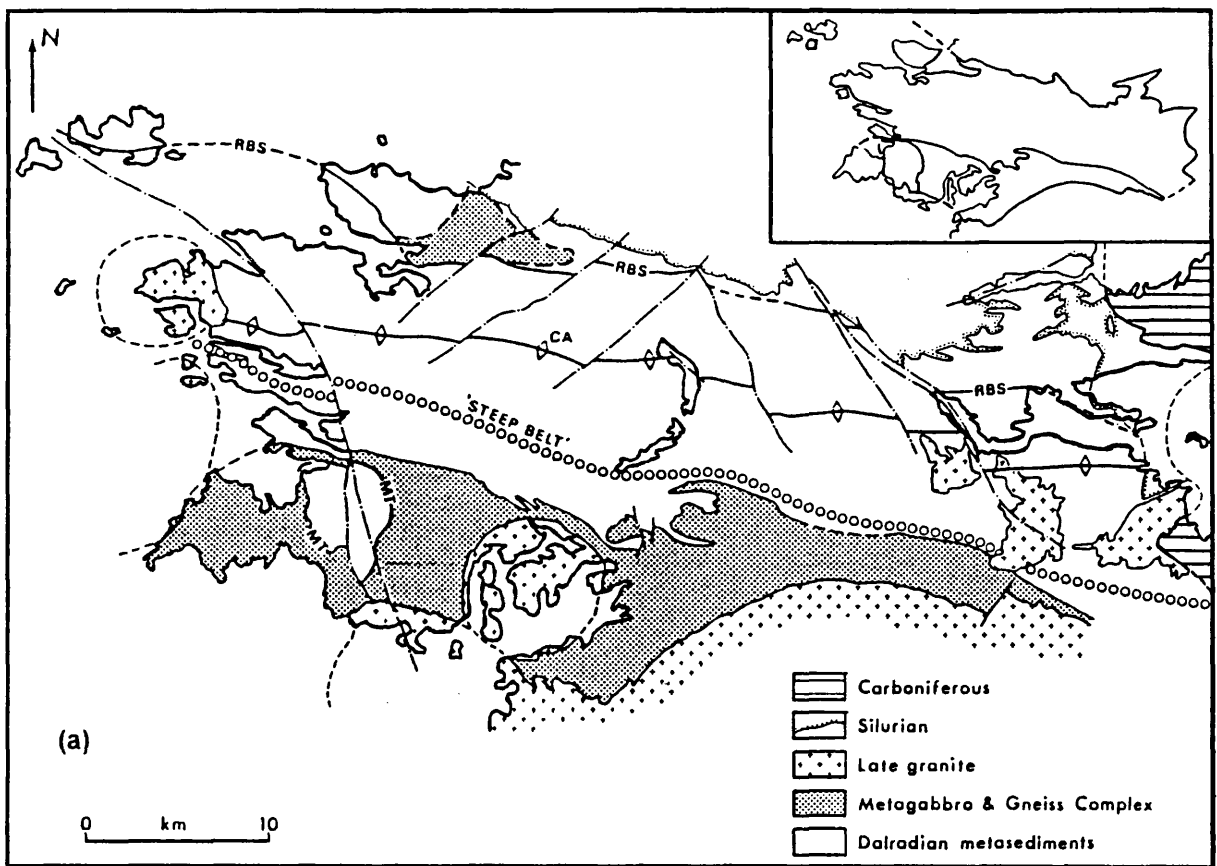


**FIGURE 1.2** (a) Major structural features of Connemara. CA, Connemara Antiform (D4); MT, Mannin Thrust; RBS, Renvyle-Bofin Slide. Diagram from Leake and Tanner (1994). (b) D3-fold traces showing the gently eastwardly plunging trend of the Connemara Antiform and the larger scale faulting trends. Diagram from Leake and Tanner (1994).

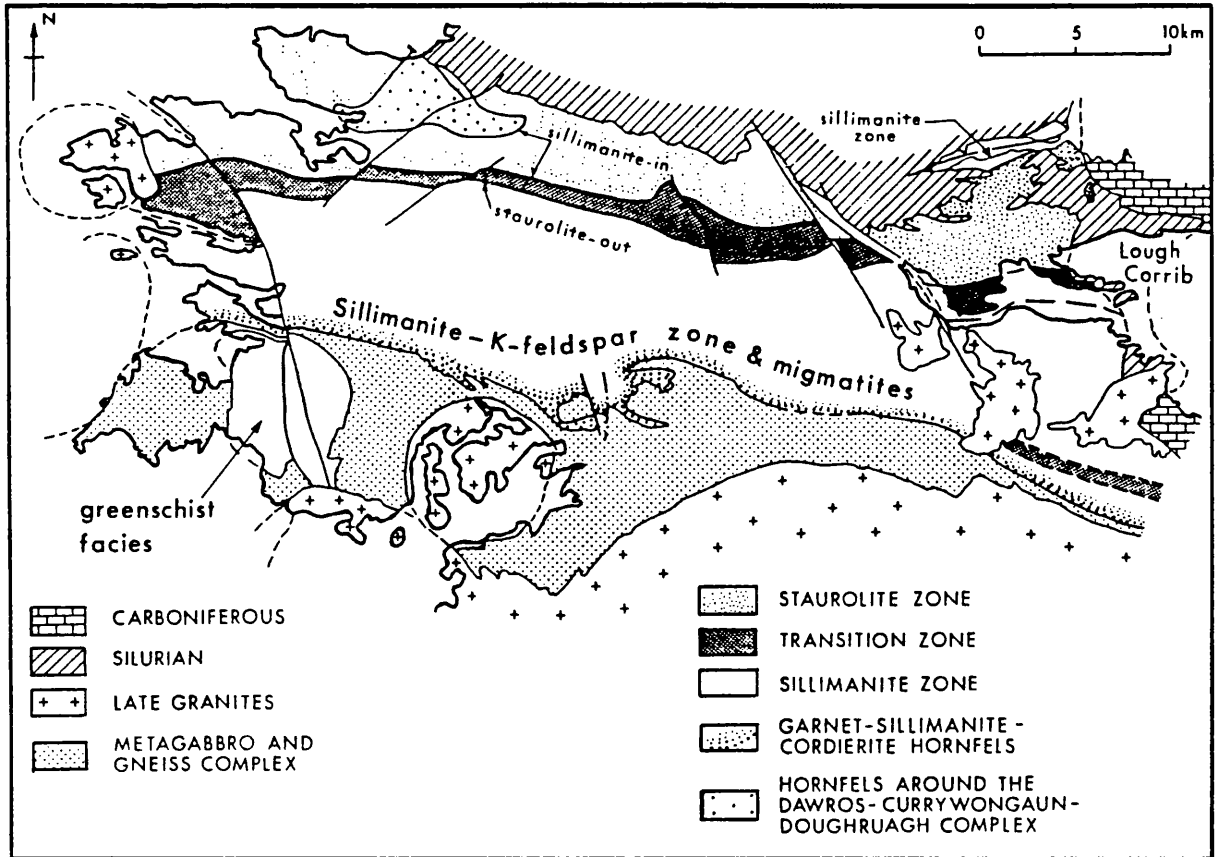


**FIGURE 1.3** Distribution of the metamorphic facies in Connemara due to the intrusion of the metagabbro gneiss complex into the Dalradian metasediments. Diagram from Leake and Tanner (1994).

### 1.1.1 The Northern Metamorphic Belt.

The metasediments of the northern metamorphic belt are believed to be entirely of Dalradian (late Proterozoic) age. They correlate with rocks of Lower Dalradian, Appin Group to the Upper Dalradian, Southern Highland Group (Tanner and Shackleton, 1979). This correlation is based on similarities with the Dalradian sequence on Islay, Scotland; Mull of Oa Phyllites, Islay Limestone, Port Askaig Tillite, Islay Quartzite. The rocks consist of pelitic and semi-pelitic schists, quartzites and marbles (a green, opicalcite variety of which is known as the Connemara Marble). Full details of the stratigraphic units can be found in Leake and Tanner (1994). Throughout the metasediments there are interbedded strata of amphibolite rocks, metamorphosed from extruded or intruded basic igneous rocks. These amphibolites are most common in the Lakes Marble Formation of the Argyll Group (Leake and Tanner, 1994).

The northern belt shows a complex deformation history. The earliest deformation episodes were of high temperature, high pressure Barrovian type metamorphism. The main east-west fabric observed was established during D2 deformation. The D1 structures have been obliterated by this later D2 event and the evidence for D1 remains only as inclusion trails in garnet and plagioclase porphyroblasts (Badley, 1976). The most prominent structural feature in the Dalradian metasediments is the Connemara Antiform (D4) which plunges gently to the east and folds previous D3 folds (Figure 1.2).

The regional metamorphism of the Dalradian rocks reached amphibolite facies throughout Connemara, grading from garnet zone in the north to upper sillimanite zone in the south (Figure 1.3).

### 1.1.2 The Southern Metamorphic Belt.

The southern belt of the Connemara metamorphic complex consists largely of metamorphosed basic and ultrabasic igneous rocks which have been injected and broken up by quartz diorite gneiss and some K-feldspar granitic gneiss. The main complex strikes east-west from Errislannan and Slyne Head to Oughterard and then southeasterly to Galway. A similar but smaller complex of metagabbro and gneiss is present in the

Dawros-Currywongaun-Doughruagh area in the Dalradian metasediments of the northern metamorphic belt.

Zircon  $^{207}\text{Pb}/^{206}\text{Pb}$  ages of  $490\pm 1\text{Ma}$  (Leake, 1970; Jagger et al., 1988) showed the intrusive complex to be of Lower Ordovician age and similar in age to the crystallisation of the Aberdeenshire gabbros (Pankhurst, 1970), the Baltimore mafic complex (Shaw and Wasserburg, 1984) and the Elkahatchee quartz diorite complex of Alabama (Russell et al., 1987). Unpublished work by Friedrich et al. (1997) indicates that more precise dating of U-Pb ages of monazite shows the gabbros to be 463-468Ma and the gneisses about 463Ma.

Throughout the whole MGS complex and in the adjacent Dalradian metasediments, there is extensive retrograde alteration effects such as sericitisation and saussuritisation of plagioclase, chloritisation of hornblende and biotite and serpentisation of ultramafic rocks. These effects are thought to be due to the circulation of hot fluids around the Galway Granite and associated plutons at  $\sim 400\text{Ma}$  (Jenkin et al., 1992; Jenkin et al., 1997; O'Reilly et al., 1997).

### 1.1.3 Geological Structure of Connemara.

There is evidence for three major periods of deformation in the Dalradian rocks; D2, D3 and D4 (Yardley, 1976; Leake and Tanner, 1994). No D1 folds are now recognised, the only evidence being quartz and iron ore helicitic fabrics in plagioclase, garnet and staurolite porphyroblasts (Tanner and Shackleton, 1979; Leake and Tanner, 1994). The earliest recognisable structures, D2, produced a pervasive schistosity in all Dalradian lithologies and resulted in at least one isoclinal fold, extending east-west through central Connemara. The oldest lithologies (Appin Group) occur in the hinge region of this fold and the succession youngs away from the central belt to the north and south. The most abundant large scale folds are tight D3 structures which form tight northward facing nappes in central and northern Connemara, possibly rooted in a steep belt to the south (Yardley, 1976). These folds formed at the metamorphic peak and have axial-planar fibrolitic fabrics in appropriate lithologies and grades (Yardley, 1976). In the steep belt there is intense rotation of fabrics into east-west parallelism.

The D4 folds are broad, open, upright structures, trending east-west, for example; the Connemara Antiform. Leake et al. (1983) have suggested a genetic relationship between the D4 structures forming in the upper plate of the Mannin Thrust complex prior to emplacement, the steep belt (Figure 1.2) being a ramp structure related to the overthrusting. The thrusting has been dated by a well defined Rb-Sr whole-rock isochron from acid mylonites in the thrust zone at 447 $\pm$ 4Ma (Tanner et al., 1989). The docking of the Dalradian with Ordovician sediments in the South Mayo Trough is pre-Upper Llandovery but the later, unconformably overlying, Silurian deposits conceal this inferred fracture zone.

#### 1.1.4 Metamorphism of Connemara.

The Dalradian rocks of Connemara are mainly of amphibolite facies with the metamorphic grade increasing southwards across a series of well defined east-west trending zones. Staurolite is restricted to the north limb of the Connemara Antiform and sillimanite to the south. Figure 1.3 shows the distribution of the index minerals and assigned metamorphic zones based on pelitic assemblages in the metasediments. The transition zone represents the appearance of sillimanite-muscovite with the gradual disappearance of staurolite.

Three major east-west striking zones which cut across the axial traces of major D3 folds are recognised in pelites with progressively higher temperature metamorphism occurring to the south. The staurolite zone is followed by a sillimanite-muscovite transition zone, still containing some staurolite and a southern sillimanite-K-feldspar zone. A higher grade subdivision of the sillimanite zone shows migmatitic melting of metasediments along the boundary of the MGS and a narrower area around the Dawros-Currywongaun-Doughruagh complex. Cordierite and garnet are common in these migmatised hornfels rocks around these intruded basic complexes.

A pervasive retrograde alteration of the Dalradian metasediments and metagabbro-gneiss complex is seen in the alteration of hornblende and biotite to chlorite, plagioclase to sericite and saussurite, garnet to chlorite, and olivine to serpentine with magnetite. Sillimanite, kyanite and andalusite, where observed, can be sericitised. This

retrogressive alteration is suggested to have occurred by the convective cell circulation of meteoric or buried seawater from the overlying Silurian strata (now eroded) driven by the large cooling igneous body of the Galway Granite, which was emplaced at ~400Ma, well after the peak metamorphic amphibolite facies conditions (Jenkin, 1988; Jenkin et al., 1992; Jenkin et al., 1997; O'Reilly et al., 1997).

Recent studies by Friedrich et al. (1997) imply that the arc magmatism and related metamorphism and D3 deformation spanned no more than 10Ma. The previous U-Pb zircon age of ~490Ma (Jagger et al., 1988) contained an inherited component and the revised U-Pb zircon age of the crystallisation of the Cashel-Lough Wheelaun metagabbro is 471.1+/-0.8Ma. The youngest intrusive phase of arc volcanism is the Oughterard Granite, yielding a U-Pb xenotime age of 462.5+/-3.3Ma (Friedrich et al., 1997). U-Pb monazite ages for Dalradian metapelites suggest that Connemara was exhumed from 18km to 10km depth between 468-463Ma. New <sup>40</sup>Ar-<sup>39</sup>Ar ages (source not given in abstract of Friedrich et al., 1997) are consistent with cooling of the high-grade areas of the Connemara region to below 400°C at 454+/-4Ma (Friedrich et al., 1997).

#### 1.1.5 Post-Tectonic Igneous Intrusions.

There are three main types of igneous activity which occurred after the main metamorphic events in Connemara:

I. The Oughterard suite of intrusions towards Lough Corrib in the east of the area (Figure 1.3). This is a fine grained granite, possibly following fault lines, the two main bodies of which lie astride the D4 Connemara Antiform. The mineralogy is quartz, oligoclase, microcline microperthite, chloritised biotite and minor muscovite. Leggo et al. (1966) estimated the emplacement to be 459+/-7Ma (based on a K-feldspar-muscovite-whole rock Rb-Sr isochron). More recently, the pluton has been dated at ~473Ma from Rb-Sr dating of muscovite by Tanner et al., 1997).

II. Leake (1978) reviewed the Galway Granite suite. This is a very large composite intrusion 60x25km in size (Figures 1.2, 1.3 and 1.4). Its satellite intrusions include the Omey and Inish Granites, the Letterfrack Granites and the Roundstone Granite. This granite phase is dated at ~400Ma (Leggo et al., 1966; Leake, 1978; Max et al., 1978). The granite was emplaced passively by stoping of country rocks (Leake, 1974). It contains large K-feldspar phenocrysts which are dark pink to red in colour (turbid in thin section), sericitised and saussuritised plagioclase (apple green in hand specimen) and biotite has been altered to chlorite, with epidote commonly present, thus indicating strong hydrothermal alteration (Jenkin et al., 1992).

III. The large number of basic igneous dykes and sills in the area are from later Carboniferous times; ~320Ma and ~305Ma (Mitchell and Mohr, 1987) and Tertiary events; ~60Ma (MacIntyre et al., 1975) and 68.5+/-0.7Ma (Mitchell and Mohr, 1986).

## 1.2 Previous Dating Studies.

Previous age determinations of events in Connemara include K-Ar and Rb-Sr investigation of micas by Giletti et al. (1961), Fitch et al. (1964) and Miller and Brown (1965). Rb-Sr whole rock isochrons by Leggo et al. (1966) and U-Pb dating of zircons by Pidgeon (1969) showed that the Galway granite and its satellite plutons were emplaced ~400Ma. Leggo et al. (1966) also reported a range of hornblende K-Ar ages of 466+/-17Ma to 440+/-17Ma for the Connemara gneisses at Cashel. Moorbath et al. (1968) and Dewey et al. (1970) considered the average K-Ar ages of five hornblendes (456+/-12Ma), 12 muscovites (448+/-5Ma) and eight biotites (442+/-6Ma) to be due to post-metamorphic uplift and cooling.

However, the two most recent studies concerning the dating of events using K-Ar dating of hornblendes, muscovites and biotites in the Dalradian rocks and the metagabbro intrusive rocks (Elias et al., 1988; Miller et al., 1991) have shown potential problems in assigning geological significance to the measured dates.

Both of these studies showed that there was an observable variation in K-Ar ages in the same mineral type in samples collected from the same areas and that the normally accepted hornblende → muscovite → biotite, oldest to youngest age sequence was varied, e.g. muscovite → biotite → hornblende. The estimated closure temperatures for  $^{40}\text{Ar}^*$  (radiogenic argon) in these minerals are as follows: hornblende =  $550\pm 50^\circ\text{C}$ ; muscovite =  $350\pm 50^\circ\text{C}$ ; biotite =  $300\pm 50^\circ\text{C}$  (Dalrymple and Lanphere, 1969; Faure, 1986). Influence of factors on closure temperature is more fully investigated in Section 1.4.

The following subsections review the findings of these two previous workers in order to put their work into perspective in the current study.

#### 1.2.1 The Findings of Elias et al. (1988).

K-Ar ages were determined for 26 hornblendes, 17 coexisting muscovites and biotites, nine muscovites and nine biotites from the Dalradian rocks. A long, complex cooling history lasting for  $\sim 75\text{Ma}$  (from  $\sim 490\text{Ma}$  to  $\sim 415\text{Ma}$ ) was deduced from the measured mineral K-Ar ages. It was observed that there were discrepancies in the expected K-Ar ages of the hornblendes when plotted on a map of the Connemara area. These age variations were not correlated with chemical composition, grain sizes or topographic locations. However, there was an apparent irregular increase in age from hornblendes in the Dalradian metasediments toward the metagabbro-gneiss complex to the south. These authors postulated that the observed variable distribution of ages was due to syn- and post-metamorphic slides or faults which had moved slices of the Dalradian metasediments from different locations and depths and hence different cooling environments to be adjacent to each other at the present erosion surface.

Elias et al. (1988) deduced from comparison of  $^{40}\text{Ar}^*$  closure temperatures from hornblende, muscovite and biotite samples collected from the same sites that there had been rapid cooling from  $\sim 1000^\circ\text{C}$  to  $\sim 550^\circ\text{C}$  ( $\sim 30^\circ\text{C}/\text{Ma}$ ) from  $490\text{Ma}$  to  $480\text{Ma}$  (Arenig-Llanvirn) during the D3, peak metamorphic phase, followed by slower cooling until  $460\text{Ma}$  to  $455\text{Ma}$  (Caradoc) when renewed uplift occurred. Geographically widespread biotite K-Ar ages and Rb-Sr ages of  $440\pm 5\text{Ma}$  (end-Ordovician) are allocated to the major

Taconic event docking Connemara Dalradian rocks against the Ordovician strata of the South Mayo Trough. At this time, widespread bursts of more rapid uplift occurred, giving the tectonic distribution of ages observed.

Elias et al. (1988) recognised the need for a closer sampling strategy to more concisely evaluate the pattern of age distributions in relation to their proposed tectonically controlled model of radiometric age distributions from mineral species in Connemara.

However, the following work by Miller et al. (1991) observed a possible link between the reduction of K-Ar ages in hornblendes and muscovites by stable isotopic exchange mechanisms with a fluid below the conventionally accepted  $^{40}\text{Ar}^*$  closure temperatures for these minerals.

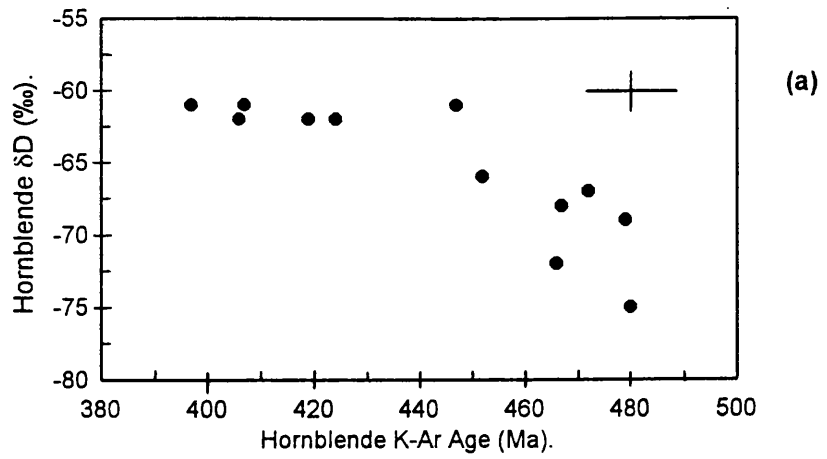
### 1.2.2 The Findings of Miller et al. (1991).

This work evaluated the importance of pervasive fluid flow throughout the Dalradian rocks and metagabbro suite in Connemara during the metamorphic phases and later with the emplacement of the Galway Granite plutons. Jenkin (1988) had recognised that two discrete palaeo-fluids had affected the Dalradian metasediments and metagabbro-gneiss complex: a high temperature magmatic influenced or derived fluid, ~480Ma and a lower temperature, ~275°C, meteoric fluid ( $\delta\text{D} = -25\text{‰}$ ,  $\delta^{18}\text{O} = +3\text{‰}$  to  $+7\text{‰}$ ). This lower temperature meteoric fluid was responsible for the widespread retrograde alteration observed throughout Connemara and was probably related to a convective circulation around the Galway Granite and its satellite plutons at ~400Ma.

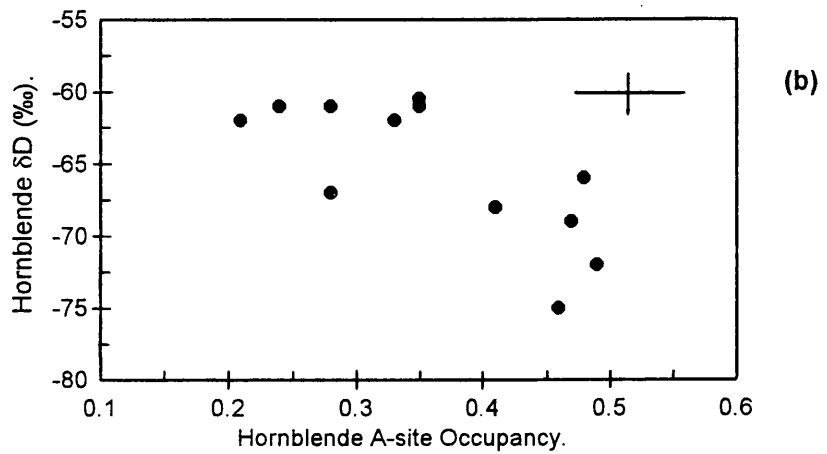
TEM work carried out by Miller et al. (1991) showed the presence of sub-microscopic phyllosilicate alteration along cleavage traces and imperfections in the hornblende samples. This phenomenon had previously been recognised by Onstott and Peacock (1987) in hornblendes derived from rocks in the central Adirondacks. It is believed that this type of alteration reduces the diffusion distance for  $^{40}\text{Ar}^*$  to travel and aids escape of  $^{40}\text{Ar}^*$  by producing conduits through the mineral structure.

Also, the effect of hydrogen stable isotope exchange displaces  $^{40}\text{Ar}^*$  from the A-site within hornblende due to the intrusion into the mineral structure of  $\text{H}^+$  as “ $\text{H}_3\text{O}^+$ ” in vacant

Miller et al. (1991).  
Dataset (12).  
 $R = -0.844; >99.9\%$ .



Miller et al. (1991).  
Dataset (12).  
 $R = -0.745; >99\%$ .



Miller et al. (1991).  
Dataset (12).  
 $R = 0.756; >99\%$ .

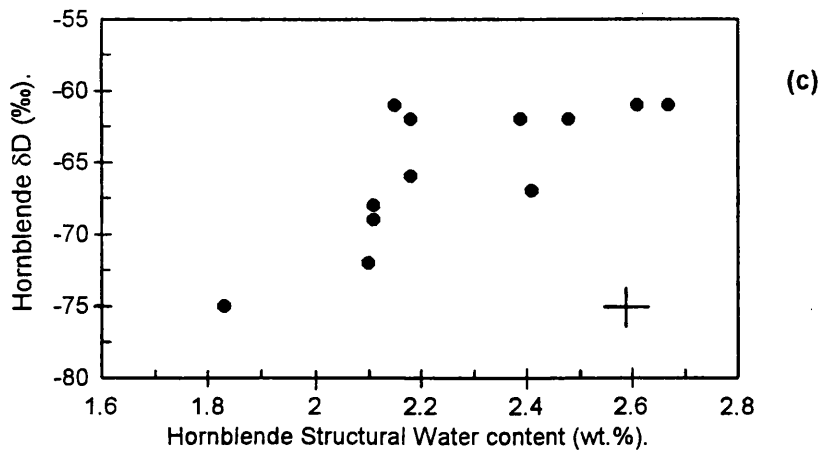


**FIGURE 1.4** Three diagrams representing the findings of Miller et al. (1991) showing: (a) Increase in hornblende  $\delta D$  as samples get younger; (b) increase in structural water content of hornblendes as  $\delta D$  increases; (c) Decrease in A-site occupancy (decrease in Na and K) as  $\delta D$  increases. All three diagrams from Miller et al. (1991). Average errors represented by the  $\text{—}+\text{—}$  symbol. Data in Appendix 12.

A-sites. Miller et al. (1991) observed the trends of: decreasing K-Ar age with increasing  $\delta D$  values; increasing  $\delta D$  values with increasing structural water content; decreasing A-site occupancy (by  $\text{Na}^+$  and  $\text{K}^+$ ) with increasing  $\delta D$  values in hornblendes (Figure 1.4). It was therefore postulated by these workers that the K-Ar ages of hornblende had been lowered by  $^{40}\text{Ar}^*$  loss due to the effect of the lower temperature fluid at  $\sim 275^\circ\text{C}$ , well below accepted  $^{40}\text{Ar}^*$  closure temperatures of  $490\text{-}550^\circ\text{C}$  in the literature (Harrison, 1981; Faure, 1986).

Work on the fluid characterisation has been further refined by O'Reilly et al. (1997) and Jenkin et al. (1997) and is discussed in Chapter 6 in this present study.

From the work of Miller et al. (1991) it is generally felt that chemical composition of the hornblendes is not related to the K-Ar ages or stable isotope values observed, although previous studies have shown correlations (O'Nions et al., 1969; Onstott and Peacock, 1987). Cosca and O'Nions (1994) have disputed the findings of compositional dependence of K-Ar ages from O'Nions et al. (1969). However, Dahl (1996) has shown that the K-Ar ages and composition correlations are related to the ionic porosity,  $Z$ , derived from the hornblende composition. These concepts are more fully discussed in Chapter 6 in relation to this current study.

### 1.3 Composition and Structure of Hornblende.

The amphibole group of minerals occur in a diverse range of igneous and metamorphic rocks and over a wide range of pressure and temperature environments. They crystallise in a large variety of regionally metamorphosed rocks from the greenschist to lower granulite facies. The essential feature of the structures of all the amphiboles is the presence of  $(\text{Si},\text{Al})\text{O}_4$  tetrahedra linked to form double chains which have the composition  $(\text{Si}_4\text{O}_{11})_n$ . Figure 1.5 shows the structure of a monoclinic amphibole down the  $a$ -axis and Figure 1.6 demonstrates the reason for the typical  $124^\circ\text{-}56^\circ$  distinguishing cleavage seen in basal sections of amphiboles. These double chains repeat along their length at intervals of approximately  $5.3\text{\AA}$ , which defines the  $c$ -axis of the unit cell. These silica chains are flanked

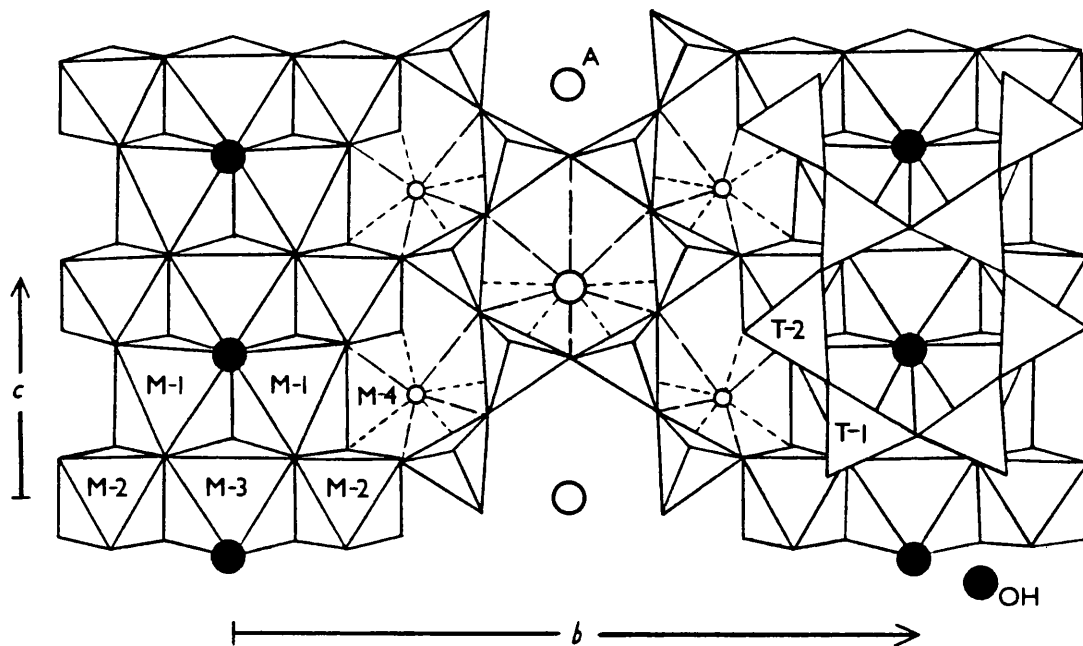


**FIGURE 1.5** Crystal structure of a monoclinic ( $C2/m$ ) amphibole projected down the  $a$ -axis. (OH) groups are located in the centre of the large holes of the rings in the  $Si_4O_{11}$  chains. M1-, M2- and M3- sites house Y-cations and are 6 coordinated. M4-sites house larger X-cations (Ca occurs in this site only, except cannilloite) in 6 to 8 coordination. A-sites house cations in 10 to 12 coordination (K occurs in this site only). Diagram from Klein and Hurlbut (1985).

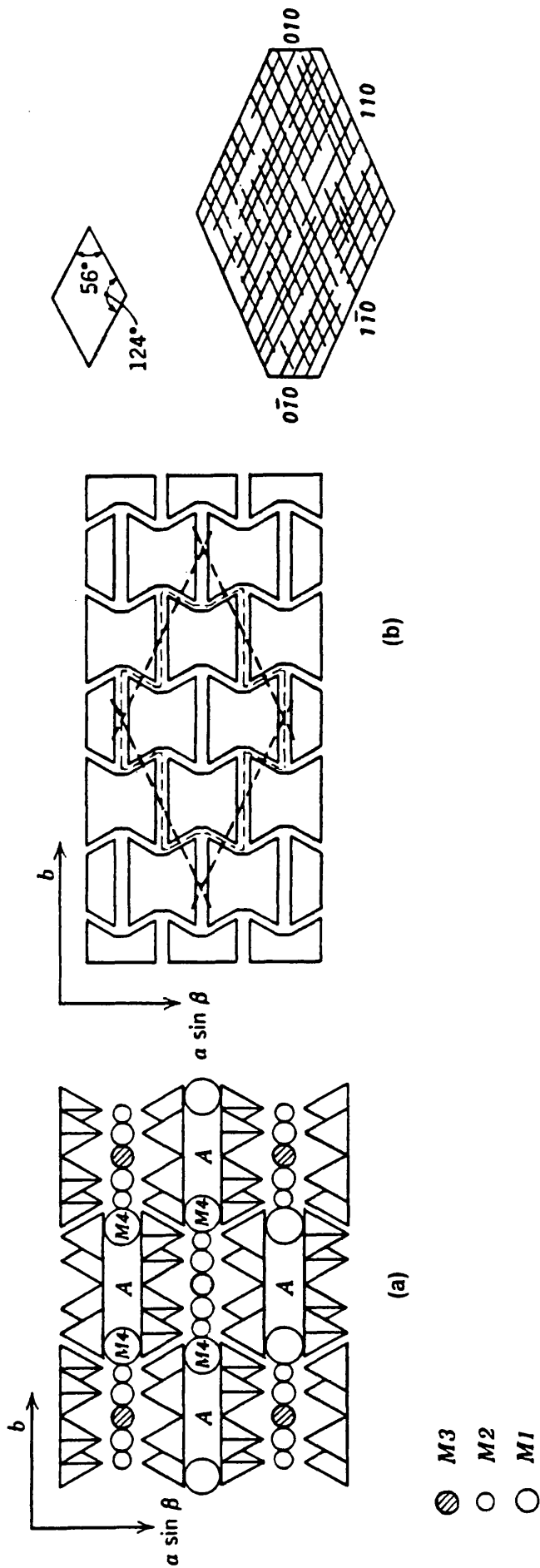


**FIGURE 1.6** (a) Schematic projection of the monoclinic amphibole structure on a plane perpendicular to the  $c$ -axis. (b) Control of cleavage angles by tetrahedral-octahedral-tetrahedral strips in the amphibole structure in comparison to naturally occurring cleavage angles. Diagram from Klein and Hurlbut (1985).

by cations in octahedral sites and OH<sup>-</sup> groups are present in amphiboles. Most of the amphiboles are monoclinic, determined by the positions of the cations in relation to the double chain structure.

The chemical composition of members of the amphibole group can be expressed by the following general formula:



Where W represents Na and K in the A-site; X represents Ca<sup>2+</sup>, Na<sup>+</sup>, Mn<sup>2+</sup>, Fe<sup>2+</sup>, Mg<sup>2+</sup> and Li<sup>+</sup> in the M4-sites; Y represents Mn<sup>2+</sup>, Fe<sup>2+</sup>, Mg<sup>2+</sup>, Fe<sup>3+</sup>, Al<sup>3+</sup> and Ti<sup>4+</sup> in the M1-, M2-, and M3-sites; Z represents Si<sup>4+</sup> and Al<sup>3+</sup> in tetrahedral sites. Complete ionic substitution can take place between Na and Ca and also between Fe<sup>2+</sup>, Mg<sup>2+</sup> and Mn<sup>2+</sup>. There is limited substitution between Fe<sup>3+</sup> and Al<sup>3+</sup> and between Ti<sup>4+</sup> and other Y-type cations and partial substitution of Al<sup>3+</sup> for Si<sup>4+</sup> in the tetrahedral sites of the double chains. Partial substitution of F<sup>-</sup> and O<sup>2-</sup> for (OH<sup>-</sup>) in the hydroxyl sites is also common.

The hornblendes are calcic amphiboles and can have a normal maximum of only two Ca per formula unit because the Ca normally resides in the M4-sites, of which only two are available in the total of seven M-sites (X+Y = 7). However, cannilloite has Ca in the A-site as well as M4-sites (Leake et al., 1997).

The relative positions of these cations are shown in Figures 1.5 and 1.6. The A-site has 10-12 coordination and can house Na and is the only site possible in which any K can reside. The M4-site houses X-type cations, Ca can only be present here. M1-, M2-, M3-sites house Y-type cations and form octahedral bands parallel to the *c*-axis. The M1-sites and M3-site are co-ordinated by four oxygens and two (OH<sup>-</sup>)/F<sup>-</sup>. M2-sites are co-ordinated by six oxygens. Figure 1.6 shows the structure of hornblende looking down the *c*-axis, giving the typical 124°-56° cleavage intersection of basal hornblende sections seen under the microscope.

Due to the presence of K in the A-sites in hornblende and the ability of this mineral species to retain <sup>40</sup>Ar\* generated from the <sup>40</sup>K by radioactive decay, this makes hornblende

an ideal mineral for dating cooling ( $^{40}\text{Ar}^*$  closure temperatures) by the very well established K-Ar dating technique (Dalrymple and Lanphere, 1969; Faure, 1986). In the Dalradian sequences and metagabbro-gneiss complex of Connemara, amphibolites and metamorphosed basic igneous intrusions are widespread (Sections 1.1 and 1.2).

The very wide range of possible calcic amphibole compositions (Leake et al., 1997) is illustrated in Figure 1.7 (accompanied by Table 1.1).

calcic amphiboles

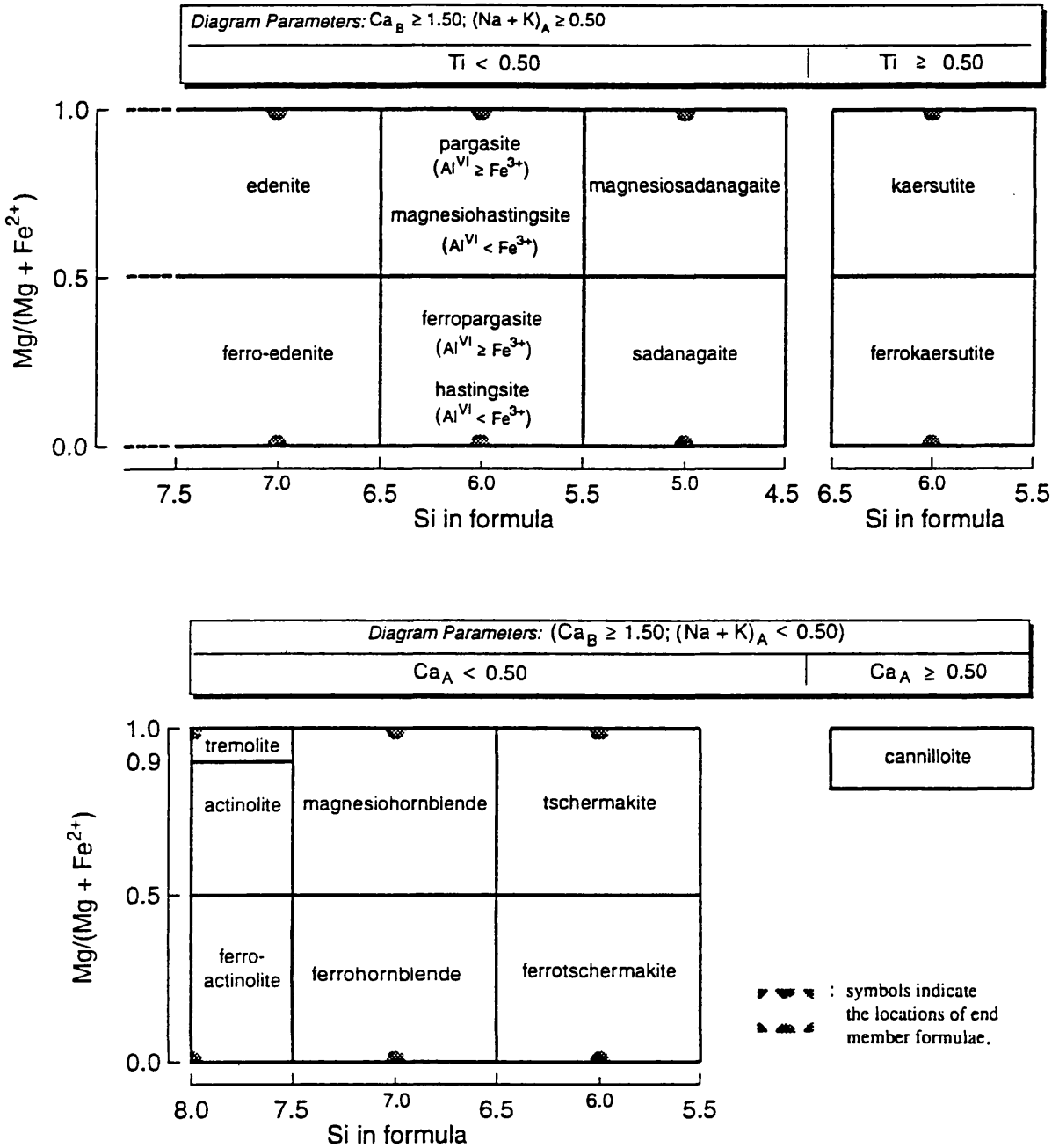


FIGURE 1.7 Classification diagram of the calcic amphiboles. Table 1.1 gives the end-member mineral formulae as shown on the diagram. From Leake et al. (1997).

### Calcic Amphiboles.

tremolite	□ Ca <sub>2</sub> Mg <sub>5</sub> Si <sub>8</sub> O <sub>22</sub> (OH) <sub>2</sub>
ferro-actinolite	□ Ca <sub>2</sub> Fe <sup>2+</sup> <sub>5</sub> Si <sub>8</sub> O <sub>22</sub> (OH) <sub>2</sub>
edenite	Na Ca <sub>2</sub> Mg <sub>5</sub> Si <sub>7</sub> Al O <sub>22</sub> (OH) <sub>2</sub>
ferro-edenite	Na Ca <sub>2</sub> Fe <sup>2+</sup> <sub>5</sub> Si <sub>7</sub> Al O <sub>22</sub> (OH) <sub>2</sub>
pargasite	Na Ca <sub>2</sub> (Mg <sub>4</sub> Al) Si <sub>6</sub> Al <sub>2</sub> O <sub>22</sub> (OH) <sub>2</sub>
ferropargasite	Na Ca <sub>2</sub> (Fe <sup>2+</sup> <sub>4</sub> Al) Si <sub>6</sub> Al <sub>2</sub> O <sub>22</sub> (OH) <sub>2</sub>
magnesiohastingsite	Na Ca <sub>2</sub> (Mg <sub>4</sub> Fe <sup>3+</sup> ) Si <sub>6</sub> Al <sub>2</sub> O <sub>22</sub> (OH) <sub>2</sub>
hastingsite	Na Ca <sub>2</sub> (Fe <sup>2+</sup> <sub>4</sub> Fe <sup>3+</sup> ) Si <sub>6</sub> Al <sub>2</sub> O <sub>22</sub> (OH) <sub>2</sub>
tschermakite	□ Ca <sub>2</sub> (Mg <sub>3</sub> AlFe <sup>3+</sup> ) Si <sub>6</sub> Al <sub>2</sub> O <sub>22</sub> (OH) <sub>2</sub>
ferrotschermakite	□ Ca <sub>2</sub> (Fe <sup>2+</sup> <sub>3</sub> AlFe <sup>3+</sup> ) Si <sub>6</sub> Al <sub>2</sub> O <sub>22</sub> (OH) <sub>2</sub>
magnesiosadanagaite	Na Ca <sub>2</sub> (Mg <sub>3</sub> (Fe <sup>3+</sup> , Al) <sub>2</sub> ) Si <sub>5</sub> Al <sub>3</sub> O <sub>22</sub> (OH) <sub>2</sub>
sadanagaite	Na Ca <sub>2</sub> (Fe <sup>2+</sup> <sub>3</sub> (Fe <sup>3+</sup> , Al) <sub>2</sub> ) Si <sub>5</sub> Al <sub>3</sub> O <sub>22</sub> (OH) <sub>2</sub>
magnesiohornblende	□ Ca <sub>2</sub> (Mg <sub>4</sub> (Al, Fe <sup>3+</sup> )) Si <sub>7</sub> Al O <sub>22</sub> (OH) <sub>2</sub>
ferrohornblende	□ Ca <sub>2</sub> (Fe <sup>2+</sup> <sub>4</sub> (Al, Fe <sup>3+</sup> )) Si <sub>7</sub> Al O <sub>22</sub> (OH) <sub>2</sub>
kaersutite	Na Ca <sub>2</sub> (Mg <sub>4</sub> Ti) Si <sub>6</sub> Al <sub>2</sub> O <sub>23</sub> (OH)
ferrokaersutite	Na Ca <sub>2</sub> (Fe <sup>2+</sup> <sub>4</sub> Ti) Si <sub>6</sub> Al <sub>2</sub> O <sub>23</sub> (OH)
cannilloite	Ca Ca <sub>2</sub> (Mg <sub>4</sub> Al) Si <sub>5</sub> Al <sub>3</sub> O <sub>22</sub> (OH) <sub>2</sub>

**TABLE 1.1** Names and formulae of calcic amphibole end-members as shown in Figure 1.7 from Leake et al. (1997). □ represents empty A-site.

## 1.4 Diffusivity in Hornblende.

### 1.4.1 Closure Temperatures in Amphiboles and Micas.

The K-Ar technique of radiometric dating is well documented in the literature. For the dating of metamorphic rocks, hornblende, muscovite and biotite are the most useful mineral species. They are common, contain measurable amounts of K and are retentive of  $^{40}\text{Ar}^*$  (radiogenic argon). The ages measured by the K-Ar dating technique represent times at which the mineral concerned cooled below its  $^{40}\text{Ar}^*$  diffusion closure temperature ( $T_c$ ). The  $T_c$  is specific for each mineral group and is defined by the following equation (Dodson, 1973):

$$E/RT_c = \ln[ART_c^2D_0 / a^2E(dT/dt)] \quad \text{Equation 1.1}$$

Where: E is the activation energy; R is the real gas constant;  $T_c$  is the closure temperature; A is a numerical constant describing the diffusion geometry;  $D_0$  is the diffusion coefficient; “a” is the characteristic diffusion radius;  $dT/dt$  is the cooling rate. The implication of this equation is that  $T_c$  is not only mineral specific but also related to the cooling rate experienced and the diffusion radii, “a”, of the observed structural components (e.g. cleavage) imposed on the mineral under investigation. Simple calculation of the  $T_c$  is difficult because the activation energy and diffusion coefficient have to be experimentally measured for each mineral species. Also, because of the great range of compositions possible within the hornblende group, this leads to a range of  $T_c$  rather than absolute values.

Harrison (1981) determined activation energies and diffusion coefficients for hornblende and applied the equation of Dodson (1973) to obtain closure temperatures of 578°C to 490°C for cooling rates of 500°C/Ma to 5°C/Ma. Harrison et al. (1985) similarly determined  $T_c$  for biotite to be 345°C for 100°C/Ma, 310°C for 10°C/Ma and 280°C for 1°C/Ma. However, the determination of “a” is quite uncertain so that  $T_c$  is poorly constrained. Is the diffusion radius the grain size of the hornblende, the cleavage spacing, the spacing between submicroscopic exsolutions or phyllosilicate alteration observed using

TEM (Onstott and Peacock, 1987; Miller et al., 1991)? Most of the values for hornblende  $T_c$  assume spherical geometry for  $^{40}\text{Ar}^*$  diffusion and observed mineral grainsize for the diffusion radius, “ $a$ ”, but clearly such a choice is largely arbitrary.

Other factors also affect activation energy and therefore closure temperature of hornblendes. Gerling et al. (1965) found that the Fe/Mg ratio controlled the activation energy for the loss of  $^{40}\text{Ar}^*$  from hornblende. O’Nions et al. (1969) showed an apparent compositional dependence on hornblende K-Ar ages from a high-grade, slowly cooled metamorphic terrain in South Norway. They found that the oldest ages were derived from hornblendes in which the “Y” sites were occupied with small positive cations,  $\text{Mg}^{2+}$  (0.66Å), and the youngest ages from hornblendes richer in  $\text{Fe}^{2+}$  (0.74Å) in the “Y” sites (ionic radii from Klein and Hurlbut, 1977). Berry and McDougall (1986) determined K-Ar ages and  $^{40}\text{Ar}$ - $^{39}\text{Ar}$  ages on amphiboles from Aileu, East Timor and found that at low grades of retrogressive metamorphism, Mg-rich hornblendes retained appreciable  $^{40}\text{Ar}^*$ , while Fe-rich hornblendes lost most of their accumulated  $^{40}\text{Ar}^*$  even at upper greenschist facies.

Also, Dahl (1996) showed that there was a relationship between  $^{40}\text{Ar}^*$  retentivity, composition and ionic porosity,  $Z$ , within calcic amphiboles. These compositional controls are described in more detail in context to the work of this thesis in Chapter 6.2.

Another potentially important effect on the  $^{40}\text{Ar}^*$  closure temperatures of minerals is from their microstructures and sub-microscopic impurities.

The effect of cummingtonite exsolution in hornblende was observed by Harrison and FitzGerald (1986) by TEM study and  $^{40}\text{Ar}$ - $^{39}\text{Ar}$  dating. They found that hornblende containing ~2.5% cummingtonite exsolution lamellae (<4µm wide) had a lower closure age than a biotite from the same sample location; 345Ma for biotite, 259Ma for hornblende. They concluded that the cummingtonite and hornblende had different  $^{40}\text{Ar}^*$  retentivities and that the creation of the exsolution lamellae allowed the channelled loss of  $^{40}\text{Ar}^*$ . The presence of areas of variable  $^{40}\text{Ar}^*$  retentivity within single hornblende crystals was observed by Kelley and Turner (1987) by laser microprobe  $^{40}\text{Ar}$ - $^{39}\text{Ar}$  investigation.

Several workers have observed the effect of mineral inclusions within amphiboles. Onstott and Peacock (1987) by TEM investigation found zones of phyllosilicate alteration

(<2 $\mu$ m wide) within hornblendes. These phyllosilicates were suspected to allow channelled  $^{40}\text{Ar}^*$  escape thus effectively reducing diffusion radius, “ $a$ ”, of the hornblende into smaller domains rather than the whole crystal and therefore effectively reducing the  $^{40}\text{Ar}^*$  closure temperature.

Twin planes are not thought to provide a significant  $^{40}\text{Ar}^*$  escape route in hornblendes as  $^{40}\text{Ar}$ - $^{39}\text{Ar}$  and TEM studies on feldspars by Parsons et al. (1988) concluded that feldspar twin boundaries are coherent and do not provide escape channels for  $^{40}\text{Ar}^*$ . If this is analogous for hornblendes with lower density of twinning then twinning does not contribute to the reduction of  $^{40}\text{Ar}^*$  closure temperature and also, the smaller “ $a$ ” diffusion domains created by phyllosilicate alterations would have a greater effect due to the smaller diffusion distances in relation to the usual scale of twinning observed in hornblendes.

The microstructure of amphiboles may also contain variable architecture of the silica tetrahedral sheets; the biopyribole effect (Velben, 1977; Klein and Hurlbut, 1984). These biopyriboles contain areas of linked tetrahedral silica sheets, (from *biotite*: mica), double chains as in amphibole and single chains as in pyroxene. The presence of biopyriboles would obviously influence the  $^{40}\text{Ar}^*$  closure temperature and network of  $^{40}\text{Ar}^*$  escape routes through the mineral.

Chemical weathering and alteration of hornblende to chlorite can allow  $^{40}\text{Ar}^*$  escape. Also, mechanical breakdown, radiation damage and excessive grinding during preparation of mineral separates may cause  $^{40}\text{Ar}^*$  loss (Faure, 1986).

The occurrence of excess Ar in minerals is well known (Dalrymple and Lanphere, 1969; Faure, 1986). This has the effect of increasing K-Ar dates, giving older than expected ages and is more pronounced in minerals containing relatively low amounts of K, such as hornblende. Excess Ar can occur due to exposure to high partial pressure of argon during regional metamorphism (Faure, 1986).

#### 1.4.2 Diffusion Mechanisms in Minerals.

Fluid diffusion through rock occurs by volume diffusion through regions of homogeneous crystals and by movement along paths of least resistance such as faults and dislocations and mineral grain boundaries on the smaller scale.

I. Exchange Mechanism. Neighbouring atoms change places with each other, no crystal defect is required. This mechanism has a large activation energy.

II. Interstitial Mechanism. Interstitial atoms which are smaller than the surrounding atoms can move between interstitial sites without disruption of the mineral lattice.

III. Vacancy Mechanism. Point vacancy defects in the mineral crystal lattice can be filled by a neighbouring atom by movement across into this site. This then generates another vacant site, previously occupied, available to be filled by a neighbouring atom. Thus progress through the crystal lattice can be achieved.

It was proposed by Miller et al. (1991) that the vacancy mechanism of diffusion and the presence of phyllosilicate alteration in the microstructures of the observed hornblendes aided the intrusion of OH<sup>-</sup> and expulsion of <sup>40</sup>Ar\* by a later sub-closure temperature fluid, increasing the δD values, giving excess H<sub>2</sub>O contents and lowering the measured K-Ar ages.

## CHAPTER 2.

### AIMS.

The immediate aims of this work were to investigate the findings of Miller et al. (1991) on a larger number of samples to confirm whether or not the correlations of increasing  $\delta D$  with decreasing K-Ar age, increasing excess  $H_2O$  content with decreasing age and other evidence for the proposed expulsion of  $^{40}Ar^*$  by  $OH^-$  invasion into hornblendes and micas was reproducible.

The work of Elias et al. (1988) and Miller et al. (1991) concentrated on samples collected mostly from the south of the Dalradian metasedimentary complex. This present work therefore concentrated on hornblende-bearing and mica-bearing rocks from the northern part of the Dalradian inlier, closer to the unconformably overlying Silurian sediments and volcanics. The purpose of this was to investigate whether, using stable isotope evidence, there was any link between circulated fluid and fluid derived from this deeply buried sedimentary pile. The ultimate aim of the research was to explain satisfactorily the reasons for the spread of K-Ar ages over nearly 100Ma in Connemara, with the probability that any such explanation(s) would have some relevance in other areas.

The hornblende compositions were estimated only by limited EMPA measurements on mineral separates by both Elias (1985) and Miller (1990). In view of the correlations of composition with  $^{40}Ar$ - $^{39}Ar$  age of hornblendes investigated by Onstott and Peacock (1987) a more detailed investigation of the minerals studied was also required.

It was hoped that ~30 samples of hornblende and ~30 samples of muscovite would be studied in this work. However, due to constraints on time and availability of K-Ar,  $\delta D$  and  $\delta^{18}O$  extraction and measuring equipment it was decided to concentrate the study on deciphering the complexities of the hornblende age, stable isotope and composition interactions (31 hornblende samples). The results from the five muscovite samples are listed in this thesis, but it is considered that this is too small a number from which to realistically derive observations of correlation. The mineral samples which yielded hornblendes and five

which gave muscovites were to be examined for K-Ar age,  $\delta D$  value,  $\delta^{18}O$  value, rock XRF composition, mineral separate wet chemical analysis and EMPA of mineral grains in polished sections to evaluate variations of composition and age within samples.

## CHAPTER. 3.

### SAMPLE COLLECTION AND PREPARATION.

#### 3.1 Sample Collection.

Rock samples of ~1kg were collected from the Dalradian inlier, MGS and Silurian outcrops of Connemara in County Galway, Western Ireland (Figure 3.1). A total of 68 rock samples were taken from a widespread area to give representative K-Ar ages and stable isotope values for the hornblende-bearing rocks. Some muscovite-bearing rocks were also collected.

Amphibolites and other metamorphosed basic igneous rocks (metagabbro, ultrabasic gabbro) were collected for hornblende mineral separation to derive K-Ar ages and stable isotope values. A small selection of pelites, semi-pelites and other mica bearing rocks were also collected to obtain corresponding K-Ar ages and stable isotope values from muscovite mineral separates. Rock samples were taken as unaltered as possible and weathered material on surfaces chipped away as much as possible in the field.

Table 3.1 gives the identification number, grid reference location, stratigraphic rock unit, metamorphic zone (where applicable) and the rock type of each collected sample. The grain size given is an estimate from observation of the rock sample hand specimen. Figure 3.1 is a sketch map of Connemara showing the locations of all samples collected, although not all samples were used. Full location details and sample descriptions are given in Appendix 1.

##### 3.1.1 Dalradian Supergroup.

The largest proportion of samples collected were from the Dalradian Supergroup. These were mostly amphibolites of various types (Table 3.1) and some mica bearing pelites, semi-pelites and psammities (Chapter 1). The sample collection was concentrated in the north of the Dalradian Supergroup, towards the unconformity of the Silurian sediments and

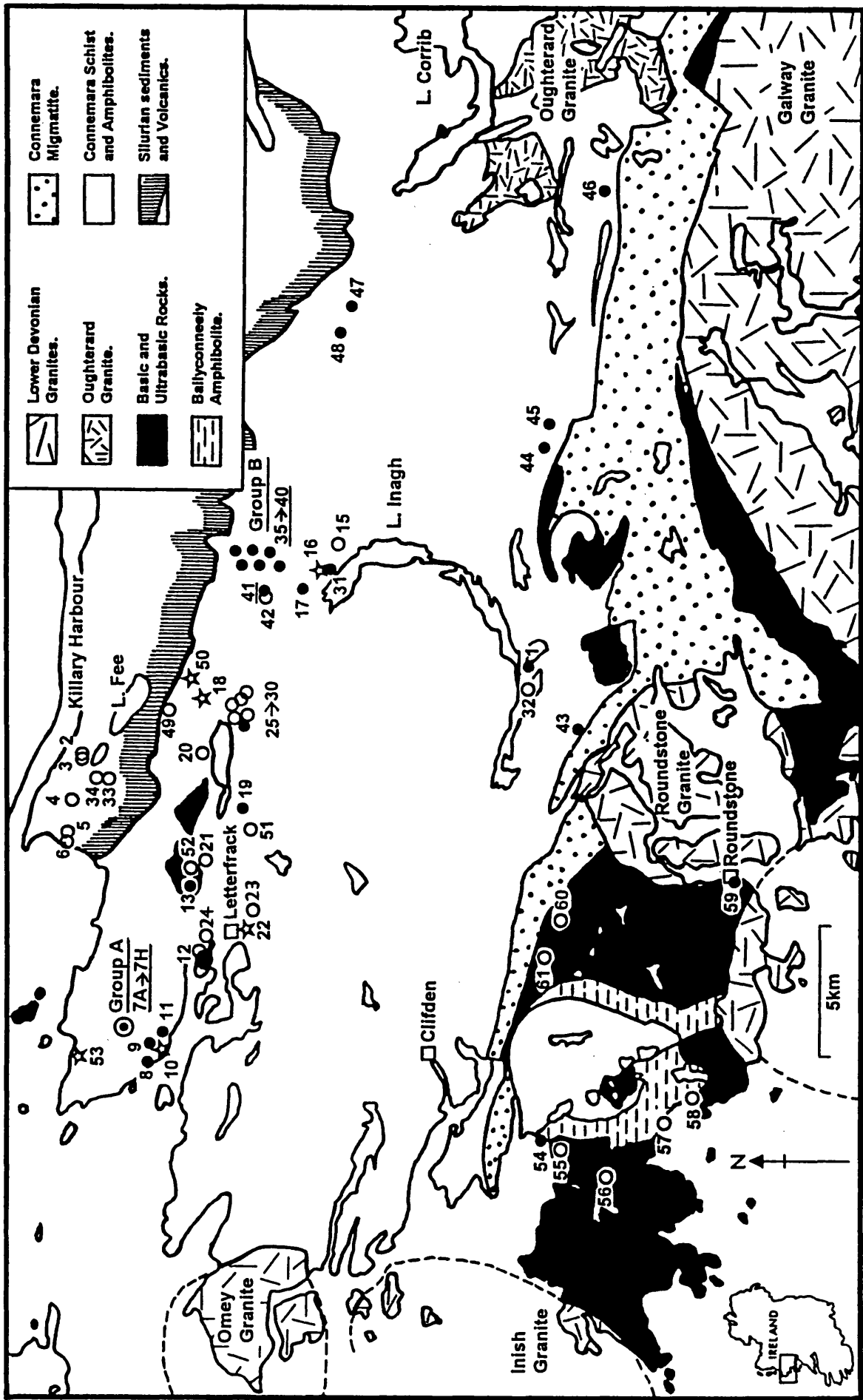


FIGURE 3.1 Map of Connemara showing sample locations. Filled circles represent hornblendes and open stars represent muscovites which were successfully separated and analysed in this study. Group-A is identified by a concentric circle symbol. Group-B is a locally clustered group of 7 samples. Open circles indicate samples collected but not used.

Sample Name.	Location. (Grid Ref.).	Stratigraphic Rock Unit.	Rock Type.	Metamorphic Zone.	Grainsize. (mm).
TJ-1	821467	Streamstown Formation.	Amphibolite (lineated).	migmatite	Fine - med. (0.5-1.5)
TJ-2	771630	Lough Muck Formation.	Mudstone (massive).	Silurian sedimentary.	Fine (<0.5)
TJ-3	824608	Lough Muck Formation.	Mudstone (massive).	Silurian sedimentary.	Very fine (<0.2)
TJ-4	752636	Lough Muck Formation.	Mudstone (massive).	Silurian sedimentary.	Very fine (<0.1)
TJ-5	744634	Lough Muck Formation.	Diorite (granular).	Silurian volcanic.	Medium (1-3)
TJ-6	740635	Lough Muck Formation.	Diorite (granular).	Silurian volcanic.	Fine - med. (0.5-3)
TJ-7A	672619	Kylemore Formation.	Amphibolite (poor lineation).	staurolite	Fine (0.2-0.8)
TJ-7B	672619	Kylemore Formation.	Amphibolite (mild lineation).	staurolite	Fine - med. (0.5-1.5)
TJ-7C	672619	Kylemore Formation.	Amphibolite (mild foliation).	staurolite	Fine - med. (0.2-1)
TJ-7D	672619	Kylemore Formation.	Amphibolite (lineated).	staurolite	Fine - med. (0.5-2)
TJ-7E	672619	Kylemore Formation.	Amphibolite (mild foliation).	staurolite	Fine - med. (0.5-2)
TJ-7F	672619	Kylemore Formation.	Amphibolite (mild foliation).	staurolite	Fine - med. (0.5-1.5)
TJ-7G	672619	Kylemore Formation.	Amphibolite (mild foliation).	staurolite	Fine - med. (0.5-1.5)

**TABLE 3.1** General descriptions and locations of rock samples collected in Connemara. Samples used for K-Ar age dating and stable isotope analysis are shown as filled circles on the map in Figure 3.1. Samples not used are shown as open circles. Full location information and hand specimen descriptions are in Appendix 1.

<b>Sample Name.</b>	<b>Location. (Grid Ref.).</b>	<b>Stratigraphic Rock Unit.</b>	<b>Rock Type.</b>	<b>Metamorphic Zone.</b>	<b>Grainsize. (mm).</b>
TJ-7H	672619	Kylemore Formation.	Amphibolite (mild foliation).	staurolite	Fine - med. (0.5-1.5)
TJ-8	660607	Lakes Marble Formation.	Amphibolite (mild foliation).	staurolite	Fine - med. (0.2-2)
TJ-9	665605	Lakes Marble Formation.	Amphibolite (foliated).	staurolite	Fine - med. (0.2-2)
TJ-10	667604	Lakes Marble Formation.	Mica schist (foliated).	staurolite	Fine - med. (0.2-3)
TJ-11	669604	Lakes Marble Formation.	Amphibolite (very foliated).	staurolite	Fine - med. (0.2-2)
TJ-12	697592	Dawros More Basic Rock.	Gabbro (granular).	staurolite	Fine - med. (0.2-2)
TJ-13	722593	Currywongaun Gabbro.	Gabbro (granular).	staurolite	Fine - med. (0.2-1)
TJ-15	841546	Ballynakill Formation.	Mica schist (foliated).	sillimanite - muscovite	Fine - med. (0.2-2)
TJ-16	836547	Ballynakill Formation.	Psammitic schist (foliated).	sillimanite - muscovite	Fine - med. (0.2-1)
TJ-17	832548	Lakes Marble Formation.	Amphibolite (massive).	sillimanite - muscovite	Fine (0.2-0.8)
TJ-18	791589	Kylemoremore Formation.	Psammitic schist (foliated).	staurolite	Fine - med. (0.2-1)
TJ-19	751580	Lakes Marble Formation.	Amphibolite (mild foliation).	staurolite	Fine - med. (0.2-1.5)
TJ-20	777587	Kylemore Formation.	Semi-pelite (massive).	staurolite	Fine (0.2-0.6)
TJ-21	728590	Lakes Marble Formation.	Semi-pelite (massive).	staurolite	Fine (0.2-0.6)
TJ-22	708575	Lakes Marble Formation.	Mica schist (foliated).	staurolite	Fine - med. (0.2-1)

**TABLE 3.1** Continued.

<b>Sample Name.</b>	<b>Location. (Grid Ref.).</b>	<b>Stratigraphic Rock Unit.</b>	<b>Rock Type.</b>	<b>Metamorphic Zone.</b>	<b>Grainsize. (mm).</b>
TJ-23	712574	Streamstown Formation.	Semi-pelite (massive).	staurolite	Fine (0.2-0.8)
TJ-24	700585	Lakes Marble Formation.	Semi-pelite (massive).	staurolite	Fine (0.2-0.8)
TJ-25	791575	Lakes Marble Formation.	Amphibolite (massive).	staurolite	Fine - med. (0.2-1)
TJ-26	789576	Lakes Marble Formation.	Amphibolite (foliated).	staurolite	Fine (0.2-0.8)
TJ-27	787577	Lakes Marble Formation.	Amphibolite (foliated).	staurolite	Fine (0.2-0.8)
TJ-28	785575	Lakes Marble Formation.	Amphibolite (massive).	staurolite	Fine - med. (0.2-1)
TJ-29	782574	Lakes Marble Formation.	Amphibolite (massive).	staurolite	Fine - med. (0.2-1)
TJ-30	783576	Lakes Marble Formation.	Amphibolite (massive).	staurolite	Fine (0.2-0.8)
TJ-31	835547	Lakes Marble Formation.	Amphibolite (massive).	sillimanite - muscovite	Fine - med. (0.2-1)
TJ-32	820467	Streamstown Formation.	Amphibolite (banded).	migmatite	Fine - med. (0.6-1)
TJ-33	768618	Lough Muck Formation.	Diorite (granular).	Silurian volcanic.	Medium (1-2)
TJ-34	770620	Lough Muck Formation.	Diorite (granular).	Silurian volcanic.	Medium (1-3)
TJ-35	838569	Lakes Marble Formation.	Amphibolite (very foliated).	staurolite	Fine - med. (0.2-2)
TJ-36	839570	Lakes Marble Formation.	Amphibolite (foliated).	staurolite	Fine - med. (0.5-2)
TJ-37	839571	Lakes Marble Formation.	Amphibolite (poor foliation).	staurolite	Fine - med. (0.5-1.5)

**TABLE 3.1** Continued.

Sample Name.	Location. (Grid Ref.).	Stratigraphic Rock Unit.	Rock Type.	Metamorphic Zone.	Grainsize. (mm).
TJ-38	838573	Lakes Marble Formation.	Amphibolite (mild foliation).	staurolite	Fine - med. (0.5-1.5)
TJ-39	839575	Lakes Marble Formation.	Amphibolite (massive).	staurolite	Fine - med. (0.2-1)
TJ-40	835566	Lakes Marble Formation.	Amphibolite (very foliated).	staurolite	Fine - med. (0.2-1.5)
TJ-41	820572	Lakes Marble Formation.	Amphibolite (massive).	staurolite	Fine - med. (0.5-1.5)
TJ-42	820572	Lakes Marble Formation.	Amphibolite (massive).	staurolite	Fine - med. (0.5-1.5)
TJ-43	783465	Lakes Marble Formation.	Amphibolite (poor foliation).	migmatite	Fine - med. (0.2-1)
TJ-44	887467	Lakes Marble Formation.	Amphibolite (massive).	migmatite	Fine - med. (0.5-1.5)
TJ-45	891465	Lakes Marble Formation.	Amphibolite (mild foliation).	migmatite	Fine - med. (0.5-1.5)
TJ-46	974449	Lakes Marble Formation.	Amphibolite (banded).	migmatite	Medium (1-2)
TJ-47	942530	Lakes Marble Formation.	Amphibolite (massive).	sillimanite - muscovite	Fine - med. (0.5-1)
TJ-48	933537	Lakes Marble Formation.	Amphibolite (poor foliation).	sillimanite - muscovite	Fine - med. (0.5-1)
TJ-49	792602	Ultrabasic Gabbro.	Serpentinite.	staurolite	Very fine (<0.2)
TJ-50	802599	Kylemore Formation.	Psammitic schist (very foliated).	staurolite	Medium (1-3)
TJ-51	747579	Lakes Marble Formation.	Amphibolite (massive).	staurolite	V. fine - med. (<0.2-1)
TJ-52	725593	Currywongaun Gabbro.	Gabbro (granular).	staurolite	Fine - med. (0.5-2)

TABLE 3.1 Continued.

Sample Name.	Location. (Grid Ref.).	Stratigraphic Rock Unit.	Rock Type.	Metamorphic Zone.	Grainsize. (mm).
TJ-53	664638	Kylemore Formation.	Pelite (mild foliation).	gamet	Fine - med. (0.5-1)
TJ-54	632466	Ballyconneely Amphibolite.	Amphibolite (massive).	greenschist	V. fine - fine. (<0.2-0.5)
TJ-55	630456	Metagabbro Gneiss Complex.	Metagabbro (granular).	greenschist	Medium (1-3)
TJ-56	618440	Metagabbro Gneiss Complex.	Metagabbro (granular).	MGS.	Fine - med. (0.5-2)
TJ-57	641423	Ballyconneely Amphibolite.	Amphibolite (massive).	greenschist	Very fine (<0.2)
TJ-58	648409	Ballyconneely Amphibolite.	Amphibolite (granular).	greenschist	Fine - med. (0.2-2)
TJ-59	721398	Metagabbro Gneiss Complex.	Amphibolite (massive).	MGS.	Fine (0.2-0.5)
TJ-60	710462	Metagabbro Gneiss Complex.	Metagabbro (granular).	MGS.	Fine - med. (0.5-1.5)
TJ-61	693469	Metagabbro Gneiss Complex.	Metagabbro (granular).	MGS.	Fine (0.2-0.5)

TABLE 3.1 Continued.

volcanic rocks because previous work by Elias et al. (1988) and Miller et al. (1991) concentrated on the south. As well as widespread samples collected to give a range of representative results within the study area, there were also three groups of samples collected to evaluate local differences.

**Group-A:** TJ-7A to TJ-7H. 8 amphibolite samples collected from a small roadside quarry north of Tully Mountain, mostly blocky with poor - mild foliation, dark grey - black. TJ-7A was adjacent to a quartz vein (10cm wide) and a smaller quartz vein (8-12mm wide) cut through TJ-7H, which displayed a contorted foliation fabric. There were observable dual grain sizes of amphiboles (~2mm hornblende grains set in a finer foliation fabric; Figure 3.2, Appendix 1 and 2). These 8 samples were collected a metre to a few metres apart from each other.

**Group-B:** TJ-35 to TJ-41. 7 amphibolite samples collected ~2km north of Lough Inagh, variously foliated, medium green colour. Observable dual grain sizes of amphiboles were also present (Appendix 1 and 2). These 7 samples were collected on a scale of tens of metres apart.

**Group-C:** TJ-8 to TJ-11. Three amphibolites and a mica schist (TJ-10) collected to the south of Tully Mountain, foliation more evident than **Group-A**, medium - dark green. Observable dual grain sizes of the amphiboles were also present (Appendix 1 and 2). These 4 samples were collected on a scale of a tens of metres apart.

Another group of six amphibolites (TJ-25 to TJ-30) was collected from the southwest of Kylemore Lough. However, due to difficulties in separating hornblende (Section 3.3) this group was not considered useful. Only TJ-29 successfully separated hornblende.

As well as the above groups, widespread selection of amphibolites (hundreds of metres to kilometres apart) occurred in the south of the Dalradian Supergroup. Also

collected were two samples of gabbro from Currywongaun (**TJ-13** and **TJ-52**), an ultrabasic gabbro just under the Silurian unconformity (**TJ-49**), several pelites, semi-pelites and psammites and other solitary amphibolites (Figure 3.1).

### 3.1.2 Silurian Rocks.

Several sedimentary rocks (**TJ-2** to **TJ-4**) were collected from the Silurian strata unconformably overlying the Dalradian Supergroup in case detrital hornblende could be studied. Also, four samples of diorite were collected from the Lough Muck Formation. Hornblende and biotite grains ~1-2mm long were observed in hand specimen. However, it was observed in electron microprobe section that they were too altered for use in this study.

### 3.1.3 Connemara Metagabbro Gneiss Complex.

Several samples of metagabbro and amphibolite (**TJ-55** to **TJ-61**) were collected from this complex on a scale of a few hundred metres to kilometres apart. It should be noted that **TJ-59** was collected within the thermal aureole of the Roundstone Granite and will therefore not be representative for the K-Ar ages of this study.

## **3.2 Sample Selection.**

Electron microprobe sections were prepared of samples which were estimated from hand specimen inspection (Appendix 1) to be good enough for possible mineral separation. This was done on the basis of large enough grainsize and lack of alteration. These sections are similar to thin sections except that they are polished with no top cover and the thickness tolerances are not as precise as a thin section (0.030mm). However for the purposes of mineral identification and petrological description they are quite adequate (Appendix 2).

Samples were selected to be mineral separated for isotope work after petrological microscope inspection of electron microprobe sections. Samples were chosen on the basis of grainsize (>0.5mm) and on how altered the amphibole or mica appeared to be.

Retrogressive hydrothermal alteration is known to occur in these rocks and evidence for this is widespread throughout the region (Yardley et al., 1987; Jenkin et al., 1992; Leake and Tanner, 1994). This retrogressive alteration takes the form of hornblende → chlorite, hornblende → epidote, biotite → chlorite, orthoclase and plagioclase → sericite and saussurite, cordierite → pinite and sillimanite → sericite (Jenkin et al., 1992). The presence of veins and sealed microcracks of quartz, chlorite and epidote in most of the samples records the effects of fluid movement through the region (Yardley, 1989).

### 3.2.1 Dalradian Supergroup.

All of the samples from **Groups-A, -B, and -C** were estimated to be suitable for mineral separation. Also, most of the samples collected in the south of the area were of use. However, it was found that the samples in the Dawros More area were too fine grained and too badly altered for use. **TJ-49** was, as suspected, serpentinised. **TJ-52** from Currywongaun had a strong igneous assemblage of altered plagioclase, orthopyroxene and clinopyroxene, mantled by hornblende and chlorite reaction rims.

Several of the mica bearing rocks were selected for muscovite separation. However, the biotite present was too chloritised to be useful for isotope work.

### 3.2.2 Silurian Rocks.

Unfortunately, none of the sediments collected were of a large enough grain size or contained enough, if any, detrital hornblende or biotite to be suitable for mineral separation.

Also, the four diorite samples were found on microscope examination to contain only highly chloritised hornblendes and biotites.

### 3.2.3 Connemara Metagabbro Gneiss Complex.

Only two samples (**TJ-54** and **TJ-59**) were found to be suitable for hornblende separation from this area. Most of the others were too altered, with a strong presence of chlorite and epidote after hornblende.

Tables 3.2 and 3.3 give a condensed overview of the samples from which hornblende and muscovite respectively were separated. Where two hornblendes are stated (2 hbl) on these tables this refers to the presence of relict or porphyroblast hornblendes (discordant inclusion trails suggest earlier D1 fabric) set in a usually finer D2 foliation fabric (Figure 3.2).

Figure 3.2 shows the typical appearance of relict hornblende grains, possibly from the D1 event (Chapter 1), found in most amphibolite samples in the north of the collection area. Figure 3.3 demonstrates variable zoning in a hornblende from **Group-A**, suggesting possible variable compositions in single grains (confirmed by EMPA; Chapters 5 and 6). Figure 3.4 shows the more uniform appearance of amphibolite samples collected in the south of the Dalradian inlier. Figure 3.5 displays biotite alteration of hornblende in cleavages, typically observed in samples from the south.

These figures show the differences between samples collected from the north limb and south limb of the Connemara Antiform:

North. Relict grains with discordant inclusion trails (D1) and zoning, set in a finer well defined foliation fabric (D2) from the metamorphism associated with the intrusion of the MGS (Chapter 1). This metamorphism was not of a high enough grade (staurolite zone; Table 3.1) to completely obliterate the previous amphibolite grade metamorphism.

South. Uniform grains only of hornblende and plagioclase are present. The MGS associated metamorphism reached a higher grade of metamorphism in the south completely obliterating the previous D1 fabric and recrystallised all hornblende. The fluid associated with widespread alteration in Connemara (~400Ma; Chapter 1) infiltrated hornblende grains along cleavages.

Sample Name.	Major Minerals Present.	Hornblende Grainsize in Section (mm).	Separated Hornblende Grainsize (µm).	Plagioclase Alteration Index (0 - 3).	Accessory Minerals Present.	Vein Minerals (vein width, mm).
TJ-1	hbl. qtz. plag.	0.2-1	90-180	1-2	Fe-Ti ox. ap. chl. bt.	qtz. chl. (0.2)
TJ-7A	2 hbl. qtz. plag.	~0.5 0.1-0.5	90-125	2	Fe-Ti ox. chl. sph. bt.	qtz. chl. (0.1)
TJ-7B	2 hbl. qtz. plag.	~0.5 0.1-0.5	90-125	2	Fe-Ti ox. py. chl. sph. bt.	qtz. chl. (0.1)
TJ-7D	2 hbl. qtz. plag.	~1 0.1-0.5	90-125	2	Fe-Ti ox. py. sph. chl. bt.	qtz. chl. py. (0.1)
TJ-7E	2 hbl. qtz. plag.	~1 0.1-0.5	90-125	2	Fe-Ti ox. sph. chl. bt.	qtz. chl. (0.1)
TJ-7F	2 hbl. qtz. plag.	~1 0.1-0.5	90-125	2	Fe-Ti ox. sph. chl. bt.	qtz. chl. (0.1)
TJ-7G	2 hbl. qtz. plag.	~1 0.1-0.5	90-125	2	Fe-Ti ox. sph. chl. bt.	qtz. chl. (0.1)
TJ-7H	2 hbl. qtz. plag.	~1 0.1-0.5	90-125	2	Fe-Ti ox. sph. chl. bt.	qtz. mus. sph. (2-4)
TJ-8	2 hbl. qtz. plag.	1-2 0.1-0.2	90-125	1	ap. sph. chl. Fe-Ti ox.	qtz. (0.1)
TJ-9	hbl. qtz. cum. plag.	0.5-1	63-125	2	ap. sph. chl. Fe-Ti ox. py.	qtz. (0.1)
TJ-11	2 hbl. qtz. plag.	0.2-0.5 0.05-0.1	90-125	1	Fe-Ti ox. sph.	qtz. (0.1-1)
TJ-13	hbl. plag.	0.2-0.5	100-180	3	Fe-Ti ox. py. sph.	-
TJ-17	hbl. qtz. plag.	0.05-0.2	90-125	0-1	Fe-Ti ox. py. sph. chl.	-
TJ-19	2 hbl. qtz. plag.	0.5-1 0.05-0.2	90-125	1	Fe-Ti ox. sph. chl.	qtz. (0.5)

**TABLE 3.2** Mineralogy of amphibolite samples selected for K-Ar age dating and stable isotope analysis. Key: hbl. = hornblende fabric; 2 hbl. = hornblende fabric and porphyroblasts; qtz. = quartz; plag. = plagioclase; Fe-Ti ox. = magnetite and ilmenite; sph. = sphene; chl. = chlorite; bt. = biotite; mus. = muscovite; epi. = epidote; cal. = calcite; cum. = cummingtonite; ap. = apatite; py. = pyrite. Full descriptions are in Appendix 2.

Sample Name.	Major Minerals Present.	Hornblende Grainsize in Section (mm).	Separated Hornblende Grainsize ( $\mu\text{m}$ ).	Plagioclase Alteration Index (0 - 3).	Accessory Minerals Present.	Vein Minerals (vein width, mm).
TJ-29	hbl. qtz. plag.	0.1-0.2	90-125	2	Fe-Ti ox. py. sph. chl.	qtz. epi. chl. ( $<0.1$ )
TJ-31	2 hbl. qtz. plag.	1-3 0.05-0.2	90-180	2	Fe-Ti ox. py. sph. chl. bt.	qtz. chl. (0.2-2)
TJ-35	2 hbl. qtz. plag.	1-3	63-125	2-3	Fe-ti ox. py. sph. chl. bt.	qtz. epi. (0.1)
TJ-36	2 hbl. qtz. plag.	2-4 0.05-0.1	63-100	2-3	Fe-Ti ox. sph. chl. bt.	-
TJ-37	2 hbl. qtz. plag.	2-3 0.1-0.2	63-100	1	Fe-Ti ox. sph. chl. bt.	-
TJ-38	2 hbl. qtz. plag.	2-4 0.05-0.2	63-125	1-2	Fe-Ti ox. sph. chl.	qtz. ( $<0.1$ )
TJ-39	hbl. qtz. plag.	0.05-0.2	100-125	2	Fe-Ti ox. sph.	-
TJ-40	2 hbl. qtz. plag.	1-3 0.05-0.1	100-125	2	cal. chl. ser. sph.	qtz. (~1)
TJ-41	hbl. qtz. plag.	0.2-0.5	100-125	2	sph. chl. bt.	qtz. epi. (0.1)
TJ-43	hbl. qtz. plag.	0.3-0.7	90-180	0-2	Fe-Ti ox. chl.	-
TJ-44	hbl. qtz. plag.	0.2-1	90-180	2-3	Fe-Ti ox. sph. chl.	qtz. (~1)
TJ-45	hbl. plag.	0.4-1	90-180	1-2	qtz. sph. ap. Fe-Ti ox. chl. bt.	qtz. ( $<0.1$ )
TJ-46	hbl. plag. qtz. Fe-Ti oxides	0.2-0.5	90-180	0-1	chl. bt. py.	-
TJ-47	hbl. plag. qtz.	0.1-0.4	90-180	2	Fe-Ti ox. py. sph. chl. bt.	chpy. epi. (0.5)
TJ-48	hbl. plag. Fe-Ti oxides	0.1-0.4	90-180	2-3	epi. qtz. sph. chl. bt.	qtz. (0.1)

TABLE 3.2 Continued.

Sample Name.	Major Minerals Present.	Hornblende Grainsize in Section (mm).	Separated Hornblende Grainsize ( $\mu$ m).	Plagioclase Alteration Index (0 - 3).	Accessory Minerals Present.	Vein Minerals (vein width, mm).
TJ-54	hbl. plag. qtz.	0.1-0.3	90-180	1	Fe-Ti ox. chl. bt.	epi. (<0.1)
TJ-59	hbl. plag. qtz.	0.2-0.4	90-125	1	Fe-Ti ox. sph. chl. bt.	qtz. (0.5)

TABLE 3.2 Continued.

Sample Name.	Major Minerals Present.	Muscovite Grainsize in Section (mm).	Separated Muscovite Grainsize ( $\mu$ m).	Plagioclase Alteration Index (0 - 3).	Accessory Minerals Present.	Vein minerals (vein width, mm).
TJ-10	qtz. mus. st. gt. bt. plag.	0.4-0.8	63-90	2	chl.	-
TJ-16	plag. qtz. mus. bt.	0.2-0.4	63-90	2	chl. zr. py.	-
TJ-18	plag. qtz. mus. chl.	0.2-0.4	90-125	1	Fe-Ti ox.	-
TJ-22	mus. qtz. plag. gt. bt.	0.5-3	90-125	1-2	Fe-Ti ox. chl. tour.	-
TJ-50	qtz. plag. mus. bt.	0.2-0.8	90-125	1-2	Fe-Ti ox. chl. Kfs.	-
TJ-53	qtz. mus. plag. gt. st. bt.	0.1-0.8	63-90	2	Fe-Ti ox. chl.	-

TABLE 3.3 Mineralogy of mica containing rocks selected for K-Ar age dating and stable isotope analysis. Key: mus. = muscovite; bt. = biotite; qtz. = quartz; plag. = plagioclase; st. = staurolite; gt. = garnet; chl. = chlorite; Fe-Ti ox. = magnetite and ilmenite; Kfs. = K-feldspar; tour. = tourmaline; zr. = zircon; py. = pyrite. Full descriptions in Appendix 2.



**FIGURE 3.2** Photomicrograph of **TJ-7D** (x10) from the north of the Dalradian outcrop. Large relic grain of hornblende showing inclusions (formed during D1) which are discordant with the surrounding D2 fabric. Quartz, altered feldspars and magnetite are also present (Appendix 2).

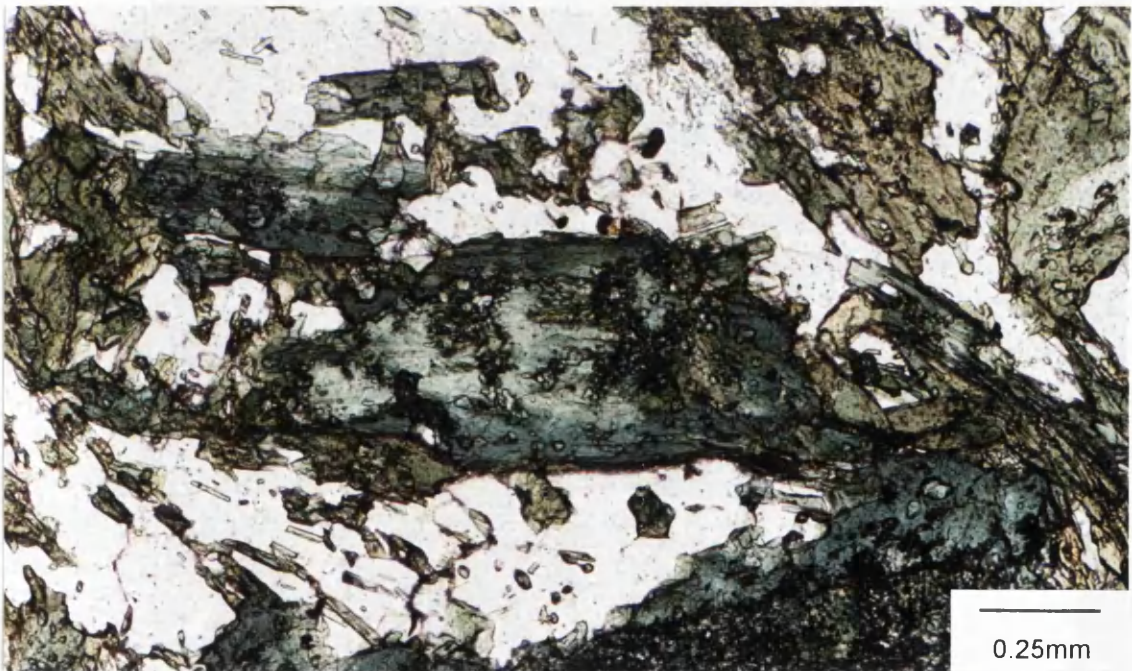


**FIGURE 3.3** Photomicrograph of **TJ-7D** (x25) from the north of the Dalradian outcrop. Another large, possibly relic grain showing zoning due to compositional differences. This is discussed in Chapters 5 and 6. Quartz, altered feldspars and magnetite are also present (Appendix 2).

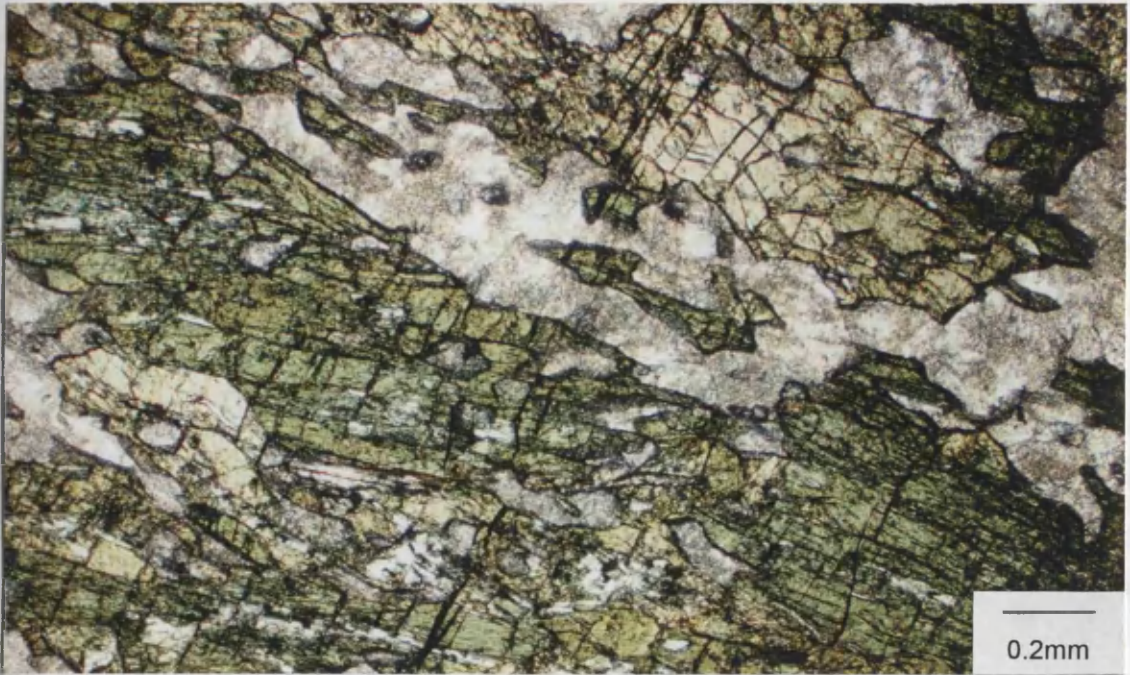


**FIGURE 3.4** Photomicrograph of TJ-44 (x40) from the south of the Dalradian outcrop. Hornblende crystals with typical pronounced cleavages. Some biotite alteration product is present. Quartz, altered feldspars and magnetite are also present (Appendix 2).

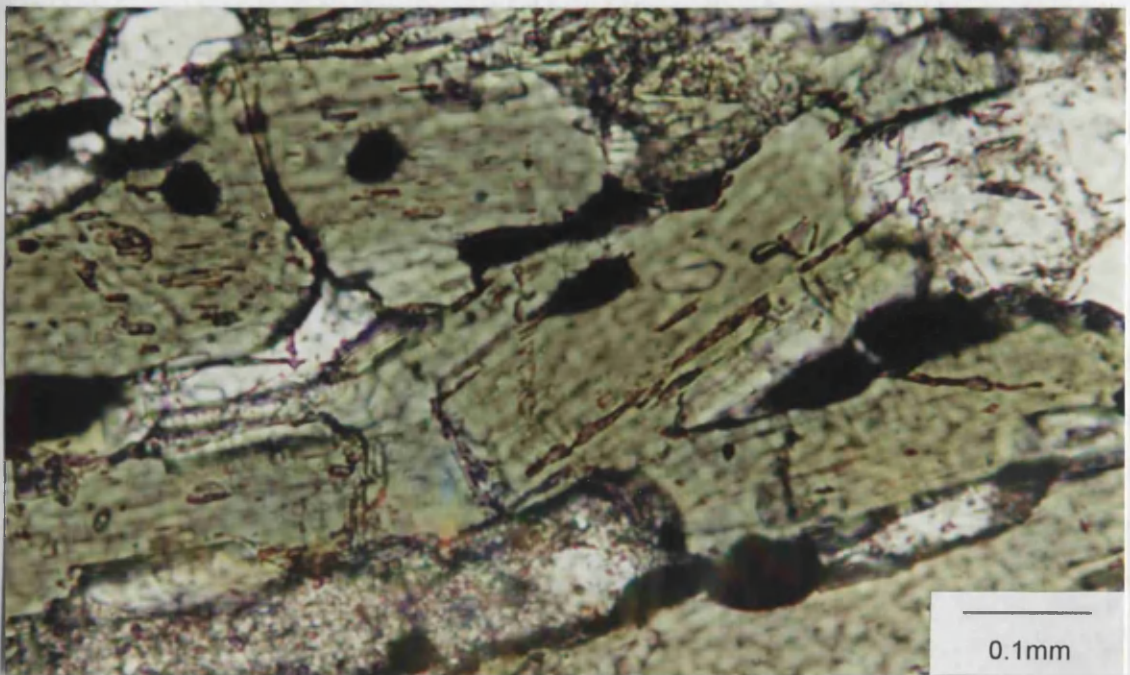


**FIGURE 3.5** Photomicrograph of TJ-44 (x64) from the south of the Dalradian outcrop. Closer view of biotite alteration along cleavage in hornblende. Quartz, altered feldspars and magnetite are also present (Appendix 2).

### 3.3 Sample Preparation.

Rock samples selected for mineral separation and isotope investigation were washed and any weathered material present was removed with the use of a small, diamond circular trimming saw.

After removal of weathered material, the block of rock was cut into slabs ~10-15mm thick. ~400g of these rock slices were used in the preparation of mineral separates, the rest being retained for further use, such as electron microprobe sections and XRF analysis. The selected pieces were further reduced in size by breaking with a hammer until they were of an acceptable size for the jaw crusher (Retsch/Glen Creston Model BB1/A). All crushing apparatus was meticulously cleaned before each sample was crushed. The jaw crusher reduced the rock fragment size to <5mm diameter. The fragment size was further reduced by passing several times through a laboratory roller crusher (Cook and Sons Ltd.), each time narrowing the gap between the rollers. After each pass through the roller crusher the sample was sieved to remove the < 150 $\mu$ m size fraction. The larger fragments were passed through until most of the sample was <150 $\mu$ m in size.

The recovered rock fragments were washed several times in tap water in a 2L conical flask to wash out the very fine rock flour generated by the crushing process. The rock flour reduces the efficiency of the magnetic separation process by causing clumping together of grains as they are passed through the magnetic separator. This usually required up to eight washes before the supernatant was clear. The sample was then dried for several days in an oven at 105°C. When dry, the sample was then again sieved to give a size fraction between 63 $\mu$ m and 125 $\mu$ m. This was again washed several times in tap water (to remove persistent fines) and given 3-4 final washes with deionised, double distilled water (DDDW) and was again dried in an oven at 105°C.

When dried, the thoroughly cleaned 63-125 $\mu$ m fragments were shaken out over a piece of glazed paper and spread thinly. A magnet was passed within 10mm over the entire exposed area of sample to remove grains of magnetite or non-monomineralic grains with a high proportion of magnetite. This process was necessary before passing the sample

through the magnetic separator because of blockages caused by the build up of magnetite on the electromagnet, which is in close proximity to the moving flow of fragments.

A Frantz Isodynamic Magnetic Separator, Model L-1 was used for the magnetic separation of hornblende from the sample. The settings of the machine were varied due to the differences in each sample to give the best separation efficiency. Generally the settings were: forward slope = 15°; side tilt = 25°; feed vibrator setting = 5.4; chute vibrator setting = 7.2. The electromagnet was set at ~0.25mA to remove the magnetic fraction first, which contained magnetite grains and other non-monomineralic magnetite containing grains. The collected lower magnetic fraction was then passed through at ~0.4-0.5mA to allow the non-iron containing quartz and feldspar fragments, non-monomineralic quartz and feldspar containing grains and a proportion of the chlorite to separate out. Thus the ~0.25-0.4mA magnetic fraction was collected. This was observed under a binocular microscope to check for chlorite content and the presence of non-monomineralic grains. If these were found in abundance the sample would then be sieved again to remove the larger size fraction until the quantity had diminished. The chlorite could be removed to an extent by finely adjusting the electromagnet current and slope of the sample splitter chute to exploit the different iron content, density and shape between chlorite and hornblende grains. It was found that in general the chlorite tended to be in the lower magnetic fraction. The magnetic separation procedure is most efficient when the sample is passed through slowly and each stage of the separation is repeated several times. Samples were checked for purity by binocular microscope and XRD.

The magnetic separation procedure was found to be very useful in creating a relatively pure hornblende separate; estimated to be 88-94% pure. However, it was found that chlorite in particular persisted in most samples and it was therefore necessary to employ the heavy liquid separation technique to further purify most samples.

Due to the toxicity of the material all heavy liquid related work was carried out in a fume cupboard and necessary protective clothing, rubber gloves and eye protection was used. The heavy liquid used was 1,1,2,2-tetrabromoethane (BDH, Laboratory Reagent). ~5-7g of hornblende was heavy liquid separated at a time, ~70ml of heavy liquid was used

for this amount of sample. The heavy liquid and mineral grains were shaken thoroughly in the separation flask to give a very slowly settling homogeneous suspension. This was allowed five minutes to settle after which the settled material was drained off through the tap at the bottom of the separation flask. The material remaining in suspension was filtered from the heavy liquid through a type 42 filter paper. This was carried out three times for each aliquot to ensure the efficiency of the technique. After the third time the settled material was filtered through a type 42 filter paper. The filtered, settled grains and also the “float-off” grains were washed through several times with acetone (AnalaR, BDH) to thoroughly remove the 1,1,2,2-tetrabromoethane. The separates were dried at 105°C and then washed four times in acetone in a 100ml conical flask, again dried at 105°C, washed four times in tap water, followed by six washes in DDDW and were finally dried at 105°C.

The purity of each sample was checked by XRD and binocular microscope, any remaining impurities were removed or broken to smaller fragments using a small metal probe and the sample was again washed to remove these fines. Sample purity was targeted at 98% pure for the isotope analysis requirements. These methods are detailed in Hutchison (1986).

Several samples which were selected for hornblende separation were unable to be separated to the required purity and were rejected from the study group. These were **TJ-7C** (from **Group-A**), **TJ-25**, **TJ-26**, **TJ-27**, **TJ-28**, **TJ-30** (most of the group collected southeast of Kylemore Lough), **TJ-32** and **TJ-55**.

It was found that the hornblende (specific gravity, **D** = 3.02-3.50) in the sample tended to settle to the bottom of the separation flask, while the chlorite (**D** = 2.6-3.3) and epidote (**D** = 3.15-3.27) remained in suspension or settled at a much slower rate. The chlorite and epidote being of a slightly lower density than the amphibole from which they formed during retrograde metamorphism. This technique also removed any remaining quartz (**D** = 2.65), alkali feldspar (**D** = 2.55-2.63) and plagioclase feldspar (**D** = 2.62-2.76) from the sample being purified (specific gravities of minerals from Deer, Howie and Zussman (1966)). This technique was quite time consuming to perform on ~30 samples and yielded usually ~2-4g of final mineral separate for isotope work.

The analysis techniques used to characterise and investigate the chemistry and isotopic properties of the selected samples are described in Chapter 4. All the information on the tables in this chapter is condensed from the sample characterisation information in Appendix 1 and 2.

## CHAPTER 4.

### ANALYTICAL WORK.

An extensive review of commonly used analytical techniques, including those described here, can be found in Potts (1987).

#### 4.1 X-Ray Diffraction.

Purity of the hornblende and muscovite mineral separates was checked by X-ray diffraction (XRD). ~0.2g of each sample was ground in acetone (Fisher Scientific, AnalaR) in an agate mortar to reduce grainsize. The slurry was then dispersed on a glass slide and the acetone allowed to dry at room temperature to give a uniform coverage. These were analysed on a computer controlled Philips PW1140 X-ray generator with a Philips PW1050/35 vertical goniometer. Samples were scanned from 4°-60° 2θ at X-ray intensity 20mA, 40kV ( $C_{O_{K\alpha}} = 1.7902\text{Å}$ ) scan speed 2°2θ/min., chart speed 1cm/min.

Hornblende mineral separates were checked for impurities of chlorite, epidote, magnetite, quartz and feldspar. Muscovite mineral separates were checked for impurities of quartz. This was done by comparison with X-ray diffraction charts of known pure mineral standards held within the Department of Geology and Applied Geology, University of Glasgow.

The detection limit of impurities was estimated to be ~5% by this XRD technique. In each case, if impurities were found (especially chlorite in hornblende), the sample would be subjected to further separation procedures (Chapter 3). The sample would be rechecked by XRD and accepted or done again. After the XRD check each sample was observed under a binocular microscope to check for any remaining impurities, which were removed by small probe if found. The level of purity aimed for was >98% hornblende (or muscovite).

## 4.2 X-Ray Fluorescence.

Rock samples of the specimens which yielded useable mineral separates (Chapter 3, Tables 3.2 and 3.3) were analysed by wavelength dispersable X-ray fluorescence spectrometry (XRF) for the major elements: Si, Ti, Al, Fe, Mn, Mg, Ca, Na, K and P on a Philips PW1450 Sequential Automatic X-ray spectrometer.

Pieces of rock trimmed for weathering and washed were broken by hammer and passed through the jaw crusher to reduce the fragment sizes to <1cm diameter (Chapter 3.3). ~150g of sample was used in each case. This was then ground to <90µm in a Siebtechnik TeMa Laboratory Disc Mill (with agate grinding barrel, disc and ring) for 20 minutes. After this the powder was further reduced to <50µm in a Fritsch Pulverisette 5/4 Laboratory Planetary Mill (with agate mortars and balls) for 30 minutes.

For major element analysis, fused glass beads were prepared by weighing out 0.3750g of rock sample (oven dried at 105°C for 24 hours) and 2.000g of Spectroflux 105 (Johnson Matthey; lithium tetraborate - lithium carbonate - lanthanum oxide mix, geochemistry laboratory designation: T-Flux) into a platinum crucible. This was heated at 1000°C for 30 minutes in a Carbolite EML 11/2 furnace (lids on crucibles), after which, each sample was agitated while being heated over a Meker burner for 5-7 minutes. The molten glass was then poured onto a preheated carbon die and pressed with a stainless steel die (also preheated) into a standard size solid glass disc (or glass bead). The beads were then cured on their carbon dies 120°C for 30 minutes on a Cutrock CHP100 hotplate, after which they were cooled to room temperature, trimmed for flash and labelled.

These were then run on the XRF spectrometer for major element analysis against blanks (beads made from Spectroflux 105 only) and internal standards held in the XRF laboratory (Appendix 3).

Pellets were prepared for trace element analysis by mixing 6g of pulverised rock sample with 2g of phenol formaldehyde resin (B and K Resins Ltd., R0214-1 resin). This was mixed for 30 minutes on a mechanical shaker, pressed at 23 tonnes for 2 minutes on a Specac Laboratory Bench Press and cured at 80°C on glass slides on refractory mounts in

an oven for 30 minutes. However, due to time restraints and equipment availability these samples were not run and were retained for possible future use.

Ferrous iron ( $\text{Fe}^{2+}$ ) content was determined by a chemical titration technique outlined in Section 4. Water and carbon dioxide were determined simultaneously by a technique also described in Section 4.

Rock XRF analysis results are in Appendix 3 and the calculated CIPW norms (Deer et al., 1966) for the amphibolites are in Appendix 3A.

### **4.3 Wet Chemical Analysis.**

#### 4.3.1 Flame Emission and Atomic Absorption Spectrophotometry.

Chemical analyses of the hornblende and muscovite mineral separates were carried out on a Thermo-Jarrell Ash Corporation, Smith-Hieftje 12, Atomic Absorption / Emission Spectrophotometer. The samples were analysed for Na, Ca, Mg, Fe (as total iron), Mn and Al as outlined in the Perkin-Elmer, "Analytical Methods for Atomic Absorption Spectrophotometry" procedure book (1971).

~0.1g of each mineral separate was weighed into a Teflon beaker (wrapped in aluminium foil to reduce static). A little DDDW (double, distilled, deionised water) was used to wash the sample to the bottom of each beaker. 5ml of conc. HF (Fisher Scientific, AnalaR) and 5ml of conc.  $\text{HNO}_3$  (BDH, AnalaR) were added. The beakers were put on a hotplate at  $105^\circ\text{C}$  overnight. After evaporation to dryness, the residue in each Teflon beaker was dissolved with 20ml of 10%  $\text{HNO}_3$ . This solution was carefully decanted and the Teflon beaker washed, into a 100ml standard flask and diluted with DDDW.

$\text{Na}^+$  content of each solution was determined by Flame Emission Spectrophotometry (FES) using a sodium-lamp with the machine detector set at 589.0nm. Comparison was made with 0, 0.5, 1.0, 1.5, 2.0 and 2.5ppm standard solutions (from NaCl, BDH, AnalaR).

$\text{Ca}^{2+}$  content of each solution was determined by Atomic Absorption Spectrophotometry (AAS) using a calcium-lamp with the machine detector set at 422.7nm.

Comparison was made with 0, 1, 2, 3, 4 and 5ppm standard solutions (from CaCO<sub>3</sub>, BDH, AnalaR).

Mg<sup>2+</sup> content of each solution was determined by AAS using a magnesium-lamp with the machine detector set at 285.2nm. Comparison was made with 0, 1, 2, 3, 4 and 5ppm standard solutions (from Mg(NO<sub>3</sub>)<sub>2</sub>, 1000ppm, BDH, SpectrosoL).

Fe<sup>3+</sup> content (total iron) of each solution was determined by AAS using an iron-lamp with the machine detector set at 248.3nm. Comparison was made with 0, 2, 4, 6, 8 and 10ppm standard solutions (from Fe(NO<sub>3</sub>)<sub>3</sub>, 1000ppm, BDH, SpectrosoL).

Mn<sup>2+</sup> content of each solution was determined by AAS using a manganese-lamp with the machine detector set at 279.5nm. Comparison was made with 0, 1, 2, 3, 4 and 5ppm standard solutions (from Mn(NO<sub>3</sub>)<sub>2</sub>, 1000ppm, BDH, SpectrosoL).

Al<sup>3+</sup> content of each solution was determined by AAS using an aluminium-lamp with the machine detector set at 309.3nm. Comparison was made with 0, 10, 20, 30, 40 and 50ppm standard solutions (from Al(NO<sub>3</sub>)<sub>3</sub>, 1000ppm, BDH, SpectrosoL).

The results of these analyses are in Appendix 4.

#### 4.3.2 Ferrous Iron Analysis.

Pulverised rock samples and hornblende and muscovite mineral separates were analysed for ferrous iron (Fe<sup>2+</sup>) content by titration with a standard potassium dichromate solution by a method described by Riley (1958a).

0.5g of pulverised rock sample (oven dried at 105°C for 24 hours) and 0.1-0.2g of hornblende or muscovite was used for each analysis. These samples were heated with conc. H<sub>2</sub>SO<sub>4</sub> (Fisher Scientific, AnalaR) and conc. HF (40%, Fisher Scientific) for 15 minutes at 160°C in platinum crucibles (with lids on) to allow complete dissolution.

Each of these was then transferred into a beaker containing ~300ml of DDDW with 10ml conc. H<sub>2</sub>SO<sub>4</sub>, 10ml of orthophosphoric acid (Prolabo, Analar), 10ml sat. H<sub>3</sub>BO<sub>3</sub> solution (Fisons, AnalaR) and 10 drops of diphenylamine-sulphonate indicator solution (0.2% w/v in DDDW, BDH Indicators) and was mixed thoroughly.

This colourless solution was immediately titrated against a standard potassium dichromate solution (2.73g in 2L DDDW, BDH, AnalaR); equivalent to 2mg Fe<sup>2+</sup> per 1ml. The quantity of titrate required to turn the solution purple was noted and the Fe<sup>2+</sup> calculated as FeO. All analyses were carried out in duplicate against an internal standard (Standard 9940, pulverised gabbro; Department of Geology and Applied Geology, University of Glasgow).

The results of this analysis are in Appendix 4.

#### 4.3.3 Water and Carbon Dioxide Analysis.

Water and carbon dioxide contents were determined to complete the XRF rock analyses. The procedure follows a technique described by Riley (1958b).

For each analysis, 0.5g of pulverised rock sample (oven dried at 105°C overnight) was weighed into a refractory boat which had been pre-ignited at 1000°C overnight in a Carbolite EML 11/2 Furnace.

A Carbolite CFM 1400 tube furnace at 1100°C, with a nitrogen flow system was used for the determinations. The nitrogen (BOC) flowing through the furnace tube was first dried by passing through, in sequence, conc. H<sub>2</sub>SO<sub>4</sub> (Fisher Scientific, AnalaR), CaCl<sub>2</sub> powder (Hopkins and Williams, AnalaR), Carbosorb AS granules (BDH, Laboratory Reagent) and Mg(ClO<sub>4</sub>)<sub>2</sub> solution (BDH, Laboratory Reagent) in U-bends.

The furnace tube contained copper wire and silver gauze to neutralise sulphur and nitrogen gaseous by-products.

The exhaust from the tube furnace was also passed through a sequence of reagents. Firstly, a sealable collection tube containing Mg(ClO<sub>4</sub>)<sub>2</sub> powder (for water absorption), saturated chromic acid solution (Hopkins and Williams, Laboratory Reagent) and finally, a sealable collection tube containing Carbosorb AS granules (for carbon dioxide absorption).

This apparatus was allowed to stabilise at 1100°C, with nitrogen flowing, for 2 hours each day before samples were run.

The first two runs were of empty, pre-ignited, refractory boats, to obtain background water and carbon dioxide values in the system not due to any sample.

Samples were run in duplicate to give reproducible results. After each sample had been heated at 1100°C for 20 minutes, the water and carbon dioxide collection tubes were sealed, wiped externally and weighed to four decimal places on a Sartorius 1207 MP2 balance. The differences in weight (from start to finish for each sample) were recorded and percentages of water and carbon dioxide derived.

The results of the rock water and carbon dioxide analysis complement the rock XRF results in Appendix 3.

#### **4.4 Electron Microprobe Analysis.**

Electron microprobe analysis was carried out on a Cameca SX50 Electron Probe Micro-Analyser (EPMA) with four internal spectrometers. Elements measured were Si, Ti, Al, Mg, Ca, Mn, Fe (as FeO), Na and K.

Electron microprobe sections, ~30µm thick, were made of all samples collected (Chapter 3). ~16-20 analyses of hornblendes and ~6-8 analyses of feldspars were carried out on each rock section of samples which had provided useable mineral separates (Chapter 3, Table 3.2). ~10-12 analyses of muscovites were carried out on the mica containing rocks (Chapter 3, Table 3.3).

Machine operating conditions were 15kV accelerating voltage with 20nA for the electron beam. Analyses were measured against standards from Micro-Analysis Consultants Ltd. Corrections were carried out for atomic number (Z), absorption (A) and fluorescence (F) automatically on a SUN computer system.

Electron microprobe analysis element oxide results are in Appendix 5 and 5A. The mineral formulae derived from these oxides are in Appendix 6 and 6A.

#### **4.5 Scanning Electron Microscope Imaging.**

Backscatter secondary electron (BSE) images of hornblendes were obtained using a Leo Microscopy Stereoscan 360 Scanning Electron Microscope (SEM) with integrated

Link Analytical AN1085S energy dispersive spectrometer microanalyser, set at 20kV accelerating voltage with 20nA for the electron beam. The images obtained were of in-situ hornblendes of selected samples (**TJ-7D**, **TJ-44** and **TJ-45**) taken from the same polished sections as used in the electron microprobe analysis. Element X-ray distribution maps for Si, Al, Fe, Mg and Ca were produced for **TJ-7D**. Sample selection was based on the EMPA results in Appendix 5 and 5A.

#### **4.6 K-Ar Dating.**

K-Ar dating of the hornblende and muscovite mineral separates was carried out at the Scottish Universities Research and Reactor Centre (SURRC) at East Kilbride, Scotland.

##### 4.6.1 Potassium Analysis.

Potassium analysis was carried out by Flame Emission Photometry (FES) on dissolved mineral separate samples.

~100mg of hornblende separate or ~15mg of muscovite separate was weighed out into an aluminium foil wrapped Teflon beaker. The foil neutralises static charges in the Teflon and makes controlled weighing of samples possible. 10ml of 40% HF (Fisher Scientific, AnalaR), 5ml of conc. HNO<sub>3</sub> (BDH, AnalaR) and 2ml of conc. H<sub>2</sub>SO<sub>4</sub> (BDH, AnalaR) were added and the aluminium foil removed. The beakers were heated overnight at 105°C until all fluid was evaporated off. The residual solid (metal sulphates, nitrates and fluoride compounds) was digested in 5ml conc. HNO<sub>3</sub> at 105°C for 1 hour. These solutions were made up to 250ml with 1000ppm NaCl (BDH, AnalaR) solution. Potassium contents were determined on a Corning EEL 450 Flame Emission Spectrophotometer, which was calibrated against known potassium standards from 0-5ppm. 3-4 analyses were carried out for each sample.

Results of these analyses are in Appendix 4 and Appendix 9.

#### 4.6.2 Argon Analysis.

Argon isotope evaluation was carried out by extraction of gases from mineral separate samples (in a glass and metal vacuum line) and were analysed by mass spectrometer.

~100mg of hornblende separate or ~15mg of muscovite separate was weighed out into a quartz-glass sample holder (closed with quartz-glass wool). Ten of these quartz-glass holders (one standard; BS133 biotite, split 9 and nine samples) were then loaded into a vertical glass sample tree, which was then connected to the vacuum line. Individual samples were dropped into the reaction chamber by manipulating iron bars in the tree with an externally held magnet.

Each sample was heated to over 1200°C for 20 minutes using a Radyne radio frequency induction heating coil.

A known volume of  $^{38}\text{Ar}$  spike was introduced after the Radyne was switched off. The liberated gases /  $^{38}\text{Ar}$  spike were passed through a zeolite trap to capture  $\text{H}_2\text{O}$  and  $\text{CO}_2$  and through a Ti sublimation pump to remove other active gases. The metal part of the line was heated by blowtorch flame to prevent  $\text{H}_2\text{O}$  condensation.

The inert gases left free in the system;  $^{36}\text{Ar}$ ,  $^{38}\text{Ar}$  and  $^{40}\text{Ar}$ , were passed through to a microcomputer controlled AE1 MS10 Mass Spectrometer. Peak heights were measured and compared and K-Ar ages calculated when potassium measurements were entered into the microcomputer program.

The results of this analysis are in Appendix 9.

#### **4.7 Hydrogen Isotope Analysis.**

Hydrogen isotope analysis of the hornblende and muscovite mineral separates was carried out at SURRC (East Kilbride).

50-60mg of each sample was weighed out on a Sartorius balance and placed in a platinum crucible in a reaction tube (previously ignited / degassed at 1200°C for 1 hour). The sample in the reaction tube was heated overnight at 120°C, under vacuum, to remove

absorbed surface water. The reaction tube was then fitted to the vacuum line and placed under vacuum, ready for commencement of H<sub>2</sub> extraction. The sample in the platinum crucible was heated for 30 minutes at 1200°C using a radio frequency induction heating coil (Cheltenham Radyne Induction Heater).

H<sub>2</sub>O vapour and H<sub>2</sub> gas was generated during the mineral sample destruction. The H<sub>2</sub>O generated was frozen into a liquid nitrogen U-bend trap while the glass line was heated by a hot-air blower. After this, the collected H<sub>2</sub>O was passed through a uranium furnace at ~500°C to be converted by chemical reduction to H<sub>2</sub> gas. This H<sub>2</sub> gas was collected in a Hg Toepler pump and the H<sub>2</sub> “yield” measured by Hg displacement.

The H<sub>2</sub> gas sample was analysed for H isotope composition on a V.G. Isogas SIRA 9 Mass Spectrometer against an internal reference gas calibrated with V-SMOW (Standard Mean Ocean Water, D/H = 155.76‰), GSIP (Greenland Ice Sheet Precipitate, D/H = -189.73‰, ref. V-SMOW) and SLAP (Standard Light Atlantic Precipitate; D/H = -482‰, ref. V-SMOW) international standards (National Bureau of Standards, 1.8.83.).

DTW -51.9‰ and LTSTD -93.68‰ international standards were also run as these were close to the measured sample results.

The results of this analysis are in Appendix 10.

#### **4.8 Oxygen Isotope Analysis.**

Oxygen isotope analysis of the hornblende and muscovite mineral separates was carried out at SURRC (East Kilbride) following the methodology of Craig (1957).

~2mg of each sample was weighed out on a Sartorius balance into a 10 port, stainless steel sample holder (two SES vein quartz standards and eight samples). This was placed under a laser target area, connected to the vacuum line apparatus used.

ClF<sub>3</sub> gas (Air Products, Special Gasses Group) was introduced to the isolated sample chamber. A sample was then incinerated at ~2000°C using a 10600nm CO<sub>2</sub> laser (Coherent Inc., System 450 CO<sub>2</sub> Surgical Laser). In the presence of ClF<sub>3</sub> the structural oxygen in the mineral sample was released after total destruction of the mineral. The O<sub>2</sub>

generated was reacted with an induction heated rod of ultra-high purity carbon (Ultra Carbon Corporation) to produce CO<sub>2</sub>. The “yield” of CO<sub>2</sub> was by calibrated capacitance manometer. The CO<sub>2</sub> was then manipulated through the glass line by a series of liquid nitrogen U-bend traps to remove other gaseous impurities.

The collected, purified CO<sub>2</sub> gas was isotopically analysed using a V.G. Isogas PRISM 3 Mass Spectrometer against internal standards held at SURRC.

The results of this analysis are in Appendix 11.

## CHAPTER 5.

### RESULTS.

Section 5.1 evaluates the results of rock XRF analysis (Appendix 3 and 3A), wet chemical analysis of mineral separates (Appendix 4) and EMPA of in-situ minerals in polished probe sections (Appendix 5 and 5A and Appendix 6 and 6A). Hornblende mineral names are given in Appendix 7 and 7A and ionic porosities,  $Z$ , are in Appendix 8.

Section 5.2 compares K-Ar age results (Appendix 9), Section 5.3 compares hydrogen isotope analysis (Appendix 10) and Section 5.4 compares oxygen isotope analysis (Appendix 11) against rock XRF analysis, wet chemical analysis of mineral separates and EMPA of in-situ minerals.

The six samples of muscovite are considered too small a set of data on which to evaluate dependable correlation coefficients and are used rather for comparison of K-Ar ages and stable isotope values with spatially nearby hornblende samples.

The progressive introduction of rock and mineral chemistry followed by isotope data gives a logical presentation of the results by giving the isotope results a set of sample characteristics with which they can be compared. The main focus of this work is to establish or reject compositional influences on the K-Ar ages and stable isotope values of the hornblendes derived from amphibolites and basic igneous rocks collected.

The sample correlation coefficients (Rollinson, 1993) were calculated using a regression analysis program in Lotus 1-2-3 (Release 5, 1996) on a personal computer (PC). The following correlation coefficients,  $R$ , (from Sachs, 1984) were used to establish whether, or to what degree, sets of data were displaying significant correlation:

For 45 samples;  $R > 0.253$  for  $>90\%$  significance;  $R > 0.299$  for  $>95\%$  significance.

For 30 samples;  $R > 0.306$  for  $>90\%$  significance;  $R > 0.361$  for  $>95\%$  significance.

For 29 samples;  $R > 0.311$  for  $>90\%$  significance;  $R > 0.367$  for  $>95\%$  significance.

For 28 samples;  $R > 0.317$  for  $>90\%$  significance;  $R > 0.374$  for  $>95\%$  significance.

For the two hornblende subgroups, **Group-A** and **Group-B**, both of 7 samples each, the correlation coefficients should be  $R > 0.669$  for >90% significance and  $R > 0.755$  for >95% significance.

For each section the R values which show >95% significance for the hornblende whole dataset are shown graphically in the figures following. Some have R values >99% and are identified as such.

Sample **TJ-59**, although shown on each graph, has not been included in the whole dataset R calculations as it was collected within the thermal aureole of the Roundstone Granite and has therefore been directly affected by the heat from this. It has been excluded from all correlation estimations.

For clarity the error bars for the average standard deviation (SD) values for the whole dataset are shown on each graph in a low density area and are represented by the following symbol: —|—. Individual SD values for each sample are in the relevant appendix for each valuation type, or can be derived from information therein.

## 5.1 **Rock and Mineral Chemistry.**

### 5.1.1 Rock Chemistry.

The results of rock XRF analysis and rock FeO, CO<sub>2</sub> and H<sub>2</sub>O determinations are in Appendix 3. CIPW normative mineral calculations (Cox et al., 1982) are given in Appendix 3A. These CIPW norms express the rock XRF results as calculated proportions of pre-metamorphosed minerals (quartz, orthoclase, albite, anorthite, diopside, hypersthene, olivine, magnetite, ilmanite and apatite) in a basaltic igneous rock type. These results show the original rocks to be of quartz-normative and olivine-normative tholeiites. This agrees with previous findings of amphibolite rock XRF appraisals in the Connemara area (Leake, 1989). This evaluation does not take into account later influences of hydrothermal metamorphism or quartz, calcite and epidote veining of the amphibolite rocks found in Connemara. Sample **TJ-48** appears to be of nepheline-normative basalt. However, this is probably an artefact of the CIPW norm calculation being affected by non-original material

from vein minerals. It is suspected that **TJ-48** would otherwise calculate as a quartz-normative or olivine-normative tholeiite, similar to the other samples.

### 5.1.2 Mineral Chemistry.

The results of the wet chemical analysis of mineral separates by AAS and FES have been recalculated as wt.% oxides ( $\text{Fe}_2\text{O}_3$ , MgO, CaO and  $\text{Na}_2\text{O}$ ) and are in Appendix 4. The FeO ( $\text{Fe}^{2+}$ ) was determined by titration of aliquots of each mineral separate (Chapter 4). K-content was also analysed by FES for the K-Ar dating technique.

EMPA results for hornblendes and muscovites are in Appendix 5 and 5A. For each sample 16-20 analyses of both schistose and larger porphyroblastic/relic hornblendes were completed. Samples collected in the north of the Dalradian inlier which displayed a foliation fabric of hornblende formed during D2 and relic grains of D1 hornblende (Chapter 3) commonly analysed as two populations of hornblende compositions (Appendix 5A, 6A and 7A). These compositions were independent of whether the analysis was from D1 relic grains or D2 fabric grains. However, in some of the larger hornblende crystals there appears to be compositional zoning present (Figures 3.2 and 3.3). Hornblende (a) and hornblende (b) types were identified in these northern samples:

Hornblende (a). Al-, Ti-, Fe-, Na-, K-rich. Commonly magnesiohornblende, occasionally tschermakite.

Hornblende (b). Si-, Mg-rich. Commonly magnesiohornblende (more Mg than coexisting hornblende (a)), occasionally actinolitic.

This dichotomy was not observed in samples collected from the southern limb of the Connemara Antiform which have experienced higher metamorphic grades (Chapters 1 and 3). The samples from the south tended to be higher in Na and K also.

Figures 5.1A-5.1F show scanning electron microscope (SEM) backscattered electron (BSE) images of selected samples to demonstrate the presence of two populations

of amphibole compositions commonly observed by EMPA in samples collected from the northern limb of the Connemara Antiform.

Figures 5.1A, 5.1B and 5.1C are of sample **TJ-7D**. The fields of view are mostly of hornblende with minor amounts of quartz, plagioclase and magnetite. These three figures show the occurrence of hornblende (b) (Mg-rich darker areas, magnesiohornblende) within hornblende (a) (relatively Fe-richer lighter surrounding areas, ferrotschermakite). The Mg-rich patches give less intense backscattering of electrons than areas richer in Fe, which has a denser nucleus than Mg (Potts, 1987). Figure 5.1A shows a patchy intergrowth of the different hornblende compositions. Figure 5.1B shows a larger Mg-rich hornblende patch within Fe-richer hornblende. Figure 5.1C demonstrates possible zoning from Mg-rich cores to Fe-rich rims. The compositional change can be gradual (Figure 5.1A) or abrupt (Figures 5.1B and 5.1C). The compositional oxide values, formulae and names for the two types observed in **TJ-7D** are in Appendix 5A, 6A and 7A.

Figures 5.1D and 5.1E are both of sample **TJ-44**. These two BSE images demonstrate the extensive alteration of hornblende to biotite and chlorite along cleavages as observed by optical microscope (Figure 3.5). This sample is from the southern limb of the Connemara Antiform and shows a uniform composition of hornblende (Appendix 5, 6 and 7). Figure 5.1F shows **TJ-45**, also from the southern limb of the Connemara Antiform, demonstrating the typical uniform hornblende composition of samples collected from this southern area and much less alteration than **TJ-44**.

The SEM element X-ray distribution maps of Figure 5.1G are of the same hornblende crystals in Figure 5.1C (sample **TJ-7D**). This figure shows the concentration of Si and Mg in the hornblende cores (as found by EMPA) and concentration of Al and Fe (less pronounced than Mg difference) in the rims. Ca is uniform across the hornblende crystals (Appendix 5A, 6A and 7A).

It should be noted that EMPA FeO and EMPA FeO/(FeO+MgO) on subsequent figures in this chapter are calculated values, using the same ratios of Fe<sub>2</sub>O<sub>3</sub>/FeO found by wet chemical analysis as outlined in the introduction to Appendix 5. Figures 5.1H and 5.1I are the results for EMPA SiO<sub>2</sub> and EMPA Al<sub>2</sub>O<sub>3</sub> plotted against calculated EMPA

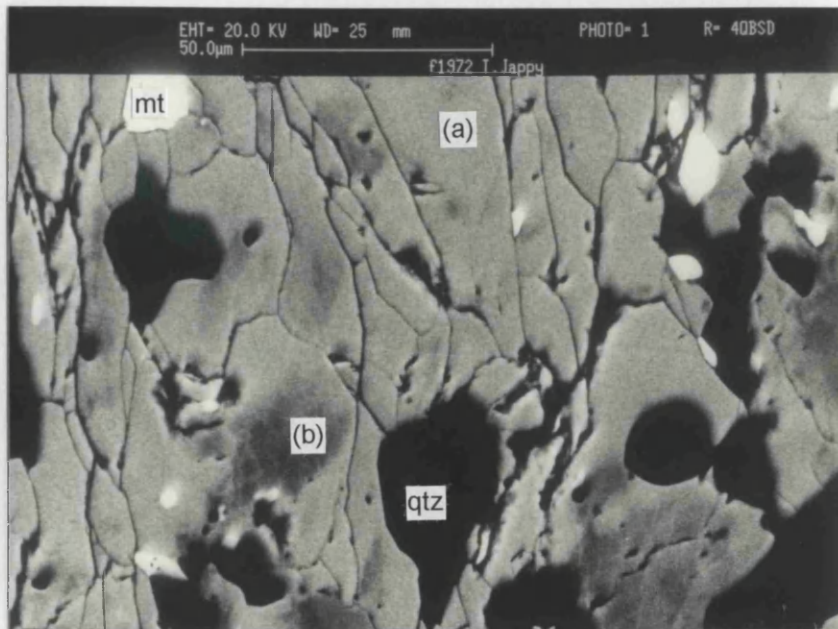


**FIGURE 5.1A** SEM backscatter electron (BSE) image of TJ-7D. Field of view mostly of hornblende: lighter areas are hornblende (a) (Al-, Fe-rich) with darker patches of hornblende (b) (Si-, Mg-rich). Key: qtz. = quartz; mt. = magnetite. Magnification x271.

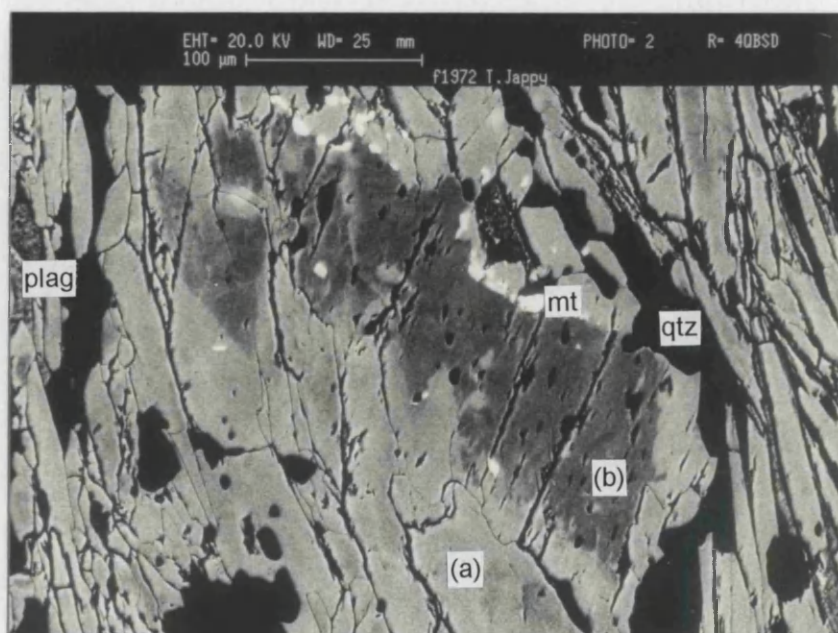


**FIGURE 5.1B** SEM backscatter electron (BSE) image of TJ-7D. Field of view mostly of hornblende: lighter areas are hornblende (a) (Al-, Fe-rich) with large, darker patch of hornblende (b) (Si-, Mg-rich). Key: qtz. = quartz; plag. = plagioclase; mt. = magnetite. Magnification x240.

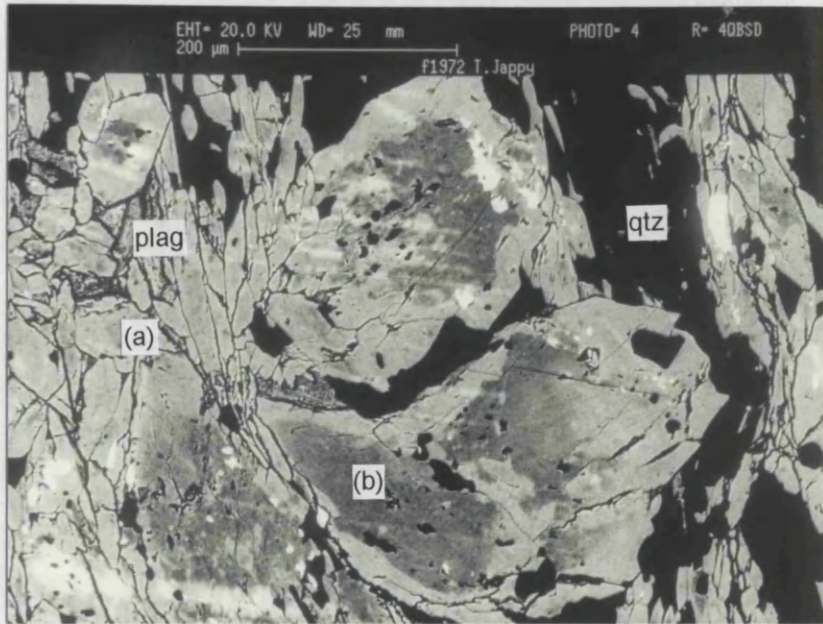


**FIGURE 5.1C** SEM backscatter electron (BSE) image of **TJ-7D**. Field of view mostly of zoned hornblendes: lighter rims of hornblende (a) (Al-, Fe-rich) with darker cores of hornblende (b) (Si-, Mg-rich). Key: qtz. = quartz; plag. = plagioclase. Magnification x157.

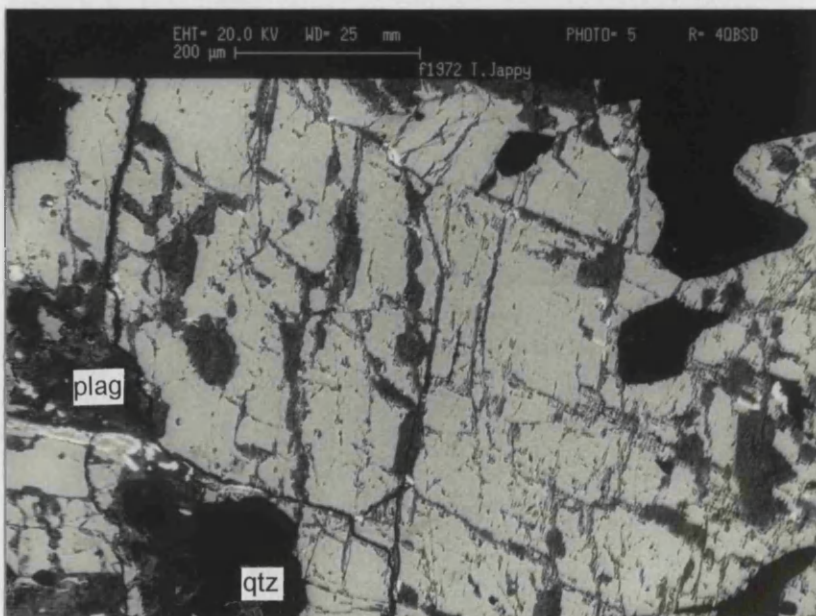


**FIGURE 5.1D** SEM backscatter electron (BSE) image of **TJ-44**. Field of view mostly hornblende of uniform composition. Alteration to biotite and chlorite along cleavages. Key: qtz. = quartz; plag. = plagioclase. Magnification x132.

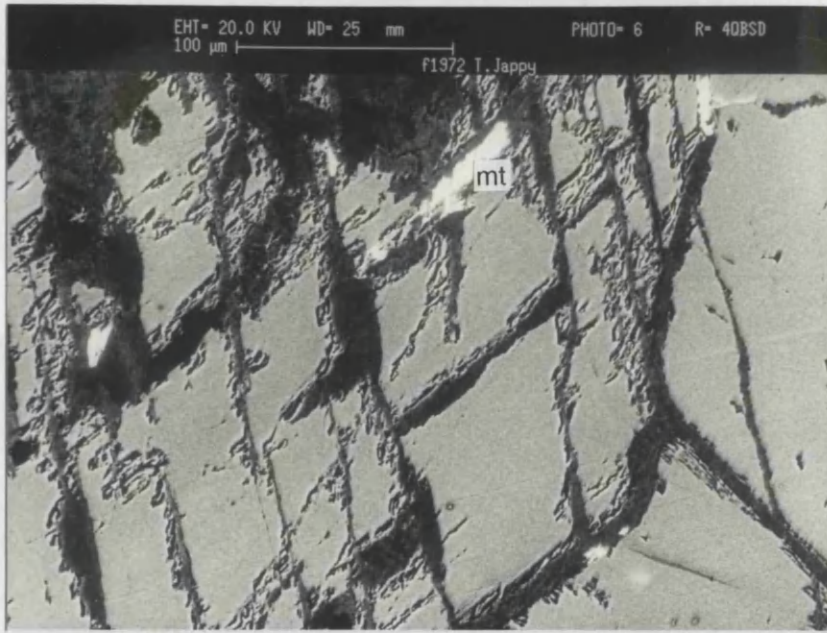


**FIGURE 5.1E** SEM backscatter electron (BSE) image of TJ-44. Field of view mostly hornblende of uniform composition. Alteration to biotite and chlorite along cleavages. Magnification x309.

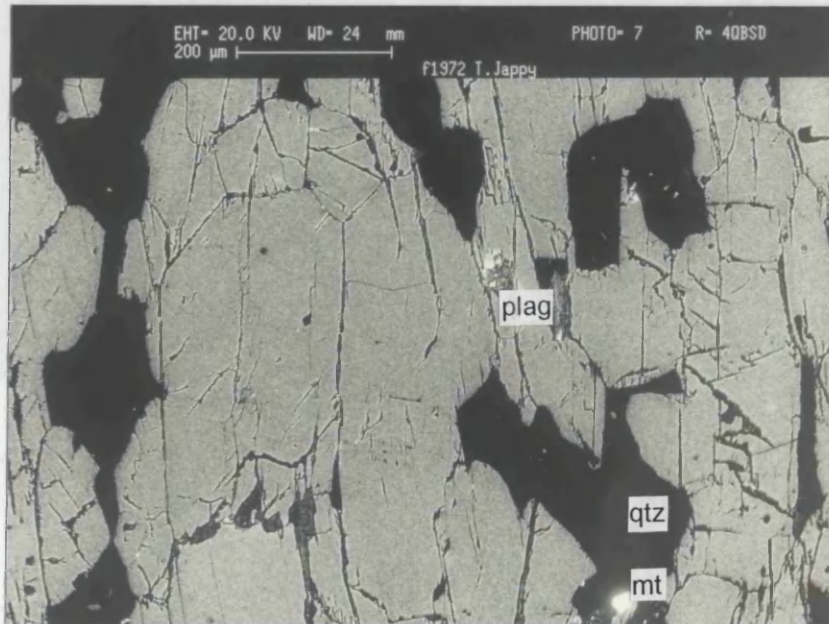


**FIGURE 5.1F** SEM backscatter electron (BSE) image of TJ-45. Field of view mostly hornblende of uniform composition. Very little alteration along cleavages. Key: qtz. = quartz; plag. = plagioclase; mt. = magnetite. Magnification x110.

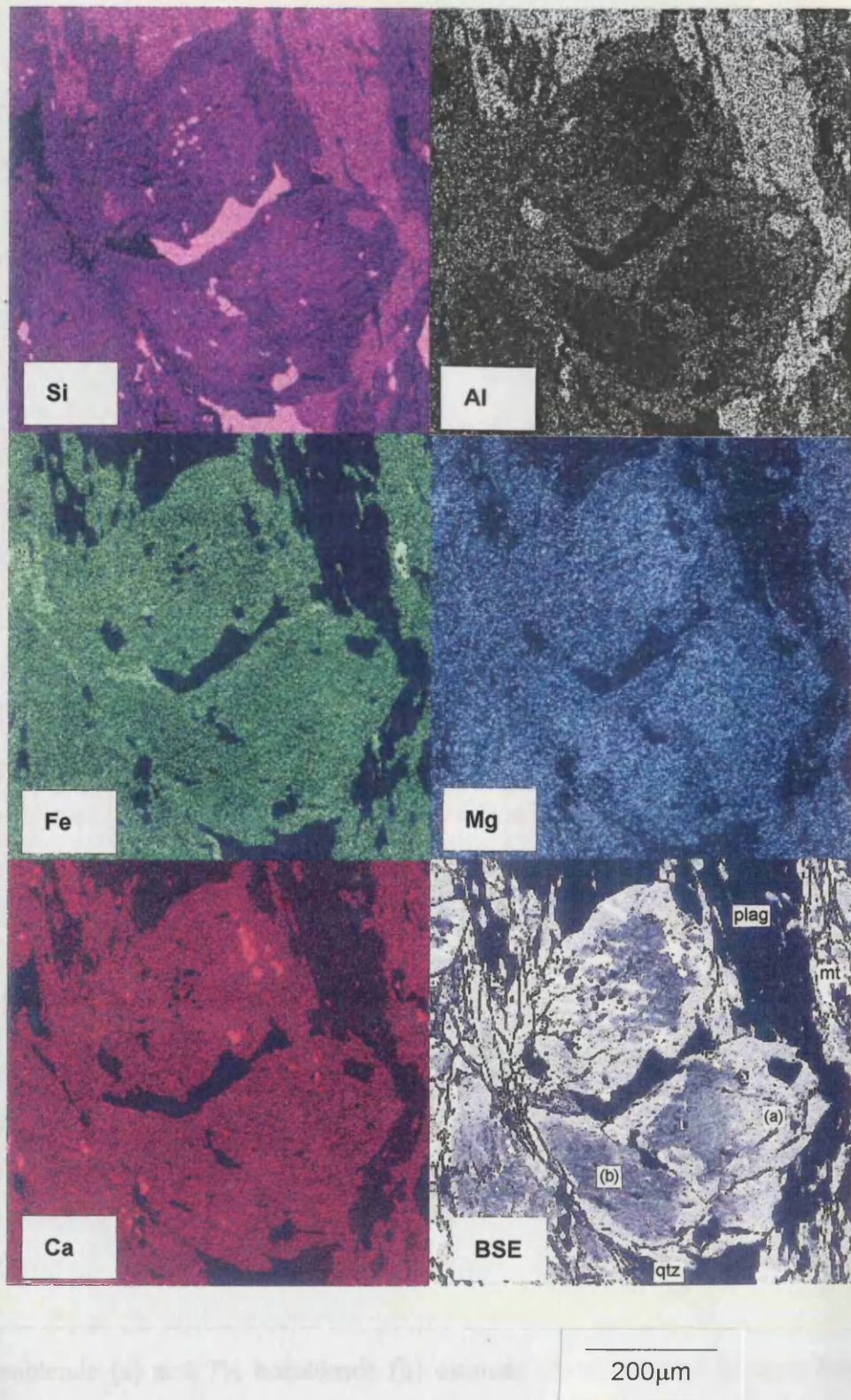


**FIGURE 5.1G** SEM element X-ray distribution maps of Si, Al, Fe, Mg and Ca of the zoned hornblende crystals of Figure 5.1C (sample TJ-7D). A backscattered electron (BSE) image is also included for comparison with Figure 5.1C. The rims of the hornblendes are relatively Al-, Fe-rich (hornblende (a)) whereas the cores are relatively Si-, Mg-rich (hornblende (b)). Compositions and formulae in Appendix 5A, 6A and 7A. Ca is uniform across cores and rims. Also: qtz. = quartz; plag. = plagioclase; mt. = magnetite.

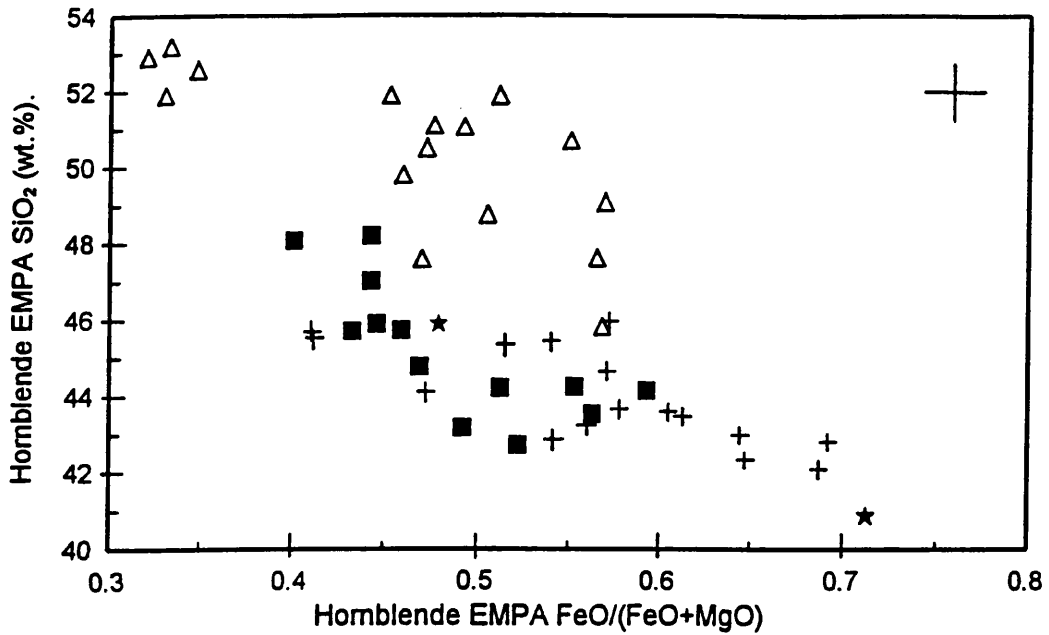
FeO/(FeO+MgO) respectively (Appendix 5 and 5A). Filled squares represent samples of uniform composition hornblende (mostly from the south of the area). Crosses represent Fe-rich hornblende (a) and open triangles represent Mg-rich hornblende (b) from samples in which two hornblende types were observed by EMPA (from the north of the area). It is demonstrated by these two graphs that hornblende (a) (Fe-rich) has similar composition to the uniform hornblende compositions (mainly from the south of the collection area), whereas the composition of hornblende (b) is offset. An interpretation of this is that hornblende (a) represents the composition moving towards equilibrium with the conditions prevalent during D2 metamorphism, during which samples closer to the MGS (in the south) were exposed to higher metamorphic grade and the north achieved only partial equilibrium, hornblende (b) representing relics of the earlier D1 associated metamorphism.

Figure 5.1J shows hornblende EMPA FeO/(FeO+MgO) (Appendix 5 and 5A) plotted against rock XRF FeO/(FeO+MgO) (Appendix 3). Hornblende (a) (Fe-rich) shows good correlation with the uniform composition hornblendes. Hornblende (b) (Mg-rich) shows a similar trend but somewhat shifted. This probably implies that both populations of hornblende grew in equilibrium with the whole rock chemistry of the amphibolite but that the conditions were different during the growth of the earlier Mg-rich hornblende (b).

To obtain a representative EMPA bulk composition (Appendix 5) with which to compare to a hornblende mineral separate K-Ar age or stable isotope value, the MgO content determined by wet chemistry on the mineral separate (Appendix 4) was used to determine the relative proportions of hornblende (a) and hornblende (b) in samples giving two populations of composition (Appendix 5A). In the case of **TJ-7D**, from BSE imaging under SEM, an observational quantitative estimate of 90% hornblende (a) and 10% hornblende (b) of the hornblende in the sample was made. This corresponds well with the 93% hornblende (a) and 7% hornblende (b) estimate of the mineral separate from MgO wt.% content of this sample (Appendix 4 and 5A).

In Appendix 5, the EMPA bulk compositions are listed along with the other "single composition" hornblendes (from the south of the collection area). These values in Appendix 5 are the EMPA values used for comparisons with isotope results in this chapter.

The hornblende mineral formulae of Appendix 6 and 6A were derived from the EMPA data of Appendix 5 and 5A. From these mineral formulae the A-site occupancy, Mg# ( $\text{MgO}/(\text{MgO}+\text{FeO})$ ), Si-content and mineral names were derived (Appendix 7 and 7A). The compositions of the hornblendes represented on the diagram in Figure 5.1K are based on the A-site and Mg# values and Si-contents of single and bulk hornblende EMPA analyses (Appendix 7). The ionic porosities (Z) of the hornblendes were calculated from values of ionic porosity of end members given by Dahl (1996), an example is given in Appendix 8.



**FIGURE 5.1H** Hornblende EMPA SiO<sub>2</sub> versus hornblende FeO/(FeO+MgO) (Appendix 5 and 5A). R for whole dataset of 45 samples = -0.675 (>99.9% significance). Symbols: filled squares = samples of uniform composition; crosses = hornblende (a) and open triangles = hornblende (b) from samples showing dual compositions. Average horizontal error = +/-0.016; average vertical error = +/-0.83wt.%.

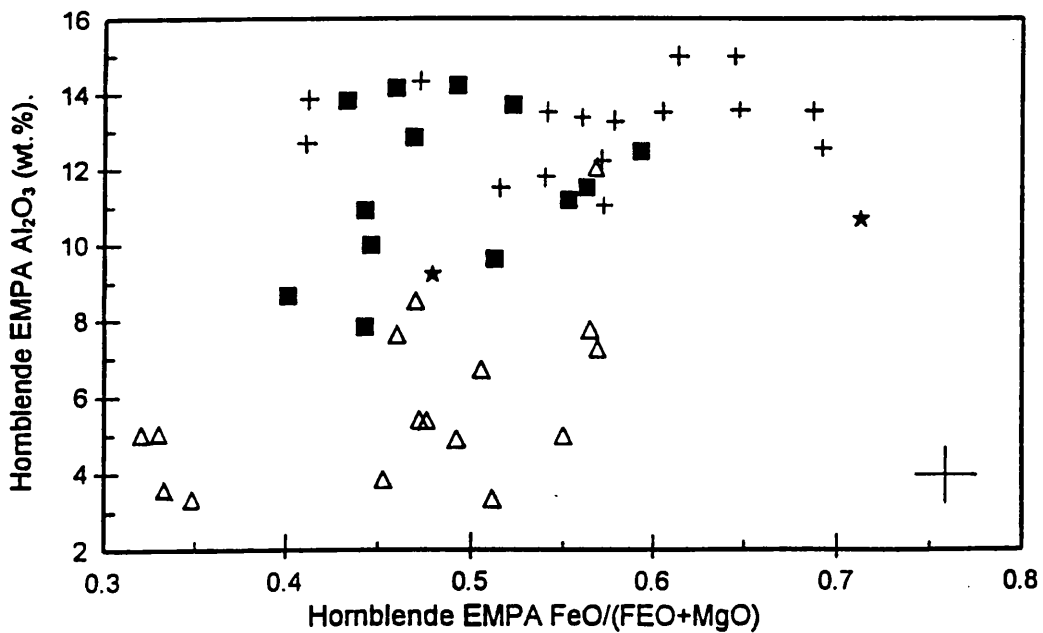


**FIGURE 5.1I** Hornblende EMPA Al<sub>2</sub>O<sub>3</sub> versus hornblende FeO/(FeO+MgO) (Appendix 5 and 5A). R for whole dataset of 45 samples = 0.518 (>99.9% significance). Symbols: filled squares = samples of uniform composition; crosses = hornblende (a) and open triangles = hornblende (b) from samples showing dual compositions. Average horizontal error = +/-0.016; average vertical error = +/-0.88wt.%.

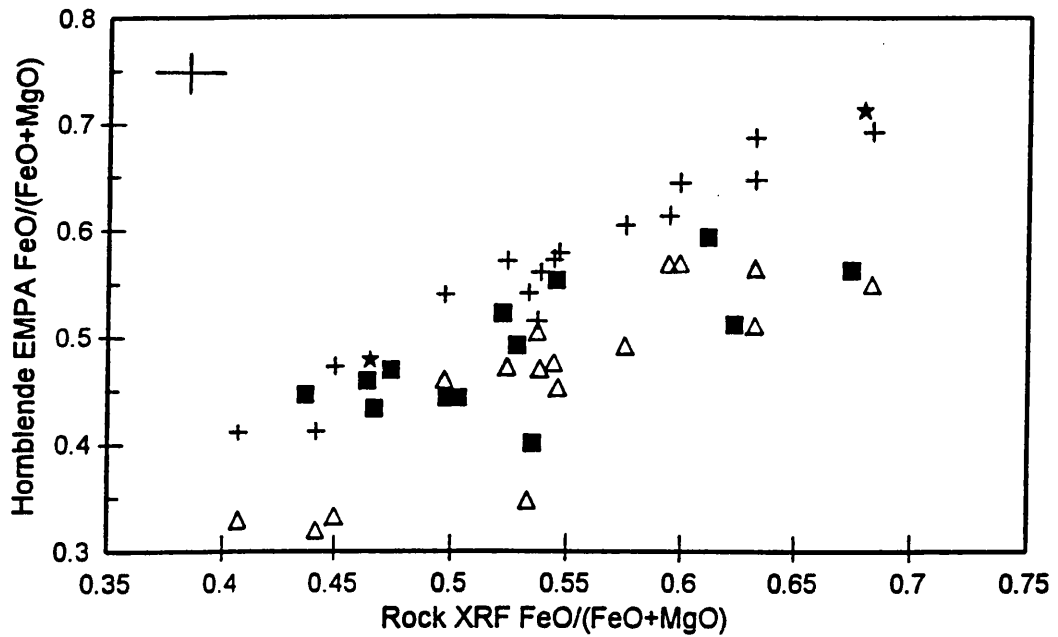


**FIGURE 5.1J** Hornblende EMPA FeO/(FeO+MgO) (Appendix 5 and 5A) versus rock XRF FeO/(FeO+MgO) (Appendix 3). R for whole dataset of 45 samples = 0.756 (>99.9% significance). Symbols: filled squares = samples of uniform composition; crosses = hornblende (a) and open triangles = hornblende (b) from samples showing dual compositions. Average horizontal error = +/-0.014; average vertical error = +/-0.016.

# CALCIC AMPHIBOLES

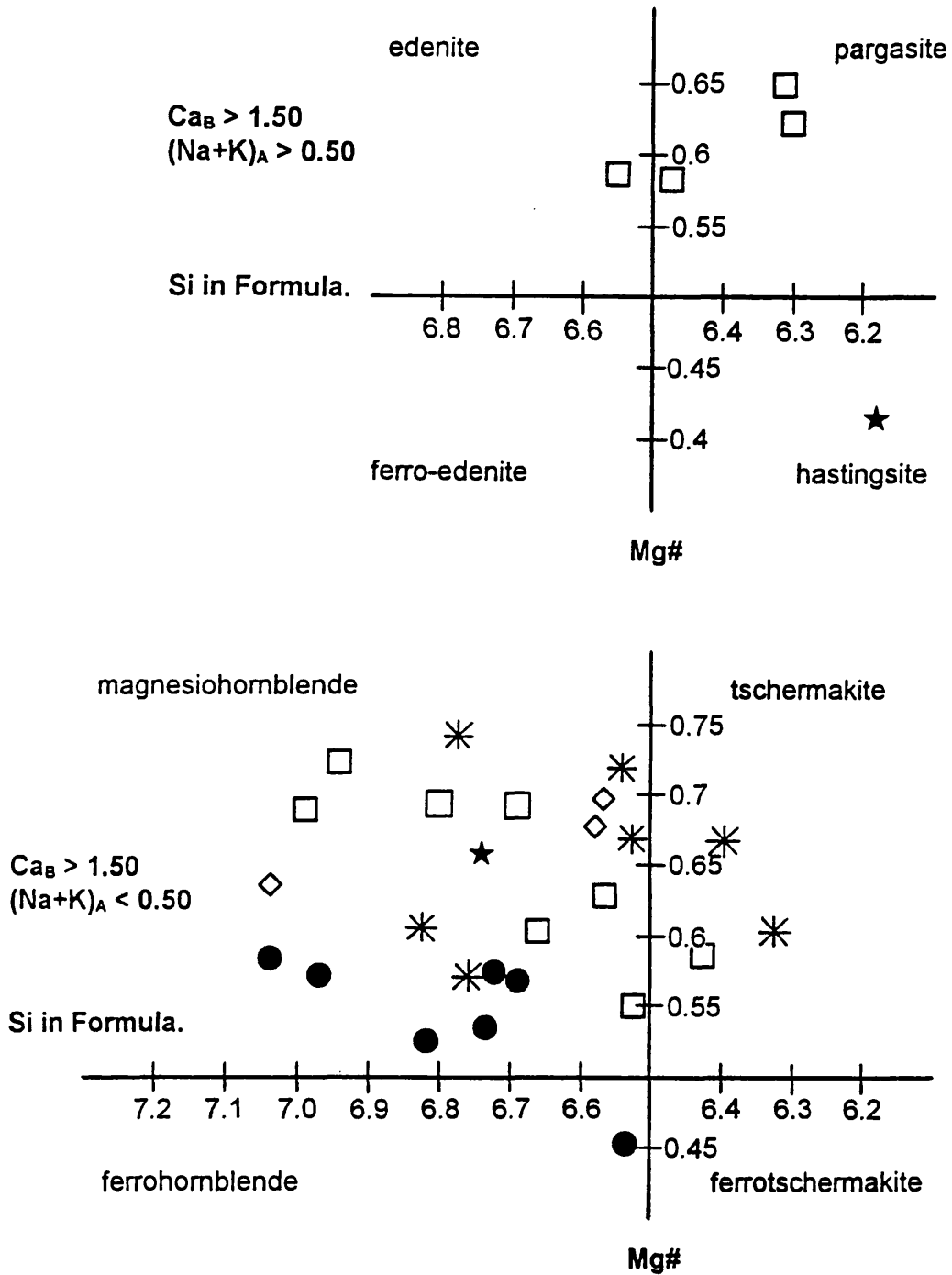


**FIGURE 5.1K** Diagram of hornblende bulk compositions (from EMPA derived formulae, Appendix 6) plotted onto part of the calcic amphibole classification diagram (Figure 1.7) of Leake et al., (1997). Symbols: **Group-A** = filled circles; **Group-B** = asterisks; **Group-C** = open diamonds; others = open squares; MGS = black stars.

## 5.2 Hornblende K-Ar Ages.

The results of the K-Ar age determinations are in Appendix 9. Table 5.1 gives a list of the ages for reference within this chapter. Figure 5.2 shows the K-Ar age distribution of these samples in relation to their geographical locations in Connemara.

K-Ar ages were determined mainly based on a single analysis for each sample due to time constraints and equipment availability. However, four samples (**TJ-35**, **TJ-36**, **TJ-38** and **TJ-41**) were analysed in duplicate to confirm repeatability within error. These are given in Appendix 9.

Figure 5.3 shows the K-Ar isochron for the hornblende whole dataset and gives a K-Ar age of 451Ma for the group. The slope of the  $^{40}\text{Ar}^*/^{36}\text{Ar}$  line is 0.029798 and the  $^{40}\text{Ar}/^{36}\text{Ar}$ -axis intercept is 295.5, the initial  $^{40}\text{Ar}/^{36}\text{Ar}$  ratio due to atmospheric composition (Dalrymple and Lanphere, 1969). Faure (1986) outlines the derivation of the K-Ar age equation:

$$t = 1/\lambda \ln[m(\lambda/\lambda_e) + 1] \quad \text{Equation 5.1}$$

Where  $t$  is the age in years (y);  $m$  is the slope of the  $^{40}\text{Ar}^*/^{36}\text{Ar}$  line;  $\lambda$  is the total decay constant of  $^{40}\text{K}$  to  $^{40}\text{Ar}$  and  $^{40}\text{Ca}$  ( $5.543 \times 10^{-10} \text{ y}^{-1}$ );  $\lambda_e$  is the decay constant of  $^{40}\text{K}$  to  $^{40}\text{Ar}$  ( $0.581 \times 10^{-10} \text{ y}^{-1}$ );  $\ln$  is the natural log of the function. The decay constants are from Steiger and Jäger (1977). The good fit of samples to the K-Ar isochron of Figure 5.3 demonstrates no unexpected deviance. However, **TJ-1** and **TJ-39** have much higher values than the group as a whole. The usefulness of the K-Ar isochron age is limited in this current study. The K-Ar age derived from each sample in relation to that sample's chemical characteristics and stable isotope values is the objective of this thesis.

The range of K-Ar ages determined for the hornblende mineral separates investigated is 410+/-9Ma to 556+/-6Ma (**TJ-39**; youngest to **TJ-38**; oldest). This range of well over 100Ma confirms the findings of the previous work (Elias, 1985; Miller, 1990) that

the ages cannot be related to one single simple cooling episode. The average age for the hornblende whole dataset (excluding **TJ-59**) is 470Ma, SD = 36Ma.

The range for **Group-A** is 412 $\pm$ 11Ma to 461 $\pm$ 11Ma (**TJ-7B** to **TJ-7D**); group average is 439Ma, SD = 19Ma. The range for **Group-B** is 410 $\pm$ 9Ma to 556 $\pm$ 6Ma (**TJ-39** to **TJ-38**); group average is 489Ma, SD = 46Ma. **Group-B** was collected from a larger area than **Group-A**, tens of metres rather than single metres apart, and shows a greater variation of age between its 7 samples than those of **Group-A**.

Four hornblende samples give K-Ar ages significantly above ~490Ma; 510 $\pm$ 16Ma (**TJ-9**), 522 $\pm$ 18Ma (**TJ-40**), 554 $\pm$ 16Ma (**TJ-43**) and 556 $\pm$ 6Ma (**TJ-38**). These samples are close to the lowest K values measured by FES for the whole dataset (Table 5.1, Figure 5.4). **TJ-38** was repeated and gave good agreement within experimental error for the K-Ar age (550 $\pm$ 18Ma and 562 $\pm$ 14Ma, Appendix 9). These hornblende ages are substantially higher than the oldest date for the main metamorphic event (Cliff et al., 1996) and may be relic ages from the D1 event or be affected by excess  $^{40}\text{Ar}$  in combination with the low K-contents, which these samples display (Table 5.1, Figure 5.4), increasing the measured hornblende K-Ar age. The main metamorphic event, having recently been demonstrated to be as young as 462.5 $\pm$ 3.3Ma (Friedrich et al., 1997) may suggest that that there could be an effect of excess  $^{40}\text{Ar}$  on the hornblende ages above this value, although the techniques used in this work are not able to recognise this condition.

The radiogenic argon,  $^{40}\text{Ar}^*$ , returns (%) for the samples were lower than expected (Appendix 9). This may be due to surface absorption of argon onto the sample and extraction apparatus at the time of analysis. This effect is corrected for by the isotope dilution technique making allowances for the presence of atmospheric argon isotopes (Dalrymple and Lanphere, 1969, Faure, 1986). The K-Ar results have larger calculated  $\pm$ -age errors as a consequence of this, i.e. -  $\sim\pm$ 12Ma instead of  $\sim\pm$ 9Ma (Miller, 1990).

### 5.2.1 K-Ar Ages - Rock XRF.

From regression analysis of hornblende K-Ar ages against rock XRF analyses (Table 5.2) probable correlations are present of age with  $\text{Fe}_2\text{O}_3$ , MgO and  $\text{FeO}/(\text{FeO}+\text{MgO})$  for

the hornblende whole dataset of 30 samples. There is also a correlation of K-Ar age with FeO in **Group-B**. Although below the accepted values for probable correlation, **Group-A** and **Group-B** variously have relatively high R values for Fe<sub>2</sub>O<sub>3</sub>, FeO, MgO and CO<sub>2</sub>.

The inference from this information is that K-Ar ages from hornblendes are related to the mafic nature and the Fe/Mg ratio of the rock analyses. No other significant correlations are observed, including Na<sub>2</sub>O and K<sub>2</sub>O values.

Figures 5.5 and 5.6 respectively demonstrate the positive trend of MgO and negative trend of FeO/(FeO+MgO) for 30 samples. Also, the relationships between average ages and average analyses for **Group-A** and **Group-B** reinforce the general trends observed (standard deviations of the group averages are given in brackets):

	<b>Group-A.</b>	<b>Group-B.</b>
Av. K-Ar Age.	439Ma (SD = 19Ma).	489Ma (SD = 46Ma).
Av. MgO	6.86wt.% (SD = 1.24wt.%).	9.75wt.% (SD = 2.17wt.%).
Av. FeO/(FeO+MgO)	0.603 (SD = 0.051).	0.482 (SD = 0.052).

### 5.2.2 K-Ar Ages - Wet Chemical Analysis of Hornblendes.

From Table 5.3 correlations are present of age with MgO and K<sub>2</sub>O in the whole dataset and with Na<sub>2</sub>O and K<sub>2</sub>O in **Group-B**. Also, elevated values of R are present for Fe<sub>2</sub>O<sub>3</sub> and FeO in **Group-A** and Fe<sub>2</sub>O<sub>3</sub>, FeO, MgO and CaO in **Group-B**. The R value for the hornblende whole dataset for FeO/(FeO+MgO) is just under the requirement for correlation.

The inference from this information is that K-Ar ages from hornblendes are related to the mafic content and the Fe/Mg ratio of the wet chemical analyses of the hornblende mineral separates. This agrees with the trends seen generally for the rock XRF data. The correlation with K<sub>2</sub>O is very strong in this case (derived from K-content values; Table 5.2, Figure 5.4).

Figures 5.7 and 5.8 respectively demonstrate the positive trend of MgO and negative trend of K<sub>2</sub>O for 30 samples. Also, the relationships between average ages and

average analyses for **Group-A** and **Group-B** reinforce the general trends observed (standard deviations of the group averages are given in brackets):

	<b>Group-A.</b>	<b>Group-B.</b>
Av. K-Ar Age.	439Ma (SD = 19Ma).	489Ma (SD = 46Ma).
Av. MgO	9.97wt.% (SD = 1.54wt.%).	11.24wt.% (SD = 1.38wt.%).
Av. K <sub>2</sub> O	0.37wt.% (SD = 0.07wt.%).	0.32wt.% (SD = 0.13wt.%).

The averages for the groups agree with the overall trends for the whole dataset. However, the overlap due to standard deviations between the two groups reduces the validity of these observations in this case.

### 5.2.3 K-Ar Ages - Hornblende EMPA.

Sample **TJ-29** gave very different values for K<sub>2</sub>O content from wet chemical analysis (0.77wt.%) to EMPA (0.21wt.%). It was felt that the EMPA results for this sample are not representative and have not been used in these evaluations. Thus giving an overall dataset of 29 samples.

The R values in Table 5.4 indicate probable correlations of K-Ar ages with FeO, MgO, K<sub>2</sub>O, FeO/(FeO+MgO), Mg# and ionic porosity (Z). **Group-B** shows probable correlations of K-Ar ages with SiO<sub>2</sub>, Fe<sub>2</sub>O<sub>3</sub>, Na<sub>2</sub>O and K<sub>2</sub>O. However, **Group-A** displays no significant correlations at all in this set.

Again the inference from this information is that K-Ar ages from hornblendes are related to the Fe and Mg values and the Fe/Mg ratio of the bulk EMPA of the hornblendes. This agrees with the trends seen generally for the rock XRF data and the wet chemical analysis.

Figures 5.9 to 5.14 respectively demonstrate the positive trends of MgO and Mg# and the negative trends of FeO, K<sub>2</sub>O, FeO/(FeO+MgO) and Z for the 29 samples. Also, the relationships between average ages and average analyses for **Group-A** and **Group-B**

reinforce the general trends observed (standard deviations for the group averages are given in brackets):

	<b>Group-A.</b>	<b>Group-B.</b>
Av. K-Ar Age.	439Ma (SD = 19Ma).	489Ma (SD = 46Ma).
Av. FeO	14.48wt.% (SD = 1.02wt.%).	10.89wt.% (SD = 1.92wt.%).
Av. MgO	9.83wt.% (SD = 1.49wt.%).	11.71wt.% (SD = 1.25wt.%).
Av. K <sub>2</sub> O	0.37wt.% (SD = 0.08wt.%).	0.30wt.% (SD = 0.11wt.%).
Av. Fe/(Fe+Mg)	0.597 (SD = 0.043).	0.480 (SD = 0.069).
Av. Mg#	0.546 (SD = 0.046).	0.654 (SD = 0.063).
Av. Z	37.921% (SD = 0.050%).	37.722% (SD = 0.095%).

The observation of relatively high values of correlation with the SiO<sub>2</sub> and Fe<sub>2</sub>O<sub>3</sub> for the whole dataset and **Group-B** is also indicative of the effect of composition on measured K-Ar age due to the overall change in character of the hornblende species. The correlations observed are seen for the oxides with the largest variation in the same way that correlations are seen in **Group-B** (range of 146Ma) but not **Group-A** (range of 49Ma).

#### 5.2.4 Summary of K-Ar Ages - Rock and Bulk Hornblende Compositions.

From comparisons of the K-Ar ages with rock XRF, wet chemical analysis and EMPA data it is observed that the greatest number of correlations are with the EMPA data. No significant correlations were expected with the rock XRF analysis due to the dilution with other mineral species and compositions. However, even in these, some correlation with iron and magnesium exists.

Therefore the MgO and possibly SiO<sub>2</sub> decreases with decreasing hornblende K-Ar age and Fe<sub>2</sub>O<sub>3</sub>, FeO, Na<sub>2</sub>O and K<sub>2</sub>O increases. The average values for **Group-A** and **Group-B** FeO/(FeO+MgO) and Z also display a decrease with increase in age. The other oxides generally have narrower ranges of compositional variation and probably do not show correlations with K-Ar age values because of this. The repeatability of correlations across

three different analysis groups shows confidently that there is a compositional control in some way of the  $^{40}\text{Ar}^*$  retention in the hornblendes from Connemara.

These compositional controls suggest that Mg-rich hornblende retains  $^{40}\text{Ar}^*$  better than the Fe-rich type. However, this is only an approximate estimation as the correlations are not perfect. This has been as observed in some previous work (Onstott and Peacock, 1987; Dahl, 1996) and may be indicative of other influences overprinting the basic composition - K-Ar age correlation.

The muscovite K-Ar ages range from  $410\pm 9\text{Ma}$  to  $460\pm 10\text{Ma}$  (Table 5.1, Appendix 9). These appear to agree with the relative ranges of local hornblende samples where present and do not offer any significant insights into the geographical distribution of the hornblende K-Ar ages.

Hornblende Sample.	Potassium (wt.%).	K-Ar Age (Ma).	Hornblende Sample.	Potassium (wt.%).	K-Ar Age (Ma).
TJ-1	0.27	448+/-10Ma	TJ-35	0.26	468+/-2Ma
TJ-7A	0.24	427+/-11Ma	TJ-36	0.22	478+/-3.5Ma
TJ-7B	0.42	412+/-11Ma	TJ-37	0.27	489+/-13Ma
TJ-7D	0.33	461+/-11Ma	TJ-38	0.15	556+/-6Ma
TJ-7E	0.31	426+/-10Ma	TJ-39	0.48	410+/-9Ma
TJ-7F	0.33	465+/-11Ma	TJ-40	0.18	522+/-18Ma
TJ-7G	0.25	436+/-11Ma	TJ-41	0.28	497+/-3.5Ma
TJ-7H	0.28	444+/-13Ma	TJ-43	0.13	554+/-16Ma
TJ-8	0.18	483+/-16Ma	TJ-44	0.43	483+/-13Ma
TJ-9	0.18	510+/-16Ma	TJ-45	0.49	452+/-11Ma
TJ-11	0.19	436+/-14Ma	TJ-46	0.40	467+/-11Ma
TJ-13	0.20	490+/-16Ma	TJ-47	0.21	478+/-13Ma
TJ-17	0.24	462+/-16Ma	TJ-48	0.15	492+/-15Ma
TJ-19	0.26	496+/-14Ma	TJ-54	0.28	448+/-14Ma
TJ-29	0.64	433+/-11Ma	TJ-59	0.40	375+/-11Ma
TJ-31	0.17	470+/-12Ma			
Muscovite Sample.	Potassium (wt.%).	K-Ar Age (Ma).	Muscovite Sample.	Potassium (wt.%).	K-Ar Age (Ma).
TJ-10	6.36	442+/-9Ma	TJ-22	7.83	410+/-9Ma
TJ-16	8.36	460+/-10Ma	TJ-50	7.94	421+/-9Ma
TJ-18	8.55	442+/-9Ma	TJ-53	4.72	437+/-10Ma

**TABLE 5.1** K-contents and K-Ar ages of hornblende mineral separates (upper table) and muscovite mineral separates (lower table). Full details of K-Ar age results in Appendix 9.

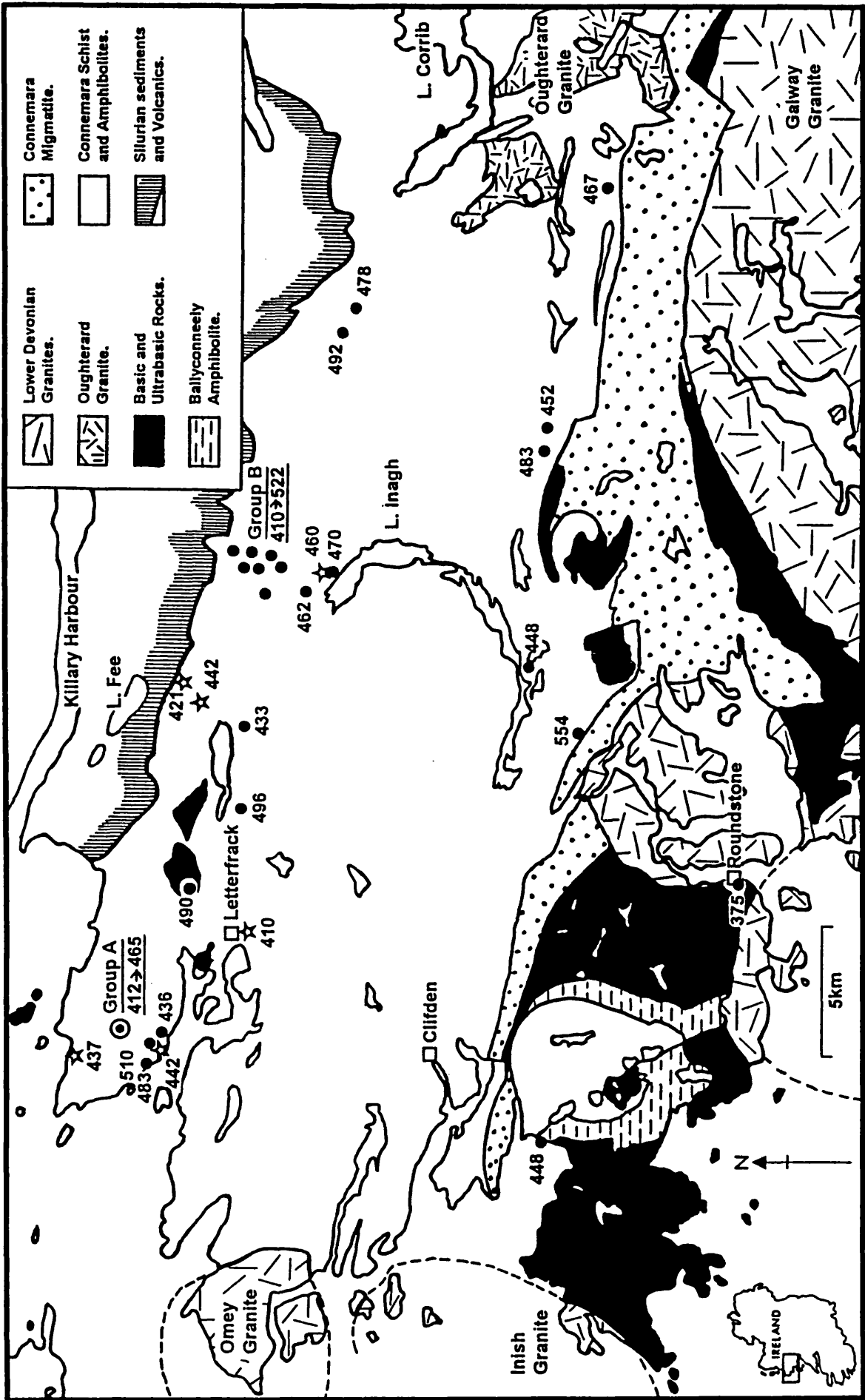
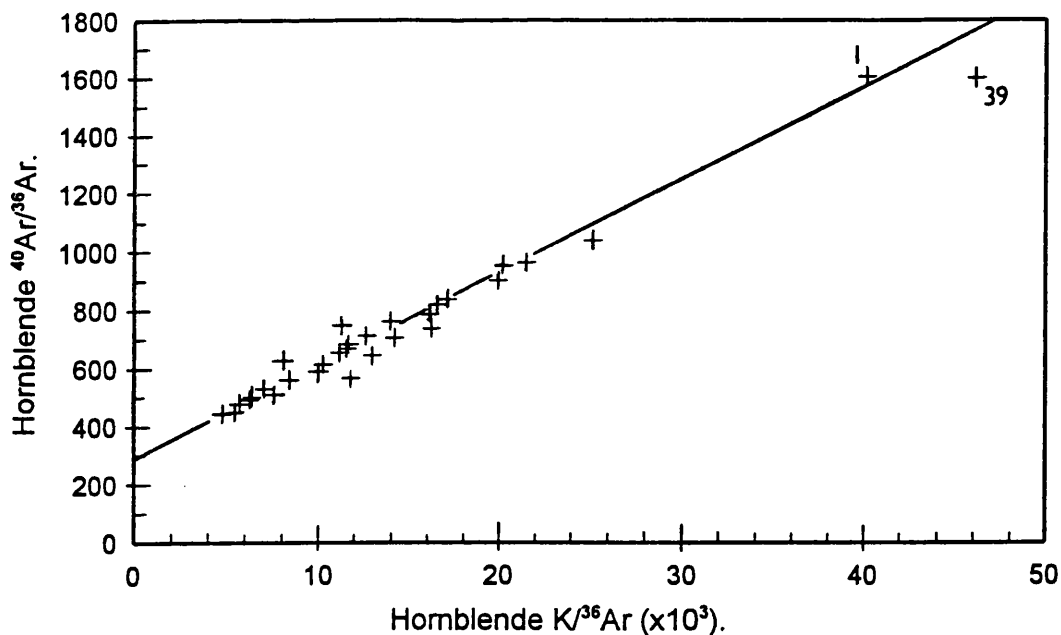
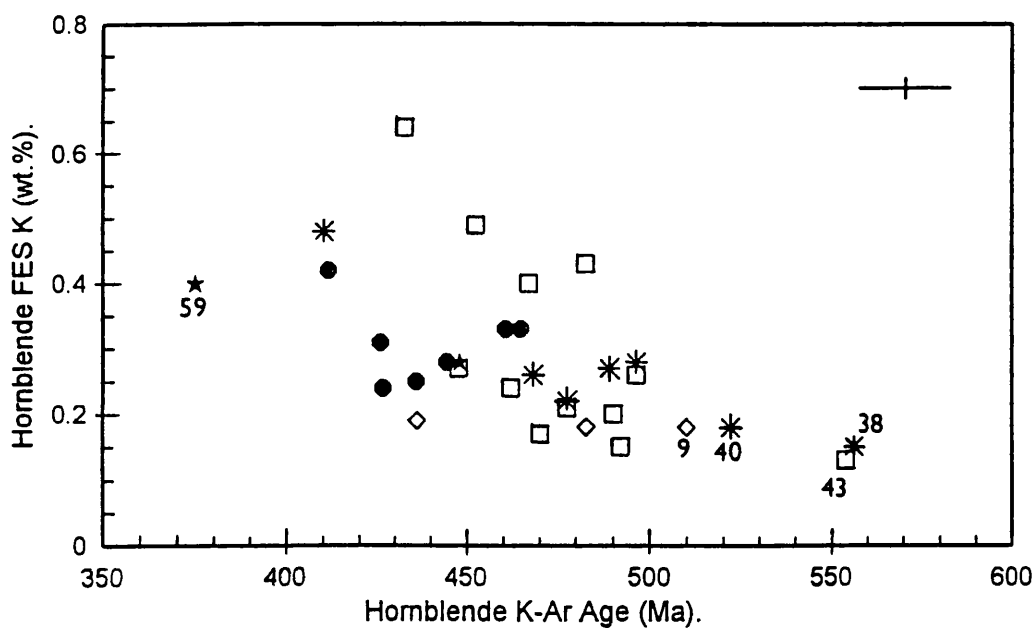


FIGURE 5.2 Map of Connemara showing K-Ar ages (Ma) of samples at locations collected. Filled circles represent hornblendes and open stars represent muscovites. Group-A is identified by a concentric circle symbol. Group-B is a locally clustered group of 7 samples.



**FIGURE 5.3** Hornblende  $^{40}\text{Ar}/^{36}\text{Ar}$  -  $\text{K}/^{36}\text{Ar}$  isochron. For clarity, each sample has been represented by a cross.  $R$  for whole dataset of 31 samples = 0.988 (>99.9% significance). The  $^{40}\text{Ar}/^{36}\text{Ar}$ -axis intercept is at 295.5; slope ( $m$ ) of line = 0.029798. The calculated K-Ar sochron age = 451.4Ma. Data for diagram in Appendix 9.



**FIGURE 5.4** Hornblende FES K versus hornblende K-Ar age.  $R$  for whole dataset = 0.576 (>99% significance).  $R$  for **Group-B** = -0.914 (>99% significance). Symbols: **Group-A** = filled octagons; **Group-B** = asterisks; **Group-C** = open diamonds; others = open squares; MGS = black stars. Average horizontal error =  $\pm 13\text{Ma}$ ; average vertical error =  $\pm 0.01\text{wt.}\%$ .

Rock XRF: Oxides.	R Dataset (30).	Probability of Trend.	R Group-A (7).	Probability of Trend.	R Group-B (7).	Probability of Trend.
SiO <sub>2</sub>	-0.041	-	0.440	-	-0.469	-
TiO <sub>2</sub>	-0.265	-	-0.005	-	-0.488	-
Al <sub>2</sub> O <sub>3</sub>	0.030	-	-0.069	-	0.082	-
Fe <sub>2</sub> O <sub>3</sub>	-0.315	>90%	0.352	-	-0.636	-
FeO	-0.100	-	0.547	-	0.686	>90%
MgO	0.433	>95%	-0.308	-	0.350	-
MnO	-0.033	-	0.326	-	0.186	-
CaO	-0.124	-	-0.360	-	0.387	-
Na <sub>2</sub> O	0.052	-	0.015	-	-0.212	-
K <sub>2</sub> O	-0.292	-	-0.282	-	-0.433	-
P <sub>2</sub> O <sub>5</sub>	-0.147	-	0.500	-	-0.290	-
CO <sub>2</sub>	-0.242	-	-0.627	-	-0.668	-
H <sub>2</sub> O	0.220	-	0.294	-	0.192	-
FeO/ (FeO+MgO)	-0.383	>95%	0.455	-	-0.073	-

**TABLE 5.2** Correlation coefficients (R) of hornblende K-Ar ages against rock XRF, FeO, H<sub>2</sub>O and CO<sub>2</sub> determinations. Whole dataset comprises 30 samples. **Group-A** and **Group-B** are of 7 samples each.

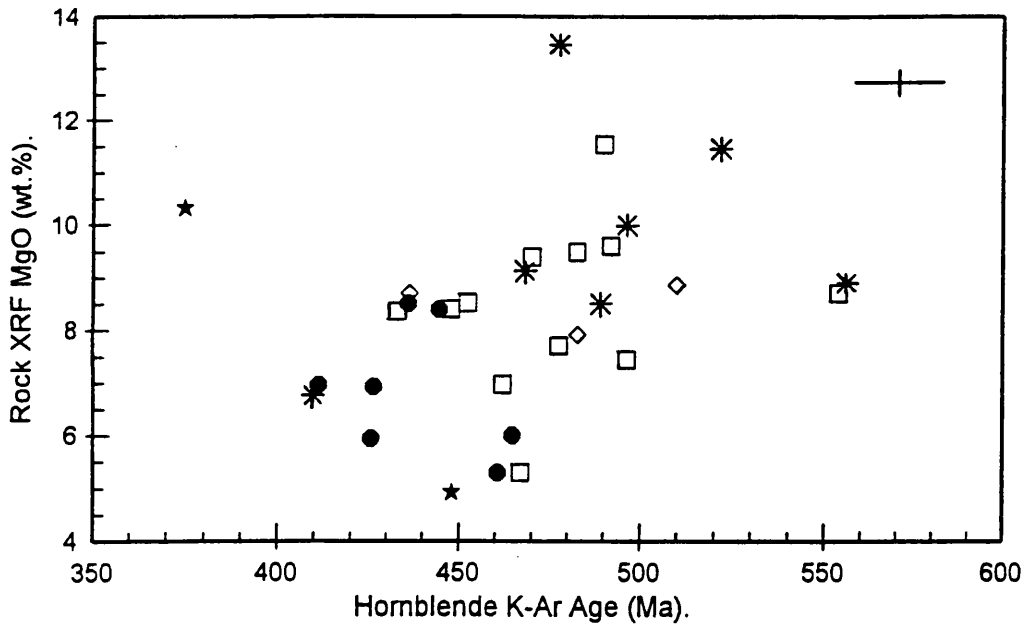


**FIGURE 5.5** Rock XRF MgO versus hornblende K-Ar age.  $R$  for whole dataset = 0.433 (>95% significance). Symbols: **Group-A** = filled octagons; **Group-B** = asterisks; **Group-C** = open diamonds; others = open squares; MGS = black stars. Average horizontal error =  $\pm 13$ Ma; average vertical error =  $\pm 0.21$ wt.%.

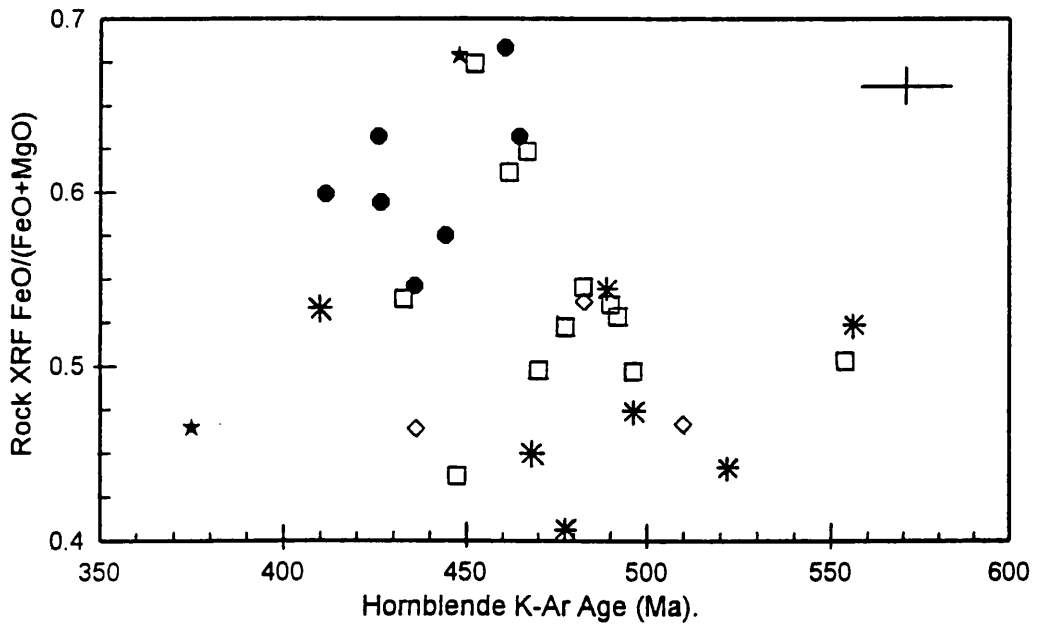


**FIGURE 5.6** Rock XRF FeO/(FeO+MgO) versus hornblende K-Ar age.  $R$  for whole dataset = -0.383 (>95% significance). Symbols: **Group-A** = filled octagons; **Group-B** = asterisks; **Group-C** = open diamonds; others = open squares; MGS = black stars. Average horizontal error =  $\pm 13$ Ma; average vertical error =  $\pm 0.014$ .

Hornblende Chemical Analyses: Oxides.	R Dataset (30).	Probability of Trend.	R Group-A (7).	Probability of Trend.	R Group-B (7).	Probability of Trend.
Fe <sub>2</sub> O <sub>3</sub>	-0.179	-	0.509	-	-0.590	-
FeO	-0.094	-	0.507	-	0.439	-
MgO	0.400	>95%	-0.123	-	0.517	-
CaO	-0.235	-	-0.170	-	0.503	-
Na <sub>2</sub> O	-0.033	-	-0.060	-	-0.752	>90%
K <sub>2</sub> O	-0.575	>99%	-0.157	-	-0.914	>99%
FeO/ (FeO+MgO)	-0.289	-	0.281	-	0.009	-

**TABLE 5.3** Correlation coefficients (R) of K-Ar ages against hornblende mineral separate wet chemical analyses. Whole dataset comprises 30 samples. **Group-A** and **Group-B** are of 7 samples each.

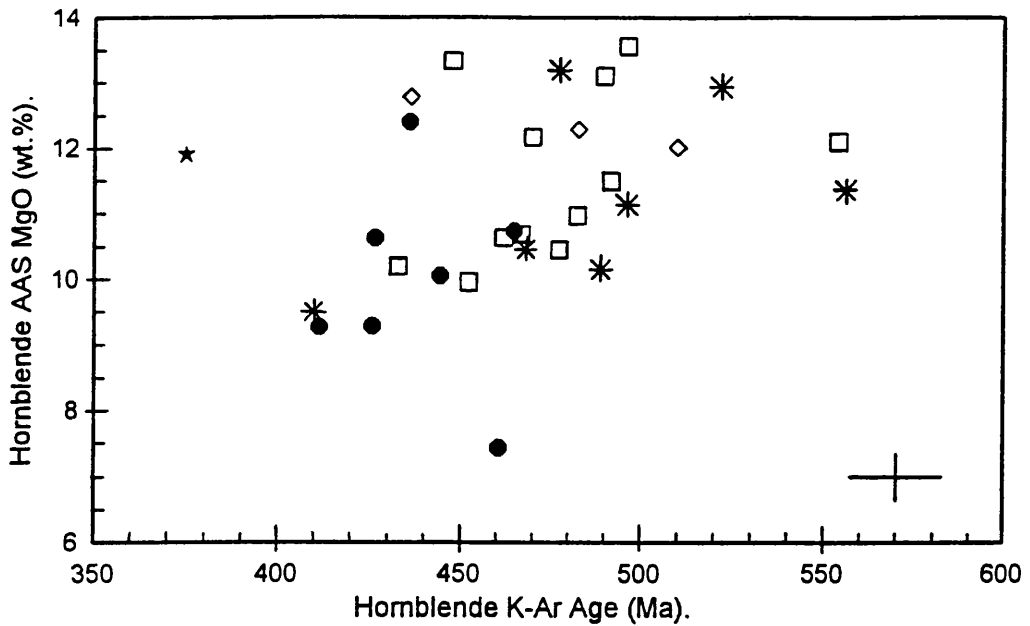


**FIGURE 5.7** Hornblende separate AAS MgO versus K-Ar age.  $R$  for whole dataset = 0.400 (>95% significance). Symbols: **Group-A** = filled octagons; **Group-B** = asterisks; **Group-C** = open diamonds; others = open squares; MGS = black stars. Average horizontal error =  $\pm 13$ Ma; average vertical error =  $\pm 0.30$ wt.%.

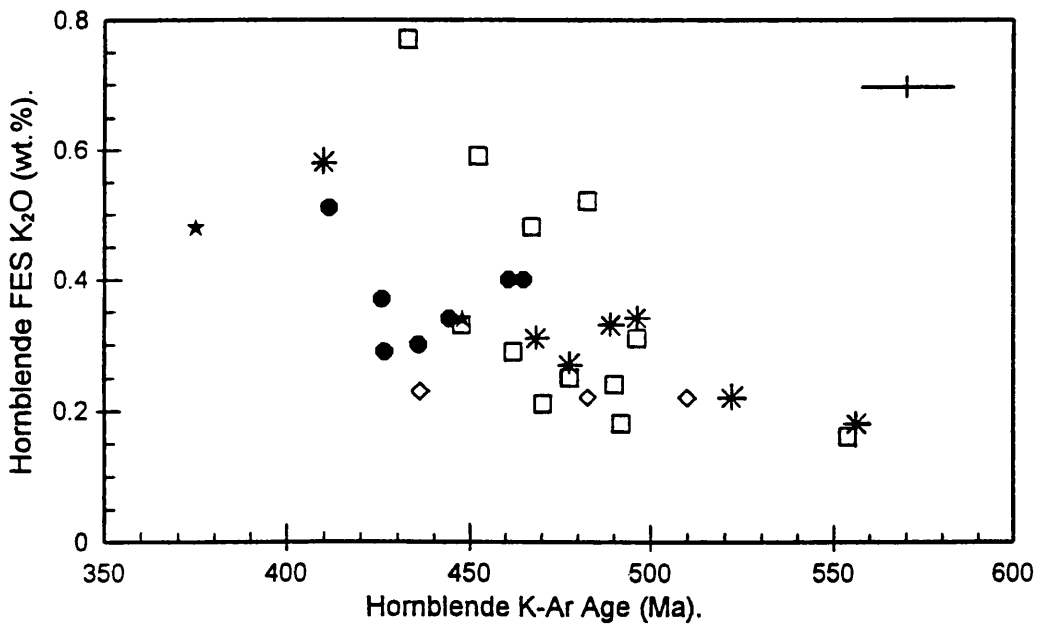


**FIGURE 5.8** Hornblende separate FES  $K_2O$  versus K-Ar age.  $R$  for whole dataset = -0.575 (>99% significance).  $R$  for **Group-B** = -0.914 (>99% significance). Symbols: **Group-A** = filled octagons; **Group-B** = asterisks; **Group-C** = open diamonds; others = open squares; MGS = black stars. Average horizontal error =  $\pm 13$ Ma; average vertical error =  $\pm 0.01$ wt.%.

Hornblende EMPA: Oxides.	R Dataset (29).	Probability of Trend.	R Group-A (7).	Probability of Trend.	R Group-B (7).	Probability of Trend.
SiO <sub>2</sub>	0.266	-	-0.135	-	0.689	>90%
TiO <sub>2</sub>	0.139	-	-0.031	-	-0.481	-
Al <sub>2</sub> O <sub>3</sub>	-0.083	-	-0.208	-	-0.489	-
Fe <sub>2</sub> O <sub>3</sub>	-0.225	-	0.256	-	-0.729	>90%
FeO	-0.368	>95%	0.303	-	0.137	-
MgO	0.525	>99%	-0.070	-	0.423	-
MnO	-0.293	-	0.536	-	-0.076	-
CaO	0.011	-	0.290	-	0.126	-
Na <sub>2</sub> O	-0.005	-	-0.035	-	-0.769	>95%
K <sub>2</sub> O	-0.427	>95%	0.226	-	-0.766	>95%
FeO/ (FeO+MgO)	-0.451	>95%	0.197	-	-0.103	-
A-site.	0.037	-	0.185	-	-0.497	-
Mg#	0.443	>95%	-0.202	-	0.102	-
Ionic Porosity (Z).	-0.487	>99%	0.055	-	-0.117	-
Plag. Alt. Index.	-0.084	-	-	-	-0.342	-

**TABLE 5.4** Correlation coefficients (R) of K-Ar ages against in-situ hornblende EMPA analyses. Whole dataset comprises 29 samples. **Group-A** and **Group-B** are of 7 samples each.

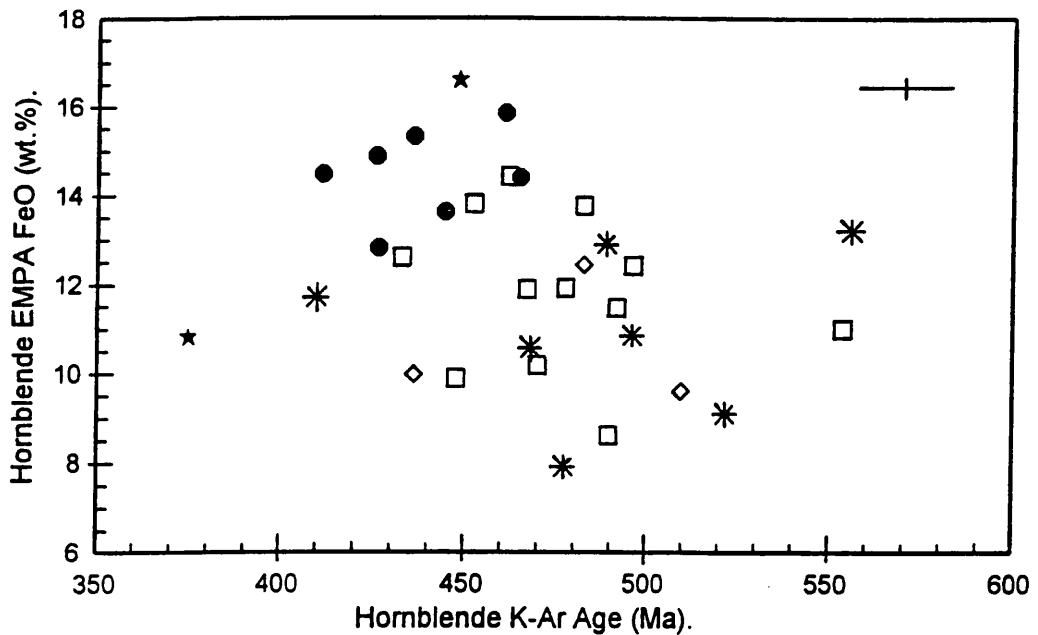


**FIGURE 5.9** Hornblende EMPA FeO versus K-Ar age.  $R$  for whole dataset =  $-0.368$  ( $>95\%$  significance). Symbols: **Group-A** = filled octagons; **Group-B** = asterisks; **Group-C** = open diamonds; others = open squares; MGS = black stars. Average horizontal error =  $\pm 13$ Ma; average vertical error =  $\pm 0.06$ wt.%.

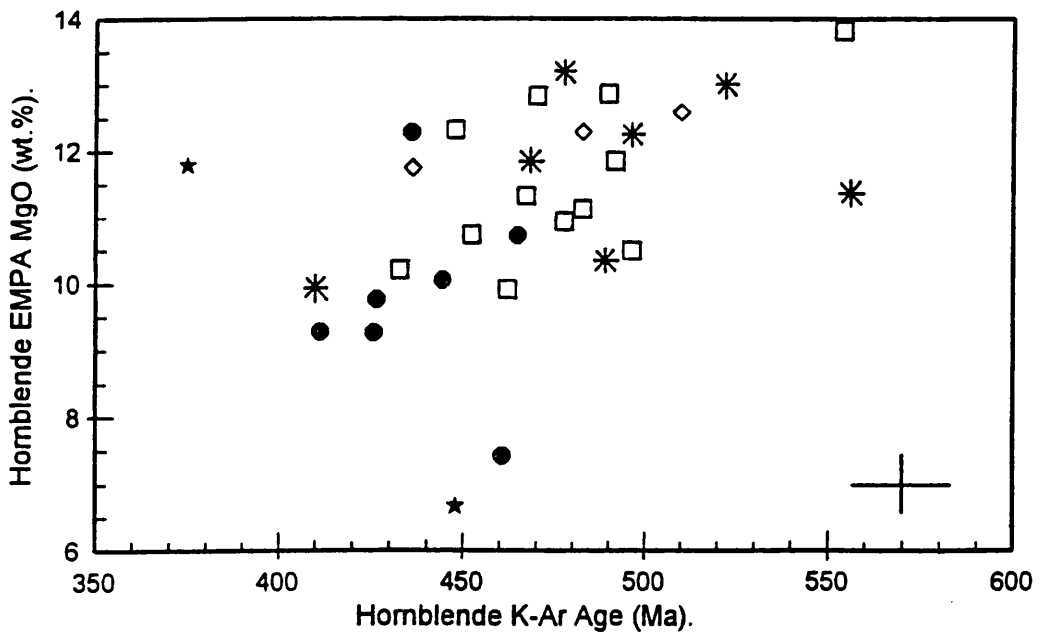


**FIGURE 5.10** Hornblende EMPA MgO versus K-Ar age.  $R$  for whole dataset =  $0.525$  ( $>99\%$  significance). Symbols: **Group-A** = filled octagons; **Group-B** = asterisks; **Group-C** = open diamonds; others = open squares; MGS = black stars. Average horizontal error =  $\pm 13$ Ma; average vertical error =  $\pm 0.57$ wt.%.

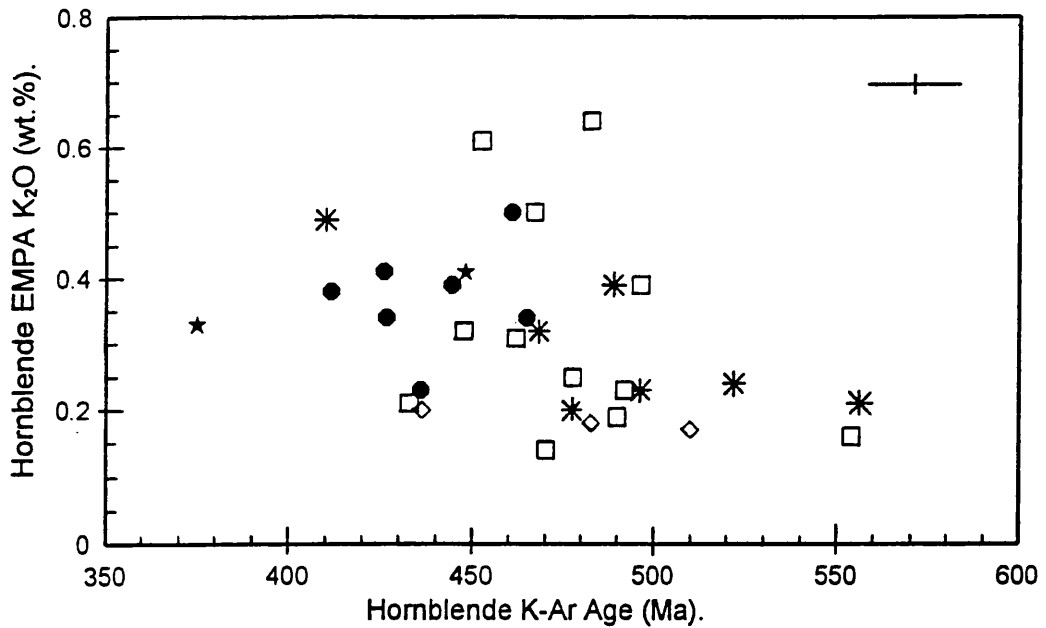


**FIGURE 5.11** Hornblende EMPA  $K_2O$  versus K-Ar age.  $R$  for whole dataset =  $-0.427$  ( $>95\%$  significance).  $R$  for **Group-B** =  $-0.766$  ( $>95\%$  significance). Symbols: **Group-A** = filled octagons; **Group-B** = asterisks; **Group-C** = open diamonds; others = open squares; MGS = black stars. Average horizontal error =  $\pm 13$ Ma; average vertical error =  $\pm 0.06$ wt.%.

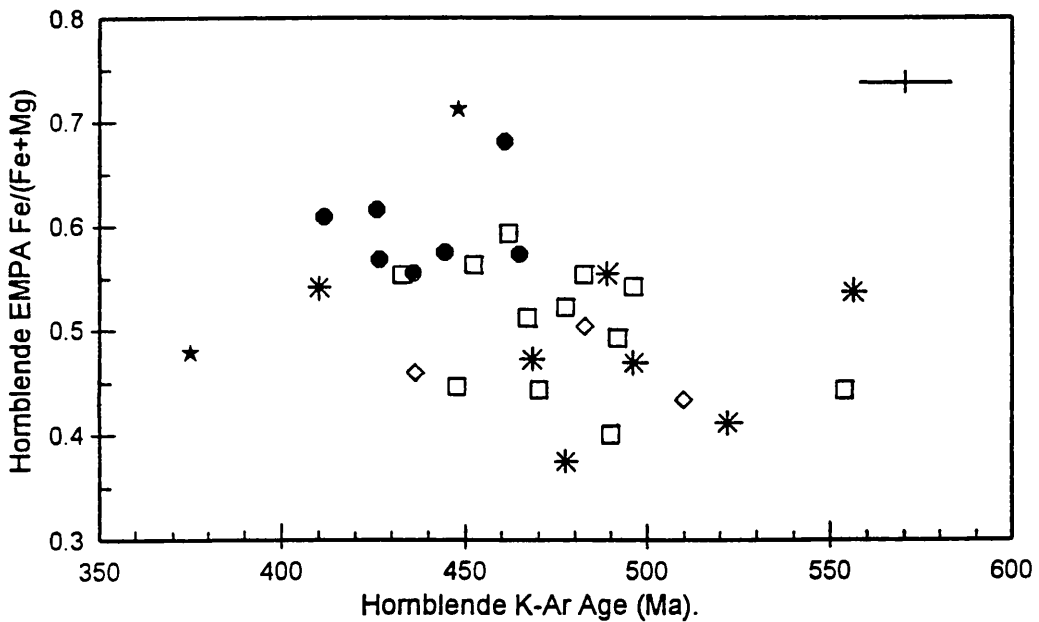


**FIGURE 5.12** Hornblende EMPA  $FeO/(FeO+MgO)$  versus K-Ar age.  $R$  for whole dataset =  $-0.451$  ( $>95\%$  significance). Symbols: **Group-A** = filled octagons; **Group-B** = asterisks; **Group-C** = open diamonds; others = open squares; MGS = black stars. Average horizontal error =  $\pm 13$ Ma; average vertical error =  $\pm 0.016$ .

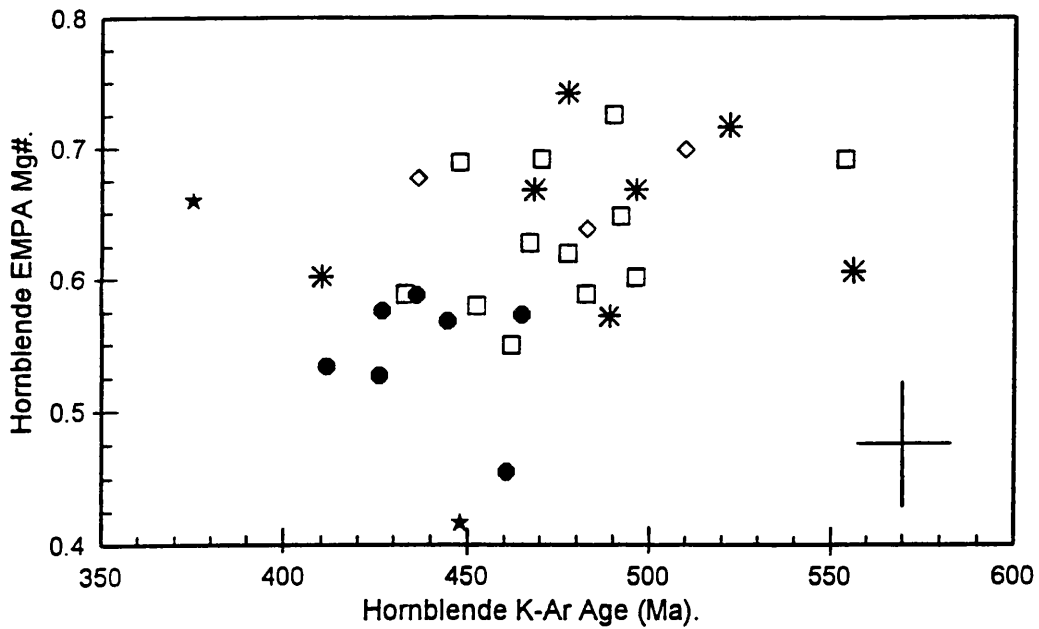


**FIGURE 5.13** Hornblende EMPA Mg# versus K-Ar age.  $R$  for whole dataset = 0.443 (>95% significance). Symbols: **Group-A** = filled octagons; **Group-B** = asterisks; **Group-C** = open diamonds; others = open squares; MGS = black stars. Average horizontal error =  $\pm 13$ Ma; average vertical error =  $\pm 0.051$ .

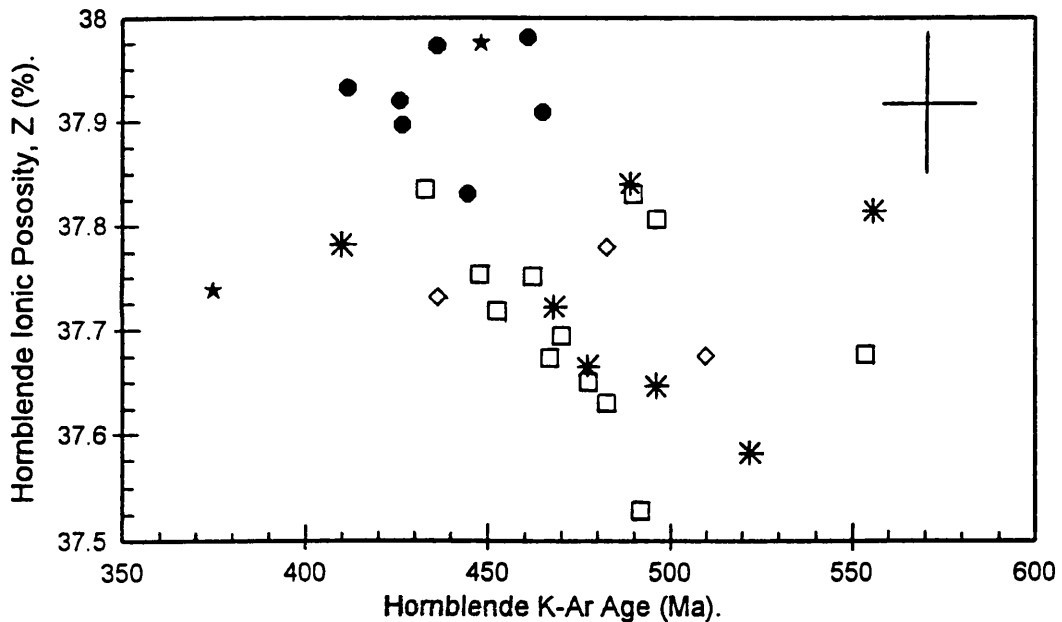


**FIGURE 5.14** Hornblende EMPA derived ionic porosity,  $Z$ , versus K-Ar age.  $R$  for whole dataset = -0.487 (>99% significance). Symbols: **Group-A** = filled octagons; **Group-B** = asterisks; **Group-C** = open diamonds; others = open squares; MGS = black stars. Average horizontal error =  $\pm 13$ Ma; average vertical error =  $\pm 0.078$ .

### 5.3 Hornblende $\delta D$ Values.

The results of the hornblende and muscovite mineral  $\delta D$  determinations are in Appendix 10. Table 5.5 gives a list of the mineral  $\delta D$  values for reference within this chapter. Figure 5.15 shows the mineral  $\delta D$  value distribution of these samples in relation to their geographical locations in Connemara.

The range of  $\delta D$  values determined for the hornblende mineral separates investigated is from -39‰ to -63‰ (TJ-11 to TJ-37 and TJ-38). The average  $\delta D$  value for the whole hornblende dataset (excluding TJ-1 and TJ-59) is -53‰ (SD = 7‰).

The range for **Group-A** is -40‰ to -57‰ (TJ-7E to TJ-7F); group average is -49‰ (SD = 6‰). The range for **Group-B** is -51‰ to -63‰ (TJ-39 to TJ-37 and TJ-38); group average is -60‰ (SD = 4‰). **Group-B** does not show such a large variation in  $\delta D$  as for K-Ar age values relative to **Group-A**. Although the two groups do have distinctly different averages.

The geographical distribution of  $\delta D$  values in Figure 5.15 display no obvious trends. However, local clusters of similar values are observed.

#### 5.3.1 $\delta D$ Values - Water Contents and K-Ar Ages.

Figure 5.16 demonstrates a decrease in hornblende water content with increasing hornblende  $\delta D$  value (both in Appendix 10). This is the opposite to that found by Miller et al. (1991) (Figure 1.4(c)). Apart from TJ-44 (containing biotite in cleavages, Figure 3.5), there are no other hornblendes with water contents above 2.4wt.% as found by Miller et al. (1991). A cluster of four samples occurs at ~2.3wt.%, but these correspond to lower  $\delta D$  values, unlike the higher water content - higher  $\delta D$  value relationship of Figure 1.4(c). The connection of water contents with hornblende composition is more fully discussed in Chapter 6.

Figure 5.17 shows a very strong correlation of decrease in hornblende K-Ar ages (Appendix 9) with increasing hornblende  $\delta D$  values. This agrees very well with the findings of Miller et al. (1991), postulating an influence of the isotopic exchange mechanism of

hydrogen and deuterium (as OH<sup>-</sup> or OD<sup>-</sup>) in disturbing hornblende K-Ar ages. Also, the relationships between average  $\delta D$  values, ages and water contents for **Group-A** and **Group-B** reinforce the general trends observed (standard deviations of the group averages are given in brackets):

	<b>Group-A.</b>	<b>Group-B.</b>
Av. $\delta D$ value.	-49‰ (SD = 6‰).	-60‰ (SD = 4‰).
Av. K-Ar Age.	439Ma (SD = 19Ma).	489Ma (SD = 46Ma).
Av. Water Content.	1.85wt.% (SD = 0.20wt.%).	2.08wt.% (SD = 0.22wt.%).

### 5.3.2 $\delta D$ Values - Rock XRF.

From regression analysis of hornblende  $\delta D$  values against rock XRF analyses (Table 5.6) correlations are present of  $\delta D$  with MgO and FeO/(FeO+MgO) for the hornblende whole dataset of 29 samples (**TJ-1** which is very far off trend at -90‰ and **TJ-59** are excluded). There is also a correlation of  $\delta D$  with CO<sub>2</sub> in **Group-B**, but this is not observed in the whole dataset or **Group-A**. Although below the accepted values for correlation, **Group-B** also has high R values for  $\delta D$  against Fe<sub>2</sub>O<sub>3</sub> and FeO.

The inference from this information is that  $\delta D$  values are related to the mafic nature and the Fe/Mg ratio of the rock analyses. Figures 5.18 and 5.19 respectively show the negative trend of MgO and positive trend of FeO/(FeO+MgO) for the 29 samples. **Group-A** and **Group-B** averages of  $\delta D$  values relative to averages for these analyses also reinforce these trends (standard deviations for the group averages are given in brackets):

	<b>Group-A.</b>	<b>Group-B.</b>
Av. $\delta D$ value.	-49‰ (SD = 6‰).	-60‰ (SD = 4‰).
Av. MgO	6.86wt.% (SD = 1.24wt.%).	9.75wt.% (SD = 2.17wt.%).
Av. FeO/(FeO+MgO)	0.603 (SD = 0.051).	0.482 (SD = 0.052).

### 5.3.3 $\delta$ D Values - Wet Chemical Analysis of Hornblendes.

From Table 5.7 correlations are present in the hornblende mineral separates of hornblende  $\delta$ D values with MgO and FeO/(FeO+MgO) in the hornblende whole dataset of 29 samples and with Na<sub>2</sub>O and K<sub>2</sub>O in **Group-B**. An elevated R value is observed for FeO in **Group-B**.

This shows again a negative correlation of hornblende  $\delta$ D values with MgO and positive with FeO/(FeO+MgO). **Group-A** and **Group-B** again show the same relative positions as with the rock XRF analyses (standard deviations of group averages are given in brackets):

	<b>Group-A.</b>	<b>Group-B.</b>
Av. $\delta$ D value.	-49‰ (SD = 6‰).	-60‰ (SD = 4‰).
Av. MgO	9.97wt.% (SD = 1.54wt.%).	11.24wt.% (SD = 1.38wt.%).
Av. FeO/(FeO+MgO)	0.594 (SD = 0.058).	0.504 (SD = 0.062).

### 5.3.4 $\delta$ D Values - Hornblende EMPA.

Sample **TJ-29** gave very different values for K<sub>2</sub>O content from wet chemical analysis (0.77wt.%) to EMPA (0.21wt.%). It was felt that the EMPA results for this sample are not representative and have not been used in these evaluations. Thus the whole dataset used for these evaluations are of 28 samples (excluding **TJ-1**, **TJ-29** and **TJ-59**).

The R values in Table 5.8 show correlations of  $\delta$ D values with FeO, MgO, FeO/(FeO+MgO) and Mg# in the hornblende whole dataset of 28 samples. However, Z is just under the requirement for >90% significant correlation. **Group-B** shows correlations of  $\delta$ D values with SiO<sub>2</sub> and Na<sub>2</sub>O and high R values for Al<sub>2</sub>O<sub>3</sub>, Fe<sub>2</sub>O<sub>3</sub>, K<sub>2</sub>O and A-site occupancy. **Group-A** shows no reliable correlations at all.

The relative values of **Group-A** and **Group-B** to each other reflect the above correlations also (standard deviations for the group averages are given in brackets):

	<b>Group-A.</b>	<b>Group-B.</b>
Av. $\delta D$ value.	-49‰ (SD = 6‰).	-60‰ (SD = 4‰).
Av. FeO	14.48wt.% (SD = 1.02wt.%).	10.89wt.% (SD = 1.92wt.%).
Av. MgO	9.83wt.% (SD = 1.49wt.%).	11.71wt.% (SD = 1.25wt.%).
Av. FeO/(FeO+MgO)	0.597 (SD = 0.043).	0.480 (SD = 0.069).
Av. Mg#	0.546 (SD = 0.046).	0.654 (SD = 0.063).

### 5.3.5 Summary of $\delta D$ Values - Rock and Bulk Hornblende Compositions.

The observed trend of increasing hornblende  $\delta D$  values with decreasing hornblende K-Ar ages by Miller et al. (1991) is strongly supported by the findings of this work. However, the correlation they observed with water content is the opposite. In fact, the water contents correlate with the chemical composition of the hornblendes, the Mg-rich hornblendes being higher in water content than their Fe-rich counterparts (Appendix 10). This is more fully discussed in Chapter 6; Section 6.3.

From the comparison of data there would appear to be a connection between the hornblende characterisation results; decreasing K-Ar age corresponds to increasing  $\delta D$  values and increasing ionic porosity. This suggests a chemical composition control of the observed interrelationships of isotopic phenomena in the hornblendes investigated.

The fluid composition derived from hornblende  $\delta D$  values is discussed in context with the  $\delta^{18}O$  values in Section 5.4.

Hornblende Sample.	$\delta D_{\text{HORNBLLENDE}}$ ( $\pm 1.5\text{‰}$ ).	Hornblende Sample.	$\delta D_{\text{HORNBLLENDE}}$ ( $\pm 1.5\text{‰}$ ).
TJ-1	-90‰	TJ-35	-60‰
TJ-7A	-49‰	TJ-36	-61‰
TJ-7B	-45‰	TJ-37	-63‰
TJ-7D	-54‰	TJ-38	-63‰
TJ-7E	-40‰	TJ-39	-51‰
TJ-7F	-57‰	TJ-40	-58‰
TJ-7G	-49‰	TJ-41	-62‰
TJ-7H	-52‰	TJ-43	-52‰
TJ-8	-52‰	TJ-44	-52‰
TJ-9	-53‰	TJ-45	-52‰
TJ-11	-39‰	TJ-46	-59‰
TJ-13	-56‰	TJ-47	-52‰
TJ-17	-44‰	TJ-48	-52‰
TJ-19	-62‰	TJ-54	-39‰
TJ-29	-50‰	TJ-59	-46‰
TJ-31	-47‰		
Muscovite Sample.	$\delta D_{\text{MUSCOVITE}}$ ( $\pm 1.5\text{‰}$ ).	Muscovite Sample.	$\delta D_{\text{MUSCOVITE}}$ ( $\pm 1.5\text{‰}$ ).
TJ-10	-40‰	TJ-22	-45‰
TJ-16	-23‰	TJ-50	-49‰
TJ-18	-36‰	TJ-53	-40‰

**TABLE 5.5**  $\delta D_{\text{MINERAL}}$  values of hornblende mineral separates (upper table) and muscovite mineral separates (lower table). Full details of  $\delta D$  results are in Appendix 10.

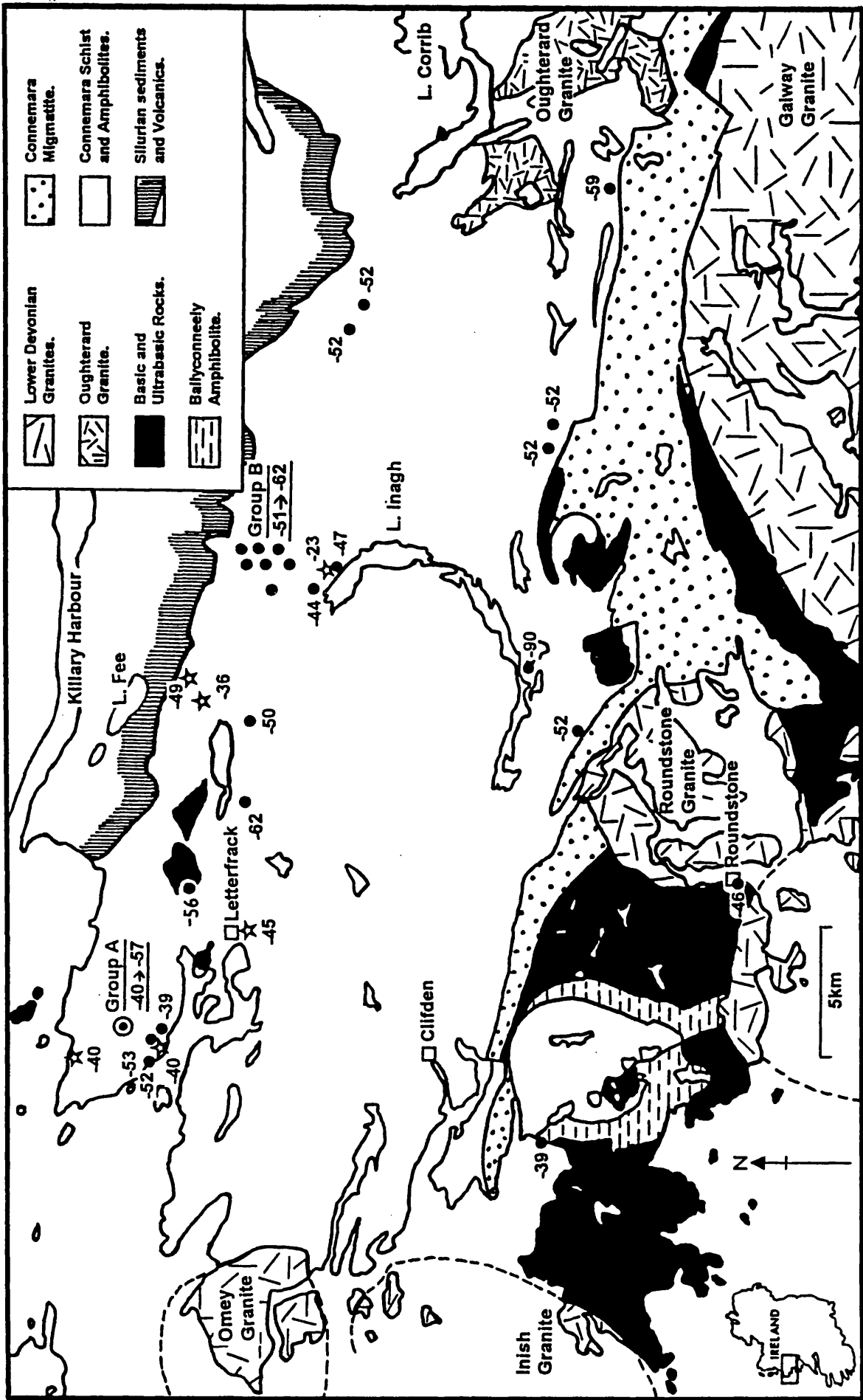


**FIGURE 5.15** Map of Connemara showing  $\delta D$  values (‰) of samples at locations collected. Filled circles represent hornblendes and open stars represent muscovites. Group-A is identified by a concentric circle symbol. Group-B is a locally clustered group of 7 samples.

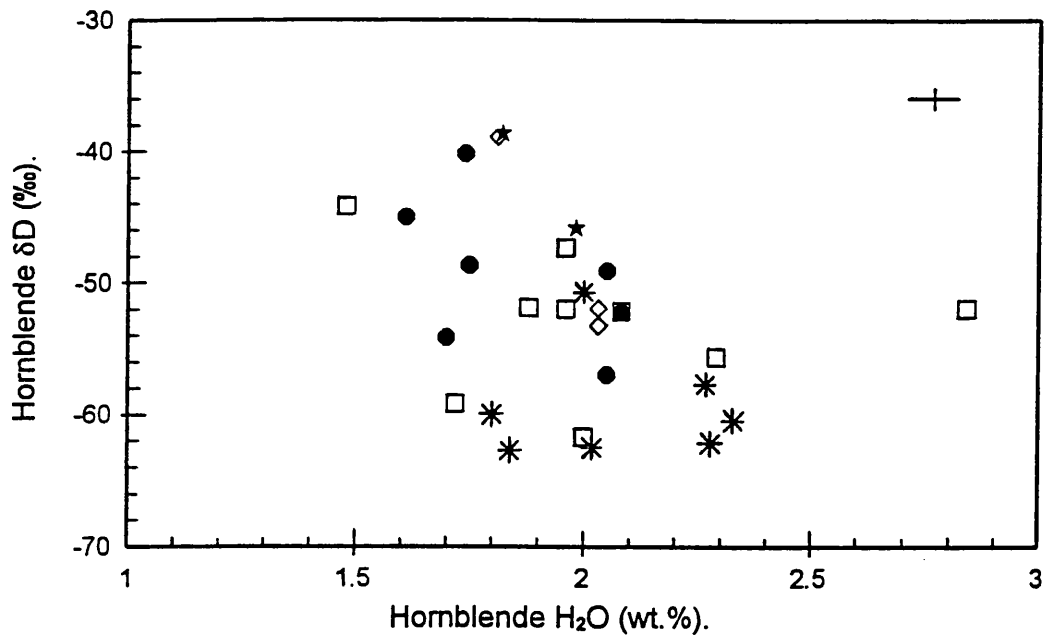


**FIGURE 5.16** Hornblende  $\delta D$  versus  $H_2O$  content.  $R$  for whole dataset =  $-0.371$  ( $>95\%$  significance). Symbols: **Group-A** = filled octagons; **Group-B** = asterisks; **Group-C** = open diamonds; others = open squares; MGS = black stars. Average vertical error =  $\pm 1.5\%$ ; average horizontal error =  $\pm 0.06\text{wt.}\%$ .

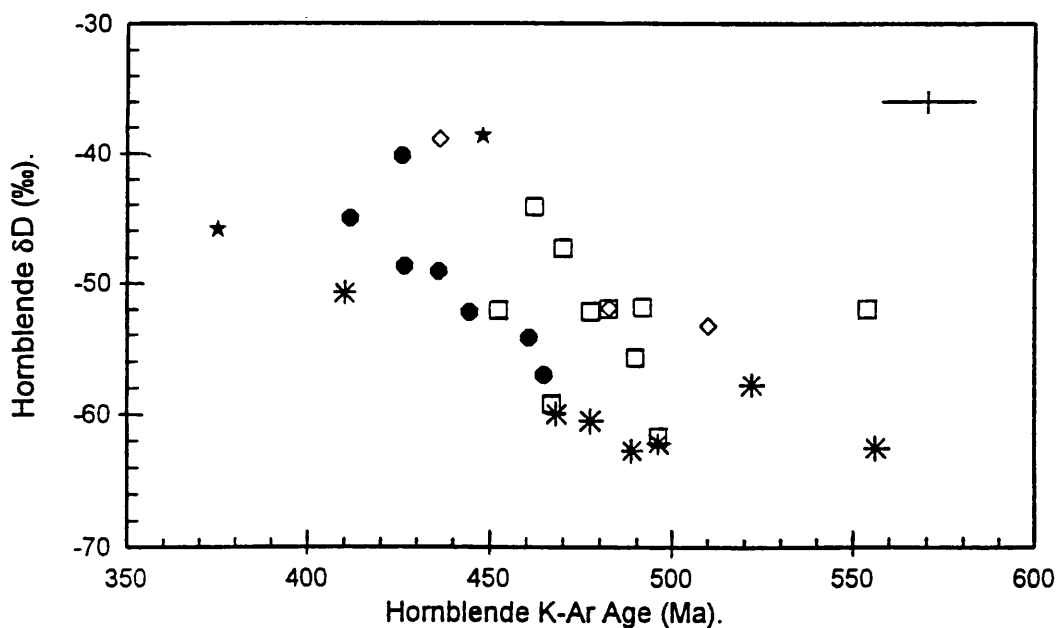


**FIGURE 5.17** Hornblende  $\delta D$  versus K-Ar age.  $R$  for whole dataset =  $-0.582$  ( $>99.9\%$  significance).  $R$  for **Group-A** =  $-0.858$  ( $>95\%$  significance).  $R$  for **Group-B** =  $-0.719$  ( $>90\%$  significance). Symbols: **Group-A** = filled octagons; **Group-B** = asterisks; **Group-C** = open diamonds; others = open squares; MGS = black stars. Average vertical error =  $\pm 1.5\%$ ; average horizontal error =  $\pm 13\text{Ma}$ .

Rock XRF: Oxides.	R Dataset (29).	Probability of Trend.	R Group-A (7).	Probability of Trend.	R Group-B (7).	Probability of Trend.
SiO <sub>2</sub>	-0.191	-	-0.245	-	0.346	-
TiO <sub>2</sub>	0.158	-	0.186	-	0.050	-
Al <sub>2</sub> O <sub>3</sub>	0.209	-	0.075	-	0.059	-
Fe <sub>2</sub> O <sub>3</sub>	0.250	-	0.057	-	0.685	-
FeO	0.209	-	-0.476	-	-0.667	-
MgO	-0.395	>95%	0.050	-	-0.376	-
MnO	0.039	-	-0.046	-	-0.467	-
CaO	0.111	-	-0.082	-	-0.097	-
Na <sub>2</sub> O	0.275	-	0.410	-	0.209	-
K <sub>2</sub> O	-0.112	-	0.314	-	0.208	-
P <sub>2</sub> O <sub>5</sub>	-0.014	-	-0.201	-	-0.144	-
CO <sub>2</sub>	0.139	-	0.359	-	0.812	>95%
H <sub>2</sub> O	-0.143	-	-0.458	-	-0.037	-
FeO/ (FeO+MgO)	0.381	>95%	-0.192	-	0.122	-

**TABLE 5.6** Correlation coefficients (R) of  $\delta D$  values against rock XRF, FeO, H<sub>2</sub>O and CO<sub>2</sub> determinations. Whole dataset comprises 29 samples. **Group-A** and **Group-B** are of 7 samples each.

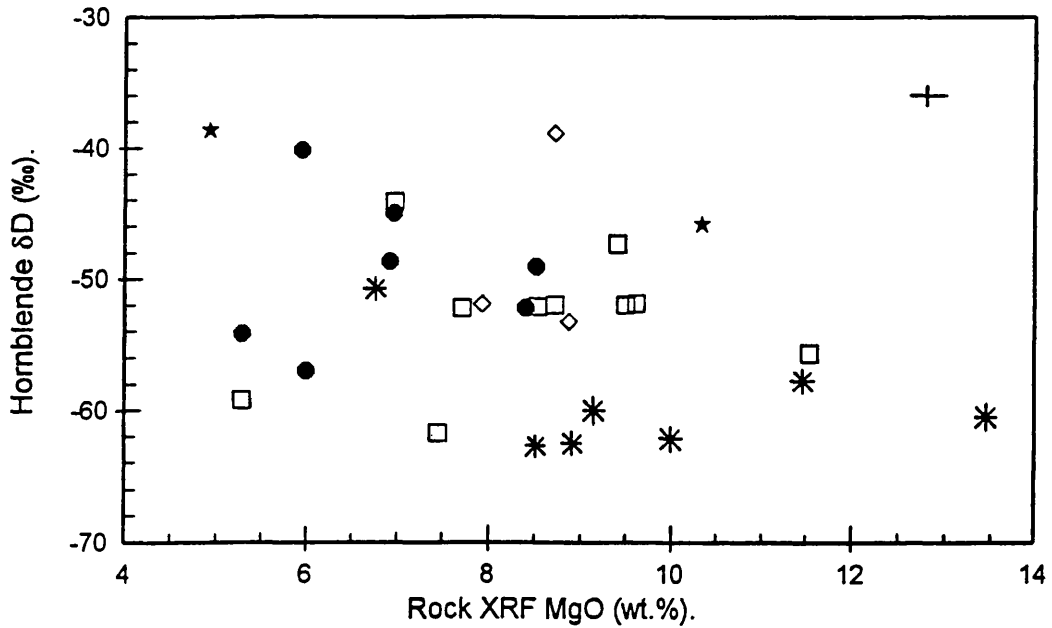


**FIGURE 5.18** Hornblende  $\delta D$  versus rock XRF MgO.  $R$  for whole dataset = -0.395 (>95% significance). Symbols: **Group-A** = filled octagons; **Group-B** = asterisks; **Group-C** = open diamonds; others = open squares; MGS = black stars. Average vertical error =  $\pm 1.5\%$ ; average horizontal error =  $\pm 0.21\text{wt.}\%$ .

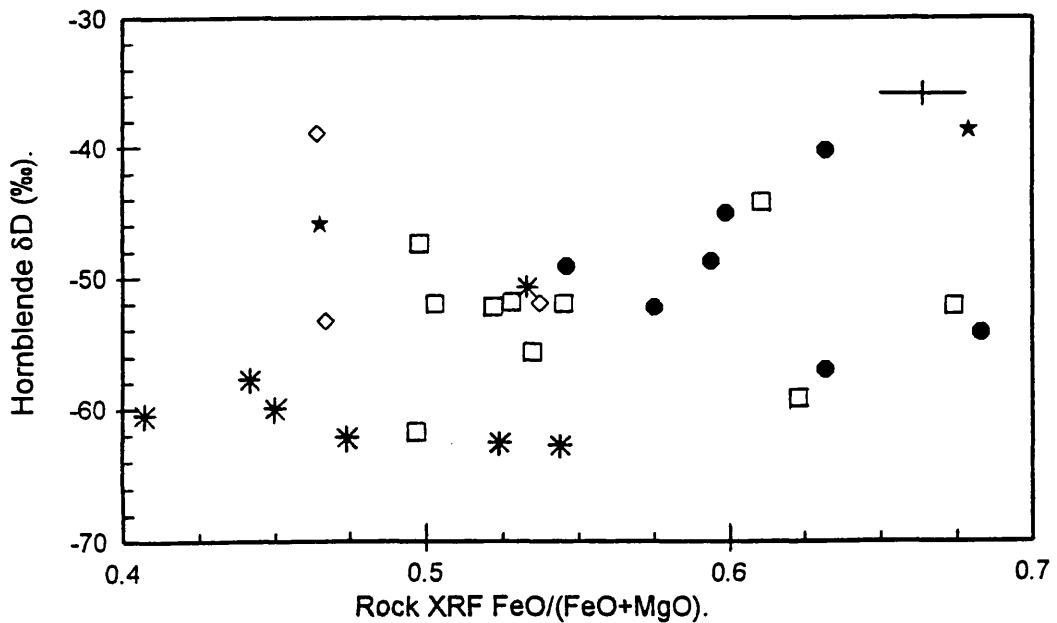


**FIGURE 5.19** Hornblende  $\delta D$  versus rock XRF FeO/(FeO+MgO).  $R$  for whole dataset = 0.381 (>95% significance). Symbols: **Group-A** = filled octagons; **Group-B** = asterisks; **Group-C** = open diamonds; others = open squares; MGS = black stars. Average vertical error =  $\pm 1.5\%$ ; average horizontal error =  $\pm 0.014$ .

Hornblende Chemical Analyses: Oxides.	R Dataset (29).	Probability of Trend.	R Group-A (7).	Probability of Trend.	R Group-B (7).	Probability of Trend.
Fe <sub>2</sub> O <sub>3</sub>	0.042	-	-0.203	-	0.337	-
FeO	0.114	-	-0.172	-	-0.516	-
MgO	-0.377	>95%	-0.041	-	-0.296	-
CaO	0.142	-	0.343	-	-0.321	-
Na <sub>2</sub> O	0.263	-	0.186	-	0.729	>90%
K <sub>2</sub> O	0.094	-	0.097	-	0.759	>95%
FeO/ (FeO+MgO)	0.328	>90%	-0.043	-	-0.158	-

**TABLE 5.7** Correlation coefficients (R) of  $\delta D$  values against hornblende mineral separates wet chemical analyses. Whole dataset comprises 29 samples. **Group-A** and **Group-B** are of 7 samples each.

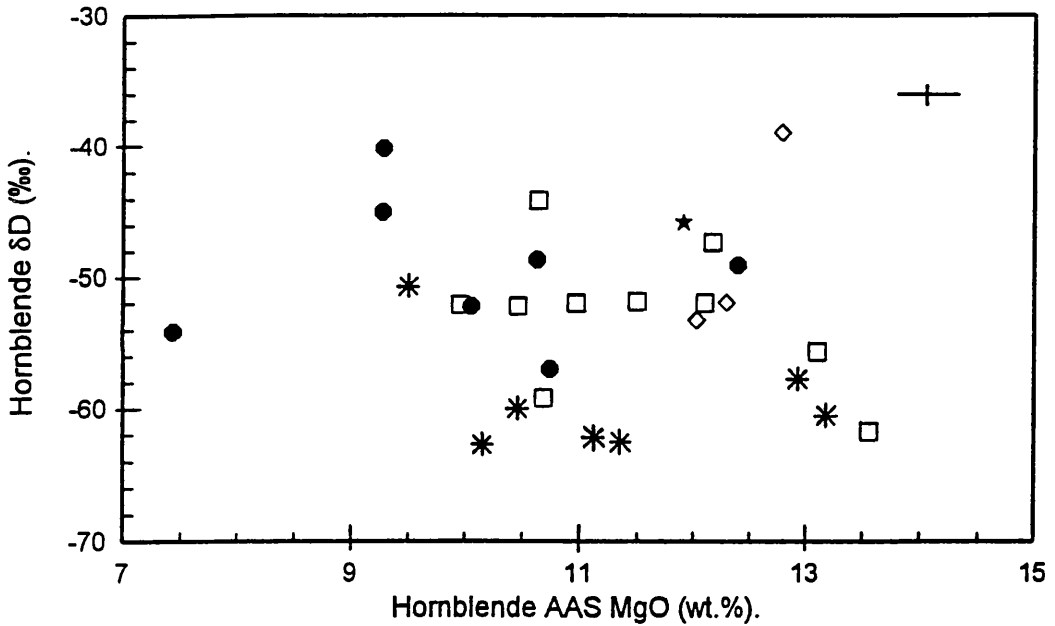


**FIGURE 5.20** Hornblende  $\delta D$  versus AAS MgO.  $R$  for whole dataset =  $-0.377$  ( $>95\%$  significance). Symbols: **Group-A** = filled octagons; **Group-B** = asterisks; **Group-C** = open diamonds; others = open squares; MGS = black stars. Average vertical error =  $\pm 1.5\%$ ; average horizontal error =  $\pm 0.30\text{wt.}\%$ .

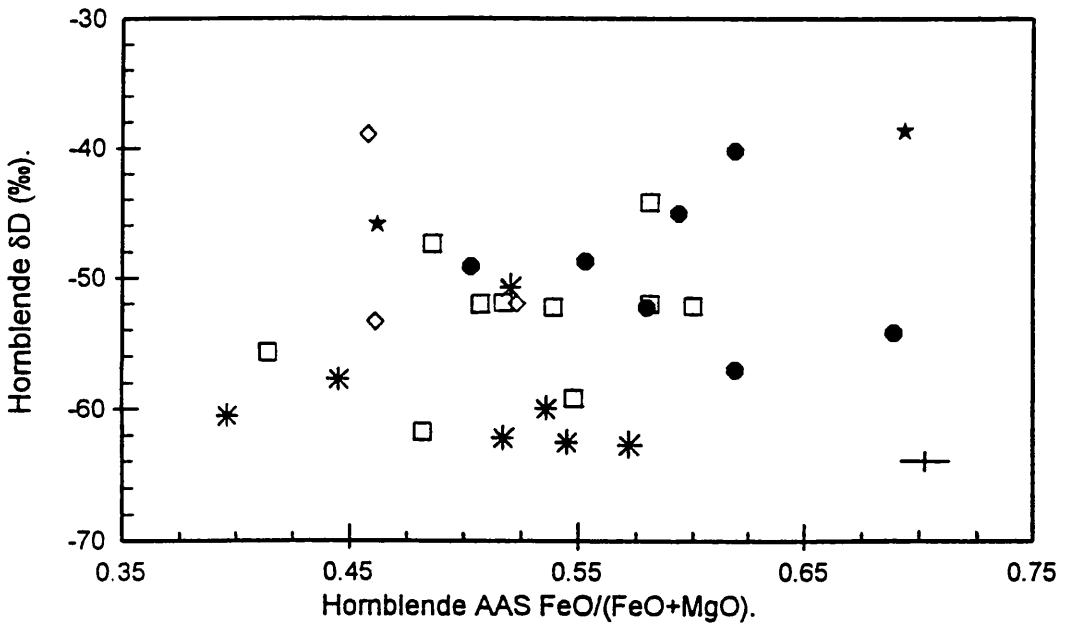


**FIGURE 5.21** Hornblende  $\delta D$  versus AAS FeO/(FeO+MgO).  $R$  for whole dataset =  $0.328$  ( $>90\%$  significance). Symbols: **Group-A** = filled octagons; **Group-B** = asterisks; **Group-C** = open diamonds; others = open squares; MGS = black stars. Average vertical error =  $\pm 1.5\%$ ; average horizontal error =  $\pm 0.010$ .

Hornblende EMPA: Oxides.	R Dataset (28).	Probability of Trend.	R Group-A (7).	Probability of Trend.	R Group-B (7).	Probability of Trend.
SiO <sub>2</sub>	-0.196	-	0.045	-	-0.709	>90%
TiO <sub>2</sub>	-0.010	-	0.203	-	0.213	-
Al <sub>2</sub> O <sub>3</sub>	0.011	-	0.068	-	0.548	-
Fe <sub>2</sub> O <sub>3</sub>	0.096	-	-0.057	-	0.599	-
FeO	0.374	>95%	-0.024	-	-0.125	-
MgO	-0.393	>95%	-0.056	-	-0.344	-
MnO	0.197	-	-0.071	-	0.184	-
CaO	-0.179	-	-0.445	-	-0.266	-
Na <sub>2</sub> O	0.185	-	0.231	-	0.765	>95%
K <sub>2</sub> O	0.048	-	-0.036	-	0.658	-
FeO/ (FeO+MgO)	0.401	>95%	0.026	-	0.082	-
A-site.	0.098	-	-0.043	-	0.626	-
Mg#	-0.399	>95%	-0.017	-	-0.043	-
Ionic Porosity (Z).	0.305	-	0.060	-	-0.048	-
Plag. Alt. Index.	0.238	-	-	-	-0.215	-

**TABLE 5.8** Correlation coefficients (R) of  $\delta D$  values against in-situ hornblende EMPA analyses. Whole dataset comprises 28 samples. **Group-A** and **Group-B** are of 7 samples each.

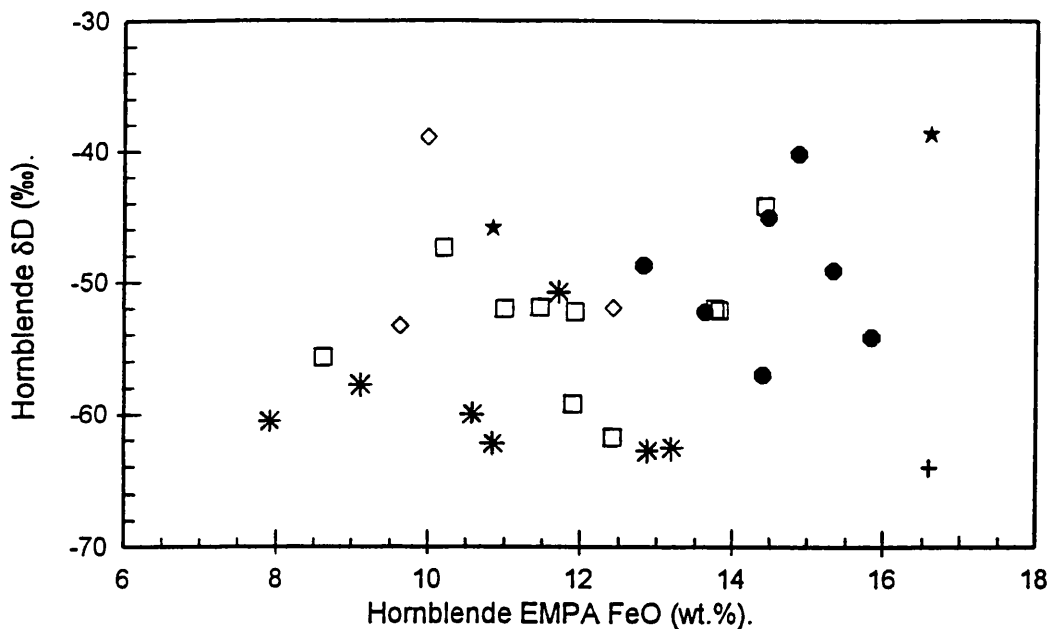


**FIGURE 5.22** Hornblende  $\delta D$  versus EMPA FeO. R for whole dataset = 0.374 (>95% significance). Symbols: **Group-A** = filled octagons; **Group-B** = asterisks; **Group-C** = open diamonds; others = open squares; MGS = black stars. Average vertical error =  $\pm 1.5\text{‰}$ ; average horizontal error =  $\pm 0.06\text{wt.}\%$ .

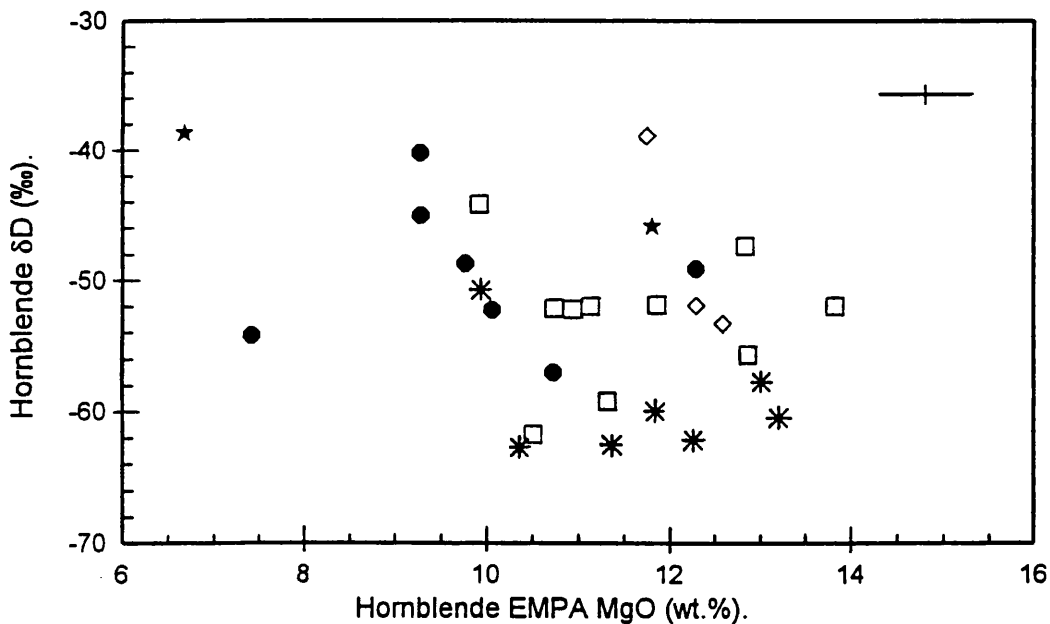


**FIGURE 5.23** Hornblende  $\delta D$  versus EMPA MgO. R for whole dataset = -0.393 (>95% significance). Symbols: **Group-A** = filled octagons; **Group-B** = asterisks; **Group-C** = open diamonds; others = open squares; MGS = black stars. Average vertical error =  $\pm 1.5\text{‰}$ ; average horizontal error =  $\pm 0.57\text{wt.}\%$ .

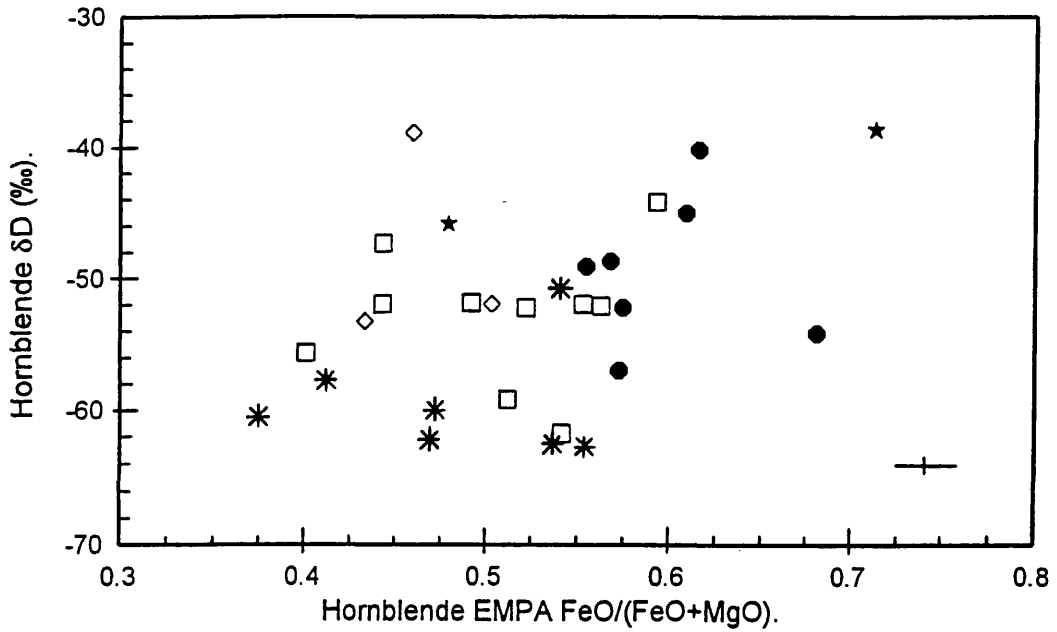


**FIGURE 5.24** Hornblende  $\delta D$  versus EMPA  $FeO/(FeO+MgO)$ .  $R$  for whole dataset = 0.401 (>95% significance). Symbols: **Group-A** = filled octagons; **Group-B** = asterisks; **Group-C** = open diamonds; others = open squares; MGS = black stars. Average vertical error =  $\pm 1.5\%$ ; average horizontal error =  $\pm 0.016$ .

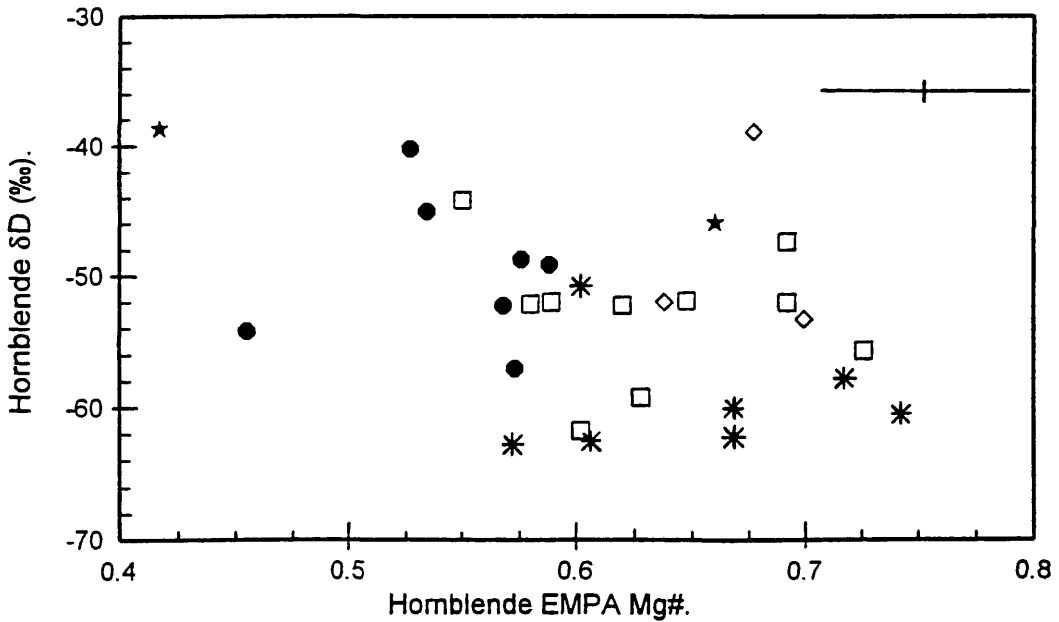


**FIGURE 5.25** Hornblende  $\delta D$  versus EMPA  $Mg\#$ .  $R$  for whole dataset = -0.399 (>95% significance). Symbols: **Group-A** = filled octagons; **Group-B** = asterisks; **Group-C** = open diamonds; others = open squares; MGS = black stars. Average vertical error =  $\pm 1.5\%$ ; average horizontal error =  $\pm 0.051$ .

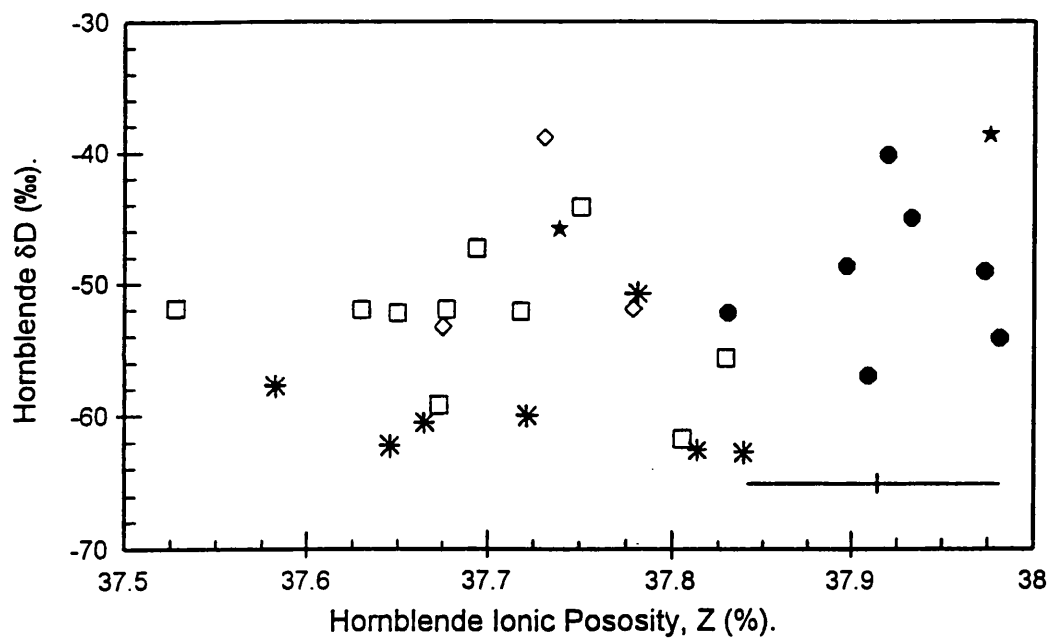


**FIGURE 5.26** Hornblende  $\delta D$  versus EMPA derived ionic positivity,  $Z$ .  $R$  for whole dataset = 0.305 (just below criteria for 90% significance). Symbols: **Group-A** = filled octagons; **Group-B** = asterisks; **Group-C** = open diamonds; others = open squares; MGS = black stars. Average vertical error =  $\pm 1.5\%$ ; average horizontal error =  $\pm 0.078$ .

## 5.4 Hornblende $\delta^{18}\text{O}$ Values.

The results of the hornblende and muscovite  $\delta^{18}\text{O}$  determinations are listed in Appendix 11. Table 5.9 gives a list of the mineral  $\delta^{18}\text{O}$  values for reference within this chapter. Figure 5.27 shows the mineral  $\delta^{18}\text{O}$  value distribution of these samples in relation to their geographical locations in Connemara.

The range of  $\delta^{18}\text{O}$  values determined for the hornblende mineral separates investigated is from +4.9‰ (TJ-9) to +9.3‰ (TJ-41 and TJ-47). The average is +7.1‰ (SD = 1.2‰) for the hornblende whole dataset of 30 samples (excluding TJ-59).

The range for **Group-A** is +5.0‰ to +8.6‰ (TJ-7D to TJ-7H); group average is +6.7‰ (SD = 1.3‰). The range for **Group-B** is +7.0‰ to +9.3‰ (TJ-36 to TJ-41); group average is 7.9‰ (SD = 0.9‰).

The geographical distribution of mineral  $\delta^{18}\text{O}$  values in Figure 5.27 shows no significant trends. However, local clusters of similar values are observed.

### 5.4.1 $\delta^{18}\text{O}$ Values - K-Ar Ages and Fluid $\delta\text{D}$ Values.

Figure 5.28 of  $\delta^{18}\text{O}$  values against hornblende K-Ar ages shows no correlation present at all, unlike the hornblende  $\delta\text{D}$  values against K-Ar ages where a strong correlation is observed (Figure 5.17). Figure 5.29 shows a general relationship of increasing hornblende  $\delta\text{D}$  values against decreasing hornblende  $\delta^{18}\text{O}$  values, however, this is just below the criterion for 90% probability of correlation. The left vertical axis of Figure 5.29 shows the measured hornblende  $\delta\text{D}$  values, whereas the right vertical axis shows the estimated fluid  $\delta\text{D}$  values for each sample (Appendix 10). This is due to the simple, temperature independent isotope fractionation factor of Graham et al. (1984), effectively displacing the fluid  $\delta\text{D}$  values to more deuterium rich levels:

$$1000\ln\alpha_{\text{HORNBLLENDE-WATER}} = -23.1\pm 2.5\text{‰} \quad \text{Equation 5.2}$$

The hydrogen isotope fractionation in hornblende is independent of temperature from 350°C to 650°C, but, from 650°C to 850°C it becomes a function of temperature (Graham et al., 1984). No data are reported for temperatures below 350°C, therefore the  $\delta D$  isotopic fractionation factor in the temperature range (270-340°C) of the activity of the retrograde fluid, RGF (O'Reilly et al., 1997), at ~400Ma has not been experimentally quantified. Equation 5.2 has been used to determine the fluid  $\delta D$  from the hornblende  $\delta D$  values in this temperature range.

Because of the range of hornblende  $\delta D$  values (-39 $\pm$ 1.5‰ to -63 $\pm$ 1.5‰) giving rise to the range of fluid  $\delta D$  values (-16 $\pm$ 1.5‰ to -40 $\pm$ 1.5‰) and the relationship with composition; Fe-rich hornblendes being more enriched in deuterium ( $\delta D = -39\pm 1.5\text{‰}$ ) from isotopic exchange with the RGF, Mg-rich hornblendes possibly retaining their original peak metamorphic (~600°C between 463Ma to 490Ma) hornblende  $\delta D$  values ( $\delta D = -63\pm 1.5\text{‰}$ ). It would appear that there has been a selective hydrogen isotope exchange due to the composition and ionic porosity of the hornblendes at these lower temperatures. Due to the lack of thermodynamic data for hornblende hydrogen isotopic fractionation at these temperatures the isotopic fractionation factor of Equation 5.2 (Graham et al., 1984) has been used as the closest approximation. For clarity, the  $\pm$  errors for  $\delta D$  are not shown beyond this point.

Also, due to the lack of thermodynamic information in the literature for the calculation of fluid  $\delta^{18}O$  from hornblende  $\delta^{18}O$ , especially at the temperatures of the retrograde fluid (RGF); 270-340°C (O'Reilly et al., 1997) the fluid  $\delta^{18}O$  values have not been calculated from the hornblende  $\delta^{18}O$  values (Appendix 11). The composition of the retrograde fluid of O'Reilly et al., (1997) is discussed fully in Chapter 6 (temperature = 270-340°C;  $\delta D = -18\pm 2\text{‰}$ ;  $\delta^{18}O = +0.5\text{‰}$  to  $+2.0\text{‰}$ ).

It has been estimated (Appendix 10) that a temperature of 470°C would have been required to give a fractionation factor of -21‰ to set the average muscovite  $\delta D$  value of -39‰ from a fluid  $\delta D$  value of -18‰. This temperature does not equate with other information known about the activities in Connemara in the period under investigation and

the relationship of muscovite  $\delta D$  values with the retrograde fluid and temperature range of 270-340°C is not understood from this present study.

From this work it is suspected that the  $\delta^{18}O$  values of the hornblendes and muscovites were set at the temperatures of formation of these minerals (>600°C) during the MGS intrusion related metamorphic peak between 463-490Ma (Friedrich et al., 1997; Cliff et al., 1996).

Figure 5.30 shows the progression of fluid  $\delta D$  values from  $\sim -40\text{‰}$  to  $\sim -16\text{‰}$ , from metamorphic/magmatic water to the  $\delta D$  value of the retrograde fluid (Jenkin et al., 1992). However, the  $\delta^{18}O$  values of the hornblende samples on this graph are the mineral values, set at time of peak metamorphism, not the retrograde fluid values. The  $\delta D$  values at  $\sim -16\text{‰}$  would be offset towards the RGF by the true retrograde fluid  $\delta^{18}O$  value on the diagram as indicated by the arrow.

#### 5.4.2 $\delta^{18}O$ Values - Rock XRF.

From regression analysis of  $\delta^{18}O$  values against rock XRF analyses (Table 5.10) a mild correlation only is present with MnO. **Group-A** shows some correlation with  $Fe_2O_3$  and  $P_2O_5$ . These are not observed in **Group-B** which shows elevated R values for  $SiO_2$  and MnO.

#### 5.4.3 $\delta^{18}O$ Values - Wet Chemical Analysis of Hornblendes.

Table 5.11 shows only a correlation of  $\delta^{18}O$  values with  $Fe_2O_3$  in **Group-B**. No other significant correlations are present.

#### 5.4.4 $\delta^{18}O$ Values - Hornblende EMPA.

The R values in Table 5.12 indicate correlations of  $\delta^{18}O$  values with  $Na_2O$ , A-site occupancy and Z for the whole dataset of 29 samples (TJ-29 and TJ-59 excluded). **Group-A** shows negative correlations with FeO, MnO and Z. **Group-B** also shows a correlation with MnO, but in this case it is positive. These opposing values for MnO

illustrate the difficulty of using the two groups only for deciding whether a correlation exists. The larger number of samples in the whole dataset is more representative.

Figures 5.30-5.32 respectively demonstrate the positive correlations of  $\delta^{18}\text{O}$  values with  $\text{Na}_2\text{O}$  and A-site occupancy and negative correlation with Z. These trends are reflected in the relative positions of **Group-A** and **Group-B** averages (standard deviations of the group averages are given in brackets):

	<b>Group-A.</b>	<b>Group-B.</b>
Av. $\delta^{18}\text{O}$	6.7‰ (SD = 1.3‰).	7.9‰ (SD = 0.9‰).
Av. $\text{Na}_2\text{O}$	1.08wt.% (SD = 0.25wt.%).	1.24wt.% (SD = 0.21wt.%).
Av. A-site value.	0.23	0.31
Av. Z.	37.921% (SD = 0.050%).	37.722% (SD = 0.095%).

The  $\delta^{18}\text{O}$  values show only very limited correlations with composition because they were set at the time of original formation of the hornblendes during the peak metamorphic grade.

Hornblende Sample.	$\delta^{18}\text{O}_{\text{HORNBLLENDE}}$ ( $\pm 0.15\text{‰}$ ).	Hornblende Sample.	$\delta^{18}\text{O}_{\text{HORNBLLENDE}}$ ( $\pm 0.15\text{‰}$ ).
TJ-1	+7.9‰	TJ-35	+7.4‰
TJ-7A	+8.0‰	TJ-36	+7.0‰
TJ-7B	+7.1‰	TJ-37	+7.3‰
TJ-7D	+5.0‰	TJ-38	+8.8‰
TJ-7E	+6.1‰	TJ-39	+7.8‰
TJ-7F	+6.5‰	TJ-40	+7.5‰
TJ-7G	+5.7‰	TJ-41	+9.3‰
TJ-7H	+8.6‰	TJ-43	+7.3‰
TJ-8	+6.1‰	TJ-44	+7.7‰
TJ-9	+4.9‰	TJ-45	+7.7‰
TJ-11	+5.3‰	TJ-46	+6.9‰
TJ-13	+7.1‰	TJ-47	+9.3‰
TJ-17	+6.7‰	TJ-48	+8.8‰
TJ-19	+6.0‰	TJ-54	+6.4‰
TJ-29	+6.2‰	TJ-59	+6.4‰
TJ-31	+7.5‰		
Muscovite Sample.	$\delta^{18}\text{O}_{\text{MUSCOVITE}}$ ( $\pm 0.15\text{‰}$ ).	Muscovite Sample.	$\delta^{18}\text{O}_{\text{MUSCOVITE}}$ ( $\pm 0.15\text{‰}$ ).
TJ-10	+11.3‰	TJ-22	+10.0‰
TJ-16	+12.0‰	TJ-50	+8.6‰
TJ-18	+8.9‰	TJ-53	+11.3‰

**TABLE 5.9**  $\delta^{18}\text{O}_{\text{MINERAL}}$  values of hornblende mineral separates (upper table) and muscovite mineral separates (lower table). Full details of the  $\delta^{18}\text{O}$  results in Appendix 11.

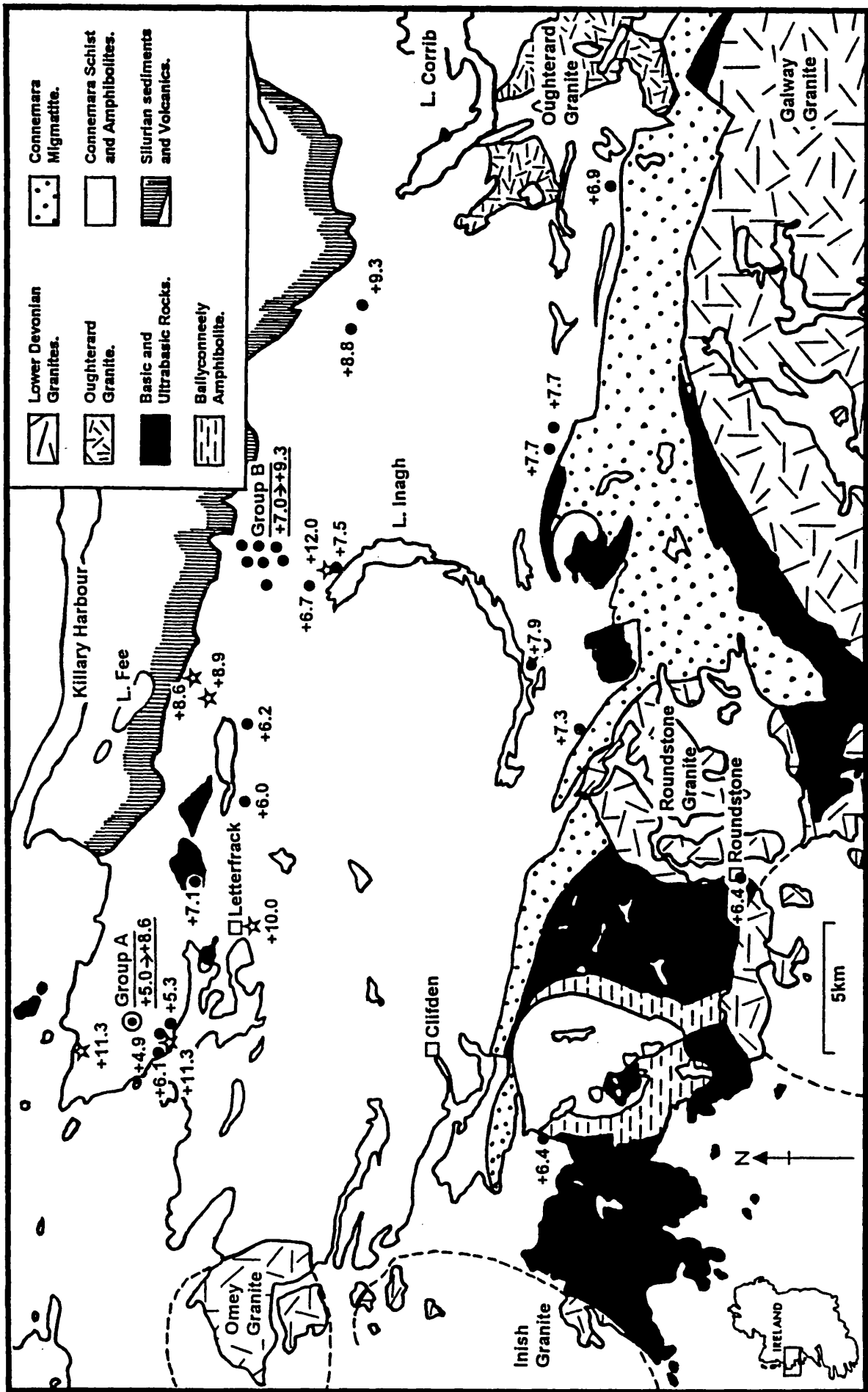
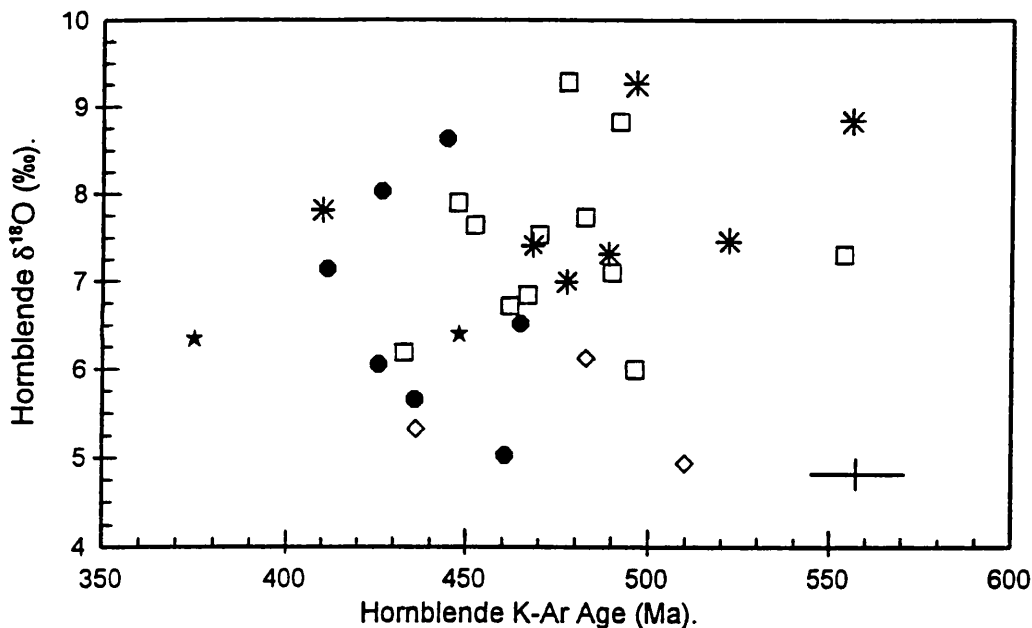
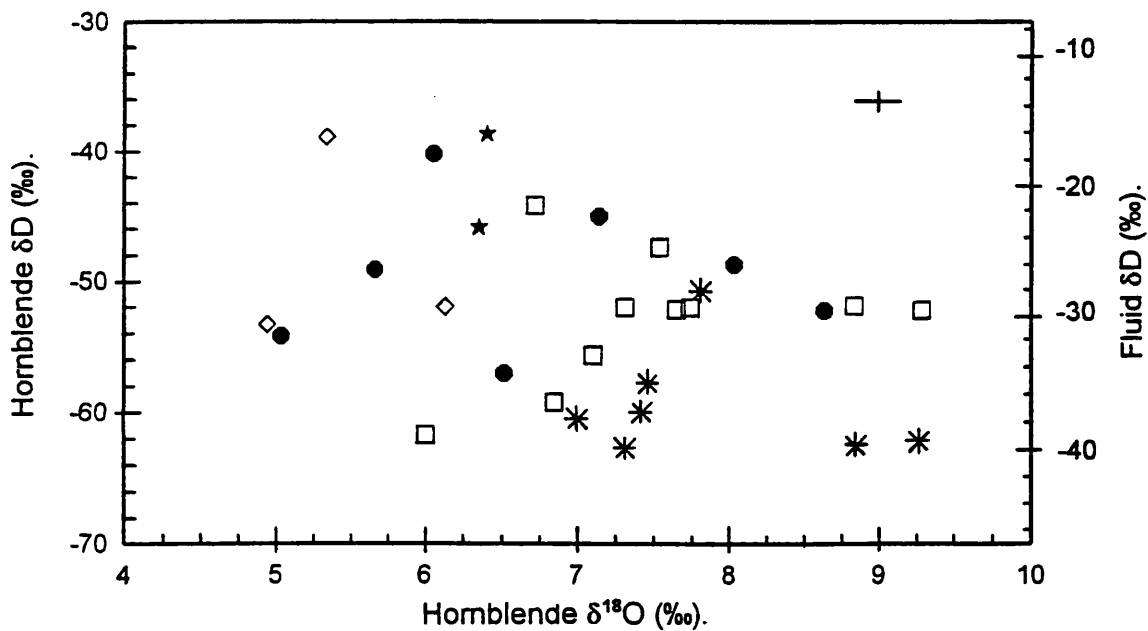


FIGURE 5.27 Map of Connemara showing  $\delta^{18}O$  values (%) of samples at locations collected. Filled circles represent hornblendes and open stars represent muscovites. Group-A is identified by a concentric circle symbol. Group-B is a locally clustered group of 7 samples.



**FIGURE 5.28** Hornblende  $\delta^{18}\text{O}$  versus K-Ar ages.  $R$  for whole dataset =  $-0.207$  (below criteria for significance). Symbols: **Group-A** = filled octagons; **Group-B** = asterisks; **Group-C** = open diamonds; others = open squares; MGS = black stars. Average horizontal error =  $\pm 13\text{Ma}$ ; average vertical error =  $\pm 0.15\text{‰}$ .



**FIGURE 5.29** Hornblende  $\delta\text{D}$  (left vertical-axis) and fluid  $\delta\text{D}$  (right vertical-axis) versus  $\delta^{18}\text{O}$ .  $R$  for whole dataset =  $-0.307$  (just below criteria for 90% significance). Symbols: **Group-A** = filled octagons; **Group-B** = asterisks; **Group-C** = open diamonds; others = open squares; MGS = black stars. Average vertical error =  $\pm 1.5\text{‰}$ ; average horizontal error =  $\pm 0.15\text{‰}$ . Data in Appendix 10 and 11. Figure 5.30 shows results in relation to fluids.

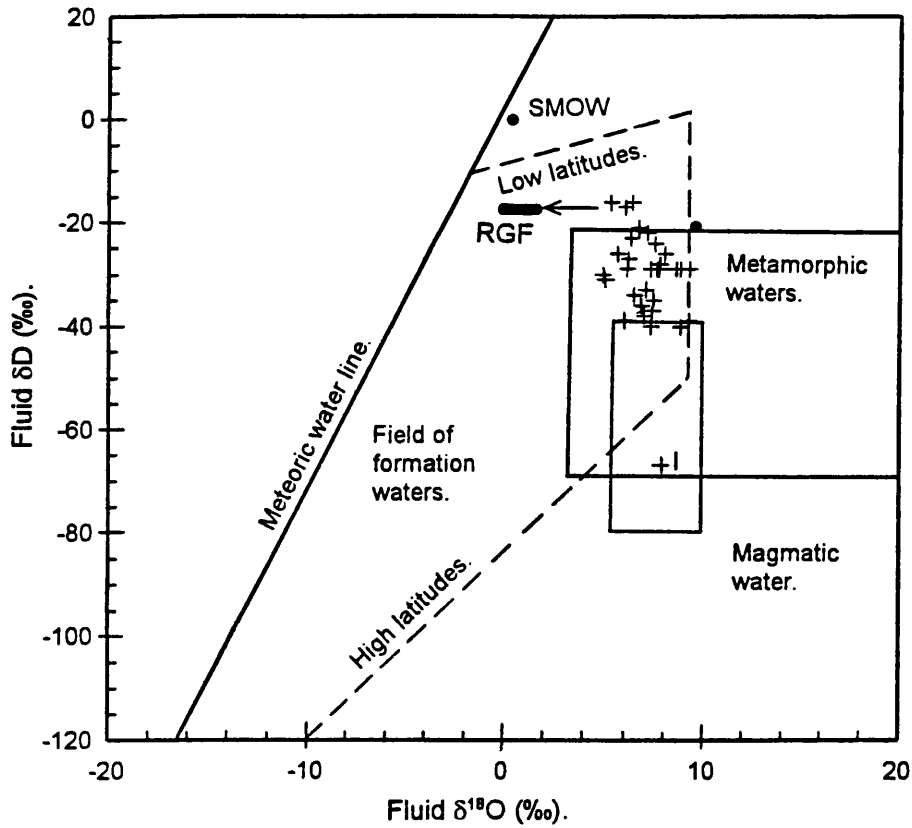


**FIGURE 5.30** Fluid  $\delta D$  versus fluid  $\delta^{18}O$ . This diagram is based on a construction from Rollinson (1993). For clarity, each hornblende sample is represented by a cross. The fluid  $\delta D$  values of the samples were calculated from the hornblende  $\delta D$  results (Appendix 10) by the method of Graham et al. (1984). However,  $\delta^{18}O$  values of the samples are the mineral values (Appendix 11) and do not represent the fluid which established the fluid  $\delta D$  values.  $R$  for whole dataset =  $-0.307$  (just below criteria for 90% significance). SMOW = Standard Mean Ocean Water ( $\delta D = 0\text{‰}$ ;  $\delta^{18}O = 0\text{‰}$ ). RGF is the retrograde fluid of Jenkin et al. (1992) which is discussed in Chapter 6. TJ-1 is shown on this diagram (not on Figure 5.29). Average vertical error =  $\pm 1.5\text{‰}$ ; average horizontal error =  $\pm 0.15\text{‰}$ .

Rock XRF: Oxides.	R Dataset (30).	Probability of Trend.	R Group-A (7).	Probability of Trend.	R Group-B (7).	Probability of Trend.
SiO <sub>2</sub>	-0.137	-	-0.374	-	0.527	-
TiO <sub>2</sub>	-0.075	-	-0.561	-	-0.115	-
Al <sub>2</sub> O <sub>3</sub>	-0.153	-	0.254	-	-0.124	-
Fe <sub>2</sub> O <sub>3</sub>	-0.067	-	-0.741	>90%	-0.112	-
FeO	0.038	-	-0.308	-	0.133	-
MgO	0.285	-	0.496	-	-0.294	-
MnO	0.318	>90%	0.151	-	0.571	-
CaO	-0.077	-	0.378	-	-0.294	-
Na <sub>2</sub> O	-0.147	-	-0.392	-	-0.094	-
K <sub>2</sub> O	0.180	-	0.019	-	0.436	-
P <sub>2</sub> O <sub>5</sub>	-0.098	-	-0.814	>95%	-0.443	-
CO <sub>2</sub>	0.202	-	0.226	-	-0.134	-
H <sub>2</sub> O	0.237	-	0.087	-	-0.041	-
FeO/ (FeO+MgO)	-0.058	-	-0.482	-	0.329	-

**TABLE 5.10** Correlation coefficients (R) of  $\delta^{18}\text{O}$  values against rock XRF, FeO, H<sub>2</sub>O and CO<sub>2</sub> determinations. Whole dataset comprises 30 samples. **Group-A** and **Group-B** are of 7 samples each.

Hornblende Chemical Analyses: Oxides.	R Dataset (30).	Probability of Trend.	R Group-A (7).	Probability of Trend.	R Group-B (7).	Probability of Trend.
Fe <sub>2</sub> O <sub>3</sub>	-0.196	-	-0.680	>90%	-0.358	-
FeO	-0.062	-	-0.489	-	0.449	-
MgO	0.045	-	0.231	-	-0.192	-
CaO	-0.241	-	-0.230	-	0.021	-
Na <sub>2</sub> O	0.230	-	-0.148	-	-0.358	-
K <sub>2</sub> O	-0.095	-	-0.148	-	-0.061	-
FeO/ (FeO+MgO)	-0.070	-	-0.351	-	0.390	-

**TABLE 5.11** Correlation coefficients (R) of  $\delta^{18}\text{O}$  values against hornblende mineral separates wet chemical analyses. Whole dataset comprises 30 samples. **Group-A** and **Group-B** are of 7 samples each.

Hornblende EMPA: Oxides.	R Dataset (29).	Probability of Trend.	R Group-A (7).	Probability of Trend.	R Group-B (7).	Probability of Trend.
SiO <sub>2</sub>	-0.204	-	0.021	-	-0.135	-
TiO <sub>2</sub>	0.126	-	-0.040	-	-0.330	-
Al <sub>2</sub> O <sub>3</sub>	0.207	-	0.399	-	-0.152	-
Fe <sub>2</sub> O <sub>3</sub>	-0.031	-	-0.078	-	-0.231	-
FeO	-0.184	-	-0.919	>99%	0.458	-
MgO	0.173	-	0.155	-	-0.093	-
MnO	-0.063	-	-0.826	>95%	0.815	>95%
CaO	-0.047	-	0.332	-	0.176	-
Na <sub>2</sub> O	0.322	>90%	-0.069	-	-0.482	-
K <sub>2</sub> O	-0.014	-	-0.140	-	-0.259	-
FeO/ (FeO+MgO)	-0.175	-	-0.538	-	0.337	-
A-site.	0.406	>95%	0.144	-	0.210	-
Mg#	0.194	-	0.542	-	-0.270	-
Ionic Porosity (Z).	-0.428	>95%	-0.900	>99%	0.042	-
Plag. Alt. Index.	-0.142	-	-	-	0.293	-

**TABLE 5.12** Correlation coefficients (R) of  $\delta^{18}\text{O}$  values against in-situ hornblende EMPA analyses. Whole dataset comprises 29 samples. **Group-A** and **Group-B** are of 7 samples each.

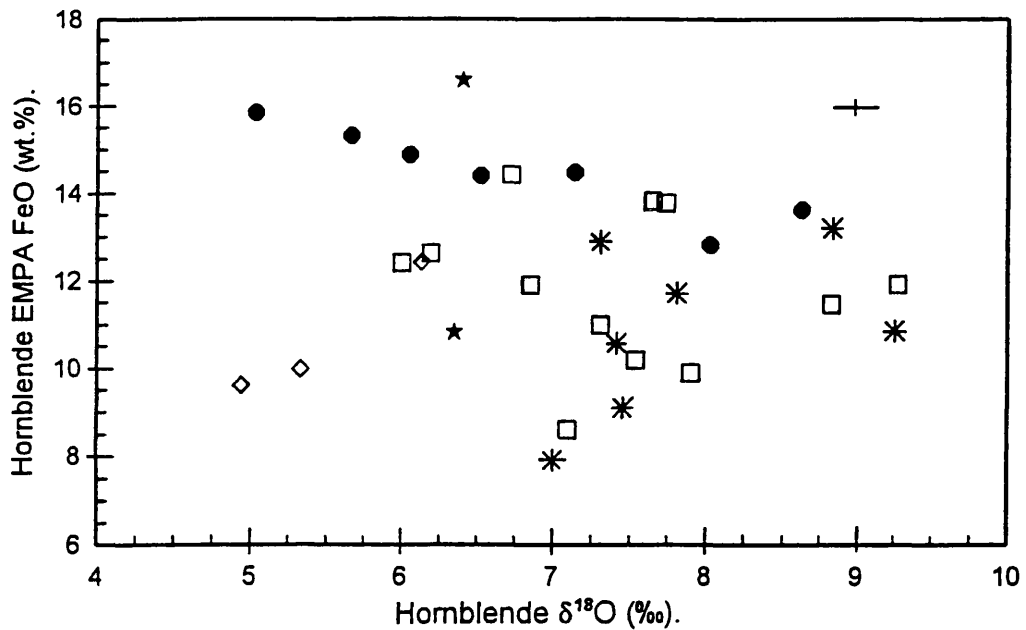


**FIGURE 5.31** EMPA FeO versus hornblende  $\delta^{18}\text{O}$ . R for whole dataset = -0.184 (below criteria for significance). R for **Group-A** = -0.919 (>99% significance). Symbols: **Group-A** = filled octagons; **Group-B** = asterisks; **Group-C** = open diamonds; others = open squares; MGS = black stars. Average horizontal error =  $\pm 0.15\text{‰}$ ; average vertical error =  $\pm 0.06\text{wt.}\%$ .

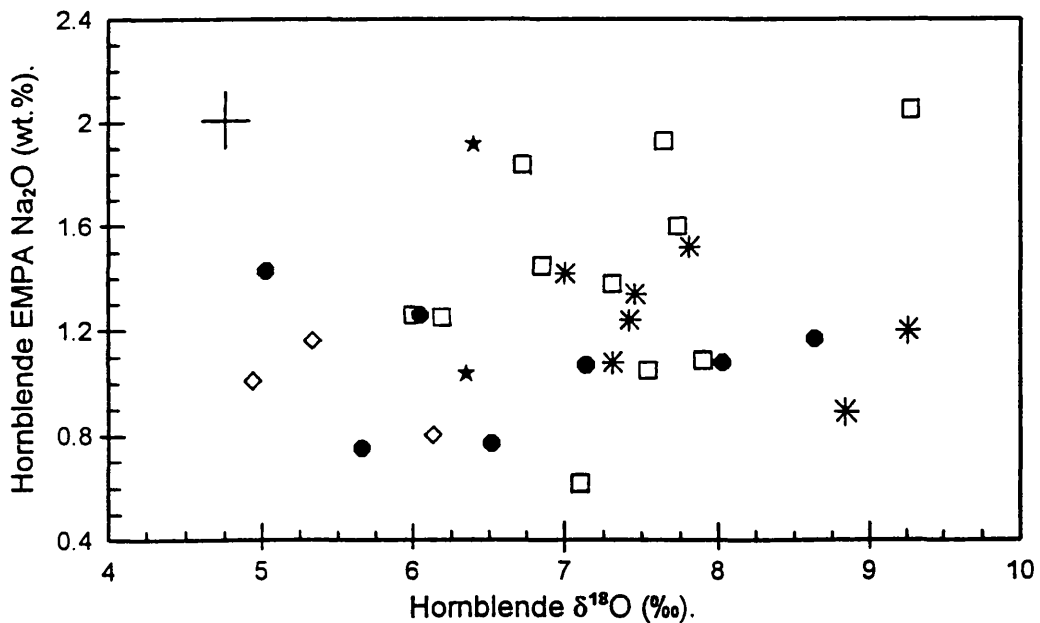


**FIGURE 5.32** EMPA  $\text{Na}_2\text{O}$  versus hornblende  $\delta^{18}\text{O}$ . R for whole dataset = 0.322 (>90% significance). Symbols: **Group-A** = filled octagons; **Group-B** = asterisks; **Group-C** = open diamonds; others = open squares; MGS = black stars. Average horizontal error =  $\pm 0.15\text{‰}$ ; average vertical error =  $\pm 0.14\text{wt.}\%$ .

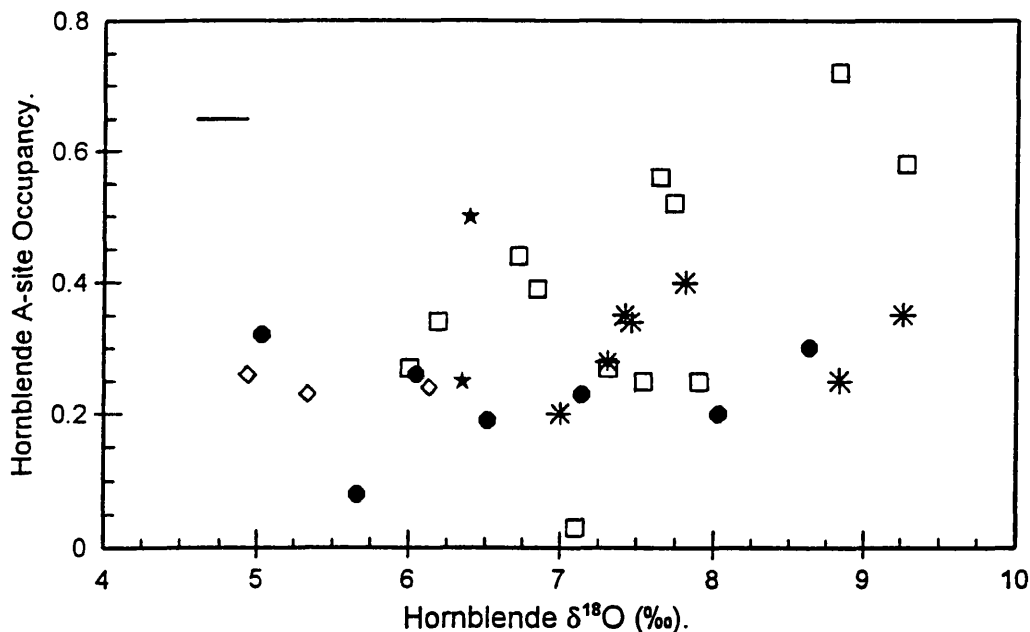


**FIGURE 5.33** EMPA derived A-site occupancy versus hornblende  $\delta^{18}\text{O}$ . R for whole dataset = 0.406 (>95% significance). Symbols: **Group-A** = filled octagons; **Group-B** = asterisks; **Group-C** = open diamonds; others = open squares; MGS = black stars. Average horizontal error =  $\pm 0.15\text{‰}$ ; average vertical error not estimated.

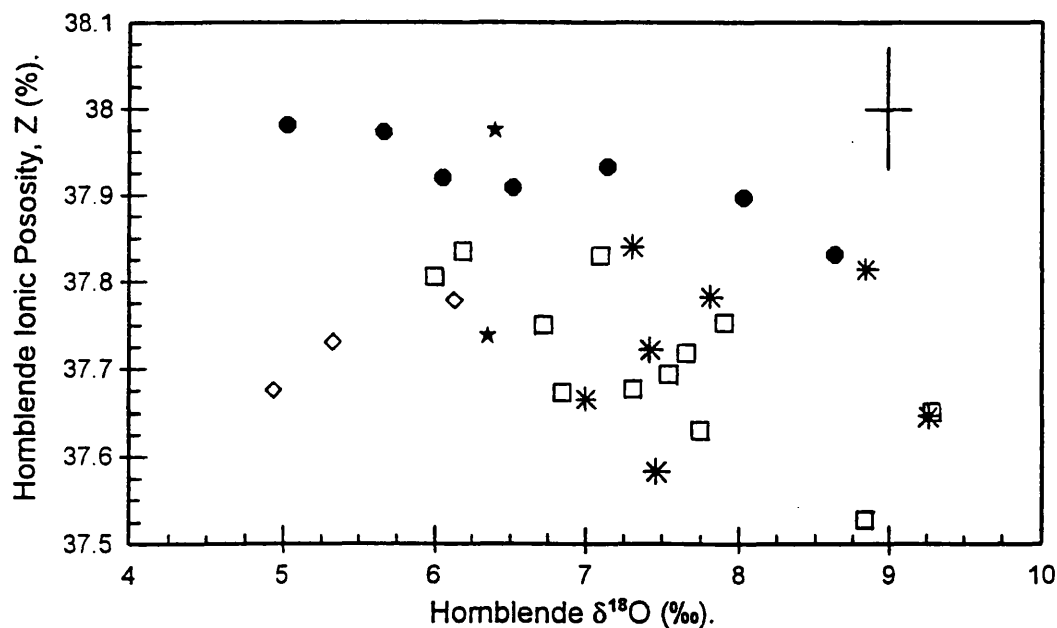


**FIGURE 5.34** EMPA derived ionic porosity, Z, versus hornblende  $\delta^{18}\text{O}$ . R for whole dataset = -0.428 (>95% significance). R for **Group-A** = -0.900 (>99% significance). Symbols: **Group-A** = filled octagons; **Group-B** = asterisks; **Group-C** = open diamonds; others = open squares; MGS = black stars. Average horizontal error =  $\pm 0.15\text{‰}$ ; average vertical error =  $\pm 0.078$ .

## 5.5 Significance of Data.

The previous sections use graphs to represent the correlations between compositional data and isotopic data. Correlation coefficients have been used to indicate whether relationships exist between data and have been used to express trends and groupings. However, some assumptions have been made in order to create a basic starting point on which to evaluate the significance of trends. The key assumption being that the data represents a single, initially homogeneous population.

The groupings of data (**Group-A, Group-B, Group-C, MGS, others**) were based on geographical location which may have much less significance on correlations with K-Ar ages and stable isotope data than compositional variation of samples considered individually. Also, influences may result from variation of metamorphic grade, variation of individual whole rock chemistry as well as mineral chemistry, variation in cooling rate, variation in grain size, variations in alteration and submicroscopic phyllosilicate development in cleavages (Miller, 1990), variations in conditions of retrograde fluid (RGF) conditions and flow through aquiferous strata and a possible influence of excess Ar recognised in some samples (Section 5.2). The group of four samples which are considered to display excess Ar (if ~490Ma is considered as the oldest possible hornblende K-Ar ages in the Dalradian rocks of Connemara) creates another problem in deciding whether to segregate these into another subgroup or regard them as part of the overall dataset. This also leads to the question of whether these samples should be excluded or retained in the datasets for stable isotope comparisons with composition since they are displaying differences in Ar retention for some reason which may or may not affect other non-Ar dependant parameters.

Another consideration is that many samples collected from the north of the area display two populations of hornblende compositions. The K-Ar dating and stable isotope analysis was carried out on separated grains (90-125 $\mu$ m) from the rocks whereas the electron microprobe data was from in-situ mineral grains (point analysis ~2 $\mu$ m). Effectively this gives a difference in the resolution of techniques used and creates a discrepancy for

comparisons. This has been addressed by estimating the probable bulk composition for EMPA from the Mg content of hornblende separated grains by wet chemistry analysis. This is outlined in Appendix 5 and 5A.

All of the above influences will have an effect to varying degrees on the statistical correlations observed in this chapter. Thus identification of key parameters controlling chemical and isotope variation on such a large dataset is difficult.

The approach of this work has been to consider the K-Ar age variation phenomenon observed in hornblende samples collected from the Dalradian rocks of Connemara as one overall dataset of 30 samples. It was decided that if the dataset of 30 samples gave a correlation of >95% significance this would be taken as an indication of a probable trend between the variables compared and a likelihood that some control of one set of data in relation to another was being observed, for example the decrease in hornblende K-Ar ages with increasing hornblende  $\delta D$  values (Figure 5.17). Observations have also been made on the emergence of apparent subgroups, for example excess Ar in hornblende, and attempts made to place these into context with the wide ranging possibilities of influencing factors.

However, truly meaningful correlations may only emerge with more detailed work on smaller subsets.

## CHAPTER 6.

### DISCUSSION.

This chapter deals sequentially with the following: Section 6.1: hornblende compositions related to K-Ar age and stable isotope results; Section 6.2: ionic porosity related to K-Ar age and stable isotope results; Section 6.3: discussion of stable isotope results with regard to possible metamorphic fluid or fluids and their possible sources; Section 6.4: possible re-estimation of fluid events based on work to date; Section 6.5: possible future work. Each section introduces and advances the realisation that composition is important in isotopic studies of hornblendes from amphibolites in Connemara.

#### 6.1 Hornblende Composition Related to K-Ar Age and Stable Isotopes.

##### 6.1.1 Consideration of Results.

From the results of Chapter 5, there is clearly a relationship between hornblende FeO, MgO, K<sub>2</sub>O and Mg#, measured K-Ar ages and hydrogen and oxygen stable isotopes. These correlations are observed across three different analytical techniques; rock XRF analysis, wet chemical analysis of hornblende separates and EMPA of in-situ hornblende grains. Had there been only one analysis type carried out, e.g. EMPA, then it could be argued that possibly the analyses would have been too imprecise without correction for bulk composition (wet chemical analysis of MgO). However, the correction of EMPA results using wet chemical analyses of MgO to give a more representative bulk EMPA composition (in samples where dual hornblende compositions are present; Appendix 5A) does give a better estimation of the EMPA bulk composition in relation to the actual mineral separates as used for K-Ar dating and stable isotope studies. This is important as good compositional estimates are required to calculate representative hornblende formulae (Appendix 6) from the complete EMPA data (Appendix 5), from which the ionic porosities, Z, are then derived, based on Mg# and A-site occupancy (Appendix 8, Dahl, 1996). Similar

correlations of composition with K-Ar age are observed with the rock XRF analyses. These are less precise than with wet chemical analyses and EMPA results due to the presence of quartz, plagioclase, chlorite, epidote, magnetite, sphene and other accessory minerals. However, the quantities (40-60%) of hornblende in the rocks have a large influence on the rock compositions; Fe<sub>2</sub>O<sub>3</sub>, FeO and MgO displaying similar correlations to that of the wet chemical mineral separate analyses and EMPA in-situ analyses of the hornblendes.

In many cases where a correlation is observed with the whole dataset, **Group-A** does not reflect the trend but **Group-B** usually does. This may be because **Group-A** (412-465Ma) does not have as wide a range of K-Ar ages in comparison to **Group-B** (410-556Ma) in relation to compositions. **Group-B** also tends to show correlations of SiO<sub>2</sub>, Fe<sub>2</sub>O<sub>3</sub> and Na<sub>2</sub>O with K-Ar age from the EMPA results (Chapter 5).

The reasons why there should be correlations of FeO, MgO, K<sub>2</sub>O and Mg# with K-Ar ages are related to ionic porosity, Z, and are discussed fully in Section 6.2. The stable isotope  $\delta$ D and  $\delta^{18}$ O values also demonstrate strong correlations with Z.

### 6.1.2 Compositional Relationships with Stable Isotopes.

The results of  $\delta$ D plotted against compositions of hornblendes again shows correlations with FeO, MgO, Mg# and Z for the whole dataset (Chapter 5). From the EMPA results (Table 5.8), **Group-A** and **Group-B** show no correlations of  $\delta$ D with FeO, MgO, Mg# and Z. But **Group-B** demonstrates correlation with SiO<sub>2</sub>, Fe<sub>2</sub>O<sub>3</sub> and Na<sub>2</sub>O (as with K-Ar ages). The general trends are observed across the rock XRF analyses, wet chemical analyses and EMPA results.

Correlations of composition with  $\delta^{18}$ O are more vague than with K-Ar ages or  $\delta$ D values. A trend with MnO is suggested but the EMPA results of **Group-A** and **Group-B** give opposite trends and therefore cancel out. There is no correlation of  $\delta^{18}$ O with Mg#. However, some correlation of  $\delta^{18}$ O with Z does exist (Table 5.12, Figure 5.33).

$\delta$ D values increase with increasing ionic porosity, the more open structure allowing the intrusion of deuterium as OD<sup>-</sup> into the hornblende crystal during isotope exchange with the ~400Ma retrogressive fluid of Jenkin et al. (1992) (Section 6.3).  $\delta^{18}$ O values show a

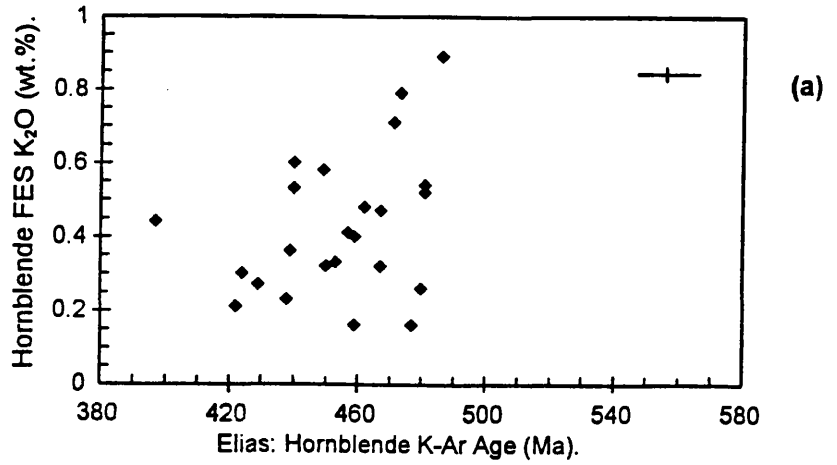
connection with Na<sub>2</sub>O, A-site occupancy and ionic porosity (from the influence of A-site rather than Mg#), but to a lesser extent than  $\delta D$ .

### 6.1.3 Evaluation with Previous Studies in Connemara.

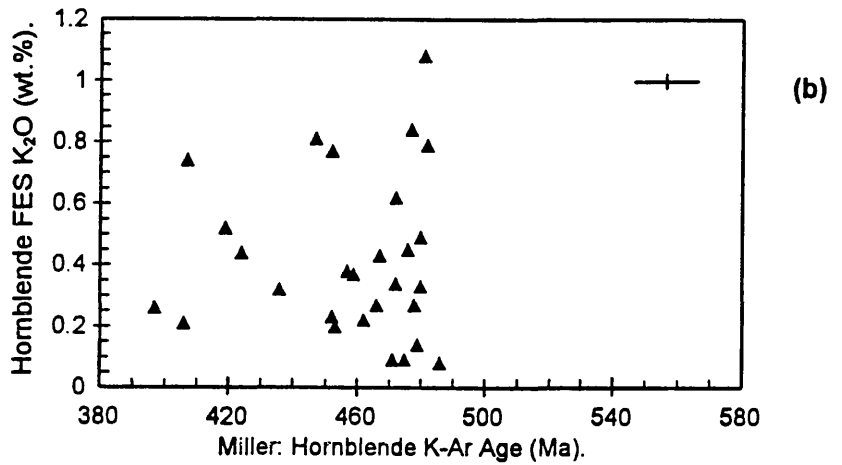
Previous K-Ar age investigations of hornblendes were carried out in Connemara, most recently by Elias et al. (1988) and Miller et al. (1991). For comparison, the K<sub>2</sub>O versus K-Ar ages are shown in Figure 6.1 for (a) Elias et al. (1988), (b) Miller et al. (1991) and (c) Jappy (1998, present study). Only the work of this present study shows correlation of K<sub>2</sub>O with K-Ar age. The previous two workers observed samples with higher K<sub>2</sub>O contents, but maximum ages of ~490Ma only, although Elias (1985) reported two samples with ages greater than 500Ma which were not considered further. Four hornblende samples with ages above 500Ma have been observed in this present study: **TJ-9** = 510 $\pm$ 16Ma; **TJ-38** = 556 $\pm$ 6Ma (two analyses); **TJ-40** = 522 $\pm$ 18Ma; **TJ-43** = 554 $\pm$ 16Ma. Samples **TJ-9** and **TJ-40** may be considered close to the ~490Ma metamorphic peak upper limit (Cliff et al., 1996). However, **TJ-38** and **TJ-43** are very much higher than would be expected from previous studies. This may be due to the effects of excess <sup>40</sup>Ar (Dalrymple and Lanphere, 1969; Faure, 1986) in these samples being amplified by the very low K contents (Figure 5.4, Figure 6.1(c), Appendix 9). Generally, these two samples, **TJ-38** and **TJ-43**, appear off the trends seen in the K-Ar ages against composition in Chapter 5. This is seen in the rock XRF figures as well as the wet chemical analysis and EMPA results. Consideration of the hornblende K-Ar age against ionic porosity diagram of Figure 5.14 would suggest that **TJ-38** and **TJ-43** should be in the region of ~490Ma to lie on the oldest age part of the group, relative to Z. This suggests a definite effect of excess <sup>40</sup>Ar displacing the true values. The four samples with ages >490Ma can therefore be attributed to excess <sup>40</sup>Ar. However, samples with low K contents but with ages <490Ma may also be affected by excess <sup>40</sup>Ar, which is undeterminable in this study.

Elias et al. (1988) investigated hornblende major element compositions of single hornblende grains by EMPA. Only three analyses per sample were carried out and it was concluded that there was no correlation of K-Ar age with composition. Miller (1990)

Elias (1985).  
Dataset (24).  
 $R = 0.340$ ; 80-90%.



Miller (1990).  
Dataset (30).  
 $R = 0.094$ ; <80%.



Jappy (1998).  
Dataset (30).  
 $R = -575$ ; >99%.

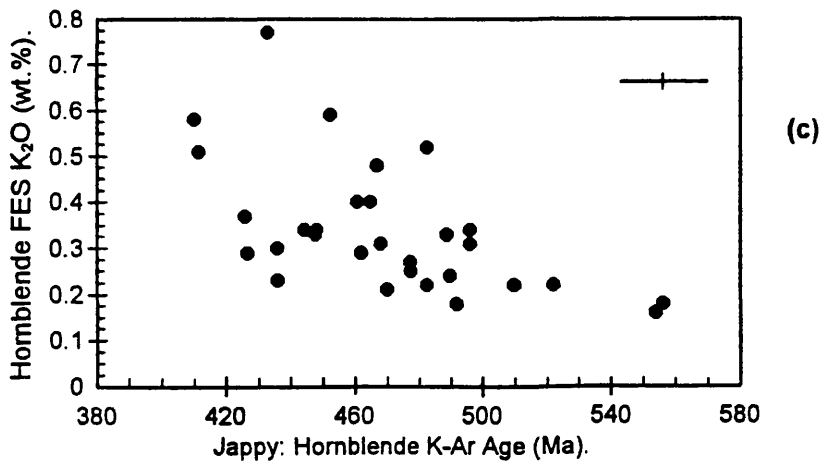
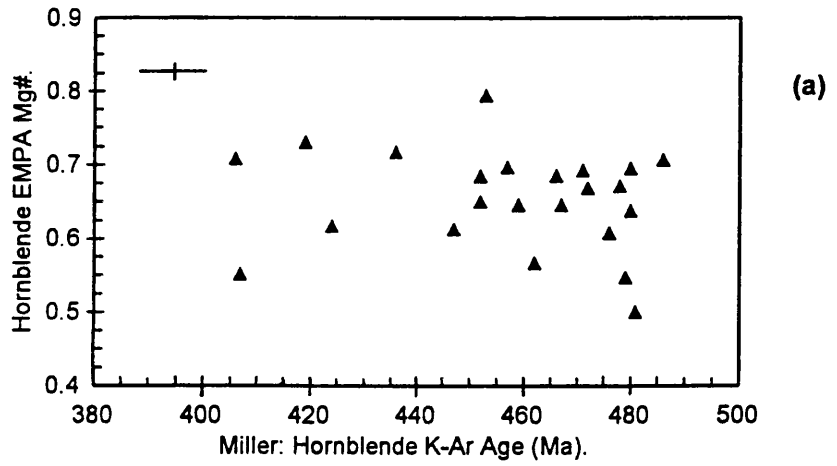
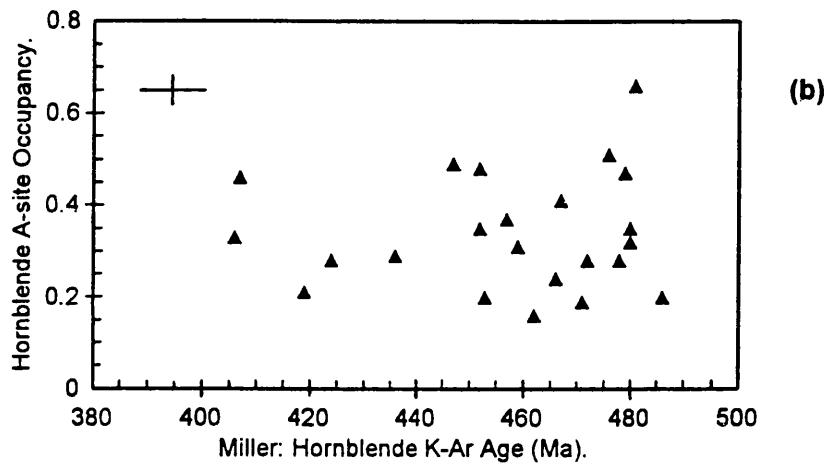


**FIGURE 6.1** Wet chemical analysis results (flame emission spectroscopy; FES) for  $K_2O$  in hornblende mineral separates against K-Ar ages (Ma): (a) Elias (1985); (b) Miller (1990); (c) Present study. Only the present study shows a significant correlation; >99%. Average errors are represented by the —+— symbol. Data in relevant sections of Appendix.

Miller (1990).  
Dataset (25).  
 $R = -0.387$ ; 90-95%.



Miller (1990).  
Dataset (25).  
 $R = 0.181$ ; <80%.



Miller (1990).  
Dataset (25).  
 $R = -0.030$ ; <80%.

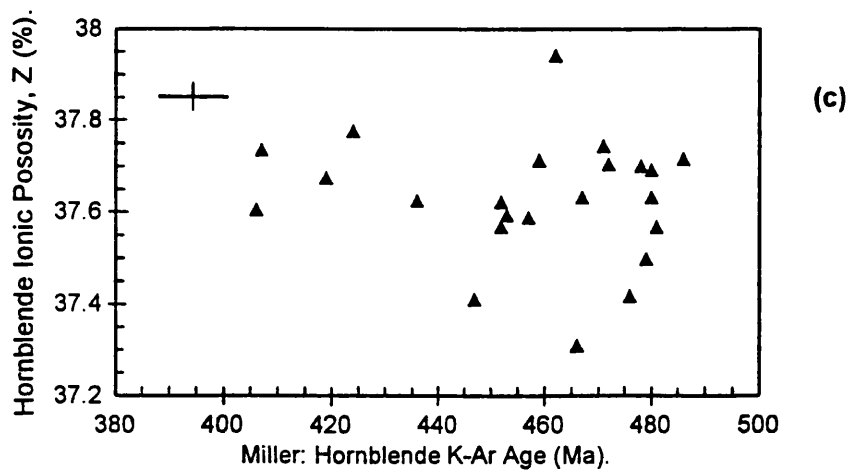


**FIGURE 6.2** Derived from Miller (1990). Comparisons of K-Ar ages (Ma) with: (a) Hornblende EMPA Mg#; (b) Hornblende A-site occupancies; (c) Calculated hornblende ionic porosities, Z. Only (a) shows a significant correlation; 90-95%. Average errors are represented by the —+— symbol. Data in relevant sections of Appendix.

similarly investigated hornblende major element compositions but determined six analyses per sample and concluded overall that although composition had no role to play in determining K-Ar age, some correlation with Fe/Mg ratios and A-site occupancy was noted.

However, because both these workers looked only at mounted, polished separated grains in reflected light and only carried out a small number of EMPA analyses per sample, the compositions obtained may not be truly representative of some samples, especially those collected in the northern part of the Dalradian, towards the Silurian unconformity where a range of compositions was observed in this study. Selection of analysis points in reflected light would not show potential analytical errors derived from impurities or cleavage alterations and obtaining representative analyses of zoned porphyroblasts would not be possible. Also, these workers did not carry out rock XRF analysis or wet chemical analysis of hornblende separates for  $\text{Fe}_2\text{O}_3$ , MgO, CaO and  $\text{Na}_2\text{O}$ . The MgO being especially important for correction of bulk EMPA compositions and formulae calculations (Appendix 5, Appendix 6). Figure 6.2 shows the lack of significant correlation between hornblende K-Ar ages with A-site occupancy and ionic porosity from Miller (1990) (Appendix 12 and 13). Also from Miller (1990), the EMPA Mg# gives a negative correlation with K-Ar age suggesting Mg-rich hornblendes are less retentive of Ar than Fe-rich types (Figure 6.2(a)).

In the present study, polished, carbon-coated rock thin sections were used, hornblende crystals being analysed in-situ in the rock fabric. Care was taken to avoid cleavages, alteration and inclusions, giving a more representative hornblende composition from 16-20 carefully selected analyses per sample. It was found that in amphibolites from the northern part of the Dalradian, two composition populations were present in single hornblende grains (Section 5.1, Appendix 5).

#### 6.1.4 Evaluation with Previous Studies in Other Areas.

O'Nions et al. (1969) carried out K-Ar dating and EMPA of hornblendes from the Bamble-Risør sector of the Fennoscandian Shield of South Norway. Separated amphibole grains were mounted, polished, carbon-coated and analysed for major element compositions by EMPA; a minimum of ten grains per sample were analysed. These workers observed an

apparent compositional dependence of K-Ar ages (1114 $\pm$ 32Ma to 970 $\pm$ 30Ma) in this area where post-metamorphic uplift and cooling were slow.

O'Nions et al. (1969) suggested that unit cell variation due to compositional variation was the cause of the K-Ar age differences. OH in amphiboles is able to equilibrate with external fluid isotopic compositions to a lower temperature in Fe-rich amphiboles than Mg-rich amphiboles (Gerling et al., 1965). OH<sup>-</sup> ions are capable of moving through the lattice of amphiboles, in response to changing partial pressures of H<sub>2</sub>O in the surrounding fluid. This mechanism is capable of continuing to lower <sup>40</sup>Ar\* closure temperatures in Fe-rich relative to Mg-rich amphiboles of the same type. A consequence of this mechanism causes the removal of <sup>40</sup>Ar\* and lowers the measured K-Ar age.

Amphiboles near the pargasite end-member (Mg-rich) begin to retain <sup>40</sup>Ar\* at higher temperatures than amphiboles near the ferropargasite end-member (Fe-rich) during cooling from temperatures characterising the upper amphibolite facies of metamorphism (Dodson, 1973; Harrison, 1981).

Onstott and Peacock (1987) studied hornblendes from amphibolite and granitic gneiss from a single outcrop in the central Adirondacks and found that significantly diverse <sup>40</sup>Ar\* - <sup>39</sup>Ar dates of 948 $\pm$ 5Ma and 907 $\pm$ 5Ma were observed. Assuming that samples from the same location have experienced the same thermal history, then the difference in ages apparently reflects a corresponding difference in closure temperature for diffusion of <sup>40</sup>Ar\*.

They carried out EMPA (minimum of 10 analyses per sample) on polished rock sections. Fe/(Fe+Mg+Mn) ratios were 0.6 and 0.8 respectively, the higher ratio corresponding to the younger <sup>40</sup>Ar\* - <sup>39</sup>Ar date. TEM investigations indicated that the samples were of homogeneous composition and devoid of exsolution features. However, zones of phyllosilicates, ~0.1-0.2 $\mu$ m wide, parallel to (110) and (1 $\bar{1}$ 0) were present. These were believed to have formed during post-metamorphic cooling, due to migrating fluids passing through the hornblendes, especially along the (110) and (1 $\bar{1}$ 0) cleavages. These sub-microscopic phyllosilicate alterations along the cleavages would have acted as conduits for <sup>40</sup>Ar\* to diffuse out of the hornblende structures; also reducing the parameter “ $\alpha$ ” in the closure temperature equation (Dodson, 1973). These phyllosilicate features are more

prominent in samples with younger  $^{40}\text{Ar}^*$ - $^{39}\text{Ar}$  dates and higher  $\text{Fe}/(\text{Fe}+\text{Mg}+\text{Mn})$  ratios. They may influence  $^{40}\text{Ar}^*$  closure temperatures by effectively partitioning a hornblende grain into smaller diffusion domains.

Diffusion parameters and determination of  $T_c$  requires a knowledge of " $a$ ", the characteristic diffusion distance (Equation 1.1). This is difficult to evaluate, even with TEM and impossible to evaluate with an optical microscope as the phyllosilicate alteration is in the microcrystalline arena. Onstott and Peacock (1987) made an estimate of " $a$ " to account for the effect of microcrystalline phyllosilicate in the calculation of  $T_c$ . However the value of  $T_c$  depends greatly on what the value of " $a$ " is taken to be. If the observed phyllosilicate channels do dictate the characteristic diffusion dimension " $a$ " then the  $^{40}\text{Ar}^*$  closure temperature ( $T_c$ ) will be greatly affected by this rather than the actual crystal sizes as previously thought (Dodson, 1973; Elias, 1985, Miller, 1990).

There was much variation of microstructure, K-Ar age and  $\delta D$  observed in hornblendes from amphibolites from the Dalradian rocks of Connemara (Miller, 1990).

Leake et al. (1988) disputed the findings of Onstott and Peacock (1987) because of the findings based on the investigation of 26 hornblendes (Elias et al., 1988). These did not show a relationship of K-Ar age with  $\text{MgO}/(\text{MgO}+\text{FeO})$  composition. However, these compositions were based on a limited EMPA investigation only (Section 6.1.3).

Cosca and O'Nions (1994) carried out  $^{40}\text{Ar}^*$ - $^{39}\text{Ar}$  step heating using the same samples which had been used for the K-Ar dating of the Bamble region of Norway (O'Nions et al., 1969) and had shown correlation with  $\text{FeO}/(\text{FeO}+\text{MgO})$ . They have stated that age plateaus measured by this method show no correlation with composition and therefore the  $^{40}\text{Ar}^*$  closure temperature is not composition dependant. Cosca and O'Nions (1994) cite previous work as supporting these findings: Elias et al. (1988); Leake et al. (1988); Cosca et al. (1992). But from the above discussion and Section 6.1.3, these compositions may not be refined enough. Cosca and O'Nions (1994) have argued that regional and local tectonic influences have created the differences in ages because the samples were collected from a widespread area. This does not account for the compositional dependency findings where samples have been collected from spatially

proximal locations such as the well studied quarry featured in Miller et al. (1991) where samples were only a few metres apart and in the present study where **Group-A** (7 samples; ~1m between samples) and **Group-B** (7 samples; ~100m between samples). Other workers to have found some degree of compositional control of hornblendes include Lee (1993) and Rex et al., (1993). Scaillet et al. (1992) found  $^{40}\text{Ar}^*$  retentivity associated with Mg-content in white micas from the Italian Alps.

Miller et al. (1991) have suggested that later, lower temperature fluids have percolated through the Connemara area and are responsible for the variability of hornblende K-Ar ages in close proximity to each other. These fluids, as suggested by Onstott and Peacock (1987) texturally changed the cleavage characteristics of the hornblende on a submicroscopic scale, allowing the influx of water as  $\text{OH}^-$ , changing the  $\delta\text{D}$  isotopic character and allowing the liberation of  $^{40}\text{Ar}^*$  in the process. They have also suggested active  $^{40}\text{Ar}^*$  replacement in A-sites by  $\text{H}_3\text{O}^+$  (Chapter 1, Figure 1.7).

## 6.2 Ionic Porosity Related to K-Ar Age and Stable Isotopes.

From the discussion of the previous section it is observed that the chemical compositions of the hornblende samples investigated in this study do have a significant influence on hornblende K-Ar ages and  $\delta\text{D}$  values.

Dahl (1996) has shown the interrelationships between chemical composition ( $X$ ), ionic porosity ( $Z$ ) and  $^{40}\text{Ar}^*$  and O diffusivity ( $D$ ) in calcic to subcalcic amphiboles. Diffusivities of silicates for a given chemical species cluster according to structural group (Fortier and Giletti, 1989). Within a structural group, relationships between diffusivity and composition are likely because composition affects bond strengths and magnitudes. The following points are relevant to the present study:

- I. Hornblendes have a flexible double-chain structure which can accommodate diverse cations and anions.

II. Positive correlations have been observed between Mg# and  $^{40}\text{Ar}^*$  retentivity in hornblendes by Gerling et al. (1965); O'Nions et al. (1969); Berry and McDougall (1986) and Onstott and Peacock (1987).

III. Other amphibole properties are known to be dependent on composition; maximum thermal stability, thermodynamic parameters, refractive indices, etc.

IV. Systematic *D-X* (diffusivity-composition) trends exist within other isostructural mineral groups, eg., Fe-Mg interdiffusion in olivine, O and  $^{40}\text{Ar}^*$  diffusion in micas (Harrison et al., 1985; Fortier and Giletti, 1991; Grove and Harrison, 1993, 1994). The location of K in mica is similar to that in amphiboles (Deer et al., 1997). However, some recent workers found no compositional dependence on  $^{40}\text{Ar}^*$  diffusion and hence K-Ar ages and  $^{40}\text{Ar}^*$ - $^{39}\text{Ar}$  ages in hornblendes (Harrison, 1981; Baldwin et al., 1990; Cosca and O'Nions, 1994).

Ionic porosity, *Z*, is a measure of a mineral's atomic packing density. *Z* is defined as the percentage of unit cell volume not occupied by ions:

$$Z(\%) = [1 - (V_i/V_c)] \times 100 \quad \text{Equation 6.1}$$

Where  $V_i$  is the total volume of ions in the unit cell and  $V_c$  is the unit cell volume at a particular temperature. Calculated from compositional and unit cell data, *Z* is a very good indicator of both M-O bond length, strength and the diffusivity of neutral species ( $^{40}\text{Ar}^*$ , He, and H and O as  $\text{H}_2\text{O}$ ).

*Z* of an amphibole decreases as:

I.  $\text{Mg}^{2+}$  replaces  $\text{Fe}^{2+}$ ;  $\text{Mg}^{2+}$  (0.66Å) is smaller than  $\text{Fe}^{2+}$  (0.74Å). All ionic radii are taken from Klein and Hurlbut (1985). Therefore  $\text{Mg}^{2+}$  replacing  $\text{Fe}^{2+}$  decreases unit cell

dimensions  $a \sin \beta$ ,  $a$ ,  $b$  and  $c$ . Parameter  $c$  decreases by kinking of double chains (Ernst, 1968; Hawthorne, 1985; Onstott and Pringle-Goodell, 1988) giving an overall shrinkage of M-sites and subsequent reduction of the A-site volume.

II.  $(\text{Al,Fe})^{3+}$  replaces  $(\text{Mg,Fe})^{2+}$ ;  $\text{Al}^{3+}$  (0.51Å) and  $\text{Fe}^{3+}$  (0.64Å) are smaller than  $\text{Fe}^{2+}$  (0.74Å). Therefore  $\text{Al}^{3+}$ - or  $\text{Fe}^{3+}$ - Tschermak's substitution and/or  $\text{Fe}^{3+}$  replacing  $\text{Fe}^{2+}$  also reduces unit cell size thus leading again to shrinkage of M-sites and A-site. Evidence supporting the above, from experimental data (Phillips et al., 1989), shows that in a synthetic tschermakitic hornblende,  $Z$  decreases from 37.9% to 37.5% as  $\text{Fe}^{3+}/(\text{Fe}^{2+}+\text{Fe}^{3+})$  increases from 0.21 to 0.47 upon  $\text{Fe}^{3+}(\text{O}^{2-})(\text{H}_2)_{0.5}\text{Fe}^{2+}_{-1}(\text{OH})_{-1}$  exchange during hydrothermal heat treatment. Also, the 0.4% decrease in  $Z$  is attributable to removal of hydroxyl from the A-sites and resultant elimination of  $(\text{Na,K})^+$  between  $\text{H}^+$  repulsion (Hawthorne and Grundy, 1973; Cameron and Gibbs, 1973).

III. A-sites are filled by  $(\text{Na,K})^+$ . Ionic porosity reduces as A-sites are filled. Synthetic amphiboles with empty A-sites give higher  $Z$  values than their counterparts of same Mg# with full A-sites. Natural clin amphiboles exhibit similar behaviour but uncertainties arise from the sensitivity of calculated Mg# and A-site occupancy because of uncertainties of  $\text{Fe}^{2+}$  and  $\text{Fe}^{3+}$  abundances (Spear, 1994). Also, the effects on  $Z$  of additional components ( $\text{F}^-$ ,  $\text{Cl}^-$  and microstructural defects) is not considered.

The central hypothesis of Dahl (1996) is that  $Z$  can predict change of diffusivity with composition among diverse minerals of a given silicate structure analogous to the  $D$ - $X$  (diffusivity-composition) link related to Mg# within the much simpler olivine group.

Age against  $Z$  predictions are best field-tested in high grade metamorphic terranes containing chemically diverse, microtexturally pristine, K bearing amphiboles in adjacent rocks. The terrain needs to be old enough for amphiboles to have cooled slowly ( $dT/dt \leq 5^\circ\text{C}/\text{Ma}$ ) under dry, static conditions such that volume diffusion most likely dominated  $^{40}\text{Ar}^*$  loss in microtexturally simple grains. Also, the amphiboles must not exhibit

excess  $^{40}\text{Ar}^*$ . Also, there must have been no reheating of the terrain if geologically meaningful age-Z trends are to be preserved.

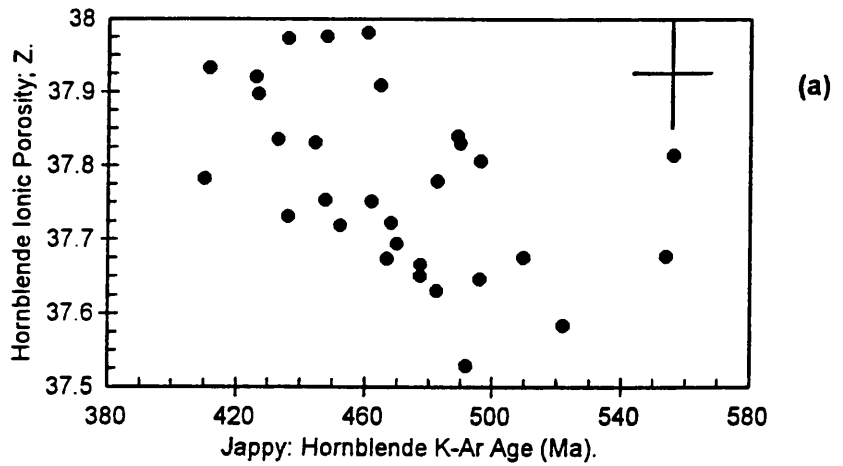
Dahl (1996) demonstrated an inverse correlation of  $^{40}\text{Ar}^*$ - $^{39}\text{Ar}$  cooling ages against Z in previous studies (Cosca and O'Nions, 1994; Kamber et al., 1995) where no obvious compositional correlation between  $^{40}\text{Ar}^*$ - $^{39}\text{Ar}$  and Mg#, A-site occupancy or Al-Tschermakite's component was previously observed (Z not previously having been considered).

The work of this thesis however does demonstrate correlations with K-Ar ages of hornblendes with analysed compositions. In fact, through rock XRF, wet chemical analyses of hornblende separates and in-situ EMPA hornblende analyses there are observable correlations with  $\text{Fe}^{2+}$ ,  $\text{Mg}^{2+}$ ,  $\text{K}^+$ ,  $\text{Fe}^{2+}/(\text{Fe}^{2+}+\text{Mg}^{2+})$ , Mg# and Z (Chapter 5). There are also observable correlations of these ions, ratios and Z with  $\delta\text{D}$ . It should be noted that the conditions of metamorphism and later retrograde activity in Connemara were not anhydrous as the ideal requirements require and that evidence of excess  $^{40}\text{Ar}$  is present in some samples. This of course would affect the precision of the diagrams and estimations.

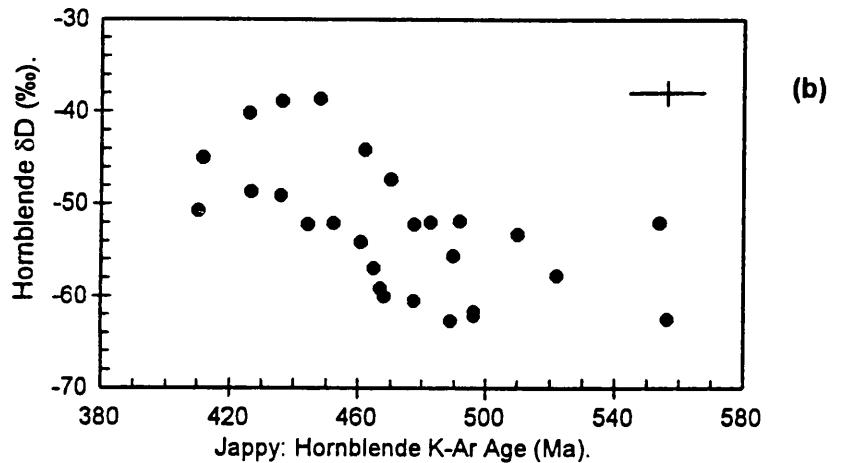
Figure 6.3 demonstrates the interrelationship of K-Ar age with  $\delta\text{D}$  and Z. The triangular diagram of Figure 6.4 combines these three elements. It can be seen from this diagram generally that samples with lower ages display a higher ionic porosity, are therefore more porous and show a higher  $\delta\text{D}$  value from a later fluid which more easily invaded these hornblendes and in turn promoted increased diffusion of  $^{40}\text{Ar}^*$  out of these hornblendes. As K-Ar age becomes older the  $\delta\text{D}$  value becomes larger in magnitude of deuterium depletion, the two effectively cancel each other out forming the trend. The key to the relationship between K-Ar age and  $\delta\text{D}$  observed by Miller (1990) is the connection to ionic porosity, Z, derived from the composition of the investigated hornblendes.

The data on this triangular diagram create a band rather than a precise line because in Connemara the conditions are not ideal for a perfect fit. That is to say, the hornblendes display microtextural complexity due to exsolution or alteration along cleavages to phyllosilicates (Miller, 1990). A later period of reheating around 400Ma due to the intrusion of the Galway Granite and related plutons had an effect on fluid movements throughout the

Jappy (1998).  
Dataset (30).  
 $R = -0.487; >99\%$ .



Jappy (1998).  
Dataset (29).  
 $R = -0.582; >99.9\%$ .



Jappy (1998).  
Dataset (29).  
 $R = -0.582; >99.9\%$ .

Miller et al. (1991).  
Dataset (12).  
 $R = -0.844; >99.9\%$ .

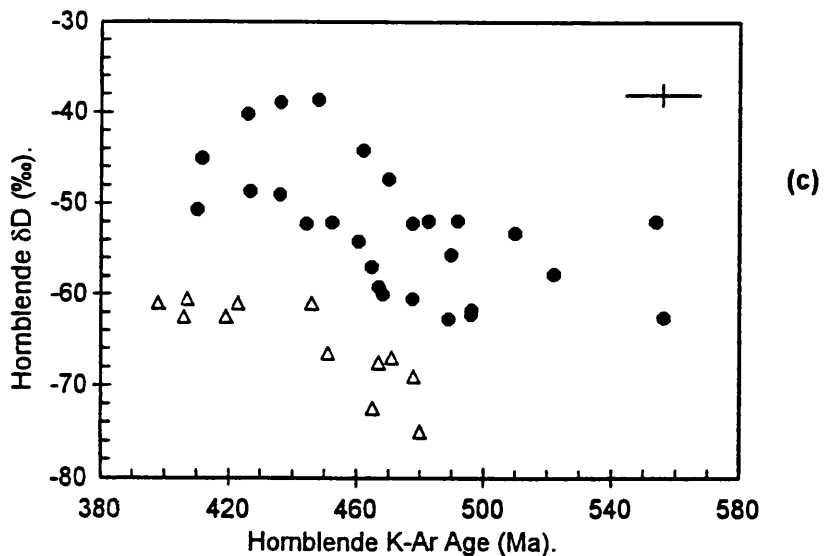


**FIGURE 6.3** From the present study. Comparisons of K-Ar ages (Ma) with: (a) Calculated hornblende ionic porosities, Z (%). (b) Hornblende  $\delta D$  (‰). (c) Hornblende  $\delta D$  (‰) from the present study; filled octagons, in comparison with Miller (1990); open triangles (see also Figure 1.7(a)). Average errors are represented by the  $\text{---}+$  symbol. Data in relevant sections of Appendix.

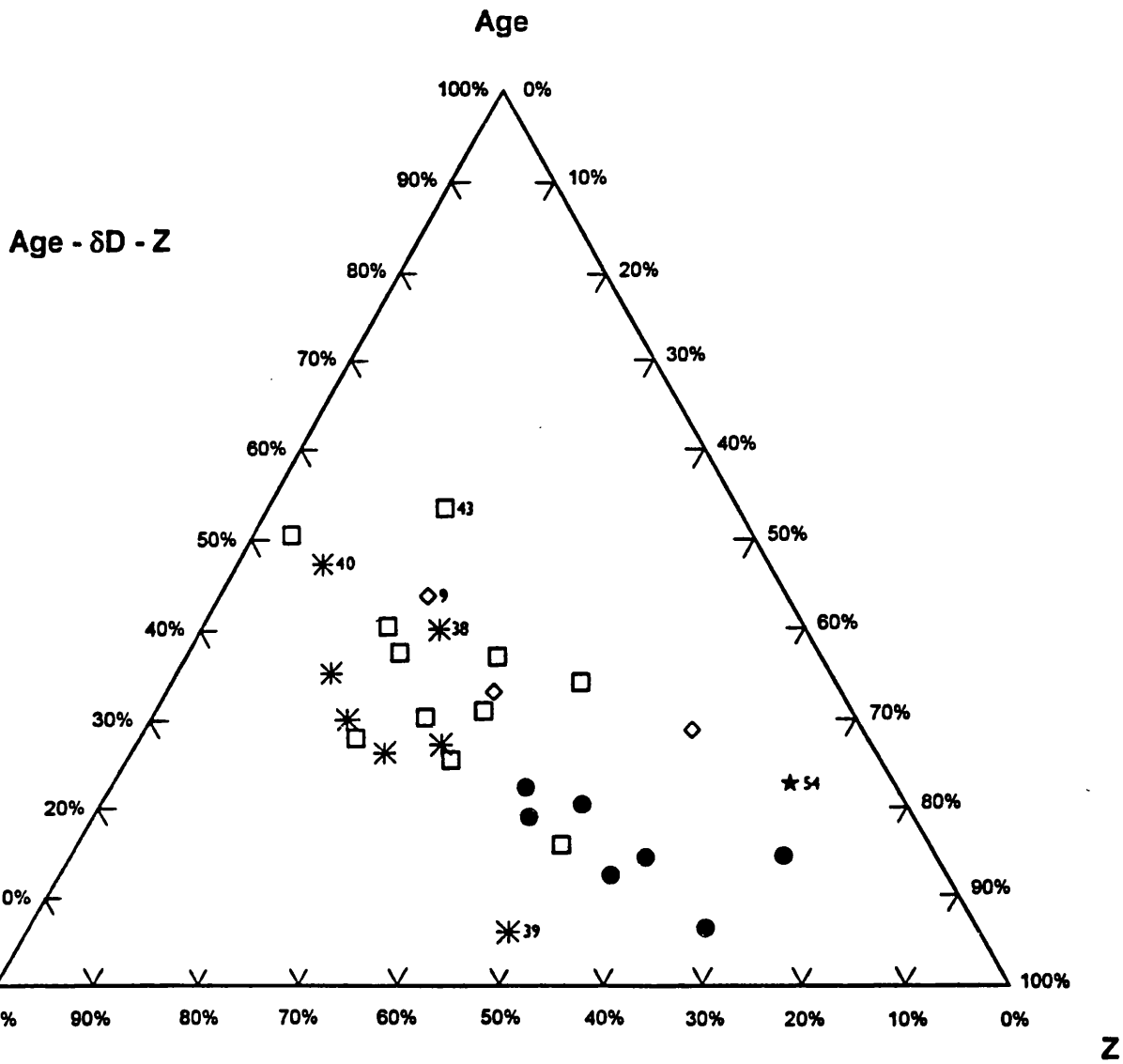


**FIGURE 6.4** [Age- $\delta D$ -Z] diagram. Percentages based on: K-Ar age range = 400Ma ( $\delta D$ -Z line) to 560Ma (apex);  $\delta D$  range = -65‰ (apex) to -35‰ (Age-Z line), ie. increasing  $\delta D$  from left to right on diagram; Z range = 37.500% ( $\delta D$ -Age line) to 38.000% (apex). Symbols: **Group-A** = filled octagons; **Group-B** = asterisks; **Group-C** = open diamonds; others = open squares; MGS = black stars. Diagram construction data in Appendix 14.

region, as observed by chloritisation and epidote retrogressive metamorphism and the microstructural effects (Jenkin et al., 1992; O'Reilly et al., 1997; Jenkin et al., 1997). The observation of excess  $^{40}\text{Ar}$  effects in hornblendes in this study will also create a divergence from the ideal conditions outlined by Dahl (1996). These influences give an overall complex history overprinting the hornblendes from the ideal conditions outlined above.

### 6.3 Origins of Hydrothermal Fluid.

Miller et al. (1991) observed a significant range of K-Ar ages in hornblendes (from 486 $\pm$ 10Ma to 397 $\pm$ 8Ma) and muscovites (478 $\pm$ 10Ma to 408 $\pm$ 8Ma) derived from metamorphic rocks in Connemara by what they considered to be a low temperature ( $\sim$ 275°C) fluid interaction. They observed correlations between K-Ar ages,  $\delta\text{D}$  values, structural water contents and calculated A-site occupancy of hornblendes and suggested that excess water as  $\text{H}_3\text{O}^+$  occupied vacant A-sites during stable isotope exchange, displacing  $^{40}\text{Ar}^*$  and hence lowering K-Ar ages. They stated that this process occurred below the normally accepted closure temperatures for  $^{40}\text{Ar}^*$  in hornblende and evidence for this is not identifiable by optical or XRD investigation.

$^{40}\text{Ar}^*$  closure temperature ( $T_c$ ) values for hornblendes were experimentally determined by Harrison (1981) as being in the range 578-490°C for cooling rates of 5°C/Ma. Other factors also affect the  $T_c$  of hornblendes: chemical composition (Gerling et al., 1965; O'Nions et al., 1969; Berry and McDougall, 1986). Mg-rich hornblendes are more retentive of  $^{40}\text{Ar}^*$  than Fe-rich equivalents (Dahl, 1996). Exsolution of cummingtonite in hornblende causes an apparent reduction of  $\sim$ 200°C in  $T_c$  to equal that of biotite. Phyllosilicate growth along cleavages leads to smaller diffusion domains (" $\alpha$ "), easier paths of escape for  $^{40}\text{Ar}^*$  and hence lower K-Ar ages (Onstott and Peacock, 1987; Baldwin et al., 1990). K-rich minerals such as K-feldspar can occur as inclusions within hornblendes, giving a falsely high K-content and therefore younger K-Ar age (Sisson and Onstott, 1986; Ross and Sharp, 1988).

### 6.3.1. Hydrothermal Palaeo-Fluids Active in Connemara.

The work of this present study indicates the range of hornblende  $\delta D$  values to be  $-39\pm 1.5\text{‰}$  to  $-63\pm 1.5\text{‰}$  indicating that they equilibrated with fluids of  $\delta D$  from  $-16\pm 1.5\text{‰}$  to  $-40\pm 1.5\text{‰}$  (Graham et al., 1984; Sheppard, 1986). The hornblendes which interacted with the fluids of  $\sim -16\pm 1.5\text{‰}$  are predominantly younger than those which interacted with the  $-40\pm 1.5\text{‰}$  fluid. The  $\delta D$ - $\delta^{18}O$  plot of water stable isotope values of Figure 5.30 shows the positions of the fluid  $\delta D$  values against hornblende  $\delta^{18}O$  values (the fluid  $\delta^{18}O$  not having been possible to properly estimate). The values of  $\delta D$  at  $\sim -40\text{‰}$  correspond to metamorphic water during the time of hornblende formation at the peak metamorphic grade at 463-490Ma (Chapter 1). This value is also at the top of the field for magmatic water and may alternatively represent the fluid  $\delta D$  values of hornblende from the original igneous extrusion or shallow intrusion of basaltic material. Yet another possibility is that the  $\sim -40\text{‰}$   $\delta D$  value for the fluid was acquired from the very large igneous intrusion of the metagabbro suite (MGS) responsible for the main metamorphic event. Considering that the metamorphic hornblende may have formed from pyroxene and olivine precursors, the fluid  $\delta D$  values could be from the MGS influence. The presence of relic hornblendes in amphibolite samples from the north of the Dalradian may be indicative of the presence of pyroxene and olivine phenocrysts set in a finer basaltic groundmass. The hornblende  $\delta^{18}O$  values may have been set during the formation of the hornblendes by the MGS metamorphism (D2), during the earlier D1 event, or be influenced by the igneous precursors.

The ubiquitous retrogressive alteration and infilled cracks indicate significant fluid infiltration throughout Connemara after peak metamorphism (Miller et al., 1991; Jenkin et al., 1992; O'Reilly et al., 1997). From  $\delta D$  and  $\delta^{18}O$  studies of fluid inclusions in Galway Granite quartz crystals and three generations of vein quartz mineralisation, O'Reilly et al. (1997) identified three discrete palaeo-fluids which have affected the Galway granite:

I. The earliest fluid was a  $H_2O$ - $CO_2$ - $NaCl$ , moderate salinity (4-10wt.%  $NaCl$  eq.) brine which deposited late magmatic molybdenite mineralised quartz veins ( $V_1$ ). This

fluid was most abundant in the western part of the Galway Granite batholith. Estimated  $V_1$  precipitation was previously estimated at  $\sim 600^\circ\text{C}$  and 1-3kb;  $\delta^{18}\text{O} = +9.5\pm 0.4\text{‰}$  ( $\delta\text{D}$  not given). More recent estimates of this fluid have yielded the fluid temperature at  $305\text{-}390^\circ\text{C}$  due to re-equilibration of  $\delta^{18}\text{O}$  in fluid inclusions during cooling. This fluid is considered to have been derived from magmatic fluids during the granite emplacement and its influence is believed to be in veins contained within the body of the granite batholith itself.

II. The second fluid (retrogressive fluid, RGF) was a  $\text{H}_2\text{O-NaCl-KCl}$ , low-moderate salinity (0-10wt.% NaCl eq.) brine which deposited  $V_2$  quartz veins which infill faults active during post-consolidation uplift of the batholith. The temperature range for precipitation of the  $V_2$  veins was  $270\text{-}340^\circ\text{C}$ ;  $\delta\text{D} = -18\pm 2\text{‰}$ ,  $\delta^{18}\text{O} = +0.5\text{‰}$  to  $+2.0\text{‰}$ . This is the fluid considered responsible for the widespread retrograde metamorphism in the Dalradian and MGS rocks of the Connemara region; chloritisation of hornblende and biotite, sericitization and saussuritization of plagioclase and reddening of K-feldspar and widespread quartz and epidote veining. This fluid is thought to have been circulated throughout these rocks as part of a large scale fluid convection system, based around the cooling Galway Granite batholith, pulling meteoric water in from the overlying accumulating Silurian strata being deposited by this time (Jenkin et al., 1997).

III. The final fluid identified by O'Reilly et al. (1997) was a  $\text{H}_2\text{O-NaCl-CaCl}_2\text{-KCl}$ , variably saline (8-28wt.% NaCl eq.) brine depositing  $V_3$  quartz veins (which also contain hematite). Geochronology suggests these veins were late Triassic in depositional age. The temperature range for precipitation of these  $V_3$  veins was  $125\text{-}205^\circ\text{C}$ ;  $\delta\text{D} = -17\text{‰}$  to  $-45\text{‰}$ ,  $\delta^{18}\text{O} = -3.0\text{‰}$  to  $+1.2\text{‰}$ . This fluid was interpreted as having resulted from the mixing of two end-members; a high  $\delta\text{D}$  fluid from convecting meteoric water or evaporated seawater and a lower  $\delta\text{D}$  fluid from basinal brine derived from the Carboniferous limestones south of the Galway Granite batholith.

The above three fluid types identified by O'Reilly et al. (1997) are all centred on the Galway Granite batholith and its associated plutons. However, the second fluid (retrogressive fluid, RGF) also passed through the whole of the Connemara metamorphic complex due to the network of faults and foliation surfaces. This RGF has caused the widespread retrograde metamorphism throughout Connemara and due to the similar  $\delta D$  values (within error) of the most deuterium rich samples, is probably responsible for the reduction of hornblende K-Ar ages observed. It may be of interest to consider that this KCl bearing fluid may have increased the K-contents of hornblendes giving a relative apparent reduction of age with no reduction of  $^{40}\text{Ar}^*$ . However, in view of the known presence of submicroscopic phyllosilicate along cleavage traces (Miller et al., 1991) the increased fluid accessibility into the hornblende would certainly allow a greater  $^{40}\text{Ar}^*$  escape potential (Harrison, 1981) and so an increase in K would be an unlikely mechanism for K-Ar age reduction in hornblendes.

From the present study, the progression of fluid  $\delta D$  towards  $\sim -16\text{‰}$  (Figure 5.30) is correlatable with the openness of the hornblende structure through composition (Mg-rich less open, Fe-rich more open). The fluid  $\delta D \sim -16 \pm 1.5\text{‰}$  value estimated from the highest (most deuterium enriched) hornblende  $\delta D$  values strongly suggests that the retrogressive fluid responsible for widespread hydration alteration throughout Connemara was indeed responsible for the microstructure effects, reduction in K-Ar age and increase in  $\delta D$  values observed in hornblendes. There is a convergence of the most susceptible samples of Fe-rich hornblende having the highest  $\delta D$  values and reset K-Ar ages approaching (within error) the time of the retrogressive fluid incursion,  $\sim 400\text{Ma}$ , associated with the Galway Granite intrusion.

The K-Ar ages of the hornblendes do not therefore represent true ages of events, but rather the mineral's susceptibility to alteration by the retrogressive fluid of  $\sim 400\text{Ma}$ . These phenomenon in the hornblendes probably represent the initial stages of this mineral's decomposition by the retrogressive fluid, effectively halted before further alteration could take place because of the short time span for which the retrogressive fluid was active.

The estimated fluid temperature range of 270-340°C for the RGF would have been insufficient to cause loss of  $^{40}\text{Ar}^*$  in hornblendes which have a  $T_c$  of 500 $\pm$ 50°C. However, a hornblende with phyllosilicate intergrowths as cleavage fluid pathways could show a significantly younger K-Ar age due to the possible effective lowering of  $T_c$  (down to ~300-350°C) due to these imperfections. The  $\delta^{18}\text{O}$  values obtained are believed to be predominantly primary and crystallochemically controlled, derived from the original metamorphism or magmatic values, because the RGF, at 270-340°C, is thought to be below the oxygen diffusion  $T_c$  of ~600°C; (Jenkin, 1988). There is some correlation of  $\delta^{18}\text{O}$  with  $\text{Fe}_2\text{O}_3$  and FeO in the hornblendes of this study; this is suspected to be from this primary crystallochemical control.

The correlation of hornblende  $\delta\text{D}$  with K-Ar age (Figure 6.3(c)) suggests that K-Ar ages are influenced by the interaction with the RGF. Younger K-Ar ages are observed with higher  $\delta\text{D}$  values. This observation is consistent with  $\delta\text{D}$  isotopic exchange having taken place with the RGF,  $^{40}\text{Ar}^*$  being displaced during the intrusion of OH<sup>-</sup> through the A-site “porosity” in the hornblende mineral structure.

It is proposed that  $\delta\text{D}$  increases as hornblende K-Ar age decreases due to the composition of the hornblende, dependant on being Mg-rich (resistant to change) or Fe-rich (susceptible to changes because of the higher ionic porosity), in it's interaction with the RGF at 270-340°C.

The relationship between  $\delta\text{D}$  and K-Ar age on Figure 5.17 and Figure 6.3(b) appears to show two lines of evolutionary trends running parallel to each other from ~490Ma to ~410Ma. The  $\delta\text{D}$  of the lower line increases from ~-64‰ to ~-44‰ and the upper line from ~-54‰ to ~-38‰. The lower trend has more samples in which relict grains were observed (Figure 3.2) in thin section (Appendix 2) and two hornblende compositions present in EMPA results (Appendix 5, 5A and 6). While the upper trend displays hornblende crystals of more uniformity in size and EMPA composition and are generally from the south of the collection area (Figure 3.1). This is a general observation but is not exclusive to either group. These observations are not apparent on consideration of  $\delta\text{D}$  or K-Ar age results alone, but when combined. This phenomenon may be due to the presence

of the relic grains retaining a more negative  $\delta D$  “memory”, displacing the samples of the lower trend.

The reason for the offset of the datapoints from Miller et al. (1991) on Figure 6.3(c) against the datapoints from this study is not clearly understood. There may have been different machine operating conditions at the time.

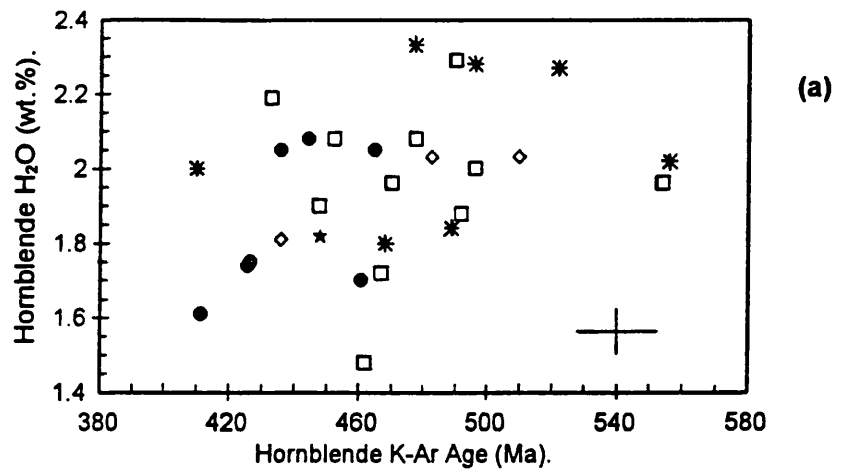
The four samples with ages greater than  $\sim 490$ Ma are obviously off the trend of the whole dataset (Figure 6.3(b)), as also observed with ionic porosity (Figure 5.14 and Figure 6.3(a)). This establishes the presence of excess  $^{40}\text{Ar}$  without the need for expensive and time consuming  $^{40}\text{Ar}^* - ^{39}\text{Ar}$  analysis on each sample, but it should be considered that the effects of excess  $^{40}\text{Ar}$  may well be influencing other samples within the dataset which are not recognised by having a K-Ar age  $> 490$ Ma but may be contributing to the scatter of results.

### 6.3.2. Structural Water in Hornblendes.

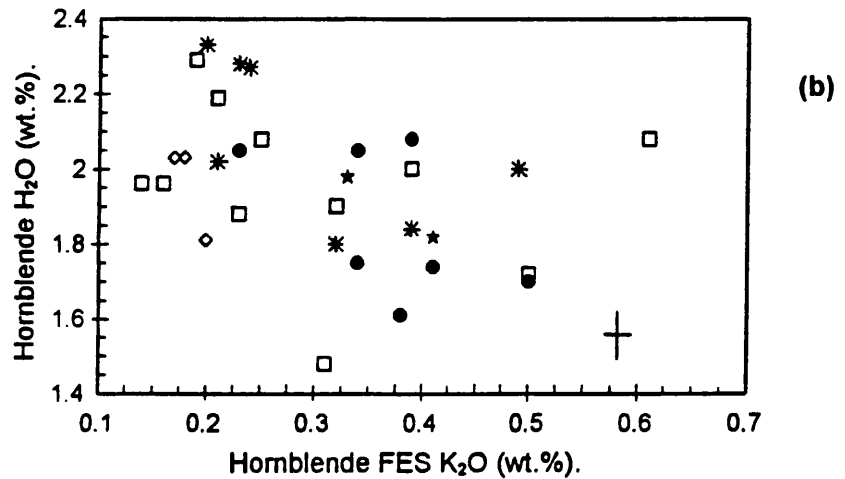
The structural water contents (wt.%) of the hornblendes studied in this work are estimated from the yield values obtained during hydrogen isotope analysis and are listed in Appendix 10.

Miller et al. (1991) observed an apparent increase in structural water content associated with a decrease of K-Ar ages and an increase in  $\delta D$  values of the investigated hornblendes. This was interpreted as being due to the forced intrusion of the external fluid into the hornblende structure, aided by phyllosilicate cleavage pathways, occupying vacant A-sites and pushing out  $^{40}\text{Ar}^*$  in the process. Hence satisfying the measured isotope values and trends between them. However, these trends with water content have not been duplicated in this present study based on 29 samples (Figures 6.5 and 6.6). In fact the opposite trend is observed for structural water content against  $\delta D$ , (Figure 6.5(c)). Also, the high structural water contents of up to  $\sim 2.8$ wt.% in hornblende as measured by Miller et al. (1991) are not generally encountered. **TJ-44** being the only sample to yield a measured water content of 2.84wt.%, similar to the excess water contents of Miller et al. (1991). This sample was collected in the southern part of the Dalradian and gives a K-Ar age of  $483 \pm 13$ Ma which is in disagreement to the lowering of ages as experienced by Miller et al.

Dataset (29).  
 $R = 0.354$ ; 90-95%.  
 Group-A (7).  
 $R = 0.514$ ; <80%.  
 Group-B (7).  
 $R = 0.218$ ; <80%.



Dataset (29).  
 $R = -0.394$ ; 95-99%.  
 Group-A (7).  
 $R = -0.541$ ; <80%.  
 Group-B (7).  
 $R = -0.615$ ; 80-90%.



Dataset (28).  
 $R = -0.464$ ; 95-99%.  
 Group-A (7).  
 $R = -0.524$ ; <80%.  
 Group-B (7).  
 $R = -0.011$ ; <80%.

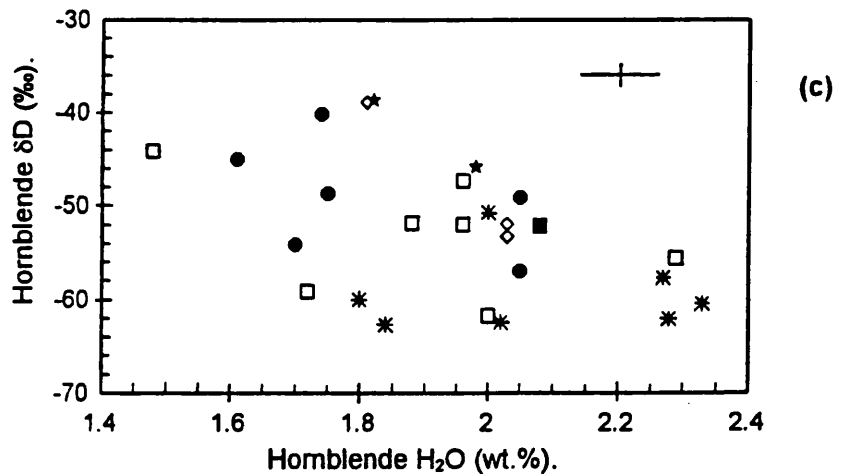
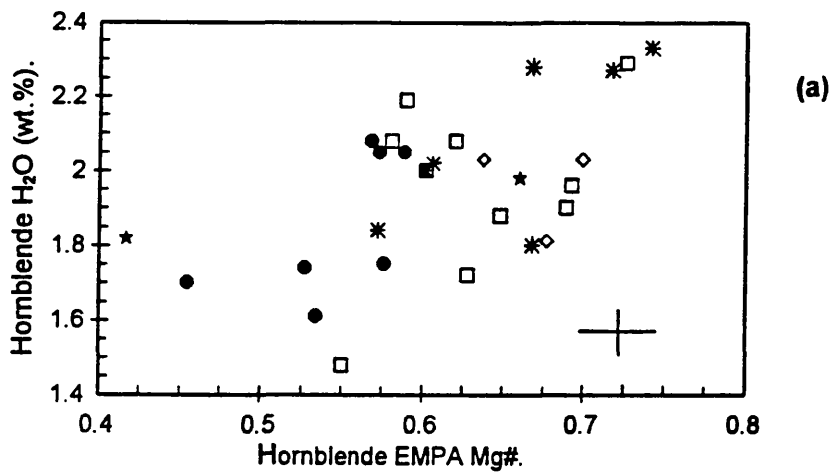
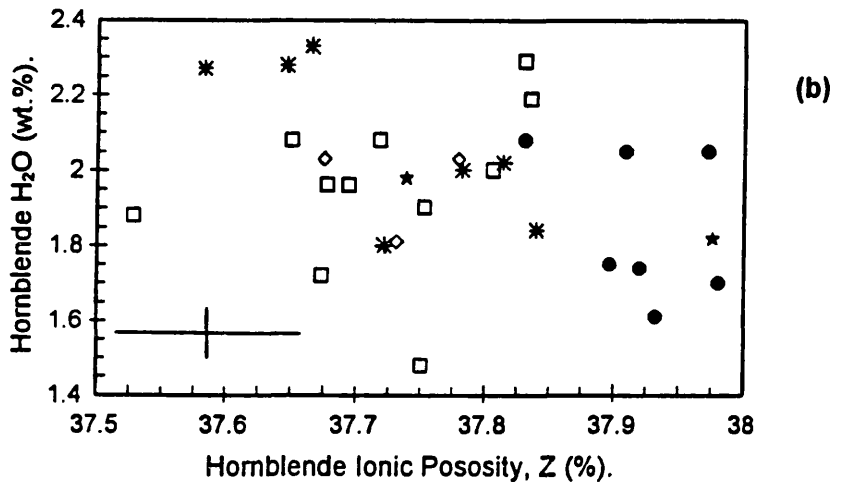


**FIGURE 6.5** From the present study. Comparisons of H<sub>2</sub>O contents (wt.%) with: (a) Hornblende K-Ar ages (Ma). (b) Hornblende K<sub>2</sub>O (wt.%). (c) Hornblende δD (‰). Data in relevant sections in Appendix. Symbols: **Group-A** = filled octagons; **Group-B** = asterisks; **Group-C** = open diamonds; others = open squares; MGS = black stars. Average errors are represented by the —+— symbol. Data in relevant sections of Appendix.

Dataset (29).  
R = 0.549; >99%.  
 Group-A (7).  
 R = 0.632; 80-90%.  
 Group-B (7).  
R = 0.723; 90-95%.



Dataset (29).  
R = -0.322; 90-95%.  
 Group-A (7).  
 R = -0.368; <80%.  
 Group-B (7).  
R = -0.760; 90-95%.



Dataset (29).  
 R = 0.236; <80%.  
 Group-A (7).  
 R = 0.184; <80%.  
 Group-B (7).  
 R = 0.171; <80%.

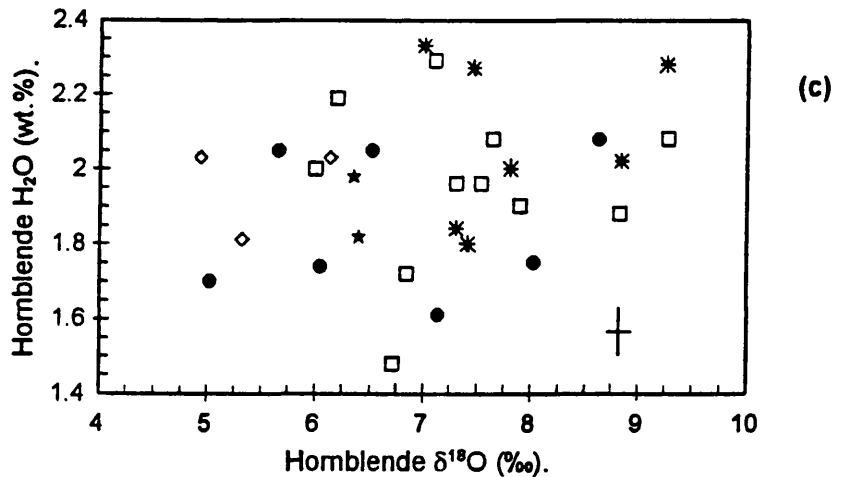


**FIGURE 6.6** From the present study. Comparisons of H<sub>2</sub>O contents (wt.%) with: (a) Hornblende Mg#. (b) Hornblende A-site occupancy. (c) Hornblende ionic positivity, Z (%). Data in relevant sections in Appendix. Symbols: **Group-A** = filled octagons; **Group-B** = asterisks; **Group-C** = open diamonds; others = open squares; MGS = black stars. Average errors are represented by the —+— symbol. Data in relevant sections of Appendix.

(1991). It is suspected that **TJ-44** was possibly influenced by the presence of biotite or chlorite alteration within cleavages (Figures 3.5, 5.1D and 5.1E) which could significantly increase the measured water content of a sample (Appendix 10). Even in quantities below the detection limit of XRD for purity checking and not observable under the binocular microscope for removing individual chlorite grains by hand picking.

**TJ-44** and **TJ-59** are not presented on the graphs of Figures 6.5 and 6.6 which show the correlations of K-Ar age,  $K_2O$  content,  $\delta D$  value, Mg#, and ionic porosity in relation to hornblende structural water content. The trend of increasing structural water content with increasing Mg# is as expected from calculated water contents from ideal formulae of hornblende end-members (Appendix 10). The figures also show a general decrease of structural water content with decreasing K-Ar ages and increasing  $K_2O$  content. This again reinforces the implication of compositional control on K-Ar ages as shown also in the relationship with ionic porosity (although much scattered; Figure 6.6(b)). No correlation of water content with  $\delta^{18}O$  was observed.

It may be possible that the increase in structural water content of the hornblendes investigated by Miller et al. (1991) was influenced by the acknowledged presence of phyllosilicate alteration in the cleavages. This would explain the increase in  $\delta D$  values with higher water contents because of the interaction of the phyllosilicates with the RGF, at 270-340°C, rather than with the hornblende itself and the network of passageways for  $^{40}Ar^*$  to escape due to the shorter diffusion distances required.

### 6.3.3. Relationships with $\delta^{18}O$ .

The [ $\delta^{18}O$ - $\delta D$ -Z] diagram of Figure 6.7 shows a similar relationship to the [Age- $\delta D$ -Z] diagram of Figure 6.4. The interpretation of this  $\delta^{18}O$ - $\delta D$ -Z diagram is that there is a strong correlation of  $\delta D$  with Z (Figure 5.26) as observed in the [Age- $\delta D$ -Z] diagram, but the correlation of  $\delta D$  with  $\delta^{18}O$  (Figure 5.29) is less obvious (just under 90%). The  $\delta^{18}O$  shows good correlation with Z because it is predominantly from the primary formation and growth of the metamorphic hornblende and reflects the equilibrium achieved with the chemical and structural character of each hornblende with the ~600°C fluid at

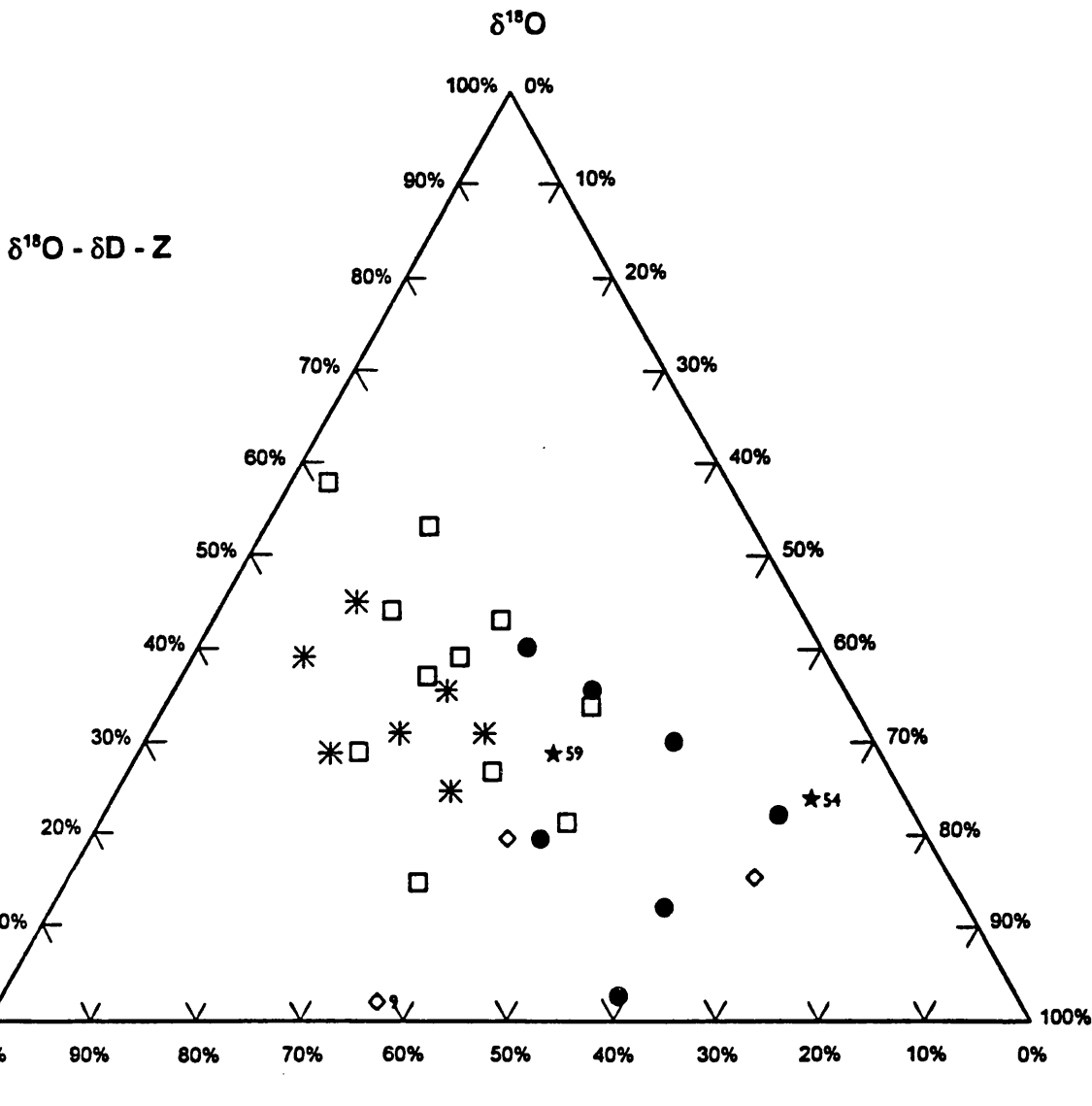


FIGURE 6.7 [ $\delta^{18}\text{O}$ - $\delta\text{D}$ -Z] diagram. Percentages based on:  $\delta^{18}\text{O}$  age range = +4.8‰ ( $\delta\text{D}$ -Z line) to +9.4‰ (apex);  $\delta\text{D}$  range = -65‰ (apex) to -35‰ ( $\delta^{18}\text{O}$ -Z line), ie. increasing  $\delta\text{D}$  from left to right on diagram; Z range = 37.500% ( $\delta\text{D}$ - $\delta^{18}\text{O}$  line) to 38.000% (apex). Symbols: **Group-A** = filled octagons; **Group-B** = asterisks; **Group-C** = open diamonds; others = open squares; MGS = black stars. Diagram construction data in Appendix 15.

~490Ma. The ionic porosity reflects the relative differences in hornblende compositions. Also, the effect of isotopic exchange with the RGF would be mostly with OH<sup>-</sup> and would affect the oxygen isotope ratios only in the hydrated component of the hornblende which is generally ~2wt.% of the whole.

#### **6.4 Relevance to Geological Synthesis in Connemara.**

From the findings of the previous sections it is thought that there is a difficulty in assigning a realistic geological significance to the ages determined by the K-Ar technique. The reasons are as follows:

I. The chemical composition and hence crystal structural properties (ionic porosity and A-site occupancy) of the investigated hornblendes have an effect on the <sup>40</sup>Ar\* closure temperature initially.

II. The susceptibility of the hornblende to infiltration by the RGF at ~400Ma is also determined by the chemical composition and ionic porosity. In hornblendes, the increase in δD values corresponds to a decrease in age. This is related to the disturbance of accumulated <sup>40</sup>Ar\* in A-sites by the hydrogen isotope exchange of OH<sup>-</sup> and OD<sup>-</sup> in the hornblende structure, effectively knocking <sup>40</sup>Ar\* out of position creating a temporary destabilisation of the A-site while the mechanism is in progress. The K-Ar “clock” is reset when the hydrogen isotope exchange mechanism has ceased. This would suggest that <sup>40</sup>Ar\* would be accumulated from ~400Ma, after the retrograde fluid activity in Connemara had passed.

III. There is chemical variation observed within hornblende on the scale of μm as determined by EMPA. Therefore, regarding the K-Ar age and δD variation with composition as measured from hornblende mineral separates, it follows that there will also be a variation in isotope values on the scale of μm.

IV. The exact date of the RGF incursion is difficult to determine from this work because of the affected K-Ar ages. The youngest hornblende K-Ar ages of  $\sim 410 \pm 10$  Ma may record the date of the effects of the RGF. Within a single sample the K-Ar age will probably be an amalgamation of slightly younger and slightly older ages, on a scale of  $\mu\text{m}$ , depending on the hornblende composition throughout the actual grains selected.

The interpretation of this work is that the hornblende K-Ar ages in the Dalradian strata were set during the  $\sim 490$  Ma main metamorphic phase associated with the regional intrusion of the MGS (Leake, 1989; Cliff et al., 1996). Also influencing these measured ages, which depend on the  $^{40}\text{Ar}^*$  retaining ability of the minerals investigated, is the variation of composition and ionic porosity, possible effects of excess Ar in some samples, lower range of peak metamorphism at 463 Ma (Friedrich et al., 1997) than previously thought and the presence of submicroscopic phyllosilicate alterations. However a greater influence on the  $^{40}\text{Ar}^*$  retention was the effect of the extensively circulated retrogressive fluid of meteoric origin associated with the cooling of the Galway Granite batholith at  $\sim 400$  Ma (Jenkin et al., 1992; O'Reilly et al., 1997; Jenkin et al., 1997). The evidence for this being the resetting of the hornblende K-Ar ages at  $\sim 400$  Ma (within error and from Elias et al., 1988 and Miler et al., 1991).

It is reasoned that the range of ages observed in this study, from  $\sim 490$  Ma down to  $\sim 410$  Ma, represent the resistance of Mg-rich or susceptibility of Fe-rich hornblende to infiltration by the  $\sim 400$  Ma RGF, disturbing the K-Ar age of each sample in proportion to the amount of imprinted hydrogen isotopic exchange (Figure 6.3(b)). It is considered that the disturbed K-Ar age, increase in  $\delta\text{D}$  value and increasing presence of submicroscopic phyllosilicate alteration in samples increasingly rich in Fe, as observed by TEM (Onstott and Peacock, 1987; Miller, 1990) are evidence of the initial stages of the retrogressive hydrothermal alteration of hornblende by the 270-340°C RGF at  $\sim 400$  Ma (O'Reilly et al., 1997; Jenkin et al., 1997). Because the RGF was only active for a relatively short period of time,  $\sim 10^4$  years (Jenkin et al., 1992; O'Reilly et al., 1997), the effects did not continue long enough to extensively alter the hornblendes (except some in the south, for example, **TJ-44**,

Figures 3.5, 5.1D and 5.1E) and stopped at the end of the RGF event. It is not considered that the later, lower temperature, Triassic fluid of O'Reilly et al. (1997) measurably affected the isotope values of the hornblendes investigated in this study. The K-Ar ages are set at ~410Ma at the youngest and the temperature of this Triassic fluid was much lower at 125-205°C. TJ-59 may however show some effects, but is a very degraded sample.

## 6.5 Future Study.

Previous TEM studies (Onstott and Peacock, 1987; Miller et al. 1991) showed different “*a*” parameters between Mg-rich and Fe-rich hornblendes. The EMPA results of this work demonstrate complex compositional variation on the scale of  $\mu\text{m}$  (Section 5.1) in samples collected in the north of the Dalradian (lower grade metamorphic zones). Also, from the northern area, there is the presence of variable composition hornblende relic grains (2-3mm in size) and a later generation of hornblende growth as metamorphic foliation fabric, from the 490Ma metamorphic peak.

A problem with the isotopic study carried out in this work is that the K-Ar age,  $\delta\text{D}$  and  $\delta^{18}\text{O}$  values are obtained from mineral separate aliquots; 100-160mg for  $^{40}\text{Ar}^*$  measurements, 60-70mg for  $\delta\text{D}$  evaluation and 8-10mg for  $\delta^{18}\text{O}$  evaluation. The  $^{40}\text{Ar}^*$  and  $\delta\text{D}$  aliquots contain hundreds of grains of ~90-125 $\mu\text{m}$  in size, the  $\delta^{18}\text{O}$  aliquots were visually estimated to contain 40-60 grains of the above sizes. From the observed compositional variation by EMPA over distances as short as 5 $\mu\text{m}$ , it is postulated that there is also a potentially large variation of composition within grains of ~90-125 $\mu\text{m}$  in size. An attempt to address this problem by using estimated bulk EMPA results (Appendix 5 and 5A) to compare with the isotope results derived from the mineral separates has been implemented in this study.

Ideally, if it were possible to measure  $^{40}\text{Ar}^*$ ,  $\delta\text{D}$  and  $\delta^{18}\text{O}$  values at the same point and at the same time as the composition measured by EMPA on a polished section, then this would probably reduce the scatter of points observed on the isotope-composition diagrams. The scale of measurement would be reduced from ~90-125 $\mu\text{m}$  to ~2 $\mu\text{m}$ . The current

technology does not at present exist to cover all these analyses at once, although it would be possible to analyse elemental composition by EMPA followed by laser probe analysis of  $^{40}\text{Ar}^*$  followed by laser probe analysis of  $\delta^{18}\text{O}$ . Laser probe technology for analysis of  $\delta\text{D}$  is not currently available. However, the use of an ion-probe instrument may address many of these requirements. The above technique as outlined could be implemented to characterise the differences between Fe-rich hornblende (a) and Mg-rich hornblende (b) in samples with two hornblende composition populations (Section 5.1).

A problem with this step by step multiple analysis would be the necessity to analyse different points on a polished section due to the damage caused by each previous analysis. Although the points would be possibly 4-5 $\mu\text{m}$  apart, this may still cause problems with changes in composition from point to point. Also, if EMPA was carried out first then the proximal  $^{40}\text{Ar}^*$  measurement may be affected by electron beam damage. If the  $^{40}\text{Ar}^*$  is carried out first, then the relatively volatile K may be affected by the structural damage and dehydration caused by the laser thermal damage in the material surrounding the vaporised analysis point. This would necessitate the other required analyses being carried out further away from the analysis point, therefore introducing the possibility of analysis incompatibility: Are K and  $^{40}\text{Ar}^*$  from different points representative of each other and combined do they give a reliable age and for which point, considering variation on a scale of  $\mu\text{m}$ ? Have either been affected by the previous destructive analysis technique? If  $\delta\text{D}$  could be measured it would also be affected by proximal structural damage and dehydration and would certainly be suspect, unless analysed at a greater distance away from the previous two analyses points, hence further increasing the potential for scatter in the results. Phyllosilicate alteration along cleavages in some samples would also have to be avoided (Figures 3.5, 5.1D and 5.1E).

However, even on the scale of  $\mu\text{m}$ , the effects of phyllosilicates occurring in cleavages on the scale of nm (Onstott and Peacock, 1987; Miller et al., 1991) are not able to be taken into consideration. Therefore, even if the analyses could be carried out at one  $\sim 2\mu\text{m}$  point (instantaneously, rather than over a  $\sim 30$  second time period, to avoid volatilisation of  $^{40}\text{Ar}^*$ , K and water), some scatter of points would still occur due to this

“unknown” phyllosilicate quantity. Ideally, an instantaneous analysis of elemental composition,  $^{40}\text{Ar}^*$ ,  $\delta\text{D}$  and  $\delta^{18}\text{O}$  values on a scale of nm, avoiding phyllosilicates in cleavage traces using transmitted electron microscopy (TEM) would give more precise measurements and better correlations of combined data. From these results profiles of K-Ar age,  $\delta\text{D}$  and  $\delta^{18}\text{O}$  variation with composition for hornblendes could be constructed. Also the “ $\alpha$ ” parameters could be realistically evaluated considering the effect of proximity, magnitude and network density of sub-microscopic phyllosilicate cleavage alteration phases in relation to the composition of the host hornblende on the nm scale. However, at present the technology in this configuration is not available and it would be necessary to carry out separate analyses, again encountering the problems outlined above concerning different analysis points and volatilisation of certain species.

In a recent publication (Siebel et al., 1998) which became available when the final conclusions to this thesis had been written, a direct correlation of  $^{40}\text{Ar}^*$ - $^{39}\text{Ar}$  ages with variable hornblende compositions on a scale of  $\mu\text{m}$  within single hornblende grains was proven.

This work by Siebel et al. (1998) investigated calcic-amphiboles from dioritic igneous rocks from the late Hercynian orogeny in northeast Bavaria. Microprobe and scanning electron microscope analyses showed (previously mineral separated) hornblende grains of two composition populations within single grains. The types were generally:

- I. Al-, Ti-, Fe-, K-, and Na-rich type.
- II. Si- and Mg-rich type.

These compositions were found to be intimately intergrown within single crystals. They correspond to the Fe-rich (hornblende (a)) and Mg-rich (hornblende (b)) compositions found in the samples which yielded two hornblende composition populations in this present work (Section 5.1, Appendix 5A and 6A).

Siebel et al. (1998) studied three hornblende samples which gave conventional K-Ar ages of 320Ma, 317Ma and 302Ma. When dated by  $^{40}\text{Ar}^*$ - $^{39}\text{Ar}$  step heating they found that the Mg-rich components correlated to high temperature Ar release, giving ages of 342Ma, 346Ma and 344Ma respectively, whereas lower to medium temperature degassing corresponded to ages younger than 325Ma, attributed to the Fe-rich composition. They suggested that the Mg-rich domains in single crystals were very resistant to Ar loss by later reheating due to Hercynian granitic intrusions.

This recent publication supports the findings of chemical variation within single crystals in this present study and confirms the direction for future investigation of hornblendes and micas in the Dalradian rocks of the Connemara region of western Ireland.

## CHAPTER 7.

### CONCLUSIONS.

#### 7.1 Conclusions: K-Ar Dating, Composition and Stable Isotope Studies of Hornblendes.

From the work of this thesis, apart from confirming the widespread (~150Ma) variation of K-Ar ages in hornblendes, there are several important points concerning results and the interpretations of previous workers on the significance of K-Ar dating studies using hornblendes from the Dalradian rocks of the Connemara region of western Ireland.

Previously unobserved relationships were found to be present between the hornblende compositions, ionic porosity, K-Ar ages and  $\delta D$  values. Also, the increasing  $\delta D$  values with reducing K-Ar ages was further confirmed (Miller et al., 1991). It appears very strongly that the  $FeO/(FeO+MgO)$  of the hornblende greatly influences the K-Ar age and  $\delta D$  values. Generally the relationships are as follows:

<u>Fe-rich hornblende.</u>	<u>Mg-rich hornblende.</u>	
Lower K-Ar age.	Higher K-Ar age.	
Higher $\delta D$ values.	Lower $\delta D$ values.	
Higher ionic porosity.	Lower ionic porosity.	] Composition related properties.
Lower $H_2O$ wt. %.	Higher $H_2O$ wt. %.	
Higher $K_2O$ wt. %.	Lower $K_2O$ wt. %.	
More phyllosilicate microstructure alteration.	Less phyllosilicate microstructure alteration.	

The reason why this study has found these relationships while Elias (1985), Elias et al. (1988) and Miller et al. (1991) did not is due to the more extensive chemical characterisation of the hornblendes. The excess water contents of lower age hornblendes observed by Miller (1990) may have been due to the undetected presence of biotite or

chlorite alteration in cleavages in some of the hornblende separates influencing the low number of samples studied (12 samples). H<sub>2</sub>O content appears to be related to the FeO/(FeO+MgO) ratio (or alternatively the Mg#) of the hornblendes investigated and varies with K-Ar age and  $\delta D$  in relation to composition, rather than the forcible removal of <sup>40</sup>Ar\* during stable isotope exchange as proposed by Miller et al. (1991). It is probable that the more open structures of the Fe-rich hornblende compositions allow easier hydrogen isotope exchange by OH<sup>-</sup> intrusion by having a higher ionic porosity and have more phyllosilicate microstructures acting as conduits for fluid circulation.

## 7.2 Results in Relation to Geology.

The results and findings of this work in relation to the geology of Connemara are summarised as follows:

I. The metasediments containing horizons of intruded or extruded tholeiitic basalt type rocks were metamorphosed by the D1 event which is now only recognised by discordant inclusion trails in relic grains of hornblende in the north of the Dalradian study area in Connemara. These grains (Section 5.1) have survived the later D2 metamorphic overprinting of the presently identifiable metamorphic zones associated with the intrusion of the MGS to the south (Figure 1.3).

II. This D2 metamorphism was responsible for the east-west trending metamorphic fabric in Connemara and the formation of the amphibolites found in the Dalradian sequence. This probably recrystallised the hornblendes formed by the earlier D1 phase, resetting the K-Ar “clocks” to between ~490Ma (Leake, 1989) and 463Ma (Friedrich et al., 1997). A group of four samples from different geographical locations have ages between 510-556Ma, well above the 490Ma previously considered as the oldest K-Ar ages in hornblendes (Miller et al., 1991). These may represent Ar retention associated with cooling from the earlier D1 event.

III. The later D3 and D4 events occurred at temperatures below the recognised temperatures of  $^{40}\text{Ar}^*$  closure for hornblende. The intrusion of the Galway Granite rocks would have thermally affected the enclosing MGS rocks only. However, the convection cell associated with this large cooling igneous body percolated fluids through the whole of the Connemara region causing retrograde alteration to varying degrees, depending on rock permeability and mineral susceptibility, across a large area. This fluid ( $\delta\text{D} = -18\pm 2\text{‰}$ ,  $\delta^{18}\text{O} = +0.5\text{‰}$  to  $+2.0\text{‰}$ ) was derived from a meteoric water source, believed to be from the overlying sedimentary pile of the Silurian sediments, sucked down into the large scale convecting cell (throughout the Connemara region) around the cooling Galway Granite batholith at  $\sim 400\text{Ma}$  (Jenkin et al., 1997; O'Reilly et al., 1997).

The findings of this study are that the hornblendes have been affected by a fluid of  $\delta\text{D} = -16\pm 1.5\text{‰}$ . The  $\delta^{18}\text{O}$  values of the fluid corresponding to  $\delta\text{D} = -16\pm 1.5\text{‰}$  were not able to be evaluated in this study and are believed to have been set at the time of formation of the amphibolites, from their basaltic precursors, during the main, MGS intrusion related D2 metamorphic event. Figure 5.30 shows the progression of fluid  $\delta\text{D}$  from  $\sim -40\text{‰}$  (metamorphic/igneous waters) to  $\sim -16\text{‰}$  (meteoric water, RGF).

IV. The Mg-rich hornblendes (lower ionic porosity) were more retentive of  $^{40}\text{Ar}^*$  than the Fe-rich varieties (higher ionic porosity) at higher temperatures during initial cooling after MGS associated metamorphism. This would create an initial differential in measured K-Ar age. The Mg-rich varieties were also more resistant to the effects of the meteoric derived, convecting retrogressive fluid than the Fe-rich hornblendes which formed phyllosilicate alteration along cleavage pathways, intruded by the fluids. This effect being controlled by the alteration potential of the hornblende due to composition and ionic porosity. The Fe-rich hornblendes have higher  $\delta\text{D}$  values than their Mg-rich counterparts because of the easier ability to equilibrate hydrogen isotopes.

In effect, it may be considered that the hydrogen isotope exchange closure temperature of the Mg-rich hornblendes was above the temperature of the retrograde fluid (RGF), at  $270\text{-}340^\circ\text{C}$ . But the RGF temperature range was above the hydrogen isotope

exchange closure temperature for the Fe-rich varieties. Samples with intermediate single compositions and samples with distinct Fe-rich (hornblende (a)) and Mg-rich (hornblende (b)) components were affected to varying degrees by the RGF. Their bulk compositions generally reflecting the degree of susceptibility. The Mg-rich hornblendes in this study are thought to show the most representative K-Ar ages, unaffected or less affected by the RGF.

It is proposed that the range in K-Ar ages, the  $\delta D$  trends and the phyllosilicate alterations are ultimately dependent on the ionic porosity and therefore the initial composition of the hornblende under investigation.

It is observed from this work that due to compositional variance it is likely that these effects can occur within single grains of a rock sample.

The factors influencing the observed K-Ar ages of the hornblendes investigated in this work create a difficulty not previously considered when measuring hornblende K-Ar ages in Connemara. The composition of the hornblendes has a greater influence on the measured K-Ar ages than previously thought (Elias et al., 1988; Miller et al., 1991). The varying compositions within single hornblende grains (on a scale of  $\mu m$ ) and therefore varying K-Ar ages within these grains would mean that the use of 90-125 $\mu m$  mineral separates could encompass a large range in hornblende compositions, K-Ar ages,  $\delta D$  and  $\delta^{18}O$  values. The values obtained from these separates are therefore averages which may, or may not (depending on each individual sample), be subject to variation and error due to this inherent compositional variation.

In conclusion, the hornblende isotope analyses in this study suggest that the hornblende K-Ar "clocks" were set at the end of the main metamorphic (D2) event, ~490-463Ma (Leake, 1989; Friedrich et al, 1997), by cooling below their  $^{40}Ar^*$  closure temperatures, ~578-490°C (Harrison, 1981). The accumulated  $^{40}Ar^*$  was disrupted by the hydrogen isotope exchange mechanism associated with the aggressively convecting RGF at ~400Ma (Jenkin et al., 1997). The intermediate K-Ar ages represent intermediate  $^{40}Ar^*$  retention between almost complete resistance to  $^{40}Ar^*$  loss (Mg-rich hornblendes) to complete  $^{40}Ar^*$  loss (Fe-rich hornblendes) and new accumulation from ~400Ma. The  $\delta D$

signature of the RGF being partially or wholly imprinted on the mineral in the process. It may be considered that these effects on the isotope values and the presence of submicroscopic phyllosilicate alteration (Onstott and Peacock, 1987; Miller, 1990) indicate the very initial stages of retrograde alteration of hornblende. The RGF event lasting only in the region of  $\sim 10^4$  years (Jenkin et al., 1992), not having a long enough time to extensively alter the hornblendes.

### 7.3 Future Work.

A practical extension of this work for investigating the combined effects of hornblende composition and occurrence of phyllosilicates within the amphibole structure on measured K-Ar ages,  $\delta D$  and  $\delta^{18}O$  could be achieved by the following operation.

An already well investigated site would be selected in an area where previous hornblende EMPA effectively showed a single composition, the hornblende grainsizes were relatively uniform, no relic grains of hornblende were present and where a large quantity of mineral separate was obtainable. For example, the roadside quarry studied by Miller (1990) (Miller et al., 1991) at grid reference 821467. A detailed study of this site for faulting, quartz veining and areas of alteration by fluid flux would be carried out. About 36 amphibolite samples ( $\sim 1$ -2kg each) would be collected from well identified points within this site, covering the full width of this quarry ( $\sim 30$ m) and with some local clusters  $\sim 50$ cm apart and also some samples next to quartz veins.

The samples collected would then be analysed by rock XRF and observations of thin sections made. Mineral separates to 60-90 $\mu$ m would be recovered and the compositions measured by XRF of the mineral separates. K-Ar ages,  $\delta D$  and  $\delta^{18}O$  values would be measured by conventional techniques to characterise the samples. This first stage would then show the K-Ar age relation to bulk composition and  $\delta D$ , as demonstrated by the present study. However, this does not take into account the effects of microstructural phyllosilicate alteration in cleavages and hence the reduction of  $^{40}Ar^*$  closure temperature due to the reduction of diffusion domains (Dodson, 1973). A study by transmission electron

microscope (TEM) on the scale of nm would be required to estimate the relative quantity and density of these. Individual grains in each sample would then be selected for elemental mapping by X-ray analysis under TEM to build up a profile of hornblende compositions, including K-content. These selected grains would then be point analysed for  $^{40}\text{Ar}^*$  and  $^{39}\text{Ar}$  by laser probe and the K-Ar and  $^{40}\text{Ar}^*$ - $^{39}\text{Ar}$  cooling ages could then be compared with the compositions (Siebel et al., 1998) and the underlying influence of the phyllosilicate microstructure. At present the  $\delta\text{D}$  may be required to be measured by conventional vacuum line extraction techniques as used in this study, or by a finer scale, but destructive ion probe technique, believed to be under development. Triangular diagrams of Age- $\delta\text{D}$ -Z, Age- $\delta\text{D}$ -phyllosilicate, Age-Mg#-phyllosilicate and other combinations could then be constructed to a finer resolution than this present study. The resolution achieved would be determined by the laser probe point analysis, estimated to be  $\sim 2\mu\text{m}$ , which is a vast improvement over the  $\sim 90\text{-}125\mu\text{m}$  of this study.

A smaller set of samples ( $\sim 12$ ) could also be collected from the location of **Group-A** (grid reference 672619), in the north of the study area, to evaluate these techniques on samples known to display compositional variation within single grains (Section 5.1).

These future advances would greatly reduce the scattering observed on the graphs in this study (due to the larger grain size observations) and establish the trends of K-Ar age with  $\delta\text{D}$ , composition and phyllosilicate alteration with greater accuracy.

## APPENDIX 1.

### SAMPLE LOCATIONS AND ROCK TYPES.

The following sample locations give grid references on the following maps: 'The Geology of Connemara', 1:63,360, University of Glasgow, 1981. 'The Geology of South Mayo', 1:63,360, University of Glasgow, 1985. In addition, Leake and Tanner (1994) and Graham et al. (1989) are reference works which contain extensive geological information of the areas studied in this thesis.

A brief description is given for each sample location (see also Figure 3.1 and Table 3.1) and hand specimen and is intended to complement the electron microprobe section descriptions which follow in Appendix 2.

#### **TJ-1 Amphibolite (lineated), Streamstown Formation.**

Grid Ref. 821467. Quarry on north side of road. Sample from small knoll ~4m from fence on east side of quarry. Dark grey - green rock, fine - medium grained (0.5-1.5mm), lineated with mild foliation, quartz veining (3-5mm wide). No weathering.

#### **TJ-2 Mudstone (massive), Lough Muck Formation.**

Grid Ref. 771630. Small hilltop ~100m behind small white church on north bank of Lough Muck. Medium - dark grey, fine grained (<0.5mm), massive with some suggestion of cleavage due to localised concentrations of mica, some graded bedding present. Slight weathering on surfaces only.

#### **TJ-3 Mudstone (massive), Lough Muck Formation.**

Grid Ref. 824608. Small quarry ~100m north of Tully Bridge. Dark grey with green tinge, very fine grained (<0.2mm), massive, extremely thin quartz veins (~0.1mm wide). Slight weathering on surfaces only.

#### **TJ-4 Mudstone (massive), Lough Muck Formation.**

Grid Ref. 752636. East side of road, ~10m from small drystone dyke. Medium grey with green tinge, very fine grained (<0.1mm), massive, thin quartz veins (~0.2mm wide). Slight weathering on surfaces only.

#### **TJ-5 Diorite (granular), Lough Muck Formation.**

Grid Ref. 744634. ~15m along private entrance road on east side of main road. Light - medium grey, medium grained (1-3mm), holocrystalline granular rock. Turbid white plagioclase, some euhedral, occasional pink K-feldspar (1-3mm). Groundmass of quartz, feldspar and darker minerals, occasional very thin veins of quartz and epidote. Some weathering on surface.

**TJ-6 Diorite (granular), Lough Muck Formation.**

Grid Ref. 740635. Rocky outcrop on shore, south west of TJ-5, ~10m west of faulted, fractured rocks. Medium grey - green, fine - medium grained (0.5-3mm), holocrystalline granular rock. Turbid white - green feldspars, 1-3mm, some euhedral, occasional dark grains, (1-2mm), occasional very thin veins of quartz and epidote. Some weathering on surface.

**TJ-7A Amphibolite (poor lineation), Kylemore Formation.**

Grid Ref. 672619. Small quarry on north side of road. Amphibolite adjacent to quartz vein (10cm thick) in west half of quarry. Two pieces of quartz vein taken also. Dark grey - green, fine grained (0.2-0.8mm), very poorly developed foliation and weak lineation. Occasional dark grains (0.5-0.8mm) set in finer groundmass. Some brown iron oxide staining and weathering on surfaces.

**TJ-7B Amphibolite (mild lineation), Kylemore Formation.**

Grid Ref. 672619. Small quarry on north side of road. Sample from 1m above TJ-7A in west half of quarry. Dark grey - green, fine - medium grained (0.5-1.5mm). Thin lenses of quartz - feldspar (4-5mm long) between groundmass of hornblende. Occasional very thin (~0.1mm) quartz veining, some brown iron oxide staining on surfaces. Pyrite crystals present (~1mm).

**TJ-7C Amphibolite (mild lineation), Kylemore Formation.**

Grid Ref. 672619. Small quarry on north side of road. Sample from 2m to the left of TJ-7A in west half of quarry. Dark grey - green, fine grained (0.2-1mm). Mildly lineated and foliated, slight knotted effect due to hornblende crystals (~1mm). Brown iron oxide staining on slightly weathered surfaces. Pyrite crystals present (~1mm).

**TJ-7D Amphibolite (lineated), Kylemore Formation.**

Grid Ref. 672619. Small quarry on north side of road. Sample from 4m to the right of TJ-7A in middle of quarry. Medium - dark green - grey, fine - medium grained (0.5-2mm). Moderate lineation and foliation, knotted on foliated surfaces due to hornblende crystals (1-2mm). Pyrite in very thin veins (<0.2mm wide). Strongly stained by brown iron oxide on surfaces.

**TJ-7E Amphibolite (mild foliation), Kylemore Formation.**

Grid Ref. 672619. Small quarry on north side of road. Sample from 7m to the right of TJ-7A in middle of quarry. Dark grey - green, fine - medium grained (0.5-2mm). Mildly foliated with some lineation. Small, thin lenses of quartz - feldspar (3-5mm long) in groundmass. Some iron oxide staining and weathering on surfaces.

**TJ-7F Amphibolite (mild foliation), Kylemore Formation.**

Grid Ref. 672619. Small quarry on north side of road. Sample from 10m to the right of TJ-7A in east half of quarry. Dark grey - green, fine - medium grained (0.5-1.5mm). Mildly foliated with some lineation. Small thin lenses of quartz - feldspar (4-6mm long),

swirling effect in places due to plastic deformation. Brown iron oxide staining and weathering on surfaces.

**TJ-7G Amphibolite (mild foliation), Kylemore Formation.**

Grid Ref. 672619. Small quarry on north side of road. Sample from 4m to the left of **TJ-7A** in west half of quarry. Dark green, fine - medium grained (0.5-1.5mm). Mildly foliated with lineation. Small thin lenses of quartz - feldspar (3-5mm long) set in groundmass. Brown iron oxide staining and weathering on surfaces.

**TJ-7H Amphibolite (mild foliation), Kylemore Formation.**

Grid Ref. 672619. Small quarry on north side of road. Sample from 12m to the right of **TJ-7A** in east half of quarry. Dark grey - green, fine - medium grained (0.5-1.5mm). Less foliated and lineated than other specimens from this quarry. Small, thin quartz - feldspar lenses (1-2mm - 4-6mm long) set in groundmass. Fabric appears smeared and contorted near quartz veining (8-12mm wide). Quartz veins have brown iron staining and cavities also. Some weathering on surfaces.

**TJ-8 Amphibolite (mild foliation), Lakes Marble Formation.**

Grid Ref. 660607. Rock outcrop on east side of north - south running fence tied to part of outcrop. Medium green - grey, fine - medium grained (0.2-2mm). Mildly foliated, knotted due to dark green hornblendes (1-2mm). Some very thin quartz veins (~0.1mm wide). Weathering 3-4mm deep.

**TJ-9 Amphibolite (foliated), Lakes Marble Formation.**

Grid Ref. 665605. Sample taken from outcrop 1m from end of east - west running fence. Medium green - grey, fine - medium grained (0.2-2mm). Moderately foliated rock, knotting on foliation surfaces due to dark green hornblendes (1-2mm). Thin quartz - feldspar lenses (3-4mm long) set in groundmass. Some pyrite crystals (~0.2mm). Weathering 2-3mm deep.

**TJ-10 Mica schist (foliated), Lakes Marble Formation.**

Grid Ref. 667604. Sample taken ~10m north of the eastern end of a drystone dyke. Medium grey - pink lustre, fine - medium grained (0.2-3mm). Moderately foliated and knotted by pink garnets (up to 3mm) with inclusions. Groundmass of muscovite and biotite (appears altered). Some layers of quartz - feldspar from original bedding. Some brown iron oxide staining and weathering on surfaces.

**TJ-11 Amphibolite (very foliated), Lakes Marble Formation.**

Grid Ref. 669604. Sample taken from outcrop at western side of and half way up field between jetty and small white house. Medium green - grey, fine - medium grained (0.2-2mm). Very foliated rock with undulating foliation surfaces, knotted due to dark green hornblendes (1-2mm). Very thin quartz - feldspar lenses (3-4mm long) set in groundmass. Some quartz veining (1mm thick). Weathering 2-3mm thick. Some brown iron oxide staining on surfaces.

**TJ-12 Gabbro (granular), Dawros More.**

Grid Ref. 697592. Small quarry exposure ~100m west along track from main road. Medium grey, fine - medium grained (0.2-2mm). Granular, white altered feldspar (0.5-2mm) set in quartz and chloritised hornblende. Weathering ~10mm deep on surface.

**TJ-13 Gabbro (granular), Currywongaun Gabbro.**

Grid Ref. 722593. 200m east of bend in road, 300m up small valley on hillside north of road. Dark grey - black, fine - medium grained (0.2-1mm). Granular, white altered feldspar (0.5-1.5mm) set in dark green - black hornblende (0.2-1mm) of no preferred orientation. Patches of pyrite (1.2mm), very thin quartz veins (0.1mm wide). Pitted surface due to weathering of mafic minerals 1-2mm deep.

**TJ-15 Mica schist (foliated), Ballynakill Formation.**

Grid Ref. 841546. Outcrop beside waterfall on river, 250m east of road, over small bridge at edge of trees, 800m north of Inagh House. Medium grey with brown iron oxide staining, fine - medium grained (0.2-2mm). Moderately foliated, quartz - feldspar patches and lenses (0.5-3mm wide), some biotite grains (~1mm). Iron oxide staining throughout rock and in cracks.

**TJ-16 Psammitic schist (foliated), Ballynakill Formation.**

Grid Ref. 836547. Outcrop 5m east of road, 100m north of small farm. Medium grey, lustrous, fine grained (0.2-1mm). Moderately foliated due to muscovite interlayered with quartz - feldspar (all fine grained). Patchy brown iron oxide infiltrated through cracks and on surfaces. Occasional pyrite grains. Some crenulations on foliation surfaces.

**TJ-17 Amphibolite (massive), Lakes Marble Formation.**

Grid Ref. 832548. West side of road, 450m north of small farm. Dark grey with green tinge, fine grained (0.2-0.8mm). Poorly foliated - massive. Small quartz - feldspar lenses (3-4mm long), thin lenses of pyrite (2-3mm long) set in groundmass of hornblende. Some minor cracking, brown iron oxide staining on surfaces. Weathering 3-4mm deep.

**TJ-18 Psammitic schist (foliated), Kylemore Formation.**

Grid Ref. 791589. Small roadside cutting, 200m north along road from junction. Medium grey with green tinge, fine - medium grained (0.2-1mm). Moderate foliation with crenulations on foliation surfaces. Muscovite interlayered with quartz - feldspar and minor chloritised biotite. Slight weathering on surfaces.

**TJ-19 Amphibolite (mild foliation), Lakes Marble Formation.**

Grid Ref. 751580. Outcrop among rhododendron bushes, 100m west of entrance to boggy land, south side of main road. Dark grey - green, fine - medium grained (0.2-1.5mm). Mild foliation, knotted appearance due to hornblende crystals (1-1.5mm). Small, thin lenses of quartz - feldspar (2-3mm long). Very minor quartz veining (0.5mm wide). Weathering 2-3mm deep, brown iron oxide staining on some surfaces.

**TJ-20 Semi-pelite (massive), Lakes Marble Formation.**

Grid Ref. 777587. Roadside quarry, north side of road. Light - medium grey, green tinge, fine grained (0.2-0.6mm). Massive, some banding due to quartz concentration from original bedding. Quartz veining, pyrite present. Weathering on surface.

**TJ-21 Semi-pelite (massive), Lakes Marble Formation.**

Grid Ref. 728590. Outcrop under tree, at edge of field opposite small white house, 300m east of bend in road (up private road). Light - medium grey, green tinge, fine grained (0.2-0.6mm). Massive, some banding due to quartz concentration from original bedding. Weathering on surface.

**TJ-22 Mica schist (foliated), Lakes Marble Formation.**

Grid Ref. 708575. Roadside cutting at entrance to Connemara national Park, south of Letterfrack. Medium grey, slight green tinge, fine - medium grained (0.2-1mm). Foliated rock, knotting due to occasional pink garnets (2-3mm). Quartz lenses and banding. Minor weathering on surface.

**TJ-23 Semi-pelite (massive), Streamstown Formation.**

Grid Ref. 712574. Connemara National Park car park (west side). Medium grey with green tinge, fine grained (0.2-0.8mm). Altered domains of rock, chloritised biotite, muscovite present. Iron oxide staining on surfaces and in cracks.

**TJ-24 Semi-pelite (massive), Lakes Marble Formation.**

Grid Ref. 700585. 200m west of road. Medium - dark grey, streaked with light grey layers, fine grained (0.2-0.8mm). Lineation from streaking effect, biotite - chlorite and quartz - feldspar domains, muscovite present.

**TJ-25 Amphibolite (massive), Lakes Marble Formation.**

Grid Ref. 791575. North of quartzite rocks on hillside. Dark grey with green tinge, fine - medium grained (0.2-1mm). Poorly foliated, Very small lenses of quartz - feldspar (<1mm long), occasional pyrite present, occasional cracks and cavities. Weathering 1-2mm deep, brown iron oxide staining on surfaces and in cavities.

**TJ-26 Amphibolite (foliated), Lakes Marble Formation.**

Grid Ref. 789576. North side of stream, ~30m west of corner of fence. Dark grey with green tinge, fine grained (0.2-0.8mm). Moderately foliated, some undulating quartz - feldspar lenses (5-6mm long). Some quartz veining (~1mm wide), chloritisation associated with this. Some cavities with brown iron oxide staining. Weathering 2-3mm deep.

**TJ-27 Amphibolite (foliated), Lakes Marble Formation.**

Grid Ref. 787577. Small outcrop in boggy ground, south side of small valley on hillside, ~5m east of fence. Moderately foliated, some undulating quartz - feldspar lenses (up to 10mm long). Some quartz veining (0.5-1mm wide), chloritisation associated with this. Some cavities and cracks with brown iron oxide staining. Weathering 2-3mm deep.

**TJ-28 Amphibolite (massive), Lakes Marble Formation.**

Grid Ref. 785575. Exposure just beneath eastern side of hilltop (~30m away), 100m south west of TJ-27. Dark grey with green tinge, fine - medium grained (0.2-1mm). Poorly foliated with some 'spotting' on surfaces. Quartz veining prominent, some patches of pyrite. Poorly weathered, slight brown iron oxide staining on surfaces.

**TJ-29 Amphibolite (massive), Lakes Marble Formation.**

Grid Ref. 782574. South facing exposure on the southern side of hilltop (~30m away), ~10m east of fence. Dark grey with green tinge, fine - medium grained (0.2-1mm). Poorly foliated with some 'spotting' on surfaces. Minor quartz veining, some pyrite. Poorly weathered, slight brown iron oxide staining on surfaces and in cracks.

**TJ-30 Amphibolite (massive), Lakes Marble Formation.**

Grid Ref. 783576. Craggy area below hilltop. Dark grey - green, fine grained (0.2-0.8mm). Poorly foliated with crenulations defining some lineation. Cavities prominent, some quartz veining. Sample strongly weathered through cracks.

**TJ-31 Amphibolite (massive), Lakes Marble Formation.**

Grid ref. 835547. Small roadside quarry, west side of road, 100m north of small farm. TJ-16 and TJ-17 are nearby. Dark grey with green tinge, fine - medium grained (0.2-1mm). Poorly foliated, quartz veining (~2mm wide) throughout sample, traces of pyrite. Minor weathering only on surface.

**TJ-32 Amphibolite (banded), Streamstown Formation.**

Grid Ref. 820467. Quarry ~70m west of TJ-1, sample taken from the eastern extremity of this quarry. Light - medium grey with green tinge, fine - medium grained (0.6-1mm). Finely banded rock. Weathering on surface <1mm.

**TJ-33 Diorite (granular), within Lough Muck formation.**

Grid Ref. 768618. Benchoona, west of Lough muck, sample taken from around the middle of this diorite body. Light - medium grey with pink and green tinge, medium grained (1-2mm). Holocrystalline, granular, light green - white turbid feldspars (1-2mm), also, grains of subhedral hornblende (1-2mm), may be chloritised. Rock is highly altered. Weathering 3-4mm deep on surface, pitted where mafic minerals have weathered out.

**TJ-34 Diorite (granular), within Lough Muck formation.**

Grid Ref. 770620. Benchoona, west of Lough Muck, sample taken from near north margin of this diorite body, near contact with Lettergesh Formation siltstones. Medium grey - pink, medium grained (1-3mm). Holocrystalline, granular, contains white altered plagioclase crystals (~3mm), finer quartz, pink feldspar and hornblende prisms (1-2mm). Rock is highly altered. Weathering 5-6mm deep, pitted where mafic minerals have weathered out.

**TJ-35 Amphibolite (very foliated), Lakes Marble Formation.**

Grid Ref. 838569. Luggastarriff area, ~20m east of old field boundaries. Medium grey - green, fine - medium grained (0.2-2mm). Pronounced foliation defined by fine grained chlorite and hornblende in groundmass, larger hornblendes (1-2mm) on foliation also. Minor quartz veining and infill of cracks, minor pyrite present. Weathering 3mm deep.

**TJ-36 Amphibolite (foliated), Lakes Marble Formation.**

Grid Ref. 839570. Outcrop north of TJ-35, on north side of old track. Medium grey with green tinge, fine - medium grained (0.5-2mm). Moderately foliated. Dark hornblende crystals (~2mm) set in finer groundmass. Weathering 1mm on surface.

**TJ-37 Amphibolite (poor foliation), Lakes Marble Formation.**

Grid Ref. 839571. Rocky outcrop on south side of old track, west of old limestone quarry. Medium grey with green tinge, fine - medium grained (0.5-1mm). Poorly foliated and lineated. Dark hornblende (~1mm) set in finer groundmass. Weathering 3mm deep.

**TJ-38 Amphibolite (mild foliation), Lakes Marble Formation.**

Grid Ref. 838573. South side of rocky mounds, ~300m north of old limestone quarry. Medium grey with green tinge, fine - medium grained (0.5-1.5mm). Mildly foliated. Dark hornblende crystals (1-1.5mm) set in finer groundmass. Individual grains of quartz - feldspar (0.5-1.5mm). Weathering 3-6mm deep.

**TJ-39 Amphibolite (masive), Lakes Marble Formation.**

Grid Ref. 839575. Rocky outcrops ~4m east of ford crossing stream, near corner of fence at forest. Medium grey with green tinge, fine - medium grained (0.2-1mm). Massive - poorly foliated. Weathering 1-2mm deep.

**TJ-40 Amphibolite (very foliated), Lakes Marble Formation.**

Grid Ref. 835566. Outcrop ~70m north-east of former bridge on narrow track. Medium grey - green, fine - medium grained (0.2-1.5mm). Pronounced foliation due to chlorite orientation. Banding of fine grained (~0.2mm) and coarser grained (1-1.5mm) crystals, banding shows minor kink folding. Minor quartz veining (~1mm wide). Weathering ~1mm deep.

**TJ-41 Amphibolite (massive), Lakes Marble Formation.**

Grid Ref. 820572. 15m north of east - west running road, 300m east of main road. Sample taken from next to a quartz vein about 5-6cm wide. Medium grey - green, fine - medium grained (0.5-1.5mm). Massive, some poor foliation - lineation. Some iron oxide staining on surfaces. Weathering 6-8mm deep.

**TJ-42 Amphibolite (massive), Lakes Marble Formation.**

Grid Ref. 820572. 15m north of east - west running road, 300m east of main road, 0.5m from TJ-41. Medium grey with green tinge, fine - medium grained (0.5-1.5mm). Massive, poor foliation and lineation. Individual grains of quartz - feldspar (0.5-1.5mm) set

in hornblende and chlorite grains of similar size range. Minor quartz veining (~2mm wide). Weathering 4-6mm deep.

**TJ-43 Amphibolite (poor foliation), Lakes Marble Formation.**

Grid Ref. 783465. Southern side of road ~1km west of Ballinafad. Exposure ~30m west of road to 'The Ranch', ~1m elevation from road surface. Medium - dark grey with green tinge, fine - medium grained (0.2-1mm). Poorly foliated with some lineation of foliated surfaces. Lenses of quartz - feldspar (1-3mm long). Faint banding in areas poorer in hornblende (bands 5-7mm thick). Weathering 2-3mm deep.

**TJ-44 Amphibolite (massive), Lakes Marble Formation.**

Grid Ref. 887467. Roadside cutting, north side of road, ~60m north east from small loch, ~2m elevation above road. Medium - dark grey, fine - medium grained (0.5-1.5mm), also, domains of finer grains (~0.5mm, granular). Massive, very poor foliation. Minor quartz veining (~1mm wide), patches of quartz. Weathering 1-2mm.

**TJ-45 Amphibolite (mild foliation), Lakes Marble Formation.**

Grid Ref. 891465. Roadside cutting, south side of road, near to east end of loch, ~1.5m elevation above road. Medium - dark grey with green tinge, fine - medium grained (0.5-1.5mm). Slightly foliated rock. Quartz - feldspar lenses (up to 15mm long) set in groundmass of hornblende. Hornblende also up to 1.5mm grainsize. Minor quartz veining (<0.05mm wide). Weathering 1-2mm deep.

**TJ-46 Amphibolite (banded), Lakes Marble Formation.**

Grid Ref. 974449. South - central part of quarry to east of road. Much quartz veining observed in quarry rocks. Medium grey, medium grained (1-2mm). Pronounced banding in rock, areas rich in quartz - feldspar, variable from ~1mm to ~3mm thick. Hornblende bands show parallel orientation of grains. Minor pyrite present. Weathering <1mm deep.

**TJ-47 Amphibolite (massive), Lakes Marble Formation.**

Grid Ref. 942530. 30m uphill from old farm building with corrugated iron roof. Medium - dark grey with green tinge, fine - medium grained (0.5-1mm). Massive rock. Stockwork veins of chalcopyrite, pyrite also present. Extensive iron oxide staining on surfaces. Weathering <1mm deep.

**TJ-48 Amphibolite (poor foliation), Lakes Marble Formation.**

Grid Ref. 933537. Exposure at top left hand corner of inclined field, surrounded by dry-stone dyke, field directly above house with 'two-tone' roofing slates. Medium - dark grey with green tinge, fine - medium grained (0.5-1mm). Poor foliation. Very thin lenses of quartz - feldspar (2-3mm long) set in hornblende groundmass. Minor quartz veining (~0.1mm wide). Some iron oxide staining on surfaces. Poorly weathered.

**TJ-49 Ultrabasic gabbro (massive), ultrabasic igneous intrusion.**

Grid Ref. 792602. Outcrop on south-west corner of stream, yellow ochre weathering over surface. Very fine grained, dark grey - black ultrabasic igneous rock, very highly serpentinised. Dark grey - black with green tinge, microcrystalline, massive. Veining and cracking present (quartz and chlorite present in veins). Mostly serpentinite. Minor pyrite. Yellow - brown weathering on surface ~2-3mm deep.

**TJ-50 Psammitic schist (very foliated), Kylemore Formation.**

Grid Ref. 802599. Located 25m south of track, in line with telegraph poles, central - south part of outcrop. Medium grey lustre, medium grained (1-3mm). Strong foliation due to parallel alignment of mica grains in layers. Granular appearance of quartz, feldspar, muscovite and biotite. Slight brown iron oxide staining on exposed surfaces. Weathering 1-2mm deep.

**TJ-51 Amphibolite (massive), Lakes Marble Formation.**

Grid Ref. 747579. South of road passing by Kylemore Abbey, small track on south side of road ~25m east of eastern entrance to abbey, outcrop near top of small rise across bog. Medium grey with green tinge, fine grained (<0.5mm) with some 1mm size crystals. Massive, very slight foliation. Highly fractured rock, quartz veining (~1mm wide). Mostly altered hornblende. Iron oxides on surfaces. Weathering up to 10mm deep.

**TJ-52 Gabbro (granular), Currywongaun gabbro.**

Grid Ref. 725593. 150m above contact with andesine porphyroblast schist of Kylemore Formation, slightly to west of the line of the road just south of the hill. Sample taken from rounded, weathered surface (brown) rock outcrop. Medium - dark grey with green tinge, fine - medium grained (0.5-2mm). Granular, mottled. Quartz, feldspar, dark minerals (pyroxene and hornblende). Brown iron oxide staining on surfaces. Weathering ~2mm deep.

**TJ-53 Pelite (mild foliation), Kylemore Formation.**

Grid Ref. 664638. Rocks on beach, below high tide mark, ~12m west of small derelict cottage with thatched roof at west end of sea wall. Light - medium grey lustrous, fine - medium grained (0.5-1mm). Slight foliation from mica, but more massive in character. Some minor quartz veining (<0.5mm wide). Banding, quartz rich lenses (3mm thick). Muscovite on surfaces stained by brown iron oxide. Poorly weathered.

**TJ-54 Amphibolite (massive), Ballyconneely Amphibolite.**

Grid Ref. 632466. South side of stream, ~20m west of road. Blocky outcrop with black oil tar stains on surface. Dark grey with green tinge, very fine - fine grained (<0.2-0.5mm). Massive appearance with some foliation. Very fine epidote veining (<0.1mm wide). Some quartz rich patches (3-4mm). Iron oxide staining on surfaces and in cavities where present.

**TJ-55 Metagabbro (granular), Metagabbro - Gneiss Complex.**

Grid Ref. 630456. Northeast corner of small beach to south of road junction (~1m elevation from beach). Parking area beside beach. Mottled, medium - dark grey with green tinge, medium grained (1-3mm). Granular, mottled due to altered feldspars 2-3mm in diameter. Groundmass ~1mm, altered white feldspars, dark green hornblende and black magnetite. Minor epidote veining (up to ~1mm wide). Poorly weathered.

**TJ-56 Metagabbro (granular), Metagabbro - Gneiss Complex.**

Grid Ref. 618440. Small quarry on north side of road, sample from back, west side of quarry, ~1.5m elevation. Medium grey with green tinge, fine - medium grained (0.5-2mm). Granular. Some cracks and quartz veining (~1mm wide). Minor pyrite present. May be highly altered rock. Weathering <1mm deep.

**TJ-57 Amphibolite (massive), Ballyconneely Amphibolite.**

Grid Ref. 641423. Ballyconneely Bay, north side of road, west corner of field next to two houses, opposite white house with red corrugated iron roof, ~10m north of road, ~1m elevation. Dark grey - green, microcrystalline. Massive. Many fine epidote veins (0.2-0.5mm). Suspected serpentinised or chloritised amphibolite. Poor weathering on surface.

**TJ-58 Amphibolite (granular), Ballyconneely Amphibolite.**

Grid Ref. 648409. Location beside car park opposite 'Calla Cove Restaurant and Coffee Shop', sample taken from ~7m behind large rock mound. Dark grey - green, fine - medium grained (0.2-2mm). Granular, very poor foliation. Light green epidote crystals, also green stained quartz, (1-2mm). Green epidote veining (0.5-1mm wide). Iron oxide staining on surfaces. Weathering 3-4mm deep.

**TJ-59 Amphibolite (massive), Metagabbro - Gneiss Complex.**

Grid Ref. 721398. Field north of road, ~200m west of telephone exchange to the west of Roundstone, outcrop ~3m into field from gate. Medium grey with green tinge, fine grained (0.2-0.5mm). Massive, very poor foliation. Sparse dark hornblendes (~1mm). Minor quartz veining (0.5mm wide). Weathering 1-2mm deep.

**TJ-60 Metagabbro (granular), Metagabbro Gneiss - Complex.**

Grid Ref. 710462. Back of quarry on north side of road, sample from ~1.5m elevation. Medium grey with green tinge, fine - medium grained (0.5-1.5mm). Mostly equigranular. Small xenoliths (~10mm across). Slight weathering only.

**TJ-61 Metagabbro (granular), Metagabbro Gneiss - Complex.**

Grid Ref. 693469. Rocky exposure ~40m east of parking area on north side of road. East of 'Alcock and Brown' landing site monument. Medium grey with green tinge, fine grained (0.2-0.5mm) and medium grained domains (1-1.5mm). Granular. Minor quartz veining (up to 1mm thick). Slight weathering only.

## APPENDIX 2.

### ELECTRON MICROPROBE SECTION DESCRIPTIONS.

The following descriptions are representative of the electron microprobe polished sections observed under a petrological microscope. These sections have been ground to a similar thickness to that of a standard thin section (0.030mm).

The descriptions are intended to give a visual modal estimation of minerals present in each rock sample and the grainsize and condition of the hornblende or muscovite (see also Table 3.2 and Figures 3.2 - 3.5).

Because of the lack of abundant polysynthetic twinning and alteration of the plagioclase, the optically estimated composition is not generally given. The analysed compositions of plagioclase feldspars, derived by EMPA, are listed in Appendix 5. The feldspar alteration indices are: 0 = unaltered; 1 = minor alteration to sericite and saussurite; 2 = extensive alteration to sericite and saussurite; 3 = completely altered to sericite and saussurite.

#### **TJ-1 Amphibolite (lineated).**

60% mid-green - yellow hornblende, euhedral - subhedral 0.2-1mm, rare alteration to chlorite at grain edges. 30% quartz, 0.2mm, granular. 5% plagioclase, subhedral - anhedral (alt. index 1-2), 0.2mm. 5% Fe-Ti oxides, irregular shapes, 0.1-0.2mm. Accessory apatite.

#### **TJ-5 Diorite.**

<10% highly chloritised hornblende, relict crystal boundaries present, 0.5-2mm. 60% altered feldspar (alt. index 2-3), 0.2-0.8mm (~40% plagioclase, ~20% K-feldspar showing carlsbad twins). 30% quartz, 0.1-0.4mm. Chlorite throughout rock, 0.1-0.4mm (<5%). Minor opaque Fe-Ti oxides, epidote and apatite.

#### **TJ-6 Diorite.**

<10% highly chloritised hornblende, relict crystal boundaries present, 1-2mm. 60% altered feldspar (alt. index 2-3), 0.2-0.8mm and 0.5-2.0mm size ranges (~40% plagioclase, ~20% K-feldspar showing carlsbad twins). 30% quartz, 0.1-0.4mm. 4% chlorite and 2% epidote throughout rock, 0.1-0.2mm. Minor opaque Fe-Ti oxides and apatite.

#### **TJ-7A Amphibolite (poor lineation).**

10% light green - light brown zoned hornblende, euhedral - subhedral, ~0.5mm, slight alteration to chlorite and biotite along cleavages, inclusions of quartz and Fe-Ti oxides. 50% mid-green - yellow hornblende, 0.1-0.5mm, slight alteration to chlorite and biotite along cleavages. 30% quartz, 0.1mm, granular. 5% plagioclase, subhedral - anhedral

(alt. index 2), 0.1mm. 5% Fe-Ti oxides, irregular shapes, 0.1-0.2mm. Minor quartz veining, chlorite also in veins (0.1mm wide). Accessory sphene associated with Fe-Ti oxides.

**TJ-7B Amphibolite (mild lineation).**

10% light green - light brown zoned hornblende, euhedral - subhedral, ~0.5mm, slight alteration to chlorite and biotite along cleavages, inclusions of quartz and Fe-Ti oxides. 50% mid-green - yellow hornblende, 0.1-0.5mm, slight alteration to chlorite and biotite along cleavages. 30% quartz, 0.1mm, granular. 5% plagioclase, subhedral - anhedral (alt. index 2), 0.1mm. 5% Fe-Ti oxides, irregular shapes, 0.1-0.2mm. Minor quartz veining, chlorite also in veins (0.1mm wide). Accessory sphene associated with Fe-Ti oxides, minor pyrite.

**TJ-7D Amphibolite (lineated).**

10% light green - light brown zoned hornblende, euhedral - subhedral, ~1mm, slight alteration to chlorite and biotite along cleavages, inclusions of quartz and Fe-Ti oxides. 50% mid-green - yellow hornblende, 0.1-0.5mm, slight alteration to chlorite and biotite along cleavages. 27% quartz, 0.1mm, granular. 5% plagioclase, subhedral - anhedral (alt. index 2), 0.1mm. 5% Fe-Ti oxides, irregular shapes, 0.1-0.2mm. 2-3% sphene associated with Fe-Ti oxides. Minor quartz veining; chlorite and pyrite also in veins (0.1mm wide).

**TJ-7E Amphibolite (mild foliation).**

10% light green - light brown zoned hornblende, euhedral - subhedral, ~1mm, slight alteration to chlorite and biotite along cleavages, inclusions of quartz and Fe-Ti oxides. 50% mid-green - yellow hornblende, 0.1-0.5mm, slight alteration to chlorite and biotite along cleavages. 28% quartz, 0.1mm, granular. 5% plagioclase, subhedral - anhedral (alt. index 2), 0.1mm. 5% Fe-Ti oxides, irregular shapes, 0.1-0.2mm. 1-2% sphene associated with Fe-Ti oxides. Minor quartz veining, chlorite also in veins (0.1mm wide). Brown iron oxide staining.

**TJ-7F Amphibolite (mild foliation).**

10% light green - light brown zoned hornblende, euhedral - subhedral, ~1mm, slight alteration to chlorite and biotite along cleavages, inclusions of quartz and Fe-Ti oxides. 50% mid-green - yellow hornblende, 0.1-0.5mm, slight alteration to chlorite and biotite along cleavages. 28% quartz, 0.1mm, granular. 5% plagioclase, subhedral - anhedral (alt. index 2), 0.1mm. 5% Fe-Ti oxides, irregular shapes, 0.1-0.2mm. 1-2% sphene associated with Fe-Ti oxides. Minor quartz veining, chlorite also in veins (0.1mm wide). Brown iron oxide staining.

**TJ-7G Amphibolite (mild foliation).**

10% light green - light brown zoned hornblende, euhedral - subhedral, ~1mm, slight alteration to chlorite and biotite along cleavages, inclusions of quartz and Fe-Ti oxides. 50% mid-green - yellow hornblende, 0.1-0.5mm, slight alteration to chlorite and biotite along cleavages. 28% quartz, 0.1mm, granular. 5% plagioclase, subhedral - anhedral (alt. index 2), 0.1mm. 5% Fe-Ti oxides, irregular shapes, 0.1-0.2mm. 1-2% sphene associated

with Fe-Ti oxides. Minor quartz veining, chlorite also in veins (0.1mm wide). Brown iron oxide staining.

**TJ-7H Amphibolite (mild foliation).**

10% light green - light brown zoned hornblende, euhedral - subhedral, ~1mm, slight alteration to chlorite and biotite along cleavages, inclusions of quartz and Fe-Ti oxides. 50% mid-green - yellow hornblende, 0.1-0.5mm, more alteration to chlorite and biotite along cleavages. 28% quartz, 0.1mm, granular. 5% plagioclase, subhedral - anhedral (alt. index 2), 0.1mm. 5% Fe-Ti oxides, irregular shapes, 0.1-0.2mm. 1-2% sphene associated with Fe-Ti oxides. Pronounced veining present (2-4mm wide) containing quartz, muscovite Fe-Ti oxides and sphene. Brown iron oxide staining.

**TJ-8 Amphibolite (mild foliation).**

20% light green - pale green hornblende, subhedral, 1-2mm, rounded and granular, minor quartz inclusions, rare alteration to chlorite at edges. 40% light green - pale green hornblende, 0.1-0.2mm, parallel alignment. 35% quartz, 0.1mm, granular. <5% plagioclase, subhedral - anhedral (alt. index 1), 0.1mm. Accessory apatite present, some brown iron staining, rare Fe-Ti oxides, minor sphene.

**TJ-9 Amphibolite (foliated).**

70% very pale green hornblende, euhedral - subhedral, 0.5-1mm, tabular, zoning in some crystals. 10% colourless, acicular cummingtonite crystals, up to 0.2mm long, low birefringence, set in groundmass. 25% quartz, 0.1mm, granular. >5% plagioclase, subhedral - anhedral (alt. index 2), 0.1mm. Accessory apatite present, some brown iron staining, rare Fe-Ti oxides, minor sphene and pyrite.

**TJ-10 Mica schist (foliated).**

35% muscovite 0.4-0.8mm, in aggregates with ~5% chloritised biotite (occurs around edges of mica aggregates). 40% quartz, 0.2-0.5mm, in aggregates and lenses. 10% staurolite, 0.5-1mm. 5% subhedral garnet (pre-syn-tectonic), 2-4mm, embayments and inclusions of quartz. Minor chlorite grains, possibly after biotite. Foliation of rock from parallel mica aggregates, knotted by garnet and staurolite porphyroblasts.

**TJ-11 Amphibolite (very foliated).**

60% very pale green pleochroic amphibole, two size fractions; 0.2-0.5mm zoned crystals and 0.05-0.1mm in matrix. 30% quartz 0.1mm. 10% plagioclase, subhedral - anhedral (alt. index 1), 0.1mm. Minor Fe-Ti oxides, minor sphene associated.

**TJ-13 Gabbro (granular).**

70% dark green - mid-green - light green hornblende, 0.2-0.6mm, subhedral - anhedral granular, relatively inclusion free, possibly some alteration at grain boundaries and along cleavages. 25% very altered plagioclase, granular (alt. index 3). 5% Fe-Ti oxides and associated sphene. Patches of pyrite ~1mm across.

**TJ-16 Psammitic schist (foliated).**

15% muscovite aggregates with ~15% chloritised biotite, mica grainsize is 0.2-0.4mm. 40% altered plagioclase, subhedral (alt. index 2), 0.1-0.2mm. 20% quartz, 0.1-0.2mm. 10% highly chloritised biotite, ~0.5mm, pleochroic haloes around zircons still present. Modest foliation in rock due to parallel micas in lenses. Muscovite and biotite more intimately intergrown than in TJ-10.

**TJ-17 Amphibolite (massive).**

65% mid-green - light yellow-green hornblende, euhedral - subhedral 0.05-0.2mm, some alteration to chlorite along grain boundaries and in cleavages. 25% quartz, 0.2mm, granular. 5% plagioclase, subhedral - anhedral (alt. index 0-1). 5% Fe-Ti oxides and associated sphene. Occasional pyrite grains.

**TJ-18 Psammitic schist (foliated).**

10% muscovite in layered aggregates, 0.2-0.4mm. 50% slightly altered plagioclase (alt. index 1), 0.2-0.4mm. 30% quartz, 0.2-0.4, mosaic texture with plagioclase. 10% chlorite, 0.1-0.3mm, with opaque Fe-Ti oxide inclusions, possibly altered biotite. Some brown iron oxide staining. Rock given foliation by layering of muscovite between psammitic layers.

**TJ-19 Amphibolite (mild foliation).**

15% mid-green - light green, hornblende, subhedral, 0.5-1mm, some quartz inclusions, minor alteration to biotite and chlorite at crystal edges and along cleavages. 45% mid-green - light green hornblende, 0.05-0.2mm, subhedral, minor chlorite present also. 35% quartz, 0.1mm, granular. <5% plagioclase, subhedral - anhedral (alt. index 1), 0.1mm. Minor opaque Fe-Ti oxides with associated sphene.

**TJ-21 Amphibolite (massive).**

50% pale green, slightly pleochroic hornblende, subhedral - anhedral, 0.05-0.1mm, chlorite alteration at grain boundaries. 25% plagioclase, anhedral (alt. index 1), 0.05-0.1mm. 20% quartz, 0.05-0.1mm, irregular boundaries. 5% opaque Fe-Ti oxides, 0.05-0.2mm. Minor epidote and cummingtonite.

**TJ-22 Mica schist (foliated).**

40% muscovite in aggregates (parallel growth), 0.5-3mm. These aggregates also contain altered plagioclase, ~20% of rock (alt. index 1-2), 0.2-1mm. 30% quartz, 0.2-1.4mm, mosaic texture in lenses and bands. Altered pre-syn-tectonic garnet, 2-3mm. ~5% chloritised biotite also present. Some chlorite crystals, accessory tourmaline and opaque Fe-Ti oxides. Foliation of rock defined by parallel muscovites.

**TJ-25 Amphibolite (massive).**

60% mid-green - yellow hornblende, subhedral, 0.1-0.4mm, chlorite evident in some grains and around edges, alteration to biotite also evident. 25% plagioclase, anhedral (alt. index 1-2), 0.05-0.2mm. 12% quartz, 0.05-0.2mm. 3% chlorite present throughout rock.

Minor Fe-Ti oxides with associated sphene. Minor biotite, epidote and pyrite. Some brown iron oxide staining.

**TJ-26 Amphibolite (foliated).**

60% mid-green - yellow hornblende, subhedral, 0.05-0.3mm, chlorite evident in some grains and around edges, alteration to biotite also evident. 25% plagioclase, anhedral (alt. index 1-2), 0.05-0.2mm. 12% quartz, 0.05-0.2mm. Quartz and feldspar occur in lenses. 3% chlorite present throughout rock. Minor Fe-Ti oxides with associated sphene. Minor biotite and epidote. Some brown iron oxide staining.

**TJ-27 Amphibolite (foliated).**

45% mid-green - yellow hornblende, subhedral, 0.1-0.4mm, chlorite evident in some grains and around edges, alteration to biotite also evident. 25% plagioclase, anhedral (alt. index 1-2), 0.05-0.2mm. 12% quartz, 0.05-0.2mm. 3% chlorite present throughout rock. Minor Fe-Ti oxides with associated sphene. Minor biotite and epidote. Veins (0.4mm wide) containing quartz, epidote and cummingtonite. Some brown iron oxide staining.

**TJ-28 Amphibolite (massive).**

60% mid-green - yellow hornblende, subhedral, 0.1-0.4mm, chlorite evident in some grains and around edges, alteration to biotite also evident. 25% plagioclase, anhedral (alt. index 1-2), 0.05-0.2mm. 12% quartz, 0.05-0.2mm. 3% chlorite present throughout rock. Minor Fe-Ti oxides with associated sphene. Minor biotite, epidote and pyrite. Some brown iron oxide staining.

**TJ-29 Amphibolite (massive).**

75% mid-green - light yellow-brown hornblende, euhedral, 0.1-0.2mm, crystals aggregated together in parallel orientations, pronounced edges and cleavages due to alteration to chlorite and biotite. 15% quartz, 0.05-0.1mm, granular. 8% plagioclase, subhedral - anhedral (alt. index 2), 0.1mm. Minor veining containing epidote and chlorite, <0.1mm wide. 2% opaque Fe-Ti oxides, sphene and pyrite.

**TJ-31 Amphibolite (massive).**

20% light green - very pale green amphibole, anhedral, 1-3mm, quartz inclusions, pronounced cleavages, alteration along cleavages and at edges of crystals, some zoning. 45% mid-green - light green hornblende crystals, acicular, 0.05-0.15mm long. 25% quartz, 0.1mm. 10% altered plagioclase (alt. index 2), 0.1mm. Occasional alteration of hornblende to biotite. Minor opaque Fe-Ti oxides, sphene and pyrite. Chlorite filled vein (0.2mm wide).

**TJ-33 Diorite (granular).**

<10% highly altered mafic minerals (chlorite alteration), occasional surviving piece of green - yellow-green hornblende (chlorite alteration), 0.5-1.0mm. 70% highly altered plagioclase, euhedral - subhedral (alt. index 3), 0.1-0.3mm, some feldspar phenocrysts 1-2mm grainsize. 15% quartz, 0.05-0.2mm. 5% chlorite, 0.2-0.5mm. Minor chloritised biotite, opaque Fe-Ti oxides, sphene and minor apatite.

**TJ-34 Diorite (granular).**

10% highly chloritised biotite, euhedral relict grains, 1-2mm. Phenocrysts of highly altered feldspar, K-feldspar and plagioclase, euhedral outlines (alt. index 2-3), 1-3mm. Feldspar ~80% of rock. 10% quartz, 0.2-0.4mm. Muscovite layers observed in biotite grains. Minor opaque Fe-Ti oxides with associated sphene. Minor apatite.

**TJ-35 Amphibolite (very foliated).**

15% light green - pale green hornblende, tabular, subhedral, 1-3mm, prominent cleavage, some alteration to chlorite and biotite. 40% light green - pale green hornblende, subhedral, 0.05-0.1mm, some alteration to chlorite and biotite also evident. 35% quartz, 0.05-0.2mm, granular. 10% plagioclase, subhedral - anhedral (alt. index 2-3), 0.05-0.2mm. Minor opaque Fe-Ti oxides with associated sphene, minor pyrite. Some quartz and epidote veins, some brown iron oxide staining.

**TJ-36 Amphibolite (foliated).**

25% light green - pale green hornblende, 2-4mm, anhedral and fractured, prominent cleavage, some alteration along cleavages and at grain boundaries, edges of crystals show cleavages 'springing' open. Opaque Fe-Ti oxides, chlorite and biotite emphasise cleavage also. 35% light green - pale green hornblende, euhedral, 0.05-0.1mm, some alteration. 30% quartz, 0.05-0.2mm, granular. 10% plagioclase, subhedral - anhedral (alt. index 2-3), 0.05-0.2mm. Minor Fe-Ti oxides with associated sphene, brown iron oxide staining also. Rock less foliated than TJ-35, more contorted around larger hornblendes.

**TJ-37 Amphibolite (poor foliation).**

25% light green - light yellow hornblende, anhedral, 2-3mm, less alteration in cleavages than in TJ-35, minor inclusions of Fe-Ti oxides, zoning in some crystals. 35% light green - light yellow hornblende, euhedral, 0.1-0.2mm, minor chlorite alteration in cleavages. 30% quartz, 0.1-0.2mm, granular. 10% plagioclase, subhedral (alt. index 1), 0.1-0.2mm. Minor opaque Fe-Ti oxides with associated sphene.

**TJ-38 Amphibolite (mild foliation).**

20% light green - light yellow-green hornblende, rounded, 2-4mm, slightly zoned, very minor inclusions of opaque Fe-Ti oxides. 45% light green - light yellow-green hornblende, 0.05-0.2mm, only minor alteration to chlorite observed. 25% quartz, 0.1-0.2mm, granular. 10% plagioclase, subhedral - anhedral (alt. index 1-2), 0.1-0.2mm. Minor opaque Fe-Ti oxides and sphene, minor quartz veining (<0.1mm wide). Brown iron oxide staining.

**TJ-39 Amphibolite (massive).**

70% turquoise green - mid-green - yellow green hornblende, 0.05-0.2mm, euhedral in aggregates, very clean and relatively unaltered. 15% quartz, 0.1-0.2mm, granular. 15% plagioclase, subhedral (alt. index 2), 0.1-0.2mm. ~1-2% opaque Fe-Ti oxides and associated sphene. Thin section much darker and turquoise coloured than the other TJ-35 - TJ-41 rock samples (all collected in same area).

**TJ-40 Amphibolite (very foliated).**

30% light green - pale green hornblende, rounded and cracked crystals, 1-3mm, inclusions and alteration along cleavages and at edges. 30% light green - pale green hornblende, euhedral - subhedral, 0.05-0.1mm, some chlorite alteration. 20% quartz, 0.05-0.1mm, granular, associated with 20% feldspars (alt. index 2), 0.05-0.1mm. Patches of calcite, chlorite and sericite. Minor sphene. Rock appears highly altered and changed.

**TJ-41 Amphibolite (massive).**

60% mid-green - light green hornblende, anhedral and rounded, 0.2-0.5mm, some alteration to biotite in cleavages, some alteration to chlorite also. 25% quartz, 0.05-0.5mm, granular. 15% altered feldspar, subhedral - anhedral (alt. index 2), 0.05-0.2mm. Minor sphene. Quartz and epidote veining. Minor brown iron oxide staining.

**TJ-42 Amphibolite (massive).**

75% mid-green - light green hornblende, subhedral - anhedral, 0.1-0.5mm, alteration to biotite (~5% estimated) and chlorite between grains. 10% plagioclase, subhedral (alt. index 1), 0.1-0.2mm. 5% quartz, 0.1-0.2mm. 5% opaque Fe-Ti oxides. Minor sphene and apatite. Quartz veining and epidote veining. Crack or vein filled with goethite.

**TJ-43 Amphibolite (poor foliation).**

65% mid-green - yellow hornblende, euhedral, 0.3-0.7mm, only very slight alteration at edges of crystals and in cleavages. 20% quartz, 0.2-0.4mm, granular. 10% variably altered plagioclase, subhedral - anhedral (alt. index 0-2), 0.2-0.4mm. 5% opaque Fe-Ti oxides.

**TJ-44 Amphibolite (massive).**

65% mid-green - light green hornblende, euhedral - subhedral, 0.2-1mm, may be altered along cleavages and cracking also observed, inclusions of quartz and feldspar, some chlorite at edges of crystals and alteration to biotite. 5% quartz, 0.2-0.5mm, granular. 30% plagioclase, subhedral - anhedral (alt. index 2-3). Only occasional Fe-Ti oxides and minor sphene.

**TJ-45 Amphibolite (mild foliation).**

70% mid-green - brown green - yellow hornblende, euhedral, 0.4-1mm, crystals in aggregates and lenses, some inclusions of quartz and plagioclase, occasional pronounced cleavage or cracks and alteration to biotite. 20% plagioclase, subhedral - anhedral (alt. index 1-2), 0.2-0.4mm. <5% quartz, 0.2-0.4mm, granular. Occasional lenses rich in opaque Fe-Ti oxides, minor sphene, accessory apatite. Some brown iron oxide staining.

**TJ-46 Amphibolite (banded).**

50% dark green - yellow hornblende, subhedral - anhedral, 0.2-0.5mm, embayments of plagioclase and quartz, some prominent cleavages and alteration to chlorite at crystal edges. 30% plagioclase, subhedral (alt. index 0-1), 0.2-0.4mm. 12% quartz, 0.2-0.4mm, granular. 8% opaque Fe-Ti oxides, 0.1-0.3mm and 1-2mm grainsize ranges, inclusions of

hornblende, plagioclase and quartz. Segregation of rock into fine mafic and felsic rich layers a few mm thick. Minor pyrite.

**TJ-47 Amphibolite (massive).**

70% mid-green - light brown hornblende, euhedral - subhedral, 0.1-0.4mm, random orientation, pronounced cleavages and some chloritised grain boundaries, some inclusions of opaque Fe-Ti oxides and plagioclase. 20% plagioclase, subhedral (alt. index 2), 0.1-0.2mm. 7% quartz, 0.1-0.2mm. 3% opaque Fe-Ti oxides, 0.3-0.5mm, inclusions and embayments of hornblende and plagioclase. Minor sphene. Epidote vein 0.5mm wide. Pyrite and chalcopyrite in vein.

**TJ-48 Amphibolite (poor foliation).**

70% mid-green - light green hornblende, subhedral, 0.1-0.4mm, pronounced cleavages with minor chlorite and biotite alteration. 15% plagioclase, subhedral - anhedral (alt. index 2-3), 0.1-0.2mm. 5% opaque Fe-Ti oxides, 0.2-0.4mm. 5% epidote, 0.1-0.2mm. 3% quartz, 0.1-0.2mm. Minor sphene.

**TJ-49 Ultrabasic gabbro (serpentinised).**

95% serpentinite. Minor chlorite, actinolite, pyrite, calcite in veins, some epidote. Grainsizes <0.05-0.2mm. Occasional completely altered plagioclase (alt. index 3). Minor pyrite.

**TJ-50 Psammitic schist (mild foliation).**

10% single grain muscovite, 0.2-0.8mm, some undulose extinction and zoning observed. 40% quartz, 0.1-0.5mm, granular mosaic. 40% altered plagioclase (alt. index 1-2) with minor k-feldspar, 0.2-1mm. 10% chloritised biotite, 0.2-0.6mm. Minor opaque Fe-Ti oxides. Minerals not very orientated.

**TJ-51 Amphibolite (massive).**

70% hornblende (green pleochroic) in total; large relict grains (20% of rock), 0.5-2mm, ragged edges, cracked, much inclusions and chloritisation and hornblende in matrix, 0.02-0.1mm, chlorite alteration. 25% altered plagioclase (alt. index 2-3), 0.02-0.05mm. 5% quartz, 0.02-0.05mm. Minor opaque Fe-Ti oxides and epidote in groundmass. Quartz vein (0.05mm wide). Minor pyrite. Brown iron oxide staining.

**TJ-52 Gabbro (granular).**

50% altered plagioclase,  $An_{58-70}$ , subhedral - anhedral, mosaic texture (alt. index 1-2), 0.5-2mm. 25% light pink - light green orthopyroxene, subhedral - anhedral, 0.5-2mm, alteration along cracks and cleavages. 20% colourless clinopyroxene, subhedral - anhedral, 0.5-2mm, alteration along cracks and cleavages also. Minor hornblende and chlorite mantling of pyroxenes. 5% sphene, euhedral, ~1mm. Minor Fe-Ti oxides. Minor chlorite in cracks in feldspars.

**TJ-53 Pelite (mild foliation).**

20% muscovite in aggregates, 0.1-0.8mm. 10% staurolite, 0.2-0.6mm, rounded with cracks. 10% garnet, very embayed with quartz, altered, remnants only left. 5% chloritised biotite, 0.2-0.4mm. 40% quartz, 0.1-0.5mm, mosaic texture (also in bands 3-4mm thick). 10% altered plagioclase (alt. index 2), 0.1-0.2mm. Opaque Fe-Ti oxides along grain boundaries of muscovite aggregates. Foliation in rock from parallel muscovites and quartz banding.

**TJ-54 Amphibolite (massive).**

60% dark green - light brown-yellow hornblende, subhedral, 0.1-0.3mm, pronounced cleavages, some alteration to chlorite and biotite, minor opaque Fe-Ti inclusions. 30% plagioclase, subhedral (alt. index 1), 0.1-0.2mm. 6% quartz, 0.1-0.2mm. 4% opaque Fe-Ti oxides, 0.1-0.3mm.

**TJ-55 Metagabbro (granular).**

65% mid-green - light green hornblende, anhedral and rounded, 0.5-2mm, highly cracked and with inclusions of highly altered feldspar, quartz and epidote, alteration along cleavages and at edges to chlorite. 15% highly altered plagioclase and K-feldspar (alt. index 3), 0.2-0.4mm. 10% quartz, undulose extinction, 0.2-1mm. 5% epidote, 0.1-0.4mm. 5% sphene, 0.5-1mm. Minor opaque Fe-Ti oxides present. Epidote vein 0.2mm wide.

**TJ-56 Metagabbro (granular).**

20% green pleochroic hornblende, anhedral with ragged edges, 0.5-2mm, highly altered to chlorite, cleavages sprung apart. 40% finer hornblende, 0.05-0.1mm, extensive chloritisation. 30% completely altered feldspar, subhedral - anhedral (alt. index 3), 0.5-1mm. 5% quartz, 0.5-1mm. 5% opaque Fe-Ti oxides with sphene. Minor epidote, apatite and pyrite.

**TJ-57 Amphibolite (massive).**

60% mid-green - light green hornblende, euhedral - subhedral, 0.05-0.2mm, some chlorite alteration, inclusions of opaque Fe-Ti oxides throughout (estimated at ~8% of rock). 30% altered plagioclase and K-feldspar (alt. index 1-2), 0.05-0.1mm. Minor quartz, calcite, epidote, sphene and pyrite.

**TJ-58 Amphibolite (granular).**

40% mid-green - light green hornblende, anhedral, mostly 0.1-0.3mm, some 0.5-1mm relict grains, chloritisation along cleavages and at edges. 30% altered plagioclase and K-feldspar (alt. index 1-2), 0.1-0.2mm, occasional plagioclase relict phenocrysts (alt. index 2), ~0.5mm. 20% epidote throughout rock in veins 0.2-1mm wide and as individual grains, subhedral - anhedral, 0.05-0.2mm. 5% quartz, 0.1-0.2mm. 5% opaque Fe-Ti oxides. Minor apatite, orange chromite, sphene and apatite.

**TJ-59 Amphibolite (massive).**

70% dark green - light green-yellow hornblende, subhedral - anhedral, 0.2-0.4mm, some larger crystals (1-2mm) in aggregates, occasional zoning, central areas of crystals display prominent dusty alteration along cleavages, spreading of cleavages also. Intergrown mosaic texture, alteration to boitite in some cleavages, inclusions of plagioclase and opaque Fe-Ti oxides. 20% plagioclase, anhedral (alt. index 1), 0.2-0.4mm. 6% quartz, 0.1-0.3mm. 4% opaque Fe-Ti oxides, sphene present. Brown iron oxide staining in patches.

**TJ-60 Metagabbro (granular).**

60% very pale green, low birefringence amphibole, subhedral mosaic texture, 0.5-2mm, sprung cleavages with chlorite alteration. 40% highly altered feldspar, anhedral patches (alt. index 3). Minor epidote, opaque Fe-Ti oxides and pyrite.

**TJ-61 Metagabbro (granular).**

50% mid-green - light green, anomalous birefringence amphibole, 0.5-0.2mm, cracked alteration to chlorite in cleavage and edges, inclusions of altered feldspar and Fe-Ti oxides. 40% altered feldspar (alt. index 2-3), 0.2-0.6mm. 6% opaque Fe-Ti oxides. 4% quartz, 0.1-0.4mm. Minor epidote, apatite and pyrite. Epidote and quartz veins.

### APPENDIX 3.

#### ROCK X-RAY FLUORESCENCE ANALYSES.

In the following analyses the FeO contents were measured by wet chemistry methods (Chapter 4). Fe<sub>2</sub>O<sub>3</sub> has been derived from the correction: Fe<sub>2</sub>O<sub>3(total)</sub> - (FeO x 1.1112) = Fe<sub>2</sub>O<sub>3</sub>. Fe/Fe+Mg in the following tables is an abbreviation for FeO/(FeO+MgO); the ratio of ferrous iron to magnesium in each sample.

H<sub>2</sub>O and CO<sub>2</sub> were measured simultaneously by the method outlined by Riley (1958), (Chapter 4).

#### Hornblende Bearing Rocks:

Oxide wt. %.	TJ-1	TJ-7A	TJ-7B	TJ-7D	TJ-7E	TJ-7F	TJ-7G
SiO <sub>2</sub>	48.57	49.35	48.03	49.26	49.01	49.45	48.30
TiO <sub>2</sub>	2.00	1.80	1.72	1.78	1.86	1.85	1.66
Al <sub>2</sub> O <sub>3</sub>	13.49	14.18	14.29	13.82	14.20	14.43	12.92
Fe <sub>2</sub> O <sub>3</sub>	6.59	1.95	2.31	3.35	3.01	2.34	2.49
FeO	6.52	10.14	10.39	11.40	10.19	10.32	10.23
MnO	0.22	0.17	0.17	0.18	0.23	0.22	0.20
MgO	8.41	6.92	6.96	5.30	5.94	6.00	8.51
CaO	9.98	11.24	11.29	10.05	9.83	10.67	11.65
Na <sub>2</sub> O	2.20	1.56	2.06	2.41	3.03	2.03	1.42
K <sub>2</sub> O	0.50	0.41	0.78	0.52	0.67	0.64	0.55
P <sub>2</sub> O <sub>5</sub>	0.35	0.20	0.22	0.38	0.27	0.25	0.23
CO <sub>2</sub>	0.11	0.09	0.77	0.06	0.12	0.11	0.09
H <sub>2</sub> O	1.58	1.63	1.68	1.66	1.60	1.75	1.86
<b>Total.</b>	<b><u>100.52</u></b>	<b><u>99.64</u></b>	<b><u>100.67</u></b>	<b><u>100.17</u></b>	<b><u>99.96</u></b>	<b><u>100.06</u></b>	<b><u>100.11</u></b>
<b>Fe/ (Fe+Mg)</b>	<b>0.437</b>	<b>0.594</b>	<b>0.599</b>	<b>0.683</b>	<b>0.632</b>	<b>0.632</b>	<b>0.546</b>

Oxide wt.%.  	TJ-7H	TJ-8	TJ-9	TJ-11	TJ-13	TJ-17	TJ-19
SiO <sub>2</sub>	47.84	51.58	47.77	48.80	44.33	47.63	52.96
TiO <sub>2</sub>	1.33	0.80	0.48	0.47	0.78	1.60	1.24
Al <sub>2</sub> O <sub>3</sub>	13.70	13.71	17.80	17.81	13.11	14.84	14.21
Fe <sub>2</sub> O <sub>3</sub>	2.41	1.35	1.20	1.11	4.64	2.35	1.97
FeO	10.73	9.20	7.78	7.55	10.03	10.94	7.37
MnO	0.24	0.18	0.18	0.13	0.21	0.35	0.19
MgO	8.40	7.93	8.87	8.71	11.54	6.97	7.45
CaO	10.87	10.88	11.09	11.96	11.49	9.35	9.97
Na <sub>2</sub> O	1.83	2.69	2.45	1.79	0.24	3.11	2.77
K <sub>2</sub> O	0.63	0.30	0.40	0.41	0.50	0.38	0.56
P <sub>2</sub> O <sub>5</sub>	0.19	0.09	0.09	0.06	0.04	0.29	0.13
CO <sub>2</sub>	0.16	0.14	0.04	0.13	0.32	0.14	0.12
H <sub>2</sub> O	1.81	1.86	1.50	2.01	2.84	1.81	1.45
<b>Total.</b>	<b><u>100.14</u></b>	<b><u>100.71</u></b>	<b><u>99.65</u></b>	<b><u>100.94</u></b>	<b><u>100.07</u></b>	<b><u>99.76</u></b>	<b><u>100.39</u></b>

Fe/ (Fe+Mg)	0.575	0.537	0.467	0.464	0.535	0.611	0.497
----------------	-------	-------	-------	-------	-------	-------	-------

Oxide wt.%.  	TJ-29	TJ-31	TJ-35	TJ-36	TJ-37	TJ-38	TJ-39
SiO <sub>2</sub>	47.26	47.47	51.12	45.94	48.16	48.59	52.07
TiO <sub>2</sub>	1.32	0.62	0.76	1.05	1.78	0.78	1.40
Al <sub>2</sub> O <sub>3</sub>	15.07	15.75	16.10	12.95	13.23	14.54	13.71
Fe <sub>2</sub> O <sub>3</sub>	2.04	1.42	0.85	2.13	1.56	1.46	2.94
FeO	9.75	9.34	7.48	9.25	10.17	9.82	7.70
MnO	0.20	0.20	0.15	0.22	0.23	0.22	0.19
MgO	8.37	9.40	9.14	13.46	8.51	8.91	6.76
CaO	10.55	11.07	10.04	9.40	11.87	11.53	10.04
Na <sub>2</sub> O	1.50	1.49	2.50	1.22	1.94	2.19	2.18
K <sub>2</sub> O	0.89	0.32	0.56	0.61	0.43	0.31	0.79
P <sub>2</sub> O <sub>5</sub>	0.28	0.07	0.14	0.45	0.23	0.11	0.17
CO <sub>2</sub>	0.60	0.18	0.00	0.36	0.07	0.13	0.66
H <sub>2</sub> O	2.48	1.92	1.24	3.12	1.73	1.69	1.81
<b>Total.</b>	<b><u>100.31</u></b>	<b><u>99.25</u></b>	<b><u>100.08</u></b>	<b><u>100.16</u></b>	<b><u>99.91</u></b>	<b><u>100.28</u></b>	<b><u>100.42</u></b>

Fe/ (Fe+Mg)	0.538	0.498	0.450	0.407	0.544	0.524	0.533
----------------	-------	-------	-------	-------	-------	-------	-------

Oxide wt.%.  	TJ-40	TJ-41	TJ-43	TJ-44	TJ-45	TJ-46	TJ-47
SiO <sub>2</sub>	47.25	52.05	50.31	46.13	46.90	53.11	46.47
TiO <sub>2</sub>	0.50	1.11	2.20	0.94	1.02	2.91	0.79
Al <sub>2</sub> O <sub>3</sub>	14.19	12.86	13.40	14.90	13.97	12.22	16.54
Fe <sub>2</sub> O <sub>3</sub>	1.23	1.44	1.74	1.32	2.05	4.30	1.94
FeO	9.08	9.02	8.82	11.38	10.95	8.76	8.41
MnO	0.16	0.27	0.14	0.24	0.29	0.22	0.20
MgO	11.46	10.00	8.72	9.50	8.53	5.30	7.71
CaO	11.18	8.31	8.45	8.48	9.84	8.19	13.12
Na <sub>2</sub> O	1.34	1.14	3.08	1.84	2.52	2.44	1.89
K <sub>2</sub> O	0.51	1.15	0.32	1.24	0.97	0.62	0.47
P <sub>2</sub> O <sub>5</sub>	0.07	0.17	0.34	0.12	0.10	0.48	0.10
CO <sub>2</sub>	0.13	0.12	0.45	0.41	0.33	0.28	0.57
H <sub>2</sub> O	3.12	2.77	1.95	3.55	2.34	1.34	1.79
<b>Total.</b>	<b><u>100.22</u></b>	<b><u>100.41</u></b>	<b><u>99.92</u></b>	<b><u>100.05</u></b>	<b><u>99.81</u></b>	<b><u>100.17</u></b>	<b><u>100.00</u></b>

Fe/ (Fe+Mg)	0.442	0.474	0.503	0.545	0.674	0.623	0.522
----------------	-------	-------	-------	-------	-------	-------	-------

Oxide wt.%.  	TJ-48	TJ-54	TJ-59
SiO <sub>2</sub>	45.80	49.07	46.33
TiO <sub>2</sub>	1.63	2.49	0.98
Al <sub>2</sub> O <sub>3</sub>	14.45	11.93	13.91
Fe <sub>2</sub> O <sub>3</sub>	2.02	5.27	3.83
FeO	10.73	10.43	8.97
MnO	0.31	0.26	0.28
MgO	9.61	4.93	10.34
CaO	8.74	9.77	11.69
Na <sub>2</sub> O	3.53	3.25	0.73
K <sub>2</sub> O	0.36	0.43	0.70
P <sub>2</sub> O <sub>5</sub>	0.36	0.30	0.13
CO <sub>2</sub>	0.07	0.09	0.13
H <sub>2</sub> O	2.37	1.65	2.48
<b>Total.</b>	<b><u>99.98</u></b>	<b><u>99.87</u></b>	<b><u>100.50</u></b>

Fe/ (Fe+Mg)	0.528	0.679	0.465
----------------	-------	-------	-------

### Average Errors of Oxides:

Oxide wt. %.	Average wt. %.	Average Error; wt. %
SiO <sub>2</sub>	48.61	0.42
TiO <sub>2</sub>	1.34	0.03
Al <sub>2</sub> O <sub>3</sub>	14.27	0.24
Fe <sub>2</sub> O <sub>3</sub>	2.41	0.03
FeO	9.45	0.10
MnO	0.21	0.02
MgO	8.34	0.21
CaO	10.41	0.18
Na <sub>2</sub> O	2.08	0.17
K <sub>2</sub> O	0.58	0.05
P <sub>2</sub> O <sub>5</sub>	0.21	0.02
CO <sub>2</sub>	0.25	0.03
H <sub>2</sub> O	2.01	0.10
Fe/ (Fe+Mg)	0.531	0.014

### Standard Deviations of Glasgow University Standards:

Oxide wt. %.	7510 G-GN		7570 G-SL		7520 G-TR	
	Average wt. %.	Average Error; wt. %	Average wt. %.	Average Error; wt. %	Average wt. %.	Average Error; wt. %
SiO <sub>2</sub>	70.14	0.46	55.07	0.42	65.78	0.54
TiO <sub>2</sub>	0.23	0.01	1.29	0.02	0.39	0.01
Al <sub>2</sub> O <sub>3</sub>	14.77	0.12	18.62	0.14	15.71	0.18
Fe <sub>2</sub> O <sub>3</sub>	2.87	0.07	10.37	0.15	3.27	0.07
MnO	0.06	0.02	0.18	0.02	0.11	0.02
MgO	1.69	0.17	2.32	0.15	0.52	0.04
CaO	2.17	0.05	1.49	0.02	1.55	0.03
Na <sub>2</sub> O	5.38	0.17	2.76	0.12	5.35	0.12
K <sub>2</sub> O	1.17	0.02	2.90	0.03	4.93	0.08
P <sub>2</sub> O <sub>5</sub>	0.06	0.01	0.23	0.01	0.06	0.00

**Muscovite Bearing Rocks:**

Oxide wt. %.	TJ-10	TJ-16	TJ-18	TJ-22	TJ-50	TJ-53
SiO <sub>2</sub>	52.52	58.66	68.40	54.91	77.35	73.79
TiO <sub>2</sub>	1.29	0.65	0.99	1.01	0.90	0.82
Al <sub>2</sub> O <sub>3</sub>	24.44	19.40	14.00	21.76	10.05	11.98
Fe <sub>2</sub> O <sub>3</sub>	3.22	2.90	1.65	1.69	2.18	3.90
FeO	6.20	4.74	4.58	5.28	2.61	2.15
MnO	0.12	0.26	0.09	0.17	0.04	0.03
MgO	2.31	2.31	1.92	2.48	1.15	1.67
CaO	0.34	1.37	0.24	1.59	0.78	0.84
Na <sub>2</sub> O	0.86	3.54	1.69	0.89	1.60	0.75
K <sub>2</sub> O	4.09	2.02	3.35	5.48	1.71	2.01
P <sub>2</sub> O <sub>5</sub>	0.24	0.17	0.15	0.11	0.14	0.17
CO <sub>2</sub>	0.23	1.13	0.22	0.72	0.15	0.14
H <sub>2</sub> O	4.02	3.26	2.64	3.92	1.59	1.93
<b>Total.</b>	<u>99.88</u>	<u>100.41</u>	<u>99.92</u>	<u>100.01</u>	<u>100.25</u>	<u>100.18</u>
<b>Fe/ (Fe+Mg)</b>	0.729	0.672	0.705	0.680	0.694	0.563

## APPENDIX 3A.

### ROCK CIPW NORM RESULTS.

These are calculated from the rock XRF oxides listed in Appendix 3 using the method in Cox et al. (1979).

The mineral abbreviations are as follows: Q = quartz ( $\text{SiO}_2$ ); Or = orthoclase ( $\text{KAlSi}_3\text{O}_8$ ); Pl = plagioclase (Ab-An); Ab = albite ( $\text{NaAlSi}_3\text{O}_8$ ); An = anorthite ( $\text{CaAl}_2\text{Si}_2\text{O}_8$ ); Di = diopside-hedenbergite (Wo-En-Fs); Wo = wollastonite ( $\text{CaSiO}_3$ ); En = enstatite ( $\text{MgSiO}_3$ ); Fs = ferrosilite ( $\text{FeSiO}_3$ ); Hy = hypersthene (En-Fs); Ol = olivine (Fo-Fa); Fo = forsterite ( $\text{Mg}_2\text{SiO}_4$ ); Fa = fayalite ( $\text{Fe}_2\text{SiO}_4$ ); Mt = magnetite ( $\text{Fe}_3\text{O}_4$ ); Il = ilmenite ( $\text{FeTiO}_3$ ); Ap = apatite ( $\text{Ca}_5(\text{PO}_4)_3(\text{F,Cl,OH})$ ); Ne = nepheline ( $(\text{Na,K})\text{AlSiO}_4$ ).

#### Hornblende Bearing Rocks:

CIPW norm wt. %.	TJ-1	TJ-7A	TJ-7B	TJ-7D	TJ-7E	TJ-7F	TJ-7G
Q	3.98	3.49	-	2.57	-	2.49	0.68
Or	2.95	2.45	4.62	3.06	3.95	3.79	3.23
Ab <u>Pl</u>	18.62	13.22	17.41	20.40	25.65	17.20	12.01
An	25.46	30.47	27.46	25.35	23.18	28.35	27.27
Wo <u>Di</u>	9.08	10.01	11.33	9.19	9.96	9.57	12.13
En	6.94	5.30	5.96	4.19	5.07	4.78	6.92
Fs	1.20	4.41	5.04	4.93	4.64	4.59	4.68
En <u>Hy</u>	14.01	11.94	7.90	9.02	7.01	10.16	14.28
Fs	2.43	9.95	6.68	10.62	6.44	9.78	9.67
Fo <u>Ol</u>	-	-	2.43	-	1.91	-	-
Fa	-	-	2.26	-	1.92	-	-
Mt	9.56	2.82	3.36	4.86	4.35	3.38	3.61
Il	3.79	3.41	3.26	3.38	3.54	3.52	3.16
Ap	0.78	0.43	0.47	0.84	0.59	0.56	0.50
<b>Total.</b>	<b><u>98.79</u></b>	<b><u>97.90</u></b>	<b><u>98.19</u></b>	<b><u>98.41</u></b>	<b><u>98.20</u></b>	<b><u>98.17</u></b>	<b><u>98.13</u></b>

CIPW norm wt.%. Q		TJ-7H	TJ-8	TJ-9	TJ-11	TJ-13	TJ-17	TJ-19
Or		-	-	-	-	-	-	3.11
		3.73	1.78	2.34	2.45	2.95	2.23	3.28
Ab	<u>Pl</u>	15.47	22.76	20.72	15.16	2.05	26.33	23.44
An		27.32	24.46	36.42	39.34	33.22	25.40	24.71
Wo	<u>Di</u>	10.56	12.09	7.54	8.20	9.82	7.98	9.99
En		5.77	6.66	4.52	4.94	6.22	4.04	6.08
Fs		4.41	4.99	2.63	2.82	2.97	3.76	3.35
En	<u>Hy</u>	10.35	11.84	2.09	9.59	17.97	4.01	12.47
Fs		7.89	8.85	1.21	5.49	8.56	3.72	6.87
Fo	<u>OI</u>	3.36	0.89	10.85	5.02	3.18	6.53	-
Fa		2.83	0.73	6.95	3.16	1.67	6.70	-
Mt		3.50	1.97	1.74	1.62	6.74	3.40	2.85
Il		2.52	1.52	0.91	0.90	1.49	3.04	2.35
Ap		0.43	0.19	0.19	0.12	0.09	0.62	0.28
<b>Total.</b>		<u>98.15</u>	<u>98.72</u>	<u>98.09</u>	<u>98.81</u>	<u>96.93</u>	<u>97.75</u>	<u>98.80</u>

CIPW norm wt.%. Q		TJ-29	TJ-31	TJ-35	TJ-36	TJ-37	TJ-38	TJ-39
Or		-	-	-	-	-	-	5.85
		5.23	1.89	3.28	3.62	2.56	1.84	4.68
Ab	<u>Pl</u>	12.69	12.59	21.14	10.33	16.42	18.51	18.46
An		31.77	35.36	31.08	28.04	26.12	28.93	25.29
Wo	<u>Di</u>	7.81	7.97	7.43	6.52	13.07	11.49	9.77
En		4.42	4.60	4.58	4.28	7.37	6.42	5.85
Fs		3.06	3.01	2.43	1.78	5.16	4.62	3.40
En	<u>Hy</u>	12.80	12.58	13.60	15.55	8.87	6.46	10.98
Fs		8.85	8.23	7.20	6.45	6.21	4.63	6.36
Fo	<u>OI</u>	2.53	4.38	3.21	9.60	3.48	6.53	-
Fa		1.94	3.16	1.87	4.38	2.69	5.18	-
Mt		2.96	2.06	1.23	3.08	2.27	2.11	4.26
Il		2.50	1.18	1.44	1.99	3.38	1.49	2.66
Ap		0.62	0.16	0.31	0.99	0.50	0.25	0.37
<b>Total.</b>		<u>97.19</u>	<u>97.17</u>	<u>98.81</u>	<u>96.61</u>	<u>98.09</u>	<u>98.44</u>	<u>97.93</u>

CIPW norm wt.%. Q		TJ-40	TJ-41	TJ-43	TJ-44	TJ-45	TJ-46	TJ-47
Or		- 3.01	5.31 6.79	- 1.89	- 7.35	- 5.73	12.38 3.67	- 2.78
Ab	<u>Pl</u>	11.33	9.65	25.12	15.58	21.35	20.66	16.00
An		31.22	26.57	21.78	28.71	23.93	20.56	35.25
Wo	<u>Di</u>	9.93	5.66	7.48	5.26	10.13	7.06	12.20
En		6.11	3.42	4.62	2.84	5.41	4.16	6.98
Fs		3.25	1.93	2.43	2.24	4.39	2.56	4.68
En	<u>Hy</u>	10.32	21.49	16.37	5.92	0.06	9.05	0.64
Fs		5.48	12.11	8.59	4.68	0.04	5.58	0.44
Fo	<u>OI</u>	8.48	-	0.52	10.44	11.06	-	8.12
Fa		4.95	-	0.31	9.09	9.90	-	6.01
Mt		1.78	2.08	2.52	1.92	2.96	6.23	2.80
Il		0.96	2.11	4.17	1.79	1.94	5.52	1.50
Ap		0.16	0.37	0.74	0.25	0.22	1.05	0.22
<b>Total.</b>		<u>96.97</u>	<u>97.49</u>	<u>96.55</u>	<u>96.08</u>	<u>97.13</u>	<u>98.49</u>	<u>97.63</u>

CIPW norm wt.%. Q		TJ-48	TJ-54	TJ-59
Or		- 2.12	2.43 2.56	- 4.12
Ab	<u>Pl</u>	24.13	27.48	6.19
An		22.51	16.69	32.61
Ne		3.13	-	-
Wo	<u>Di</u>	7.74	12.45	10.26
En		4.44	6.36	6.52
Fs		2.96	5.79	3.09
En	<u>Hy</u>	-	5.92	16.91
Fs		-	5.38	8.00
Fo	<u>OI</u>	13.66	-	1.63
Fa		10.03	-	0.86
Mt		2.92	7.64	5.56
Il		3.10	4.73	1.87
Ap		0.78	0.65	0.28
<b>Total.</b>		<u>97.48</u>	<u>98.10</u>	<u>97.87</u>

## APPENDIX 4.

### MINERAL SEPARATES CHEMICAL ANALYSES.

The following results were obtained from mineral separates using wet chemistry techniques as described in Chapter 4.

FeO was analysed using the titration method outlined in Chapter 4. Fe<sub>(total)</sub> was measured by AAS and calculated as Fe<sub>2</sub>O<sub>3(total)</sub>. Fe<sub>2</sub>O<sub>3</sub> has been derived from the correction: Fe<sub>2</sub>O<sub>3(total)</sub> - (FeO x 1.1112) = Fe<sub>2</sub>O<sub>3</sub>. Fe/Fe+Mg in the following tables is an abbreviation for FeO/(FeO+MgO); the ratio of ferrous iron to magnesium in each sample.

#### Hornblende mineral separates:

Oxide wt. %.	TJ-1	TJ-7A	TJ-7B	TJ-7D	TJ-7E	TJ-7F	TJ-7G	TJ-7H
Fe <sub>2</sub> O <sub>3</sub>	5.03	4.00	3.41	6.30	4.63	4.02	3.88	3.64
FeO	9.48	13.13	13.54	16.49	15.06	14.40	12.52	13.87
MgO	13.33	10.63	9.27	7.43	9.28	10.74	12.39	10.05
CaO	11.69	11.54	11.30	10.99	12.21	11.79	12.63	11.45
Na <sub>2</sub> O	1.17	1.19	1.18	1.49	1.23	0.87	0.84	1.11
K <sub>2</sub> O	0.33	0.29	0.51	0.40	0.37	0.40	0.30	0.34
Fe/ (Fe+Mg)	0.416	0.553	0.594	0.689	0.619	0.619	0.503	0.580

Oxide wt. %.	TJ-8	TJ-9	TJ-11	TJ-13	TJ-17	TJ-19	TJ-29	TJ-31
Fe <sub>2</sub> O <sub>3</sub>	3.70	3.04	2.79	7.51	3.09	4.05	4.07	3.26
FeO	13.45	10.26	10.80	9.26	14.78	12.63	11.28	11.50
MgO	12.29	12.02	12.78	13.10	10.64	13.56	10.20	12.17
CaO	12.45	11.61	11.75	11.40	11.22	11.45	11.02	12.03
Na <sub>2</sub> O	0.91	1.16	1.30	0.72	2.10	1.32	1.39	1.19
K <sub>2</sub> O	0.22	0.22	0.23	0.24	0.29	0.31	0.77	0.21
Fe/ (Fe+Mg)	0.523	0.461	0.458	0.414	0.581	0.482	0.525	0.486

Oxide wt.%. TJ-35	TJ-36	TJ-37	TJ-38	TJ-39	TJ-40	TJ-41	TJ-43
Fe <sub>2</sub> O <sub>3</sub>	3.55	5.68	3.61	3.34	4.81	3.09	3.78
FeO	12.08	8.65	13.56	13.58	10.30	10.36	12.44
MgO	10.46	13.18	10.15	11.36	9.50	12.93	12.10
CaO	11.50	10.68	11.75	11.56	10.99	11.66	9.94
Na <sub>2</sub> O	1.27	1.54	1.08	0.99	1.60	1.33	1.39
K <sub>2</sub> O	0.31	0.27	0.33	0.18	0.58	0.22	0.16
Fe/ (Fe+Mg)	0.536	0.396	0.572	0.545	0.520	0.445	0.507

Oxide wt.%. TJ-44	TJ-45	TJ-46	TJ-47	TJ-48	TJ-54	TJ-59
Fe <sub>2</sub> O <sub>3</sub>	3.16	4.01	6.40	3.69	3.11	6.25
FeO	15.21	14.94	12.97	12.21	12.31	10.24
MgO	10.97	9.96	10.69	10.46	11.50	11.91
CaO	10.36	10.58	11.61	11.98	10.70	11.91
Na <sub>2</sub> O	1.53	1.78	1.50	1.85	3.01	1.14
K <sub>2</sub> O	0.52	0.59	0.48	0.25	0.18	0.48
Fe/ (Fe+Mg)	0.581	0.600	0.548	0.539	0.517	0.462

Average Error Values: Based on above hornblende data.

Oxide wt.%. Average	Average	Average
	wt.%. Error.	
Fe <sub>2</sub> O <sub>3</sub>	4.16	+/-0.05
FeO	12.42	+/-0.06
MgO	11.21	+/-0.30
CaO	11.43	+/-0.19
Na <sub>2</sub> O	1.38	+/-0.02
K <sub>2</sub> O	0.34	+/-0.01
Fe/ (Fe+Mg)	0.526	+/-0.010

**Muscovite mineral separates:**

<b>Oxide wt.%.  </b>	<b>TJ-10</b>	<b>TJ-16</b>	<b>TJ-18</b>	<b>TJ-22</b>	<b>TJ-50</b>	<b>TJ-53</b>
<b>Fe<sub>2</sub>O<sub>3</sub></b>	2.97	1.46	4.59	1.56	4.65	3.06
<b>FeO</b>	0.75	0.51	1.17	1.35	1.38	1.70
<b>MgO</b>	1.38	1.36	1.43	1.36	1.44	1.49
<b>Na<sub>2</sub>O</b>	1.63	0.86	0.69	0.86	0.85	1.11
<b>K<sub>2</sub>O</b>	7.66	10.07	10.30	9.44	9.57	5.69
<b>Fe/ (Fe+Mg)</b>	0.352	0.273	0.450	0.498	0.489	0.533

## APPENDIX 5.

### ELECTRON MICROPROBE ANALYSIS RESULTS. (estimated bulk analyses).

The following are the EMPA results for 16-20 point analyses for hornblende samples taken from polished rock sections. Standard deviations are given for each oxide measured, except FeO and Fe<sub>2</sub>O<sub>3</sub> which were estimated based on the results of wet chemistry analysis (Appendix 4).

The iron measured by EMPA was initially assumed as Fe<sub>2</sub>O<sub>3(total)</sub>. The ratio of Fe<sub>2</sub>O<sub>3</sub>/FeO as found by wet chemical analysis for each hornblende separate sample (Appendix 4) was used to split the measured EMPA Fe<sub>2</sub>O<sub>3(total)</sub> value into the same Fe<sub>2</sub>O<sub>3</sub>/FeO relative proportions as the mineral separate. The correction Fe<sub>2</sub>O<sub>3(total)</sub> - (FeO x 1.1112) = Fe<sub>2</sub>O<sub>3</sub> was also used on this ratio. These are the Fe<sub>2</sub>O<sub>3</sub> and FeO wt.% values given for each sample in the following tables.

Fe/(Fe+Mg) in the following tables is an abbreviation for FeO/(FeO+MgO); the ratio of ferrous iron to magnesium in each sample, assuming the Fe<sub>2</sub>O<sub>3</sub>/FeO relative proportions as estimated from wet chemical analysis.

In all cases the values were normalised to give a total of 98%, allowing 2% for the presence of H<sub>2</sub>O, CO<sub>2</sub> and halogens, which were not analysed in the mineral separates.

The samples which have an asterisk below the sample number are representative, bulk compositions of samples which displayed two composition populations as measured by EMPA (Chapter 5, Appendix 5A). The bulk composition (Appendix 5) for these samples was estimated by using the MgO value from the AAS analysis (Appendix 4) to calculate a representative intermediate composition (bulk), from compositions (a) and (b) (Appendix 5A). The % ratio of compositions (a) to (b) is given in each case in Appendix 5A. This phenomenon was encountered in samples collected in the north of the Dalradian exposure. Samples collected in the south did not display this and were generally of uniform, single composition.

The EMPA results for muscovite are based on 10-12 point analyses for each sample. The analyses were not as variable as observed for the hornblende samples. Each sample has been normalised to give a total of 96%, allowing 4% for the presence of H<sub>2</sub>O, CO<sub>2</sub> and halogens, which were not analysed for in the mineral separates.

**Hornblende Analyses: Single and bulk (\*) compositions.**

Oxide wt.%. TJ-1 (SD)	TJ-7A (SD) *	TJ-7B (SD) *	TJ-7D (SD) *	TJ-7E (SD) *
SiO <sub>2</sub>	45.89 (0.51)	45.82 (0.57)	45.66 (0.69)	45.71 (0.43)
TiO <sub>2</sub>	0.95 (0.23)	0.30 (0.06)	0.28 (0.08)	0.35 (0.05)
Al <sub>2</sub> O <sub>3</sub>	9.99 (0.46)	12.03 (0.50)	11.59 (0.61)	9.78 (0.44)
Fe <sub>2</sub> O <sub>3</sub>	5.22	3.90	3.63	4.55
FeO	9.90	12.82	14.47	14.87
MnO	0.30 (0.05)	0.28 (0.05)	0.27 (0.06)	0.37 (0.07)
MgO	12.32 (0.23)	9.77 (0.32)	9.28 (0.56)	9.27 (0.37)
CaO	12.03 (0.11)	11.68 (0.38)	11.36 (0.32)	11.40 (0.38)
Na <sub>2</sub> O	1.09 (0.09)	1.08 (0.09)	1.07 (0.15)	1.26 (0.14)
K <sub>2</sub> O	0.32 (0.04)	0.34 (0.05)	0.38 (0.08)	0.41 (0.07)
<b>Total.</b>	<b><u>98.01</u></b>	<b><u>98.02</u></b>	<b><u>97.99</u></b>	<b><u>97.97</u></b>
Fe/ (Fe+Mg)	0.446	0.568	0.609	0.616

Oxide wt.%. TJ-7F (SD) *	TJ-7G (SD) *	TJ-7H (SD) *	TJ-8 (SD) *	TJ-9 (SD)
SiO <sub>2</sub>	47.08 (0.60)	48.45 (0.85)	45.39 (0.57)	45.70 (0.67)
TiO <sub>2</sub>	0.16 (0.04)	0.18 (0.05)	0.34 (0.07)	0.30 (0.08)
Al <sub>2</sub> O <sub>3</sub>	8.34 (0.44)	7.28 (0.61)	11.44 (0.79)	13.82 (1.08)
Fe <sub>2</sub> O <sub>3</sub>	4.01	1.27	3.55	2.42
FeO	14.40	15.33	13.63	9.62
MnO	0.34 (0.06)	0.32 (0.05)	0.28 (0.05)	0.21 (0.04)
MgO	10.73 (0.49)	12.29 (0.78)	10.06 (0.66)	12.58 (0.48)
CaO	11.82 (0.40)	11.87 (0.43)	11.77 (0.40)	12.16 (0.12)
Na <sub>2</sub> O	0.77 (0.11)	0.75 (0.11)	1.17 (0.16)	1.01 (0.07)
K <sub>2</sub> O	0.34 (0.06)	0.23 (0.05)	0.39 (0.07)	0.17 (0.04)
<b>Total.</b>	<b><u>97.99</u></b>	<b><u>97.97</u></b>	<b><u>98.02</u></b>	<b><u>97.99</u></b>
Fe/ (Fe+Mg)	0.573	0.555	0.575	0.433

Oxide wt. %.	TJ-11 (SD)	TJ-13 (SD)	TJ-17 (SD)	TJ-19 (SD) *	TJ-29 (SD) *
SiO <sub>2</sub>	45.73 (0.50)	48.07 (1.78)	44.15 (0.92)	45.45 (0.53)	43.62 (0.79)
TiO <sub>2</sub>	0.40 (0.05)	0.47 (0.13)	0.55 (0.17)	0.35 (0.06)	0.46 (0.11)
Al <sub>2</sub> O <sub>3</sub>	14.16 (0.78)	8.66 (1.62)	12.46 (0.97)	11.81 (1.00)	12.93 (1.08)
Fe <sub>2</sub> O <sub>3</sub>	2.56	6.55	3.01	3.95	4.53
FeO	9.98	8.62	14.43	12.42	12.62
MnO	0.19 (0.04)	0.25 (0.03)	0.34 (0.05)	0.31 (0.05)	0.29 (0.05)
MgO	11.75 (0.28)	12.86 (1.08)	9.92 (0.36)	10.51 (0.47)	10.21 (0.68)
CaO	11.90 (0.12)	11.75 (0.14)	10.98 (0.14)	11.51 (0.48)	11.91 (0.29)
Na <sub>2</sub> O	1.16 (0.08)	0.62 (0.13)	1.84 (0.18)	1.26 (0.19)	1.25 (0.15)
K <sub>2</sub> O	0.20 (0.03)	0.19 (0.03)	0.31 (0.06)	0.39 (0.06)	0.21 (0.06)
<b>Total.</b>	<u>98.03</u>	<u>98.04</u>	<u>97.99</u>	<u>97.96</u>	<u>98.03</u>
Fe/ (Fe+Mg)	0.459	0.401	0.593	0.542	0.553

Oxide wt. %.	TJ-31 (SD)	TJ-35 (SD) *	TJ-36 (SD) *	TJ-37 (SD) *	TJ-38 (SD) *
SiO <sub>2</sub>	47.01 (1.88)	44.11 (0.82)	47.20 (0.99)	45.99 (1.02)	46.51 (1.71)
TiO <sub>2</sub>	0.52 (0.17)	0.40 (0.04)	0.30 (0.05)	0.50 (0.09)	0.31 (0.07)
Al <sub>2</sub> O <sub>3</sub>	10.92 (2.55)	14.33 (1.15)	11.06 (0.79)	11.06 (0.91)	10.04 (1.52)
Fe <sub>2</sub> O <sub>3</sub>	2.87	3.08	4.96	3.42	3.24
FeO	10.20	10.58	7.92	12.89	13.20
MnO	0.22 (0.04)	0.29 (0.04)	0.17 (0.05)	0.23 (0.05)	0.32 (0.05)
MgO	12.83 (1.21)	11.84 (0.58)	13.20 (0.47)	10.36 (0.73)	11.37 (1.02)
CaO	12.28 (1.97)	11.79 (0.31)	11.52 (0.30)	12.09 (0.43)	11.90 (0.33)
Na <sub>2</sub> O	1.05 (0.29)	1.24 (0.11)	1.42 (0.18)	1.08 (0.12)	0.89 (0.18)
K <sub>2</sub> O	0.14 (0.06)	0.32 (0.07)	0.20 (0.04)	0.39 (0.07)	0.21 (0.06)
<b>Total.</b>	<u>98.04</u>	<u>97.98</u>	<u>97.95</u>	<u>98.01</u>	<u>97.99</u>
Fe/ (Fe+Mg)	0.443	0.472	0.375	0.554	0.537

Oxide wt.%. *	TJ-39 (SD)	TJ-40 (SD)	TJ-41 (SD)	TJ-43 (SD)	TJ-44 (SD)
SiO <sub>2</sub>	42.85 (0.81)	45.51 (0.78)	44.76 (1.18)	48.20 (0.34)	44.24 (0.52)
TiO <sub>2</sub>	0.43 (0.10)	0.35 (0.06)	0.34 (0.11)	1.01 (0.12)	0.79 (0.11)
Al <sub>2</sub> O <sub>3</sub>	13.53 (0.83)	13.85 (1.09)	12.85 (1.55)	7.84 (0.28)	11.18 (0.47)
Fe <sub>2</sub> O <sub>3</sub>	5.45	2.71	3.41	3.33	2.85
FeO	11.71	9.11	10.85	11.00	13.77
MnO	0.33 (0.08)	0.23 (0.04)	0.35 (0.05)	0.22 (0.03)	0.28 (0.04)
MgO	9.94 (0.58)	13.01 (0.86)	12.26 (1.01)	13.82 (0.30)	11.13 (0.27)
CaO	11.78 (0.34)	11.65 (0.33)	11.74 (0.17)	11.01 (0.38)	11.54 (0.18)
Na <sub>2</sub> O	1.52 (0.15)	1.34 (0.16)	1.20 (0.16)	1.38 (0.08)	1.60 (0.09)
K <sub>2</sub> O	0.49 (0.08)	0.24 (0.07)	0.23 (0.06)	0.16 (0.03)	0.64 (0.07)
<b>Total.</b>	<b><u>98.03</u></b>	<b><u>98.00</u></b>	<b><u>97.99</u></b>	<b><u>97.97</u></b>	<b><u>98.02</u></b>
Fe/ (Fe+Mg)	0.541	0.412	0.469	0.443	0.553

Oxide wt.%. *	TJ-45 (SD)	TJ-46 (SD)	TJ-47 (SD)	TJ-48 (SD)	TJ-54 (SD)
SiO <sub>2</sub>	43.54 (0.50)	44.21 (0.55)	42.71 (1.16)	43.17 (0.69)	40.89 (0.55)
TiO <sub>2</sub>	0.63 (0.08)	1.27 (0.12)	0.47 (0.16)	0.41 (0.04)	0.58 (0.06)
Al <sub>2</sub> O <sub>3</sub>	11.52 (0.24)	9.62 (0.50)	13.70 (1.49)	14.23 (0.66)	10.69 (0.47)
Fe <sub>2</sub> O <sub>3</sub>	3.69	5.86	3.35	2.89	8.43
FeO	13.82	11.90	11.93	11.47	16.60
MnO	0.39 (0.04)	0.35 (0.06)	0.28 (0.05)	0.26 (0.04)	0.48 (0.05)
MgO	10.74 (0.31)	11.32 (0.38)	10.94 (0.74)	11.85 (0.52)	6.68 (0.27)
CaO	11.13 (0.23)	11.51 (0.26)	12.32 (0.29)	10.43 (0.26)	11.30 (0.22)
Na <sub>2</sub> O	1.93 (0.15)	1.45 (0.09)	2.05 (0.18)	3.06 (0.29)	1.92 (0.16)
K <sub>2</sub> O	0.61 (0.05)	0.50 (0.07)	0.25 (0.06)	0.23 (0.05)	0.41 (0.05)
<b>Total.</b>	<b><u>98.00</u></b>	<b><u>97.99</u></b>	<b><u>98.00</u></b>	<b><u>98.00</u></b>	<b><u>97.98</u></b>
Fe/ (Fe+Mg)	0.563	0.512	0.522	0.492	0.713

Oxide wt.%.  	TJ-59 (SD)	
SiO <sub>2</sub>	45.90	(1.29)
TiO <sub>2</sub>	0.61	(0.09)
Al <sub>2</sub> O <sub>3</sub>	9.23	(1.06)
Fe <sub>2</sub> O <sub>3</sub>	5.90	
FeO	10.84	
MnO	0.31	(0.05)
MgO	11.80	(0.65)
CaO	12.07	(0.21)
Na <sub>2</sub> O	1.04	(0.12)
K <sub>2</sub> O	0.33	(0.05)
<b>Total.</b>	<b>98.03</b>	

Fe/  
(Fe+Mg) 0.479

**Average Standard Deviations:** Based on the above data for hornblende.

Oxide wt.%.  	Average wt.%.  	Average SD.  
SiO <sub>2</sub>	45.32	(0.83)
TiO <sub>2</sub>	0.47	(0.09)
Al <sub>2</sub> O <sub>3</sub>	11.28	(0.88)
MnO	0.30	(0.05)
MgO	11.26	(0.57)
CaO	11.68	(0.34)
Na <sub>2</sub> O	1.31	(0.14)
K <sub>2</sub> O	0.32	(0.06)
Fe <sub>2</sub> O <sub>3</sub>	3.83	(0.04)
FeO	12.09	(0.06)
Fe/ (Fe+Mg)	0.518	(0.016)

FeO, Fe<sub>2</sub>O<sub>3</sub> and FeO/(FeO+MgO) standard deviations are derived from the chemical analysis data in Appendix 4.

### Muscovite Analyses:

Oxide wt. %.	TJ-10 (SD)	TJ-16 (SD)	TJ-18 (SD)	TJ-22 (SD)	TJ-50 (SD)
SiO <sub>2</sub>	47.12 (0.38)	47.04 (0.46)	46.32 (0.32)	46.82 (0.24)	45.15 (1.24)
TiO <sub>2</sub>	0.18 (0.07)	0.53 (0.22)	0.92 (0.12)	0.63 (0.05)	1.07 (0.17)
Al <sub>2</sub> O <sub>3</sub>	35.23 (0.68)	35.54 (0.57)	33.02 (0.30)	36.02 (0.37)	33.36 (0.87)
Fe <sub>2</sub> O <sub>3</sub>	1.96	0.93	3.20	0.57	3.62
FeO	0.50	0.24	0.81	0.51	1.08
MnO	0.01 (0.01)	0.02 (0.02)	0.02 (0.02)	0.01 (0.01)	0.02 (0.01)
MgO	0.67 (0.11)	0.76 (0.08)	0.69 (0.08)	0.59 (0.05)	0.67 (0.04)
CaO	-	-	-	-	-
Na <sub>2</sub> O	1.61 (0.11)	0.72 (0.04)	0.53 (0.08)	0.89 (0.08)	0.49 (0.04)
K <sub>2</sub> O	8.76 (0.14)	10.24 (0.18)	10.48 (0.30)	9.98 (0.26)	10.54 (0.35)
<b>Total.</b>	<u>96.04</u>	<u>96.02</u>	<u>95.99</u>	<u>96.02</u>	<u>96.00</u>

Oxide wt. %.	TJ-53 (SD)
SiO <sub>2</sub>	45.98 (0.19)
TiO <sub>2</sub>	0.32 (0.08)
Al <sub>2</sub> O <sub>3</sub>	35.18 (0.40)
Fe <sub>2</sub> O <sub>3</sub>	2
FeO	1.11
MnO	0.02 (0.02)
MgO	0.68 (0.06)
CaO	-
Na <sub>2</sub> O	1.11 (0.07)
K <sub>2</sub> O	9.59 (0.27)
<b>Total.</b>	<u>95.99</u>

## APPENDIX 5A.

### ELECTRON MICROPROBE ANALYSIS RESULTS. (dual hornblende analyses).

These analyses represent the analyses where the EMPA results clustered, even within individual grains. In each case (a) represents the Al-, Ti-, Fe-, Na-, K-rich hornblende and (b) the Si-, Mg-rich hornblende analyses (Chapter 5).

The bulk composition for each sample in Appendix 5 is representative of the proportions of (a) and (b) relative to the AAS MgO result (Appendix 4).

For example, **TJ-7E**:

(a) has 7.23wt.% MgO.

(b) has 12.75wt.% MgO.

AAS = 9.28wt.% MgO (Appendix 4).

This gives 37% of (a) and 67% of (b)

These proportions are then used to calculate the representative value for each oxide to produce the bulk composition. The introduction to Appendix 5 outlines Fe<sub>2</sub>O<sub>3</sub>, FeO and MgO ratios and evaluations.

Oxide wt.%. (a)	(SD)	TJ-7A (b)	(SD)	Oxide wt.%. (a)	(SD)	TJ-7B (b)	(SD)
SiO <sub>2</sub>	43.46 (0.48)	45.82	(0.57)	SiO <sub>2</sub>	42.98 (0.47)	49.06	(0.98)
TiO <sub>2</sub>	0.40 (0.03)	0.30	(0.06)	TiO <sub>2</sub>	0.41 (0.10)	0.12	(0.05)
Al <sub>2</sub> O <sub>3</sub>	14.99 (0.39)	12.03	(0.50)	Al <sub>2</sub> O <sub>3</sub>	15.00 (0.43)	7.25	(0.84)
Fe <sub>2</sub> O <sub>3</sub>	3.83	3.90		Fe <sub>2</sub> O <sub>3</sub>	3.65	3.60	
FeO	13.36	12.82		FeO	14.57	14.34	
MnO	0.29 (0.06)	0.28	(0.05)	MnO	0.27 (0.06)	0.28	(0.06)
MgO	8.43 (0.30)	9.77	(0.32)	MgO	8.05 (0.43)	10.85	(0.72)
CaO	11.37 (0.26)	11.68	(0.38)	CaO	11.26 (0.31)	11.49	(0.34)
Na <sub>2</sub> O	1.39 (0.15)	1.08	(0.09)	Na <sub>2</sub> O	1.36 (0.12)	0.70	(0.19)
K <sub>2</sub> O	0.45 (0.06)	0.34	(0.05)	K <sub>2</sub> O	0.44 (0.07)	0.31	(0.10)
<b>Total.</b>	<b><u>97.97</u></b>	<b><u>98.02</u></b>		<b>Total.</b>	<b><u>97.99</u></b>	<b><u>98.00</u></b>	
Fe/ (Fe+Mg)	0.613	0.568		Fe/ (Fe+Mg)	0.644	0.569	
% from AAS MgO	0%	100%		% from AAS MgO	66%	44%	

Oxide wt.%. <b>Oxide wt.%. TJ-7D (SD) (a)</b>	<b>TJ-7D (SD) (b)</b>	Oxide wt.%. <b>Oxide wt.%. TJ-7E (SD) (a)</b>	<b>TJ-7E (SD) (b)</b>		
SiO <sub>2</sub>	42.80 (0.67)	50.70 (1.16)	SiO <sub>2</sub>	42.09 (0.40)	51.87 (0.48)
TiO <sub>2</sub>	0.45 (0.07)	0.20 (0.07)	TiO <sub>2</sub>	0.46 (0.06)	0.16 (0.04)
Al <sub>2</sub> O <sub>3</sub>	12.57 (0.84)	4.97 (0.97)	Al <sub>2</sub> O <sub>3</sub>	13.56 (0.47)	3.34 (0.38)
Fe <sub>2</sub> O <sub>3</sub>	5.41	4.46	Fe <sub>2</sub> O <sub>3</sub>	4.83	4.08
FeO	15.97	13.76	FeO	15.78	13.33
MnO	0.38 (0.06)	0.40 (0.06)	MnO	0.37 (0.07)	0.36 (0.06)
MgO	7.12 (0.43)	11.27 (0.40)	MgO	7.23 (0.32)	12.75 (0.45)
CaO	11.30 (0.33)	11.41 (0.36)	CaO	11.38 (0.34)	11.42 (0.44)
Na <sub>2</sub> O	1.47 (0.17)	0.60 (0.09)	Na <sub>2</sub> O	1.72 (0.18)	0.48 (0.08)
K <sub>2</sub> O	0.51 (0.07)	0.19 (0.05)	K <sub>2</sub> O	0.56 (0.09)	0.16 (0.05)
<b>Total.</b>	<b><u>97.98</u></b>	<b><u>97.96</u></b>	<b>Total.</b>	<b><u>97.98</u></b>	<b><u>97.95</u></b>

Fe/ (Fe+Mg)	0.692	0.550	Fe/ (Fe+Mg)	0.687	0.511
% from AAS MgO	93%	7%	% from AAS MgO	63%	37%

Oxide wt.%. <b>Oxide wt.%. TJ-7F (SD) (a)</b>	<b>TJ-7F (SD) (b)</b>	Oxide wt.%. <b>Oxide wt.%. TJ-7G (SD) (a)</b>	<b>TJ-7G (SD) (b)</b>		
SiO <sub>2</sub>	42.33 (1.21)	47.61 (0.53)	SiO <sub>2</sub>	43.65 (0.53)	51.89 (1.04)
TiO <sub>2</sub>	0.38 (0.06)	0.13 (0.04)	TiO <sub>2</sub>	0.39 (0.08)	0.05 (0.03)
Al <sub>2</sub> O <sub>3</sub>	13.57 (1.09)	7.76 (0.37)	Al <sub>2</sub> O <sub>3</sub>	13.27 (0.49)	3.85 (0.68)
Fe <sub>2</sub> O <sub>3</sub>	4.25	3.98	Fe <sub>2</sub> O <sub>3</sub>	4.05	3.58
FeO	15.30	14.30	FeO	13.18	11.63
MnO	0.36 (0.06)	0.34 (0.06)	MnO	0.26 (0.04)	0.35 (0.05)
MgO	8.34 (0.58)	11.00 (0.48)	MgO	9.61 (0.40)	14.02 (1.01)
CaO	11.62 (0.36)	11.84 (0.41)	CaO	11.93 (0.37)	12.00 (0.46)
Na <sub>2</sub> O	1.39 (0.22)	0.70 (0.10)	Na <sub>2</sub> O	1.32 (0.10)	0.42 (0.12)
K <sub>2</sub> O	0.49 (0.08)	0.32 (0.06)	K <sub>2</sub> O	0.42 (0.07)	0.12 (0.04)
<b>Total.</b>	<b><u>98.03</u></b>	<b><u>97.98</u></b>	<b>Total.</b>	<b><u>98.08</u></b>	<b><u>97.91</u></b>

Fe/ (Fe+Mg)	0.647	0.565	Fe/ (Fe+Mg)	0.578	0.453
% from AAS MgO	10%	90%	% from AAS MgO	37%	63%

Oxide wt.%. TJ-7H (SD) (a)	TJ-7H (SD) (b)	Oxide wt.%. TJ-8 (SD) (a)	TJ-8 (SD) (b)
SiO <sub>2</sub> 43.60 (0.41)	51.06 (1.08)	SiO <sub>2</sub> 45.34 (0.69)	48.74 (0.87)
TiO <sub>2</sub> 0.41 (0.07)	0.12 (0.08)	TiO <sub>2</sub> 0.33 (0.10)	0.21 (0.09)
Al <sub>2</sub> O <sub>3</sub> 13.51 (0.54)	4.89 (1.58)	Al <sub>2</sub> O <sub>3</sub> 11.52 (0.28)	6.71 (0.65)
Fe <sub>2</sub> O <sub>3</sub> 3.62	3.34	Fe <sub>2</sub> O <sub>3</sub> 4.51	2.86
FeO 13.89	12.82	FeO 11.67	12.89
MnO 0.24 (0.04)	0.39 (0.08)	MnO 0.36 (0.06)	0.34 (0.05)
MgO 9.05 (0.64)	13.25 (0.72)	MgO 10.99 (0.59)	12.62 (0.45)
CaO 11.91 (0.34)	11.33 (0.57)	CaO 11.81 (0.72)	12.72 (0.32)
Na <sub>2</sub> O 1.36 (0.15)	0.55 (0.21)	Na <sub>2</sub> O 1.20 (0.37)	0.69 (0.12)
K <sub>2</sub> O 0.45 (0.07)	0.20 (0.07)	K <sub>2</sub> O 0.24 (0.06)	0.17 (0.04)
<b>Total. 98.04</b>	<b>97.95</b>	<b>Total. 97.97</b>	<b>97.95</b>

Fe/ (Fe+Mg)	0.605	0.492	Fe/ (Fe+Mg)	0.515	0.505
% from AAS MgO	76%	24%	% from AAS MgO	21%	79%

Oxide wt.%. TJ-19 (SD) (a)	TJ-19 (SD) (b)	Oxide wt.%. TJ-29 (SD) (a)	TJ-29 (SD) (b)
SiO <sub>2</sub> 45.45 (0.53)	49.78 (1.96)	SiO <sub>2</sub> 43.23 (0.79)	47.58 (0.75)
TiO <sub>2</sub> 0.35 (0.06)	0.23 (0.08)	TiO <sub>2</sub> 0.47 (0.12)	0.39 (0.07)
Al <sub>2</sub> O <sub>3</sub> 11.81 (1.00)	7.63 (2.08)	Al <sub>2</sub> O <sub>3</sub> 13.37 (1.07)	8.52 (1.12)
Fe <sub>2</sub> O <sub>3</sub> 3.95	3.56	Fe <sub>2</sub> O <sub>3</sub> 4.58	4.03
FeO 12.42	11.14	FeO 12.76	11.23
MnO 0.31 (0.05)	0.24 (0.05)	MnO 0.30 (0.05)	0.22 (0.06)
MgO 10.51 (0.47)	12.73 (1.22)	MgO 9.97 (0.67)	12.66 (0.74)
CaO 11.51 (0.48)	12.05 (0.35)	CaO 11.87 (0.29)	12.32 (0.35)
Na <sub>2</sub> O 1.26 (0.19)	0.43 (0.16)	Na <sub>2</sub> O 1.29 (0.15)	0.86 (0.16)
K <sub>2</sub> O 0.39 (0.06)	0.18 (0.06)	K <sub>2</sub> O 0.21 (0.06)	0.20 (0.06)
<b>Total. 97.96</b>	<b>97.97</b>	<b>Total. 98.05</b>	<b>98.01</b>

Fe/ (Fe+Mg)	0.54	0.46	Fe/ (Fe+Mg)	0.56	0.47
% from AAS MgO	100%	0%	% from AAS MgO	91%	9%

Oxide wt.%. (a)	(SD)	TJ-35 (b)	(SD)	Oxide wt.%. (a)	(SD)	TJ-36 (b)	(SD)
SiO <sub>2</sub>	44.11	(0.82)	53.19	(0.97)	SiO <sub>2</sub>	45.67	(0.93)
TiO <sub>2</sub>	0.40	(0.04)	0.15	(0.03)	TiO <sub>2</sub>	0.37	(0.06)
Al <sub>2</sub> O <sub>3</sub>	14.33	(1.15)	3.58	(0.62)	Al <sub>2</sub> O <sub>3</sub>	12.70	(0.83)
Fe <sub>2</sub> O <sub>3</sub>	3.08		2.52		Fe <sub>2</sub> O <sub>3</sub>	4.62	
FeO	10.58		8.63		FeO	8.60	
MnO	0.29	(0.04)	0.22	(0.05)	MnO	0.19	(0.05)
MgO	11.84	(0.58)	17.27	(0.56)	MgO	12.34	(0.44)
CaO	11.79	(0.31)	12.06	(0.32)	CaO	11.61	(0.29)
Na <sub>2</sub> O	1.24	(0.11)	0.33	(0.09)	Na <sub>2</sub> O	1.63	(0.18)
K <sub>2</sub> O	0.32	(0.07)	0.05	(0.02)	K <sub>2</sub> O	0.24	(0.04)
<b>Total.</b>	<b><u>97.98</u></b>		<b><u>98.00</u></b>		<b>Total.</b>	<b><u>97.97</u></b>	<b><u>97.99</u></b>

Fe/ (Fe+Mg)	0.472		0.333		Fe/ (Fe+Mg)	0.411		0.330
% from AAS MgO	100%		0%		% from AAS MgO	78%		22%

Oxide wt.%. (a)	(SD)	TJ-37 (b)	(SD)	Oxide wt.%. (a)	(SD)	TJ-38 (b)	(SD)
SiO <sub>2</sub>	45.95	(1.02)	51.10	(1.41)	SiO <sub>2</sub>	44.64	(1.98)
TiO <sub>2</sub>	0.50	(0.09)	0.15	(0.06)	TiO <sub>2</sub>	0.39	(0.08)
Al <sub>2</sub> O <sub>3</sub>	11.04	(0.91)	5.37	(0.81)	Al <sub>2</sub> O <sub>3</sub>	12.23	(1.76)
Fe <sub>2</sub> O <sub>3</sub>	2.56		3.18		Fe <sub>2</sub> O <sub>3</sub>	3.35	
FeO	13.85		11.96		FeO	13.61	
MnO	0.23	(0.05)	0.32	(0.06)	MnO	0.30	(0.05)
MgO	10.35	(0.73)	13.16	(0.91)	MgO	10.22	(1.19)
CaO	12.07	(0.43)	12.03	(0.50)	CaO	11.94	(0.31)
Na <sub>2</sub> O	1.08	(0.12)	0.54	(0.11)	Na <sub>2</sub> O	1.08	(0.21)
K <sub>2</sub> O	0.39	(0.07)	0.17	(0.05)	K <sub>2</sub> O	0.24	(0.07)
<b>Total.</b>	<b><u>98.02</u></b>		<b><u>97.98</u></b>		<b>Total.</b>	<b><u>98.00</u></b>	<b><u>98.01</u></b>

Fe/ (Fe+Mg)	0.572		0.476		Fe/ (Fe+Mg)	0.571		0.472
% from AAS MgO	100%		0%		% from AAS MgO	68%		32%

Oxide wt. %.	TJ-39 (SD) (a)	TJ-39 (SD) (b)	Oxide wt. %.	TJ-40 (SD) (a)	TJ-40 (SD) (b)
SiO <sub>2</sub>	42.85 (0.81)	52.57 (0.91)	SiO <sub>2</sub>	45.51 (0.78)	52.91 (2.01)
TiO <sub>2</sub>	0.43 (0.10)	0.08 (0.03)	TiO <sub>2</sub>	0.35 (0.06)	0.13 (0.07)
Al <sub>2</sub> O <sub>3</sub>	13.53 (0.83)	3.34 (0.54)	Al <sub>2</sub> O <sub>3</sub>	13.85 (1.09)	5.03 (1.84)
Fe <sub>2</sub> O <sub>3</sub>	5.45	4.03	Fe <sub>2</sub> O <sub>3</sub>	2.71	2.43
FeO	11.71	8.67	FeO	9.11	8.19
MnO	0.33 (0.08)	0.38 (0.08)	MnO	0.23 (0.04)	0.21 (0.05)
MgO	9.94 (0.58)	16.21 (0.49)	MgO	13.01 (0.86)	17.44 (0.89)
CaO	11.78 (0.34)	12.18 (0.32)	CaO	11.65 (0.33)	11.11 (0.35)
Na <sub>2</sub> O	1.52 (0.15)	0.38 (0.07)	Na <sub>2</sub> O	1.34 (0.16)	0.49 (0.16)
K <sub>2</sub> O	0.49 (0.08)	0.11 (0.03)	K <sub>2</sub> O	0.24 (0.07)	0.06 (0.03)
<b>Total.</b>	<b><u>98.03</u></b>	<b><u>97.95</u></b>	<b>Total.</b>	<b><u>98.00</u></b>	<b><u>98.00</u></b>
Fe/ (Fe+Mg)	0.541	0.348	Fe/ (Fe+Mg)	0.412	0.320
% from AAS MgO	100%	0%	% from AAS MgO	100%	0%

## APPENDIX 6.

### ELECTRON MICROPROBE MINERAL FORMULAE. (from bulk EMPA results).

The following mineral formulae for the hornblende samples were derived from the electron microprobe results in Appendix 5.

The cation molar contents were calculated on the basis of 23 oxygens per unit formula for hornblende (Deer et al., 1966). Number of cations for each site are given in brackets. For the general amphibole formula in Chapter 1 (page 17): T-site = Z-type cations; C-site = Y-type cations; B-site = X-type cations; A-site = W-type cations.

#### Hornblende Mineral Formulae:

	CATION.	TJ-1	TJ-7A	TJ-7B	TJ-7D	TJ-7E	TJ-7F	TJ-7G
<u>T-site (8)</u>	Si	6.68	6.72	6.73	6.53	6.81	6.96	7.03
	Al <sup>IV</sup>	1.32	1.28	1.27	1.47	1.19	1.04	0.97
<u>C-site (5)</u>	Al <sup>VI</sup>	0.39	0.80	0.75	0.66	0.53	0.42	0.28
	Ti	0.11	0.04	0.04	0.05	0.04	0.02	0.02
	Fe <sup>3+</sup>	0.58	0.42	0.41	0.59	0.50	0.44	0.14
	Mg	2.68	2.13	2.04	1.66	2.06	2.36	2.66
	Fe <sup>2+</sup>	1.21	1.57	1.76	1.99	1.85	1.76	1.86
	Mn	0.03	0.04	-	0.05	0.02	-	0.04
<u>B-site (2)</u>	Fe <sup>2+</sup>	-	-	0.02	-	-	-	-
	Mn	0.01	-	0.04	-	0.03	0.04	-
	Ca	1.88	1.83	1.80	1.82	1.82	1.87	1.84
	Na	0.11	0.17	0.14	0.18	0.15	0.09	0.16
<u>A-site(0-1)</u>	Na	0.20	0.13	0.16	0.23	0.21	0.12	0.05
	K	0.05	0.07	0.07	0.09	0.07	0.07	0.03

	CATION.	TJ-7H	TJ-8	TJ-9	TJ-11	TJ-13	TJ-17	TJ-19
<b><u>T-site (8)</u></b>	Si	6.69	7.03	6.56	6.57	6.93	6.53	6.66
	Al <sup>IV</sup>	1.31	0.97	1.44	1.43	1.07	1.47	1.34
<b><u>C-site (5)</u></b>	Al <sup>VI</sup>	0.67	0.36	0.91	0.97	0.40	0.70	0.70
	Ti	0.04	0.03	0.03	0.04	0.05	0.06	0.04
	Fe <sup>3+</sup>	0.39	0.37	0.26	0.28	0.71	0.34	0.44
	Mg	2.21	2.68	2.69	2.52	2.76	2.19	2.30
	Fe <sup>2+</sup>	1.68	1.52	1.11	1.19	1.04	1.71	1.52
	Mn	0.01	0.04	-	-	0.04	-	-
<b><u>B-site (2)</u></b>	Fe <sup>2+</sup>	-	-	0.05	0.01	-	0.08	-
	Mn	0.03	-	0.03	0.03	-	0.04	0.04
	Ca	1.86	1.97	1.87	1.83	1.82	1.74	1.81
	Na	0.11	0.03	0.05	0.13	0.18	0.14	0.15
<b><u>A-site(0-1)</u></b>	Na	0.23	0.20	0.23	0.20	-	0.39	0.20
	K	0.07	0.04	0.03	0.03	0.03	0.05	0.07

	CATION.	TJ-29	TJ-31	TJ-35	TJ-36	TJ-37	TJ-38	TJ-39
<b><u>T-site (8)</u></b>	Si	6.43	6.80	6.40	6.77	6.75	6.82	6.33
	Al <sup>IV</sup>	1.57	1.20	1.60	1.23	1.25	1.18	1.67
<b><u>C-site (5)</u></b>	Al <sup>VI</sup>	0.68	0.66	0.86	0.62	0.66	0.55	0.69
	Ti	0.05	0.03	0.04	0.03	0.05	0.04	0.04
	Fe <sup>3+</sup>	0.50	0.31	0.33	0.53	0.29	0.35	0.60
	Mg	2.24	2.76	2.57	2.82	2.27	2.49	2.19
	Fe <sup>2+</sup>	1.53	1.23	1.20	0.98	1.70	1.57	1.45
	Mn	-	0.01	-	0.02	0.03	-	0.03
<b><u>B-site (2)</u></b>	Fe <sup>2+</sup>	0.03	-	0.08	-	-	0.05	-
	Mn	0.04	0.02	0.04	-	-	0.04	0.01
	Ca	1.88	1.90	1.83	1.77	1.91	1.87	1.86
	Na	0.05	0.08	0.05	0.23	0.09	0.04	0.13
<b><u>A-site(0-1)</u></b>	Na	0.30	0.22	0.30	0.17	0.21	0.21	0.31
	K	0.04	0.03	0.05	0.03	0.07	0.04	0.09

	CATION.	TJ-40	TJ-41	TJ-43	TJ-44	TJ-45	TJ-46	TJ-47
<b><u>T-site (8)</u></b>	Si	6.53	6.52	6.98	6.54	6.48	6.56	6.30
	Al <sup>IV</sup>	1.47	1.48	1.02	1.46	1.52	1.44	1.70
<b><u>C-site (5)</u></b>	Al <sup>VI</sup>	0.88	0.72	0.32	0.50	0.50	0.23	0.67
	Ti	0.03	0.04	0.11	0.09	0.07	0.14	0.05
	Fe <sup>3+</sup>	0.29	0.37	0.37	0.32	0.41	0.66	0.37
	Mg	2.79	2.66	2.99	2.45	2.38	2.50	2.40
	Fe <sup>2+</sup>	1.01	1.21	1.21	1.64	1.64	1.47	1.47
	Mn	-	-	-	-	-	-	0.04
<b><u>B-site (2)</u></b>	Fe <sup>2+</sup>	0.09	0.11	0.12	0.07	0.08	0.01	-
	Mn	0.03	0.05	0.03	0.04	0.05	0.05	-
	Ca	1.79	1.83	1.71	1.83	1.77	1.83	1.95
	Na	0.09	0.01	0.14	0.06	0.10	0.11	0.05
<b><u>A-site(0-1)</u></b>	Na	0.29	0.32	0.24	0.40	0.45	0.30	0.53
	K	0.05	0.03	0.03	0.12	0.11	0.09	0.05

	CATION.	TJ-48	TJ-54	TJ-59
<b><u>T-site (8)</u></b>	Si	6.32	6.29	6.73
	Al <sup>IV</sup>	1.68	1.71	1.27
<b><u>C-site (5)</u></b>	Al <sup>VI</sup>	0.78	0.22	0.33
	Ti	0.04	0.06	0.07
	Fe <sup>3+</sup>	0.32	0.98	0.65
	Mg	2.59	1.53	2.58
	Fe <sup>2+</sup>	1.27	2.14	1.33
	Mn	-	0.07	0.04
<b><u>B-site (2)</u></b>	Fe <sup>2+</sup>	0.14	-	-
	Mn	0.04	-	-
	Ca	1.64	1.86	1.90
	Na	0.18	0.14	0.10
<b><u>A-site(0-1)</u></b>	Na	0.68	0.43	0.20
	K	0.04	0.07	0.05

## APPENDIX 6A.

### ELECTRON MICROPROBE MINERAL FORMULAE. (from dual hornblende analyses).

The following mineral formulae for dual hornblende compositions were derived from the electron microprobe results in Appendix 5A.

The cation molar contents were calculated on the basis of 23 oxygens per unit formula for hornblende (Deer et al., 1966). Site allocation is discussed in the introduction to Appendix 6.

#### Hornblende Mineral Formulae:

	CATION.	TJ-7A (a)	TJ-7A (b)	TJ-7B (a)	TJ-7B (b)
<u>T-site (8)</u>	Si	6.40	6.72	6.36	7.19
	Al <sup>IV</sup>	1.60	1.28	1.64	0.81
<u>C-site (5)</u>	Al <sup>VI</sup>	1.00	0.80	0.98	0.44
	Ti	0.04	0.04	0.04	0.02
	Fe <sup>3+</sup>	0.42	0.42	0.41	0.41
	Mg	1.85	2.13	1.78	2.37
	Fe <sup>2+</sup>	1.65	1.57	1.79	1.76
	Mn	0.04	0.04	-	-
<u>B-site (2)</u>	Fe <sup>2+</sup>	-	-	0.02	-
	Mn	-	-	0.04	0.04
	Ca	1.80	1.83	1.79	1.81
	Na	0.20	0.17	0.15	0.15
<u>A-site(0-1)</u>	Na	0.19	0.13	0.24	0.04
	K	0.09	0.07	0.09	0.05
<u>% in Bulk.</u>		<u>0%</u>	<u>100%</u>	<u>44%</u>	<u>56%</u>

	CATION.	TJ-7D (a)	TJ-7D (b)	TJ-7E (a)	TJ-7E (b)
<b><u>T-site (8)</u></b>	Si	6.44	7.38	6.36	7.55
	Al <sup>IV</sup>	1.56	0.62	1.64	0.45
<b><u>C-site (5)</u></b>	Al <sup>VI</sup>	0.68	0.25	0.78	0.13
	Ti	0.05	0.03	0.05	0.02
	Fe <sup>3+</sup>	0.61	0.49	0.49	0.46
	Mg	1.60	2.48	1.79	2.78
	Fe <sup>2+</sup>	2.01	1.70	1.89	1.61
	Mn	0.05	0.05	-	-
<b><u>B-site (2)</u></b>	Fe <sup>2+</sup>	-	-	0.11	0.02
	Mn	-	-	0.05	0.04
	Ca	1.82	1.81	1.84	1.79
	Na	0.18	0.19	-	0.14
<b><u>A-site(0-1)</u></b>	Na	0.25	-	0.51	-
	K	0.11	0.04	0.11	0.04
<b><u>% in Bulk.</u></b>		<u>7%</u>	<u>93%</u>	<u>37%</u>	<u>63%</u>

	CATION.	TJ-7F (a)	TJ-7F (b)	TJ-7G (a)	TJ-7G (b)
<b><u>T-site (8)</u></b>	Si	6.33	7.03	6.45	7.51
	Al <sup>IV</sup>	1.67	0.97	1.55	0.49
<b><u>C-site (5)</u></b>	Al <sup>VI</sup>	0.72	0.38	0.76	0.17
	Ti	0.05	0.02	0.04	0.01
	Fe <sup>3+</sup>	0.49	0.44	0.44	0.38
	Mg	1.86	2.42	2.11	3.02
	Fe <sup>2+</sup>	1.88	1.74	1.63	1.41
	Mn	0.05	-	0.02	0.01
<b><u>B-site (2)</u></b>	Fe <sup>2+</sup>	0.04	0.03	-	-
	Mn	0.05	0.04	0.02	0.03
	Ca	1.86	1.87	1.89	1.86
	Na	0.05	0.06	0.09	0.11
<b><u>A-site(0-1)</u></b>	Na	0.35	0.14	0.28	0.01
	K	0.09	0.05	0.07	0.02
<b><u>% in Bulk.</u></b>		<u>90%</u>	<u>10%</u>	<u>63%</u>	<u>37%</u>

	CATION.	TJ-7H (a)	TJ-7H (b)	TJ-8 (a)	TJ-8 (b)
<u>T-site (8)</u>	Si	6.46	7.42	6.69	7.13
	Al <sup>IV</sup>	1.54	0.58	1.31	0.87
<u>C-site (5)</u>	Al <sup>VI</sup>	0.81	0.26	0.70	0.29
	Ti	0.04	0.02	0.04	0.03
	Fe <sup>3+</sup>	0.41	0.37	0.50	0.31
	Mg	2.00	2.87	2.41	2.75
	Fe <sup>2+</sup>	1.72	1.48	1.44	1.58
	Mn	0.02	-	-	0.04
<u>B-site (2)</u>	Fe <sup>2+</sup>	-	0.07	0.08	-
	Mn	0.01	0.04	0.05	-
	Ca	1.89	1.76	1.87	2.00
	Na	0.10	0.13	-	-
<u>A-site(0-1)</u>	Na	0.29	0.03	0.34	0.19
	K	0.09	0.03	0.05	0.03
<u>% in Bulk.</u>		<u>24%</u>	<u>76%</u>	<u>79%</u>	<u>21%</u>

	CATION.	TJ-19 (a)	TJ-19 (b)	TJ-29 (a)	TJ-29 (b)
<u>T-site (8)</u>	Si	6.66	7.18	6.38	6.94
	Al <sup>IV</sup>	1.34	0.82	1.62	1.06
<u>C-site (5)</u>	Al <sup>VI</sup>	0.70	0.48	0.70	0.41
	Ti	0.04	0.03	0.05	0.02
	Fe <sup>3+</sup>	0.44	0.38	0.52	0.44
	Mg	2.30	2.74	2.19	2.75
	Fe <sup>2+</sup>	1.52	1.35	1.54	1.37
	Mn	-	0.02	-	0.01
<u>B-site (2)</u>	Fe <sup>2+</sup>	-	-	0.02	-
	Mn	0.04	0.01	0.04	0.02
	Ca	1.81	1.87	1.88	1.93
	Na	0.15	0.12	0.06	0.05
<u>A-site(0-1)</u>	Na	0.20	-	0.31	0.20
	K	0.07	0.03	0.04	0.04
<u>% in Bulk.</u>		<u>100%</u>	<u>0%</u>		

	CATION.	TJ-35 (a)	TJ-35 (b)	TJ-36 (a)	TJ-36 (b)
<u>T-site (8)</u>	Si	6.40	7.54	6.59	7.38
	Al <sup>IV</sup>	1.60	0.46	1.41	0.62
<u>C-site (5)</u>	Al <sup>VI</sup>	0.86	0.14	0.75	0.22
	Ti	0.04	0.02	0.04	0.01
	Fe <sup>3+</sup>	0.33	0.27	0.49	0.55
	Mg	2.57	3.65	2.65	3.40
	Fe <sup>2+</sup>	1.20	0.92	1.04	0.82
	Mn	-	-	0.03	-
<u>B-site (2)</u>	Fe <sup>2+</sup>	0.08	0.10	-	0.12
	Mn	0.04	0.03	-	0.02
	Ca	1.83	1.83	1.79	1.68
	Na	0.05	0.04	0.21	0.18
<u>A-site(0-1)</u>	Na	0.30	0.05	0.24	0.01
	K	0.05	0.02	0.05	0.02
<u>% in Bulk.</u>		<u>100%</u>	<u>0%</u>	<u>22%</u>	<u>78%</u>

	CATION.	TJ-37 (a)	TJ-37 (b)	TJ-38 (a)	TJ-38 (b)
<u>T-site (8)</u>	Si	6.75	7.39	6.58	7.32
	Al <sup>IV</sup>	1.25	0.61	1.42	0.68
<u>C-site (5)</u>	Al <sup>VI</sup>	0.66	0.31	0.70	0.24
	Ti	0.05	0.02	0.04	0.02
	Fe <sup>3+</sup>	0.29	0.35	0.37	0.33
	Mg	2.27	2.84	2.25	2.98
	Fe <sup>2+</sup>	1.70	1.44	1.64	1.43
	Mn	0.03	0.04	-	-
<u>B-site (2)</u>	Fe <sup>2+</sup>	-	-	0.03	0.07
	Mn	-	-	0.04	0.04
	Ca	1.91	1.87	1.89	1.84
	Na	0.09	0.13	0.04	0.05
<u>A-site(0-1)</u>	Na	0.21	0.03	0.26	0.09
	K	0.07	0.03	0.05	0.03
<u>% in Bulk.</u>		<u>100%</u>	<u>0%</u>	<u>32%</u>	<u>68%</u>

	CATION.	TJ-39 (a)	TJ-39 (b)	TJ-40 (a)	TJ-40 (b)
<b><u>T-site (8)</u></b>	Si	6.33	7.51	6.53	7.46
	Al <sup>IV</sup>	1.67	0.49	1.47	0.54
<b><u>C-site (5)</u></b>	Al <sup>VI</sup>	0.69	0.08	0.88	0.29
	Ti	0.04	0.01	0.03	0.02
	Fe <sup>3+</sup>	0.60	0.43	0.29	0.25
	Mg	2.19	3.45	2.79	3.67
	Fe <sup>2+</sup>	1.45	1.03	1.01	0.77
	Mn	0.03	-	-	-
<b><u>B-site (2)</u></b>	Fe <sup>2+</sup>	-	0.01	0.09	0.20
	Mn	0.01	0.04	0.03	0.03
	Ca	1.86	1.86	1.79	1.68
	Na	0.13	0.09	0.09	0.09
<b><u>A-site(0-1)</u></b>	Na	0.31	0.01	0.29	0.05
	K	0.09	0.02	0.05	0.02
<b><u>% in Bulk.</u></b>		<b><u>100%</u></b>	<b><u>0%</u></b>	<b><u>100%</u></b>	<b><u>0%</u></b>

## APPENDIX 7.

### MINERAL NAMES. (from bulk mineral formulae).

The hornblendes were named according to the classification of Leake et al. (1997), (Figure 1.7), depending on A-site occupancy, Mg# ( $Mg/(Mg+Fe^{2+})$ ) and Si-contents from Appendix 6 (Figure 5.1K).

SAMPLE.	A-site occupancy.	Mg#.	Si-content.	Mineral name.
TJ-1	0.25	0.689	6.68	magnesiohornblende.
TJ-7A	0.20	0.576	6.72	magnesiohornblende.
TJ-7B	0.23	0.534	6.73	magnesiohornblende.
TJ-7D	0.32	0.455	6.53	ferrohornblende.
TJ-7E	0.26	0.527	6.81	magnesiohornblende.
TJ-7F	0.19	0.573	6.96	magnesiohornblende.
TJ-7G	0.08	0.588	7.03	magnesiohornblende.
TJ-7H	0.30	0.568	6.69	magnesiohornblende.
TJ-8	0.24	0.638	7.03	magnesiohornblende.
TJ-9	0.26	0.699	6.56	magnesiohornblende.
TJ-11	0.23	0.677	6.57	magnesiohornblende.
TJ-13	0.03	0.726	6.93	magnesiohornblende.
TJ-17	0.44	0.550	6.53	magnesiohornblende.
TJ-19	0.27	0.602	6.66	magnesiohornblende.
TJ-29	0.34	0.589	6.43	tschermakite.
TJ-31	0.25	0.692	6.80	magnesiohornblende.

<b>SAMPLE.</b>	<b>A-site occupancy.</b>	<b>Mg#.</b>	<b>Si- content.</b>	<b>Mineral name.</b>
TJ-35	0.35	0.668	6.40	tschermakite.
TJ-36	0.20	0.742	6.77	magnesiohornblende.
TJ-37	0.28	0.572	6.75	magnesiohornblende.
TJ-38	0.25	0.606	6.82	magnesiohornblende.
TJ-39	0.40	0.602	6.33	tschermakite.
TJ-40	0.34	0.717	6.53	magnesiohornblende.
TJ-41	0.35	0.668	6.52	magnesiohornblende.
TJ-43	0.27	0.692	6.98	magnesiohornblende.
TJ-44	0.52	0.589	6.54	edenite.
TJ-45	0.56	0.580	6.48	pargasite.
TJ-46	0.39	0.628	6.56	magnesiohornblende.
TJ-47	0.58	0.620	6.30	pargasite.
TJ-48	0.72	0.648	6.32	pargasite.
TJ-54	0.50	0.417	6.29	hastingsite.
TJ-59	0.25	0.660	6.73	magnesiohornblende.

## APPENDIX 7A.

### MINERAL NAMES. (from dual hornblende analyses).

Hornblendes named according to the classification of Leake et al. (1997), (Figure 1.7).

SAMPLE.	A-site occupancy.	Mg#.	Si- content.	Mineral name.
TJ-7A (a)	0.28	0.529	6.40	tschermakite.
TJ-7A (b)	0.20	0.576	6.72	magnesianhornblende.
TJ-7B (a)	0.33	0.496	6.36	ferrotschermakite.
TJ-7B (b)	0.09	0.574	7.19	magnesianhornblende.
TJ-7D (a)	0.36	0.443	6.44	ferrotschermakite.
TJ-7D (b)	0.04	0.593	7.38	magnesianhornblende.
TJ-7E (a)	0.62	0.472	6.36	ferropargasite.
TJ-7E (b)	0.04	0.630	7.55	actinolite.
TJ-7F (a)	0.44	0.492	6.33	ferrotschermakite.
TJ-7F (b)	0.19	0.578	7.03	magnesianhornblende.
TJ-7G (a)	0.35	0.564	6.45	tschermakite.
TJ-7G (b)	0.03	0.682	7.51	actinolite.
TJ-7H (a)	0.38	0.538	6.46	tschermakite.
TJ-7H (b)	0.06	0.649	7.42	magnesianhornblende.
TJ-8 (a)	0.39	0.613	6.69	magnesianhornblende.
TJ-8 (b)	0.22	0.635	7.13	magnesianhornblende.
TJ-19 (a)	0.27	0.602	6.66	magnesianhornblende.
TJ-19 (b)	0.03	0.670	7.18	magnesianhornblende.
TJ-29 (a)	0.35	0.584	6.38	tschermakite.
TJ-29 (b)	0.24	0.667	6.94	magnesianhornblende.

<b>SAMPLE.</b>	<b>A-site occupancy.</b>	<b>Mg#.</b>	<b>Si- content.</b>	<b>Mineral name.</b>
TJ-35 (a)	0.35	0.668	6.40	tschermakite.
TJ-35 (b)	0.07	0.782	7.54	actinolite.
TJ-36 (a)	0.29	0.718	6.59	magnesiohornblende.
TJ-36 (b)	0.03	0.783	7.38	magnesiohornblende.
TJ-37 (a)	0.28	0.572	6.75	magnesiohornblende.
TJ-37 (b)	0.06	0.664	7.39	magnesiohornblende.
TJ-38 (a)	0.31	0.574	6.58	magnesiohornblende.
TJ-38 (b)	0.12	0.665	7.32	magnesiohornblende.
TJ-39 (a)	0.40	0.602	6.33	tschermakite.
TJ-39 (b)	0.03	0.768	7.51	actinolite.
TJ-40 (a)	0.34	0.717	6.53	magnesiohornblende.
TJ-40 (b)	0.07	0.791	7.46	magnesiohornblende.

## APPENDIX 8.

### IONIC POROSITIES OF HORNBLENDES.

The ionic porosity, Z, for the bulk composition hornblende mineral separates were calculated using the A-site and Mg# (Appendix 6 and 7).

For example, TJ-7E: (from Appendix 7).

A-site component = 0.26;      Non-A-site component = 0.74;  
Mg# = 0.527  
Si-content = 6.81

Assuming A-site component has completely full A-sites.

26% x 0.527 = 0.137 due to Mg component.  
= 0.123 due to Fe component.

Assuming non-A-site component has completely empty A-sites.

74% x 0.527 = 0.390 due to Mg component.  
= 0.350 due to Fe component.

Total. = 1.000 (one formula unit).

Si-content pushes end-member formulae into edenite/ferro-edenite and magnesiohornblende/ferrohornblende fields on Figure 1.7 (Leake et al., 1997). The ionic porosity is then calculated by multiplying the above proportions of one formula unit with the relevant ionic porosity values for end members from Dahl (1996). All Z values are ionic porosity %.

<b>edenite.</b>	Na Ca <sub>2</sub> Mg <sub>5</sub> Si <sub>7</sub> Al O <sub>22</sub> (OH) <sub>2</sub>	<b>Z = 36.52%</b>
<b>ferro-edenite.</b>	Na Ca <sub>2</sub> Fe <sup>2+</sup> <sub>5</sub> Si <sub>7</sub> Al O <sub>22</sub> (OH) <sub>2</sub>	<b>Z = 38.31%</b>
<b>magnesiohornblende.</b>	Ca <sub>2</sub> (Mg <sub>4</sub> (Al,Fe <sup>3+</sup> )) Si <sub>7</sub> Al O <sub>22</sub> (OH) <sub>2</sub>	<b>Z = 37.50%</b>
<b>ferrohornblende.</b>	Ca <sub>2</sub> (Fe <sup>2+</sup> <sub>4</sub> (Al,Fe <sup>3+</sup> )) Si <sub>7</sub> Al O <sub>22</sub> (OH) <sub>2</sub>	<b>Z = 38.80%</b>
<b>pargasite.</b>	Na Ca <sub>2</sub> (Mg <sub>4</sub> Al) Si <sub>6</sub> Al <sub>2</sub> O <sub>22</sub> (OH) <sub>2</sub>	<b>Z = 36.85%</b>
<b>ferropargasite.</b>	Na Ca <sub>2</sub> (Fe <sup>2+</sup> <sub>4</sub> Al) Si <sub>6</sub> Al <sub>2</sub> O <sub>22</sub> (OH) <sub>2</sub>	<b>Z = 38.30%</b>
<b>tschermakite.</b>	□ Ca <sub>2</sub> (Mg <sub>3</sub> AlFe <sup>3+</sup> ) Si <sub>6</sub> Al <sub>2</sub> O <sub>22</sub> (OH) <sub>2</sub>	<b>Z = 36.90%</b>
<b>ferrotschermakite.</b>	□ Ca <sub>2</sub> (Fe <sup>2+</sup> <sub>3</sub> AlFe <sup>3+</sup> ) Si <sub>6</sub> Al <sub>2</sub> O <sub>22</sub> (OH) <sub>2</sub>	<b>Z = 38.20%</b>

TJ-1	A-site. = 0.25 Mg# = 0.689	edenite. ferro-edenite. magnesiohornblende. ferrohornblende.	0.172 0.078 0.517 0.233	<b>Z = 37.753%</b>
TJ-7A	A-site. = 0.20 Mg# = 0.576	edenite. ferro-edenite. magnesiohornblende. ferrohornblende.	0.115 0.085 0.461 0.339	<b>Z = 37.897%</b>
TJ-7B	A-site. = 0.23 Mg# = 0.534	edenite. ferro-edenite. magnesiohornblende. ferrohornblende.	0.123 0.107 0.411 0.359	<b>Z = 37.933%</b>
TJ-7D	A-site = 0.32 Mg# = 0.455	edenite. ferro-edenite. magnesiohornblende. ferrohornblende.	0.146 0.174 0.309 0.371	<b>Z = 37.981%</b>
TJ-7E	A-site. = 0.26 Mg# = 0.527	edenite. ferro-edenite. magnesiohornblende. ferrohornblende.	0.137 0.123 0.390 0.350	<b>Z = 37.920%</b>
TJ-7F	A-site. = 0.19 Mg# = 0.573	edenite. ferro-edenite. magnesiohornblende. ferrohornblende.	0.109 0.081 0.464 0.346	<b>Z = 37.909%</b>
TJ-7G	A-site. = 0.08 Mg# = 0.588	edenite. ferro-edenite. magnesiohornblende. ferrohornblende.	0.047 0.033 0.541 0.379	<b>Z = 37.973%</b>
TJ-7H	A-site. = 0.30 Mg# = 0.568	edenite. ferro-edenite. magnesiohornblende. ferrohornblende.	0.170 0.130 0.398 0.302	<b>Z = 37.831%</b>
TJ-8	A-site. = 0.24 Mg# = 0.638	edenite. ferro-edenite. magnesiohornblende. ferrohornblende.	0.153 0.087 0.485 0.275	<b>Z = 37.779%</b>
TJ-9	A-site. = 0.26 Mg# = 0.699	edenite. ferro-edenite. magnesiohornblende. ferrohornblende.	0.182 0.078 0.517 0.223	<b>Z = 37.675%</b>

TJ-11	A-site. = 0.23 Mg# = 0.677	edenite. ferro-edenite. magnesiohomblende. ferrohomblende.	0.156 0.074 0.521 0.249	Z = 37.731%
TJ-13	A-site. = 0.03 Mg# = 0.726	edenite. ferro-edenite. magnesiohomblende. ferrohomblende.	0.022 0.008 0.704 0.266	Z = 37.830%
TJ-17	A-site. = 0.44 Mg# = 0.550	edenite. ferro-edenite. magnesiohomblende. ferrohomblende.	0.242 0.198 0.308 0.252	Z = 37.751%
TJ-19	A-site. = 0.27 Mg# = 0.602	edenite. ferro-edenite. magnesiohomblende. ferrohomblende.	0.163 0.107 0.439 0.291	Z = 37.806%
TJ-29	A-site. = 0.34 Mg# = 0.589	pargasite. ferropargasite. magnesiohomblende. ferrohomblende.	0.200 0.140 0.389 0.271	Z = 37.835%
TJ-31	A-site. = 0.25 Mg# = 0.692	edenite. ferro-edenite. magnesiohomblende. ferrohomblende.	0.173 0.077 0.519 0.231	Z = 37.694%
TJ-35	A-site. = 0.35 Mg# = 0.668	pargasite. ferropargasite. magnesiohomblende. ferrohomblende.	0.234 0.116 0.434 0.216	Z = 37.722%
TJ-36	A-site. = 0.20 Mg# = 0.742	edenite. ferro-edenite. magnesiohomblende. ferrohomblende.	0.148 0.052 0.594 0.206	Z = 37.665%
TJ-37	A-site. = 0.28 Mg# = 0.572	edenite. ferro-edenite. magnesiohomblende. ferrohomblende.	0.160 0.120 0.412 0.308	Z = 37.840%
TJ-38	A-site. = 0.25 Mg# = 0.606	edenite. ferro-edenite. magnesiohomblende. ferrohomblende.	0.152 0.098 0.455 0.295	Z = 37.814%
TJ-39	A-site. = 0.40 Mg# = 0.602	pargasite. ferropargasite. magnesiohomblende. ferrohomblende.	0.241 0.159 0.361 0.239	Z = 37.782%

TJ-40	A-site. = 0.34 Mg# = 0.717	edenite. ferro-edenite. magnesiohornblende. ferrohornblende.	0.244 0.096 0.473 0.187	Z = 37.583%
TJ-41	A-site. = 0.35 Mg# = 0.668	edenite. ferro-edenite. magnesiohornblende. ferrohornblende.	0.234 0.116 0.434 0.216	Z = 37.646%
TJ-43	A-site. = 0.27 Mg# = 0.692	edenite. ferro-edenite. magnesiohornblende. ferrohornblende.	0.187 0.083 0.505 0.225	Z = 37.677%
TJ-44	A-site. = 0.52 Mg# = 0.589	edenite. ferro-edenite. magnesiohornblende. ferrohornblende.	0.306 0.214 0.283 0.197	Z = 37.630%
TJ-45	A-site. = 0.56 Mg# = 0.580	pargasite. ferropargasite. magnesiohornblende. ferrohornblende.	0.325 0.235 0.255 0.185	Z = 37.718%
TJ-46	A-site. = 0.39 Mg# = 0.628	edenite. ferro-edenite. magnesiohornblende. ferrohornblende.	0.245 0.145 0.383 0.227	Z = 37.673%
TJ-47	A-site. = 0.58 Mg# = 0.620	pargasite. ferropargasite. magnesiohornblende. ferrohornblende.	0.360 0.220 0.260 0.160	Z = 37.650%
TJ-48	A-site. = 0.72 Mg# = 0.648	pargasite. ferropargasite. magnesiohornblende. ferrohornblende.	0.467 0.253 0.181 0.099	Z = 37.528%
TJ-54	A-site. = 0.50 Mg# = 0.417	pargasite. ferropargasite. magnesiohornblende. ferrohornblende.	0.209 0.291 0.209 0.291	Z = 37.976%
TJ-59	A-site. = 0.25 Mg# = 0.660	edenite. ferroedenite. magnesiohornblende. ferrohornblende.	0.165 0.085 0.495 0.255	Z = 37.739%

## APPENDIX 9.

### K-Ar AGE ISOTOPE DATA.

#### Hornblende Mineral Separates:

Sample.	Weight (mg).	Potassium (wt.%).	$^{40}\text{Ar}/^{36}\text{Ar} / \text{K}/^{36}\text{Ar}$ .	Radiogenic $^{40}\text{Ar}$ (%).	K-Ar Age (Ma).
TJ-1	116.57	0.27	1606 / 40117	73.7	<u>448+/-10Ma</u>
TJ-7A	118.96	0.24	902 / 19966	61.9	<u>427+/-11Ma</u>
TJ-7B	94.55	0.42	645 / 12947	53.9	<u>412+/-11Ma</u>
TJ-7D	149.55	0.33	963 / 21501	68.1	<u>461+/-11Ma</u>
TJ-7E	130.21	0.31	1038 / 25123	67.5	<u>426+/-10Ma</u>
TJ-7F	118.67	0.33	952 / 29197	65.4	<u>465+/-11Ma</u>
TJ-7G	125.48	0.25	787 / 16194	59.0	<u>436+/-11Ma</u>
TJ-7H	122.00	0.28	587 / 10018	50.0	<u>444+/-13Ma</u>
TJ-8	117.71	0.18	493 / 6271	40.9	<u>483+/-16Ma</u>
TJ-9	148.35	0.18	501 / 6381	43.5	<u>510+/-16Ma</u>
TJ-11	144.68	0.19	508 / 7570	42.7	<u>436+/-14Ma</u>
TJ-13	106.73	0.20	477 / 5713	39.2	<u>490+/-16Ma</u>
TJ-17	100.68	0.24	451 / 5448	36.9	<u>462+/-16Ma</u>
TJ-19	152.08	0.26	560 / 8421	49.9	<u>496+/-14Ma</u>
TJ-29	141.66	0.64	737 / 16215	62.6	<u>433+/-11Ma</u>
TJ-31	150.88	0.17	762 / 13965	57.2	<u>470+/-12Ma</u>

Sample.	Weight (mg).	Potassium (wt.%).	$^{40}\text{Ar}/^{36}\text{Ar} / \text{K}/^{36}\text{Ar}$ .	Radiogenic $^{40}\text{Ar}$ (%).	K-Ar Age (Ma).
TJ-35	148.65	0.26	537 / 8230	47.8	470+/-14Ma
	149.74	0.26	836 / 17127	63.3	466+/-11Ma <u>468+/-2Ma</u>
TJ-36	148.98	0.22	497 / 6912	43.7	474+/-15Ma
	149.86	0.22	653 / 11166	54.2	481+/-13Ma <u>478+/-4Ma</u>
TJ-37	158.45	0.27	667 / 11549	56.5	<u>489+/-13Ma</u>
TJ-38	144.53	0.15	492 / 5466	41.5	550+/-18Ma
	150.94	0.15	747 / 11308	58.0	562+/-14Ma <u>556+/-6Ma</u>
TJ-39	114.95	0.48	1599 / 46131	77.2	<u>410+/-9Ma</u>
TJ-40	151.58	0.18	444 / 4779	37.9	<u>522+/-18Ma</u>
TJ-41	149.46	0.28	567 / 8728	50.7	493+/-14Ma
	150.27	0.28	712 / 12621	59.3	500+/-13Ma <u>497+/-3.5Ma</u>
TJ-43	123.20	0.13	627 / 8128	48.8	<u>554+/-16Ma</u>
TJ-44	110.87	0.43	612 / 10247	53.8	<u>483+/-13Ma</u>
TJ-45	139.41	0.49	706 / 14192	60.1	<u>452+/-11Ma</u>
TJ-46	107.18	0.40	819 / 16583	62.7	<u>467+/-11Ma</u>
TJ-47	125.92	0.21	682 / 11645	54.2	<u>478+/-13Ma</u>
TJ-48	137.26	0.15	531 / 7047	43.6	<u>492+/-15Ma</u>
TJ-54	116.26	0.28	511 / 7639	44.2	<u>448+/-14Ma</u>
TJ-59	147.28	0.40	565 / 11759	50.4	<u>375+/-11Ma</u>

Errors of each sample based on single analysis, except **TJ-35**, **TJ-36**, **TJ-38** and **TJ-41**, which are based on two analyses (SD given). Average hornblende K-Ar age = 470Ma. Average of hornblende K-Ar age errors = +/-13Ma.

**Muscovite Mineral Separates:**

<b>Sample.</b>	<b>Weight (mg).</b>	<b>Potassium (wt.%).</b>	<b><math>^{40}\text{Ar}/^{36}\text{Ar} / \text{K}/^{36}\text{Ar}</math>.</b>	<b>Radiogenic <math>^{40}\text{Ar}</math> (%).</b>	<b>K-Ar Age (Ma).</b>
<b>TJ-10</b>	16.15	6.36	2283 / 66776	85.2	<b><u>442+/-9Ma</u></b>
<b>TJ-16</b>	18.39	8.36	2979 / 87118	88.8	<b><u>460+/-10Ma</u></b>
<b>TJ-18</b>	17.25	8.55	2439 / 72872	86.9	<b><u>442+/-9Ma</u></b>
<b>TJ-22</b>	13.28	7.83	1688 / 51269	81.1	<b><u>410+/-9Ma</u></b>
<b>TJ-50</b>	19.30	7.94	1454 / 42264	80.0	<b><u>421+/-9Ma</u></b>
<b>TJ-53</b>	17.69	4.72	919 / 21961	68.6	<b><u>437+/-10Ma</u></b>

Errors of each sample based on single analysis. Average muscovite K-Ar age = 435Ma. Average of muscovite K-Ar age errors = +/-9Ma.

APPENDIX 10.

HYDROGEN ISOTOPE DATA.

Hornblende Mineral Separates:

Sample.	Weight (mg).	Manometer (cm of Hg).	Yield ( $\mu\text{M}/\text{mg}$ ).	$\text{H}_2\text{O}^+$ (wt.%).	$\delta\text{D}_{\text{HORNBLLENDE}}$ ( $\pm 1.5\text{‰}$ ).	$\delta\text{D}_{\text{FLUID}}$ ( $\pm 1.5\text{‰}$ ).
TJ-1	57.8	19.0	1.054	1.90	<u>-90‰</u>	-67‰
TJ-7A	50.8	16.0	0.971	1.75	<u>-49‰</u>	-26‰
TJ-7B	55.8	16.1	0.891	1.61	<u>-45‰</u>	-22‰
TJ-7D	40.1	12.9	0.945	1.70	<u>-54‰</u>	-31‰
TJ-7E	59.5	18.1	0.965	1.74	<u>-40‰</u>	-17‰
TJ-7F	62.3	21.5	1.139	2.05	<u>-57‰</u>	-34‰
TJ-7G	68.5	22.8	1.139	2.05	<u>-49‰</u>	-26‰
TJ-7H	63.0	21.9	1.152	2.08	<u>-52‰</u>	-29‰
TJ-8	55.4	19.4	1.129	2.03	<u>-52‰</u>	-29‰
TJ-9	52.3	18.5	1.128	2.03	<u>-53‰</u>	-30‰
TJ-11	57.7	18.2	1.002	1.81	<u>-39‰</u>	-16‰
TJ-13	53.3	20.7	1.270	2.29	<u>-56‰</u>	-33‰
TJ-17	28.8	8.8	0.822	1.48	<u>-44‰</u>	-21‰
TJ-19	53.5	18.6	1.110	2.00	<u>-62‰</u>	-39‰
TJ-29	58.8	21.6	1.213	2.19	<u>-50‰</u>	-27‰
TJ-31	57.5	19.4	1.087	1.96	<u>-47‰</u>	-24‰

Sample.	Weight (mg).	Manometer (cm of Hg).	Yield ( $\mu\text{M}/\text{mg}$ ).	$\text{H}_2\text{O}^+$ (wt.%).	$\delta\text{D}_{\text{HORNBLENDE}}$ (+/-1.5‰).	$\delta\text{D}_{\text{FLUID}}$ (+/-1.5‰).
TJ-35	59.1	18.5	0.998	1.80	<u>-60‰</u>	-37‰
TJ-36	58.4	22.6	1.292	2.33	<u>-61‰</u>	-38‰
TJ-37	53.7	17.4	1.019	1.84	<u>-63‰</u>	-40‰
TJ-38	59.8	20.5	1.119	2.02	<u>-63‰</u>	-40‰
TJ-39	54.2	18.8	1.110	2.00	<u>-51‰</u>	-28‰
TJ-40	54.4	20.9	1.259	2.27	<u>-58‰</u>	-35‰
TJ-41	54.5	21.0	1.265	2.28	<u>-62‰</u>	-39‰
TJ-43	53.9	18.4	1.087	1.96	<u>-52‰</u>	-29‰
TJ-44	58.5	26.6	1.575	2.84	<u>-52‰</u>	-29‰
TJ-45	62.9	21.9	1.154	2.08	<u>-52‰</u>	-29‰
TJ-46	58.1	17.6	0.955	1.72	<u>-59‰</u>	-36‰
TJ-47	60.9	21.3	1.152	2.08	<u>-52‰</u>	-29‰
TJ-48	63.4	20.3	1.043	1.88	<u>-52‰</u>	-29‰
TJ-54	66.1	20.5	1.012	1.82	<u>-39‰</u>	-16‰
TJ-59	66.4	22.0	1.099	1.98	<u>-46‰</u>	-23‰

Single analysis only for each sample, except TJ-1, TJ-7F, TJ-35, TJ-43 and TJ-44 which are based on two analyses (within errors, averages shown). Average hornblende  $\delta\text{D} = -52‰$ . Average error for hornblende  $\delta\text{D} = \pm 1.5‰$  (estimated due to method and equipment).

The water content (wt.%) of each sample was derived by multiplying the yield ( $\mu\text{M}/\text{mg}$ ) by a factor of 1.8015. Average hornblende water content = 1.96wt.%. Average error for hornblende water content = 0.06wt.% (based on 3% estimated error).

Fluid  $\delta\text{D}$  values are derived from the hornblende  $\delta\text{D}$  values by the temperature independent fractionation factor of Graham et al. (1984):

$$1000\ln\alpha_{\text{HORNBLENDE-WATER}} = -23.1 \pm 2.5‰$$

### Muscovite Mineral Separates:

Sample.	Weight (mg).	Manometer (cm of Hg).	Yield ( $\mu\text{M}/\text{mg}$ ).	$\text{H}_2\text{O}^+$ (wt.%).	$\delta\text{D}_{\text{MUSCOVITE}}$ (+/-1.5‰).
TJ-10	51.8	28.3	1.919	3.46	<u>-40‰</u>
TJ-16	53.9	35.4	2.428	4.37	<u>-23‰</u>
TJ-18	61.1	38.2	2.352	4.24	<u>-36‰</u>
TJ-22	51.6	32.8	2.310	4.16	<u>-45‰</u>
TJ-50	56.3	32.2	2.069	3.73	<u>-49‰</u>
TJ-53	50.6	24.0	1.605	2.89	<u>-40‰</u>

The water content (wt.%) of each sample was derived by multiplying the yield ( $\mu\text{M}/\text{mg}$ ) by a factor of 1.8015.

Single analysis only for each sample. Average muscovite  $\delta\text{D} = -39‰$ . Average error for muscovite  $\delta\text{D} = +/-1.5‰$  (estimated due to method and equipment).

The  $\text{H}_2\text{O}^+$  (wt.%) content of each sample was derived by multiplying the yield ( $\mu\text{M}/\text{mg}$ ) by a factor of 1.8015. Average muscovite water content = 3.81wt.%. Average error for muscovite water content = +/-0.11wt.% (based on 3% estimated error).

Fluid  $\delta\text{D}$  values were derived from the muscovite  $\delta\text{D}$  values by the method outlined by Suzuoki and Epstein (1976), from Rollinson (1993), where  $T$  is the absolute temperature ( $^{\circ}\text{K}$ ).

$$1000\ln\alpha_{\text{MUSCOVITE-WATER}} = 19.1 - 22.1(10^6/T^2)$$

At 600°C:  $\delta\text{D } 1000\ln\alpha_{\text{MUSCOVITE-WATER}} = -10‰$ . Giving a range of fluid  $\delta\text{D}$  values of -39‰ to -13‰ (average = -29‰) at 600°C.

At 300°C:  $\delta\text{D } 1000\ln\alpha_{\text{MUSCOVITE-WATER}} = -48‰$ . Giving a range of fluid  $\delta\text{D}$  values of -1‰ to +25‰ (average = +9‰) at 300°C.

Average muscovite  $\delta\text{D} = -39‰$ . A fluid temperature of 470°C would be required to give a fractionation factor of -21‰ (based on the above equation) for an average fluid  $\delta\text{D} = -18‰$  (Chapter 6).

**Calculated Water Contents of Amphibole End-Members:**

magnesiohornblende	$\square \text{Ca}_2 (\text{Mg}_4(\text{Al}, \text{Fe}^{3+})) \text{Si}_7\text{AlO}_{22} (\text{OH})_2$	$\text{H}_2\text{O} = 2.21\%$
ferrohornblende	$\square \text{Ca}_2 (\text{Fe}^{2+}_4 (\text{Al}, \text{Fe}^{3+})) \text{Si}_7\text{AlO}_{22} (\text{OH})_2$	$\text{H}_2\text{O} = 1.92\%$
edenite	$\text{Na Ca}_2 \text{Mg}_5 \text{Si}_7\text{AlO}_{22} (\text{OH})_2$	$\text{H}_2\text{O} = 2.16\%$
ferro-edenite	$\text{Na Ca}_2 \text{Fe}^{2+}_5 \text{Si}_7\text{AlO}_{22} (\text{OH})_2$	$\text{H}_2\text{O} = 1.82\%$
pargasite	$\text{Na Ca}_2 (\text{Mg}_4\text{Al}) \text{Si}_6\text{Al}_2\text{O}_{22} (\text{OH})_2$	$\text{H}_2\text{O} = 2.15\%$
ferropargasite	$\text{Na Ca}_2 (\text{Fe}^{2+}_4\text{Al}) \text{Si}_6\text{Al}_2\text{O}_{22} (\text{OH})_2$	$\text{H}_2\text{O} = 1.87\%$
tschermakite	$\square \text{Ca}_2 (\text{Mg}_3(\text{Al}, \text{Fe}^{3+})) \text{Si}_6\text{Al}_2\text{O}_{22} (\text{OH})_2$	$\text{H}_2\text{O} = 2.21\%$
ferrotschermakite	$\square \text{Ca}_2 (\text{Fe}^{2+}_3 (\text{Al}, \text{Fe}^{3+})) \text{Si}_6\text{Al}_2\text{O}_{22} (\text{OH})_2$	$\text{H}_2\text{O} = 1.98\%$
magnesiohastingsite	$\text{Na Ca}_2 (\text{Mg}_4 \text{Fe}^{3+}) \text{Si}_6\text{Al}_2\text{O}_{22} (\text{OH})_2$	$\text{H}_2\text{O} = 2.29\%$
hastingsite	$\text{Na Ca}_2 (\text{Fe}^{2+}_4 \text{Fe}^{3+}) \text{Si}_6\text{Al}_2\text{O}_{22} (\text{OH})_2$	$\text{H}_2\text{O} = 1.98\%$
tremolite	$\square \text{Ca}_2 \text{Mg}_5 \text{Si}_6\text{O}_{22} (\text{OH})_2$	$\text{H}_2\text{O} = 2.21\%$
ferro-actinolite	$\square \text{Ca}_2 \text{Fe}^{2+}_5 \text{Si}_6\text{O}_{22} (\text{OH})_2$	$\text{H}_2\text{O} = 1.92\%$
Fe-chlorite - Mg-chlorite	Range of $\text{H}_2\text{O} = 10.54\text{-}12.93\%$	
Fe-biotite - Mg-biotite	Range of $\text{H}_2\text{O} = 3.52\text{-}4.31\%$	
muscovite - paragonite	Range of $\text{H}_2\text{O} = 4.52\text{-}4.71\%$	

The above values show the relatively higher water contents in Fe-rich compared to Mg-rich varieties of hornblende. The  $\square$  symbol represents empty A-sites. Hornblende water contents calculated from Leake et al. (1997). Chlorite, biotite and muscovite water contents from Klein and Hurlbut (1985).

## APPENDIX 11.

### OXYGEN ISOTOPE DATA.

#### Hornblende mineral Separates:

Sample.	Weight (mg).	$\delta^{18}\text{O}_{\text{HORNBLLENDE}}$ ( $\pm 0.15\text{‰}$ ).	Average $\delta^{18}\text{O}$ (‰).
TJ-1	1.9	+7.712‰	<u>+7.9‰</u>
	1.6	+8.096‰	
TJ-7A	2.3	+8.025‰	<u>+8.0‰</u>
TJ-7B	1.9	+7.188‰	<u>+7.1‰</u>
	2.4	+7.088‰	
TJ-7D	2.1	+4.784‰	<u>+5.0‰</u>
	1.6	+5.283‰	
TJ-7E	2.2	+6.179‰	<u>+6.1‰</u>
	2.3	+5.922‰	
TJ-7F	2.0	+6.672‰	<u>+6.5‰</u>
	2.0	+6.361‰	
TJ-7G	2.5	+5.684‰	<u>+5.7‰</u>
	2.7	+5.639‰	
TJ-7H	1.7	+8.371‰	<u>+8.6‰</u>
	1.6	+8.395‰	
TJ-8	2.8	+6.043‰	<u>+6.1‰</u>
	1.8	+6.226‰	
TJ-9	1.9	+5.068‰	<u>+4.9‰</u>
	1.5	+4.821‰	
TJ-11	2.2	+5.333‰	<u>+5.3‰</u>
TJ-13	2.2	+7.095‰	<u>+7.1‰</u>
TJ-17	3.0	+6.833‰	<u>+6.7‰</u>
	1.7	+6.615‰	

Sample.	Weight (mg).	$\delta^{18}\text{O}_{\text{HORNBLENDE}}$ (+/-0.15‰).	Average $\delta^{18}\text{O}$ (‰).
TJ-19	1.8	+6.081‰	<u>+6.0‰</u>
TJ-29	1.3 1.5	+6.201‰ +6.178‰	<u>+6.2‰</u>
TJ-31	1.9	+7.539‰	<u>+7.5‰</u>
TJ-35	1.7 1.7	+7.423‰ +7.409‰	<u>+7.4‰</u>
TJ-36	2.0 2.1	+7.061‰ +6.940‰	<u>+7.0‰</u>
TJ-37	2.3	+7.307‰	<u>+7.3‰</u>
TJ-38	1.7	+8.839‰	<u>+8.8‰</u>
TJ-39	2.0	+7.808‰	<u>+7.8‰</u>
TJ-40	2.0	+7.461‰	<u>+7.5‰</u>
TJ-41	1.5 2.4	+9.518‰ +9.008‰	<u>+9.3‰</u>
TJ-43	2.1 1.9	+7.242‰ +7.375‰	<u>+7.3‰</u>
TJ-44	2.9	+7.737‰	<u>+7.7‰</u>
TJ-45	1.9	+7.646‰	<u>+7.7‰</u>
TJ-46	2.6	+6.852‰	<u>+6.9‰</u>
TJ-47	1.9	+9.278‰	<u>+9.3‰</u>
TJ-48	2.1	+8.830‰	<u>+8.8‰</u>
TJ-54	2.3	+6.394‰	<u>+6.4‰</u>
TJ-59	1.7	+6.351‰	<u>+6.4‰</u>

Most samples analysed in duplicate, some only single as indicated. Average hornblende  $\delta^{18}\text{O} = +7.1‰$ . Average error of hornblende  $\delta^{18}\text{O} = +/-0.15‰$  (estimated due to method and equipment). Fluid  $\delta^{18}\text{O}$  not evaluated due to lack of information in the literature.

### Muscovite Mineral Separates:

Sample.	Weight (mg).	$\delta^{18}\text{O}_{\text{MUSCOVITE}}$ (+/-0.15‰).	Average $\delta^{18}\text{O}$ (‰).
TJ-10	1.6	+11.278‰	<u>+11.3‰</u>
TJ-16	1.6	+11.982‰	<u>+12.0‰</u>
TJ-18	1.6	+8.925‰	<u>+8.9‰</u>
TJ-22	1.8	+9.973‰	<u>+10.0‰</u>
TJ-50	1.9	+8.616‰	<u>+8.6‰</u>
TJ-53	2.1	+11.282‰	<u>+11.3‰</u>

Single analysis only for each sample. Average muscovite  $\delta^{18}\text{O} = +10.4\text{‰}$ . Average error for muscovite  $\delta^{18}\text{O} = \pm 0.15\text{‰}$  (estimated due to method and equipment).

Fluid  $\delta^{18}\text{O}$  values are derived from the muscovite  $\delta^{18}\text{O}$  values by the method outlined by O'Neil and Taylor (1967) from Rollinson (1993). Where  $T$  is the absolute temperature ( $^{\circ}\text{K}$ ):

$$1000\ln\alpha_{\text{MUSCOVITE-WATER}} = -3.89 + 2.38(10^6/T^2)$$

At  $600^{\circ}\text{C}$   $1000\ln\alpha_{\text{MUSCOVITE-WATER}} = -0.768\text{‰}$ . Giving a range of fluid  $\delta^{18}\text{O}$  values of  $+9.4\text{‰}$  to  $+12.8\text{‰}$  (average =  $+11.2\text{‰}$ ) at  $600^{\circ}\text{C}$ .

At  $470^{\circ}\text{C}$   $1000\ln\alpha_{\text{MUSCOVITE-WATER}} = +0.419\text{‰}$ . Giving a range of fluid  $\delta^{18}\text{O}$  values of  $+8.2\text{‰}$  to  $+11.6\text{‰}$  (average =  $+10.0\text{‰}$ ) at  $470^{\circ}\text{C}$ . See Chapter 6 and Appendix 10.

At  $300^{\circ}\text{C}$   $1000\ln\alpha_{\text{MUSCOVITE-WATER}} = +3.355\text{‰}$ . Giving a range of fluid  $\delta^{18}\text{O}$  values of  $+5.2\text{‰}$  to  $+8.6\text{‰}$  (average =  $+7.0\text{‰}$ ) at  $300^{\circ}\text{C}$ .

Due to the limited availability of experimental data of  $\delta^{18}\text{O}$  thermodynamics below  $400^{\circ}\text{C}$  (O'Neil and Taylor, 1967; Bottinga and Javoy, 1973; Rollinson, 1993) the above estimations are only theoretical estimates.

## APPENDIX 12.

### K-Ar AGES AND $\delta D$ VALUES FROM PREVIOUS STUDIES.

Elias et al. (1988): K-Ar Age Results.

Sample.	K (wt.%).	Age (Ma).	Sample.	K (wt.%).	Age (Ma).
EL-8	0.16	477+/-10Ma	EL-60	0.53	440+/-8Ma
EL-30	0.33	453+/-9Ma	EL-66	0.32	450+/-9Ma
EL-31	0.60	440+/-8Ma	EL-75	0.16	459+/-9Ma
EL-32	0.47	467+/-9Ma	EL-76	0.44	397+/-8Ma
EL-33	0.48	462+/-9Ma	EL-82	0.36	439+/-8Ma
EL-34	0.40	459+/-9Ma	EL-85	0.23	438+/-9Ma
EL-35	0.26	480+/-10Ma	EL-87	0.58	449+/-9Ma
EL-36	0.32	467+/-9Ma	EL-90	0.71	471+/-9Ma
EL-38	0.27	429+/-8Ma	EL-92	0.41	457+/-9Ma
EL-41	0.30	424+/-8Ma	EL-93	0.79	473+/-9Ma
EL-42	0.21	422+/-8Ma	EL-94	0.89	486+/-9Ma
EL-43	0.52	481+/-9Ma	EL-F	1.24	478+/-10Ma
EL-44	0.54	481+/-9Ma	EL-G	1.24	478+/-10Ma

Sample **EL-F** supplied by Prof. B. E. Leake (**BEL-1248**).

Sample **EL-G** supplied by Dr. G. R. T. Jenkin (**GJ-60**).

Miller et al. (1991): K-Ar Age Results.

Sample.	K (wt.%).	Age (Ma).	Sample.	K (wt.%).	Age (Ma).
WM-108	0.20	453+/-10Ma	WM-200	0.34	472+/-10Ma
WM-109	0.38	457+/-10Ma	WM-201	0.42	349+/-8Ma
WM-111	0.49	480+/-10Ma	WM-220	0.21	406+/-8Ma
WM-124	0.45	476+/-10Ma	WM-224	0.26	397+/-8Ma
WM-128	0.23	452+/-9Ma	WM-225	0.77	452+/-9Ma
WM-135	0.08	486+/-10Ma	WM-228	1.08	481+/-10Ma
WM-136	0.09	475+/-10Ma	WM-232	0.43	467+/-9Ma
WM-137	0.09	471+/-10Ma	WM-234	0.27	466+/-10Ma
WM-138	0.27	478+/-10Ma	WM-235	0.81	447+/-9Ma
WM-139	0.52	419+/-9Ma	WM-237	0.74	407+/-8Ma
WM-146	0.84	477+/-10Ma	WM-238	0.33	480+/-10Ma
WM-155	0.79	482+/-10Ma	WM-242	0.62	472+/-9Ma
WM-165	0.14	479+/-10Ma	WM-244	0.32	436+/-9Ma
WM-167	0.44	424+/-9Ma	WM-248	0.22	462+/-9Ma
WM-183	0.20	334+/-7Ma	WM-249	0.37	459+/-9Ma

Miller et al. (1991): Stable Isotope Results.

Sample.	$\delta^{18}\text{O}$ (SMOW) (‰).	$\delta\text{D}$ (SMOW) (‰).	$\text{H}_2\text{O}^+$ (wt. %).
WM-128	+8.6‰	-66.2‰	2.18
WM-139	+9.6‰	-62.4‰	2.48
WM-165	+8.7‰	-68.8‰	2.11
WM-167	+9.0‰	-61.8‰	2.39
WM-220	+8.8‰	-62.4‰	2.18
WM-224	-	-61.2‰	2.15
WM-232	+8.5‰	-67.7‰	2.11
WM-234	+6.4‰	-72.7‰	2.10
WM-235	-	-61.4‰	2.61
WM-237	-	-60.9‰	2.67
WM-238	+6.6‰	-75.1‰	1.83
WM-242	+5.5‰	-67.0‰	2.41

### APPENDIX 13.

#### IONIC POROSITIES FROM PREVIOUS STUDY.

The ionic porosity (Z) for the hornblende mineral separates EMPA from Miller (1990) were calculated using the method as outlined in Appendix 8. The relevant data was taken from Miller (1990).

<b>WM-108</b>	A-site. = 0.20 Mg# = 0.794	edenite. ferro-edenite. magnesiohornblende. ferrohornblende.	0.159 0.041 0.635 0.165	<b>Z = 37.593%</b>
<b>WM-109</b>	A-site. = 0.37 Mg# = 0.696	edenite. ferro-edenite. magnesiohornblende. ferrohornblende.	0.258 0.112 0.438 0.192	<b>Z = 37.588%</b>
<b>WM-111</b>	A-site. = 0.32 Mg# = 0.695	edenite. ferro-edenite. magnesiohornblende. ferrohornblende.	0.222 0.098 0.473 0.207	<b>Z = 37.631%</b>
<b>WM-124</b>	A-site = 0.51 Mg# = 0.607	pargasite. ferropargasite. tschermakite. ferrotschermakite.	0.310 0.200 0.297 0.193	<b>Z = 37.416%</b>
<b>WM-128</b>	A-site. = 0.48 Mg# = 0.649	edenite. ferro-edenite. magnesiohornblende. ferrohornblende.	0.312 0.168 0.337 0.183	<b>Z = 37.568%</b>
<b>WM-135</b>	A-site. = 0.20 Mg# = 0.706	edenite. ferro-edenite. magnesiohornblende. ferrohornblende.	0.141 0.059 0.565 0.235	<b>Z = 37.715%</b>
<b>WM-137</b>	A-site. = 0.19 Mg# = 0.692	edenite. ferro-edenite. magnesiohornblende. ferrohornblende.	0.131 0.059 0.561 0.249	<b>Z = 37.743%</b>
<b>WM-138</b>	A-site. = 0.28 Mg# = 0.671	edenite. ferro-edenite. magnesiohornblende. ferrohornblende.	0.188 0.092 0.483 0.237	<b>Z = 37.700%</b>

<b>WM-139</b>	A-site. = 0.21 Mg# = 0.730	edenite. ferro-edenite. magnesiohornblende. ferrohornblende.	0.153 0.057 0.577 0.213	<b>Z = 37.674%</b>
<b>WM-165</b>	A-site. = 0.47 Mg# = 0.547	pargasite. ferropargasite. tschermakite. ferrotschermakite.	0.257 0.213 0.290 0.240	<b>Z = 37.497%</b>
<b>WM-167</b>	A-site. = 0.28 Mg# = 0.617	edenite. ferro-edenite. magnesiohornblende. ferrohornblende.	0.173 0.107 0.444 0.276	<b>Z = 37.776%</b>
<b>WM-183</b>	A-site. = 0.11 Mg# = 0.791	edenite. ferro-edenite. magnesiohornblende. ferrohornblende.	0.087 0.023 0.704 0.186	<b>Z = 37.675%</b>
<b>WM-201</b>	A-site. = 0.43 Mg# = 0.709	edenite. ferro-edenite. magnesiohornblende. ferrohornblende.	0.305 0.125 0.404 0.166	<b>Z = 37.519%</b>
<b>WM-220</b>	A-site. = 0.33 Mg# = 0.708	edenite. ferro-edenite. magnesiohornblende. ferrohornblende.	0.234 0.096 0.474 0.196	<b>Z = 37.604%</b>
<b>WM-225</b>	A-site. = 0.35 Mg# = 0.684	edenite. ferro-edenite. magnesiohornblende. ferrohornblende.	0.239 0.111 0.445 0.205	<b>Z = 37.622%</b>
<b>WM-228</b>	A-site. = 0.66 Mg# = 0.500	pargasite. ferropargasite. tschermakite. ferrotschermakite.	0.330 0.330 0.170 0.170	<b>Z = 37.567%</b>
<b>WM-232</b>	A-site. = 0.41 Mg# = 0.645	edenite. ferro-edenite. magnesiohornblende. ferrohornblende.	0.264 0.146 0.381 0.209	<b>Z = 37.631%</b>
<b>WM-234</b>	A-site. = 0.24 Mg# = 0.685	pargasite. ferropargasite. tschermakite. ferrotschermakite.	0.164 0.076 0.521 0.239	<b>Z = 37.309%</b>
<b>WM-235</b>	A-site. = 0.49 Mg# = 0.612	pargasite. ferropargasite. tschermakite. ferrotschermakite.	0.300 0.190 0.312 0.198	<b>Z = 37.409%</b>

<b>WM-237</b>	A-site. = 0.46 Mg# = 0.551	edenite. ferro-edenite. magnesiohornblende. ferrohornblende.	0.253 0.207 0.298 0.242	<b>Z = 37.735%</b>
<b>WM-238</b>	A-site. = 0.35 Mg# = 0.637	edenite. ferro-edenite. magnesiohornblende. ferrohornblende.	0.223 0.127 0.414 0.236	<b>Z = 37.691%</b>
<b>WM-242</b>	A-site. = 0.28 Mg# = 0.668	edenite. ferro-edenite. magnesiohornblende. ferrohornblende.	0.187 0.093 0.481 0.239	<b>Z = 37.703%</b>
<b>WM-244</b>	A-site. = 0.29 Mg# = 0.717	edenite. ferro-edenite. magnesiohornblende. ferrohornblende.	0.208 0.082 0.509 0.201	<b>Z = 37.624%</b>
<b>WM-248</b>	A-site. = 0.16 Mg# = 0.566	edenite. ferro-edenite. magnesiohornblende. ferrohornblende.	0.091 0.069 0.475 0.365	<b>Z = 37.941%</b>
<b>WM-249</b>	A-site. = 0.31 Mg# = 0.645	edenite. ferro-edenite. magnesiohornblende. ferrohornblende.	0.200 0.110 0.445 0.245	<b>Z = 37.712%</b>

## APPENDIX 14.

### DATA FOR AGE- $\delta$ D-Z DIAGRAM.

The following data were used to construct the triangular diagram of Figure 6.4. The range for each component was multiplied by a factor to bring the highest possible value for that component to equal 150. The minimum for each component was subtracted from the value of each sample and the remainder multiplied by the relevant factor. These are shown below.

The data for K-Ar ages are from Appendix 9,  $\delta$ D from Appendix 10 and Z from Appendix 8.

Range for Age.	400Ma to 560Ma	=	160Ma x 0.9375	= 150
Range for $\delta$ D.	-35‰ to -65‰	=	30‰ x 5	= 150
Range for Z.	37.500% to 38.000%.	=	0.500% x 300	= 150

Each component was calculated as a percentage and then plotted on the triangular diagram of Figure 6.4.

Sample.	Age.	$\delta$ D.	Z.	Total.	Percentages on Diagram.		
					Age.	$\delta$ D.	Z.
TJ-1	45	-	58	-	-	-	-
TJ-7A	25	70	119	<u>214</u>	12	33	55
TJ-7B	11	50	130	<u>191</u>	6	26	68
TJ-7D	57	95	144	<u>296</u>	19	32	49
TJ-7E	23	25	126	<u>174</u>	13	14	73
TJ-7F	61	105	123	<u>289</u>	21	36	43
TJ-7G	34	70	142	<u>246</u>	14	28	58
TJ-7H	41	85	99	<u>225</u>	18	38	44
TJ-8	78	85	84	<u>247</u>	32	34	34
TJ-9	103	90	53	<u>246</u>	42	37	21

Sample.	Age.	δD.	Z.	Total.	Percentages on Diagram.		
					Age.	δD.	Z.
TJ-11	34	20	69	<u>123</u>	28	16	56
TJ-13	84	105	99	<u>288</u>	29	37	34
TJ-17	58	45	75	<u>178</u>	33	25	42
TJ-19	90	135	92	<u>317</u>	28	43	29
TJ-29	31	75	101	<u>207</u>	15	36	49
TJ-31	66	60	58	<u>184</u>	36	33	31
TJ-35	64	125	67	<u>256</u>	25	49	26
TJ-36	73	130	50	<u>253</u>	29	51	20
TJ-37	83	140	102	<u>325</u>	26	43	31
TJ-38	146	140	94	<u>380</u>	38	37	25
TJ-39	9	80	85	<u>174</u>	5	46	49
TJ-40	114	115	25	<u>254</u>	45	45	10
TJ-41	91	135	44	<u>270</u>	34	50	16
TJ-43	144	85	53	<u>282</u>	51	30	19
TJ-44	78	85	39	<u>202</u>	39	42	19
TJ-45	49	85	65	<u>199</u>	24	43	33
TJ-46	63	120	51	<u>234</u>	27	51	22
TJ-47	73	85	45	<u>203</u>	36	42	22
TJ-48	86	85	8	<u>179</u>	48	47	5
TJ-54	45	20	143	<u>208</u>	21	10	69
TJ-59	-	55	72	-	-	-	-

## APPENDIX 15.

### DATA FOR $\delta^{18}\text{O}$ - $\delta\text{D}$ -Z DIAGRAM.

The following data were used to construct the triangular diagram of Figure 6.7. The range for each component was multiplied by a factor to bring the highest possible value for that component to equal 150. The minimum for each component was subtracted from the value for each sample and the remainder multiplied by the relevant factor. These are shown below.

The data for  $\delta^{18}\text{O}$  are from Appendix 11,  $\delta\text{D}$  from Appendix 10 and ionic porosity, Z, from Appendix 8.

$$\text{Range for } \delta^{18}\text{O.} \quad +4.8\text{‰ to } +9.4\text{‰} \quad = \quad 4.6\text{‰} \times 32.6 \quad = \quad 150$$

$$\text{Range for } \delta\text{D.} \quad -35\text{‰ to } -65\text{‰} \quad = \quad 30\text{‰} \times 5 \quad = \quad 150$$

$$\text{Range for Z.} \quad 37.500\% \text{ to } 38.000\% \quad = \quad 0.500\% \times 300 \quad = \quad 150$$

Each component was calculated as a percentage and then plotted on the triangular diagram of Figure 6.7.

Sample.	$\delta^{18}\text{O}$ .	$\delta\text{D}$ .	Z.	Total.	Percentages on Diagram.		
					$\delta^{18}\text{O}$ .	$\delta\text{D}$ .	Z.
TJ-1	101	-	58	-	-	-	-
TJ-7A	104	70	119	<u>293</u>	35	24	41
TJ-7B	75	50	130	<u>255</u>	29	20	51
TJ-7D	7	95	144	<u>246</u>	3	38	59
TJ-7E	42	25	126	<u>193</u>	22	13	65
TJ-7F	55	105	123	<u>283</u>	20	37	43
TJ-7G	29	70	142	<u>241</u>	12	29	59
TJ-7H	124	85	99	<u>308</u>	40	28	32
TJ-8	42	85	84	<u>211</u>	20	40	40
TJ-9	3	90	53	<u>146</u>	2	62	36

Sample.	$\delta^{18}\text{O}$ .	$\delta\text{D}$ .	Z.	Total.	Percentages on Diagram.		
					$\delta^{18}\text{O}$ .	$\delta\text{D}$ .	Z.
TJ-11	16	20	69	<u>105</u>	15	19	66
TJ-13	75	105	99	<u>279</u>	27	38	35
TJ-17	62	45	75	<u>182</u>	34	25	41
TJ-19	39	135	92	<u>266</u>	15	51	34
TJ-29	46	75	101	<u>222</u>	21	34	45
TJ-31	88	60	58	<u>206</u>	43	29	28
TJ-35	85	125	67	<u>277</u>	31	45	24
TJ-36	72	130	50	<u>252</u>	28	52	20
TJ-37	82	140	102	<u>324</u>	25	43	32
TJ-38	130	140	94	<u>364</u>	36	38	26
TJ-39	98	80	85	<u>263</u>	37	31	32
TJ-40	88	115	25	<u>228</u>	39	50	11
TJ-41	147	135	44	<u>326</u>	45	42	13
TJ-43	82	85	53	<u>220</u>	37	39	24
TJ-44	95	85	39	<u>219</u>	43	39	18
TJ-45	95	85	65	<u>245</u>	38	35	27
TJ-46	69	120	51	<u>240</u>	29	50	21
TJ-47	147	85	45	<u>277</u>	53	31	16
TJ-48	130	85	8	<u>223</u>	58	38	4
TJ-54	52	20	143	<u>215</u>	24	9	67
TJ-59	52	55	72	<u>179</u>	29	31	40

## REFERENCES.

Anderton, R., Bridges, P.H., Leeder, M.R. and Sellwood, B.W. (1979). "A Dynamic Stratigraphy of the British Isles: A Study in Crustal Evolution." George Allen and Unwin, London.

Badley, M.E. (1976). "Stratigraphy, structure and metamorphism of Dalradian rocks of the Maumturk Mountains, Connemara, Ireland." *Journal of the Geological Society, London*, Vol. 132, pp.87-96.

Baldwin, S.L., Harrison, T.M. and FitzGerald, J.D. (1990). "Diffusion of  $^{40}\text{Ar}$  in metamorphic hornblende." *Contributions to Mineralogy and Petrology*, Vol. 105, pp.691-703.

Berry, R.F. and McDougall, I. (1986). "Interpretation of  $^{40}\text{Ar}/^{39}\text{Ar}$  and K-Ar dating evidence from the Aileu Formation, East Timor." *Chemical Geology (Isotope Geoscience Section)*, Vol. 59, pp.43-58.

Cameron, M.E. and Gibbs, G.V. (1973). "The crystal structure and bonding of fluoro-tremolite: A comparison with hydroxyl-tremolite." *American Mineralogist*, Vol. 58, pp.879-888.

Cliff, R.A., Yardley, B.W.D. and Bussy, F.R. (1996). "U-Pb and Rb-Sr geochronology of magmatism and metamorphism in the Dalradian of Connemara, western Ireland." *Journal of the Geological Society, London*, Vol. 153, pp.109-120.

Cosca, M.A., Sutter, J.F. and Essene, E.J. (1992). "Cooling and inferred uplift/erosion history of the Grenville orogen, Ontario: constraints from  $^{40}\text{Ar}/^{39}\text{Ar}$  thermochronology." *Tectonics*, Vol. 10, pp.959-977.

Cosca, M.A. and O'Nions, R.K. (1994). "A re-examination of the influence of composition on argon retentivity in metamorphic calcic amphiboles." *Chemical Geology*, Vol. 112, pp.39-56.

Cox, K.G., Bell, J.D. and Pankhurst, R.J. (1979). "The Interpretation of Igneous Rocks." George Allen and Unwin, London.

Craig, H. (1957). "Isotopic standards for carbon and oxygen and correction factors for mass-spectrometric analysis of carbon dioxide." *Geochimica et Cosmochimica Acta*, Vol. 12, pp.133-149.

Dahl, P.S. (1996). "The effects of composition on retentivity of argon and oxygen in hornblende and related amphiboles: A field-tested empirical model." *Geochimica et Cosmochimica Acta*, Vol. 60, pp.3687-3700.

Dalrymple, G.B. and Lanphere, M.A. (1969). "Potassium-Argon Dating. Principles, Techniques and Applications to Geochronology." W. H. Freeman and Company, San Francisco.

Deer, W.A., Howie, R.A. and Zussman, J. (1966). "An Introduction to the Rock-Forming Minerals." Longman Group Ltd., U.K.

Dewey, J.F., McKerrow, W.S. and Moorbath, S. (1970). "The relationship between isotopic ages, uplift and sedimentation during Ordovician times in western Ireland." *Scottish Journal of Geology*, Vol. 6, pp.133-145.

Dewey, J.F. and Shackleton, R.M. (1984). "A model for the evolution of the Grampian tract in the early Caledonides and Appalachians." *Nature*, Vol. 312, pp.115-121.

Dodson, M.H. (1973). "Closure temperature in cooling geochronological and petrological systems." *Contributions to Mineralogy and Petrology*, Vol. 40, pp.259-274.

Elias, E.M. (1985). "K-Ar and Rb-Sr isotope studies in Connemara, Western Ireland." Ph.D. thesis, Department of Geology and Applied Geology, University of Glasgow, Scotland.

Elias, E.M., MacIntyre, R.M., and Leake, B.E. (1988). "The cooling history of Connemara, western Ireland, from K-Ar and Rb-Sr age studies." *Journal of the Geological Society, London*, Vol. 145, pp.649-660.

Ernst, W.G. (1968). "Amphiboles." Springer-Verlag.

Faure, G. (1986). "Principles of Isotope Geology." 2<sup>ND</sup> Edition, John Wiley and Sons, Inc., New York.

Fitch, F.J., Miller, J.A. and Brown, P.E. (1964). "Age of Caledonian orogeny and metamorphism in Britain." *Nature*, Vol. 204. pp.275-278.

Fortier, S.M. and Giletti, B.J. (1989). "An empirical model for predicting diffusion coefficients in silicate minerals." *Science*, Vol. 245, pp.1481-1484.

Fortier, S.M. and Giletti, B.J. (1991). "Volume self-diffusion of oxygen in biotite, muscovite and phlogopite micas." *Geochimica et Cosmochimica Acta*, Vol. 55, pp.1319-1330.

Friedrich, A.M., Hodges, K.V. and Bowring, S.A. (1997). "Geochronologic constraints on the tectonic evolution of Connemara." *Geology* (in press).

Gerling, E.K., Kol'tsova, T.V., Petrov, B.V. and Zul'fikarova, Z.K. (1965). "On the suitability of amphiboles for age determination by the K-Ar method." *Geochem. Intl.*, Vol. 2, pp.148-154.

Giletti, B.J., Moorbath, S. and Lambert Sr., R.J. (1961). "A geochronological study of the metamorphic complexes of the Scottish Highlands." *Journal of the Geological Society, London*, Vol. 117, pp.233-272.

Graham, C.M., Harmon, R.S. and Sheppard, S.M.F. (1984). "Experimental hydrogen isotope studies: hydrogen isotope exchange between amphibole and water." *American Mineralogist*, Vol. 69, pp128-138.

Graham, J.R., Leake, B.E. and Ryan, P.D. (1989). "The Geology of South Mayo, western Ireland." Scottish Academic Press.

Grove, M. and Harrison, T.M. (1993). "Compositional controls governing argon loss in biotite." (abstract), *Transactions of the American Geophysical Union*, Vol. 74, p.339.

Grove, M. and Harrison, T.M. (1994). "Argon loss from F-OH phlogopite." (abstract), *United States Geological Survey*, Vol. 1107 p.119.

Harrison, T.M. (1981). "Diffusion of  $^{40}\text{Ar}$  in hornblende." *Contributions to Mineralogy and Petrology*, Vol. 78, pp.324-331.

Harrison, T.M., Duncan, I. and McDougall, I. (1985). "Diffusion of  $^{40}\text{Ar}$  in biotite: Temperature, pressure and compositional effects." *Geochimica et Cosmochimica Acta*, Vol. 49, pp.2461-2468.

Harrison, T.M. and FitzGerald, J.D. (1986). "Exsolution in hornblende and its consequences for  $^{40}\text{Ar}/^{39}\text{Ar}$  age spectra and closure temperature." *Geochimica et Cosmochimica Acta*, Vol. **50**, pp.247-253.

Hawthorne, F.C. and Grundy, H.D. (1973). "The crystal chemistry of the amphiboles. II. Refinement of the crystal structure of oxy-kaersutite." *Mineralogical Magazine*, Vol. **39**, pp.390-400.

Hawthorne, F.C. (1983). "The crystal chemistry of the amphiboles." *Canadian Mineralogist*, Vol. **21**, pp.171-480.

Hutchison, C.S. (1974). "Laboratory Handbook of Petrographic Techniques." John Wiley and Sons, Inc., New York.

Hutton, D.H.W. and Dewey, J.F. (1986). "Palaeozoic terrane accretion in the western Irish Caledonides." *Tectonics*, Vol. **5**, pp.1115-1124.

Hutton, D.H.W. (1987). "Strike-slip terranes and a model for the evolution of the British and Irish Caledonides." *Geological Magazine*, Vol. **124**, pp.405-425.

Jagger, M.D., Aftalion, M., Max, M.D. and Leake, B.E. (1988). "U-Pb zircon ages of basic rocks and gneisses intruded into the Dalradian rocks of Cashel, Connemara, western Ireland." *Journal of the Geological Society, London*, Vol. **145**, pp.645-648.

Jenkin, G.R.T. (1988). "Stable isotope studies in the Caledonides of SW Connemara, Ireland." Ph.D. thesis, Department of Geology and Applied Geology, University of Glasgow, Scotland.

Jenkin, G.R.T., Fallick, A.E. and Leake, B.E. (1992). "A stable isotope study of retrograde alteration in SW Connemara, Ireland." *Contributions to Mineralogy and Petrology*, Vol. **110**, pp.269-288.

Jenkin, G.R.T., O'Reilly, C.O., Feely, M. and Fallick, A.E. (1997). "The geometry of mixing of surface and basinal fluids in the Galway Granite, Connemara, Western Ireland." *In press*.

Kamber, B.S., Blenkinsop, T.G., Villa, I.M. and Dahl, P.S. (1995). "Transpressive deformation in the Northern Marginal Zone, Limpopo Belt, Zimbabwe." *Journal of Geology*, Vol. **103**, 493-508.

Klein, C. and Hurlbut, Jr., C.S. (eds.), after Dana, J.D. (1985). "Manual of Mineralogy." 20<sup>TH</sup> Edition, John Wiley and Sons, Inc., New York.

Leake, B.E. (1970). "The origin of the Connemara migmatites of the Cashel district, Connemara, Ireland." *Journal of the Geological Society, London*, Vol. **125**, pp.219-276.

Leake, B.E., Elias, E.M. and Farrow, C.M. (1988). "The relationship of argon retentivity and chemical composition of hornblende." *Geochimica et Cosmochimica Acta*, Vol. **52**, p.2165.

Leake, B.E. (1989). "The metagabbros, orthogneisses and paragneisses of the Connemara complex, western Ireland." *Journal of the Geological Society, London*, Vol. **146**, pp.575-596.

Leake, B.E. and Tanner, P.W.G. (1994). "The Geology of the Dalradian and Associated Rocks of Connemara, Western Ireland." Royal Irish Academy.

Leake, B.E., Woolley, A.R., Birch, W.D., Gilbert, M.C., Grice, J.D., Hawthorne, F.C., Kato, A., Kisch, H.J., Krivovichev, V.G., Linthout, K., Laird, J. and Mandarino, J. (1997). "Nomenclature of Amphiboles: Report of the Subcommittee on Amphiboles of the International Mineralogical Association Commission on New Minerals and Mineral Names." *Mineralogical Magazine*, Vol. 61, pp.295-321.

Lee, J.K.W. (1993). "The argon release mechanisms of hornblende in vacuo." *Chemical Geology (Isotope Geoscience Section)*, Vol. 106, pp.133-170.

Leggo, P.J., Compston, W. and Leake, B.E. (1966). "Geochronology of the Connemara granites and its bearing on the antiquity of the Dalradian Series." *Journal of the Geological Society, London*, Vol. 122, pp.91-118.

Max, M. D., Long, C.B. and Geohegan, M. (1978). "The Galway Granite." *Geological Survey of Ireland Bulletin*, Vol. 2, pp.223-233.

Miller, J.A. and Brown, P.E. (1965). "Potassium-argon age studies in Scotland." *Geological Magazine*, Vol. 102, pp.106-134.

Miller, W.M. (1990). "Fluid disturbed K-Ar mineral ages from the Dalradian rocks of Connemara, western Ireland." Ph.D. thesis, Department of Geology and Applied Geology, University of Glasgow, Scotland.

Miller, W.M., Fallick, A.E., Leake, B.E., MacIntyre, R.M. and Jenkin, G.R.T. (1991). "Fluid disturbed hornblende K-Ar ages from the Dalradian rocks of Connemara, western Ireland." *Journal of the Geological Society, London*, Vol. 148, pp.985-992.

Mitchell, J.G. and Mohr, P. (1986). "K-Ar systematics in Tertiary dolerites from West Connacht, Ireland." *Scottish Journal of Geology*, Vol. 22, pp.225-240.

- Mitchell, J.G. and Mohr, P. (1987). "Carboniferous dykes of West Connacht, Ireland." *Transactions of the Royal Society of Edinburgh: Earth Sciences*, Vol. 78, pp.33-151.
- Moorbath, S., Bell, K., Leake, B.E. and McKerrow, W.S. (1968). "Geochronological studies in Connemara and Murrisk, western Ireland." In: Hamilton, E.I. and Farquhar, R.M. (eds.), "Radiometric Dating For Geologists." Interscience. pp.259-298.
- O'Neil, J.R. and Taylor, H.P. Jr. (1967). "The oxygen isotope and cation exchange chemistry of feldspars." *American Mineralogist*, Vol. 52, pp1414-1437.
- O'Nions, R.K., Smith, D.G.W., Baadsgaard, H. and Morton, R.D. (1969). "Influence of chemical composition on argon retentivity in metamorphic calcic amphiboles from South Norway." *Earth and Planetary Science Letters*, Vol. 5, pp339-345.
- Onstott, T.C. and Peacock, M.W. (1987). "Argon retentivity of hornblendes: A field experiment in a slowly cooled metamorphic terrane." *Geochimica et Cosmochimica Acta*, Vol. 51, pp.2891-2903.
- Onstott, T.C. and Pringle-Goodell, L. (1988). "The influence of microstructures on the relationship between argon retentivity and chemical composition of hornblende." *Geochimica et Cosmochimica Acta*, Vol. 52, pp.2167-2168.
- O'Reilly, C.O., Jenkin, G.R.T., Feely, M., Alderton, D.H.M. and Fallick, A.E. (1997). "A fluid inclusion and stable isotope study of 200Ma of fluid evolution in the Galway Granite, Connemara, Ireland." *In press*.
- Pankhurst, R.J. (1970). "The geochronology of the basic igneous complexes of Aberdeenshire." *Scottish Journal of Geology*, Vol. 6, pp.83-107.

Perkin-Elmer, (1971). "Analytical Methods for Atomic Absorption Spectrophotometry." Perkin-Elmer Ltd., Norwalk, Connecticut, USA.

Phillips, M.W., Draheim, J.E., Popp, R.K., Clowe, C.A. and Pinkerton, A.A. (1989). "Effects of oxidation-dehydration in tschermakitic hornblende." *American Mineralogist*, Vol. 74, pp.764-773.

Pidgeon, R.T. (1969). "Zircon U-Pb ages from the Galway Granite and the Dalradian, Connemara, Ireland." *Scottish Journal of Geology*, Vol. 5, pp.375-392.

Potts, P.J. (1987). "A Handbook of Silicate Rock Analysis." Blackie Academic and Professional, Chapman and Hall, London.

Rex, D.C. Guise, P.G. and Wartho, J.-A. (1993). "Disturbed  $^{40}\text{Ar}$ - $^{39}\text{Ar}$  spectra from hornblendes: Thermal loss or contamination." *Chemical Geology (Isotope Geoscience Section)*, Vol. 103, pp.271-281.

Riley, J.P. (1958a). "The rapid analysis of silicate rocks and minerals." *Analytica Chimica Acta*, Vol. 19, pp.413-428.

Riley, J.P. (1958b). "Simultaneous determination of water and carbon dioxide in rocks and minerals." *Analyst*, Vol. 83, pp.42-49.

Rollinson, H.R. (1993). "Using Geochemical Data: Evaluation, Presentation, Interpretation." Longman Scientific and Technical, U.K.

Ross, J.A. and Sharp, W.D. (1988). "The effects of sub-blocking temperature metamorphism on the K-Ar systematics of hornblendes:  $^{40}\text{Ar}$ - $^{39}\text{Ar}$  dating of polymetamorphic garnet amphibolite from the Franciscan Complex, California." *Contributions to Mineralogy and Petrology*, Vol. 100, pp.213-221.

Russell, G.S., Odom, A.L. and Russell, C.W. (1987). "U-Pb and Rb-Sr isotopic evidence for the age and origin of granitic rocks in the Northern Alabama Piedmont." In: Drummond, M.S. and Green, N.L. (eds.) "Granites of Alabama." Geological Survey of Alabama. Tuscaloosa, pp.239-249.

Sachs, L. (1984). "Applied Statistics: A Handbook of Techniques." Springer-Verlag, New York.

Scaillet, S., Feraud, G., Balleve, M. and Amouric, M. (1992). "Mg/Fe and [(Mg,Fe)Si-Al<sub>2</sub>] compositional control on argon behaviour in high-pressure white micas: A  $^{40}\text{Ar}/^{39}\text{Ar}$  continuous laser-probe study from the Dora-Maria nappe of the internal Western Alps, Italy." *Geochimica et Cosmochimica Acta*, Vol. 56, pp.2851-2872.

Shaw, H.F. and Wasserburg, G.J. (1984). "Isotopic constraints on the origin of the Appalachian mafic complexes." *American Journal of Science*, Vol. 284, pp.319-349.

Sheppard, S.M.F. (1986). "Characterisation and isotopic variations in natural waters." In: Valley, J.W., Taylor, H.P. Jr, O'Neil J.R. (eds.). "Stable Isotopes in High Temperature Geological Processes." (Reviews in Mineralogy 16). Mineralogical Society of America, Washington DC, pp.165-183.

Siebel, W., Henjes-Kunst, F. and Rhede, D. (1998). "High-temperature memory in calcic amphiboles and constraints on compositional control of their  $^{40}\text{Ar}/^{39}\text{Ar}$  ages." *Geology*, Vol. 26, pp.31-34.

Sisson, V.B. and Onstott, T.C. (1986). "Dating blueschist metamorphism: A combined  $^{40}\text{Ar}/^{39}\text{Ar}$  and electron microprobe approach." *Geochimica et Cosmochimica Acta*, Vol. 50, pp.2111-2117.

Soper, N.J. and Hutton, D.H.W. (1984). "Late Caledonian sinistral displacements in Britain: implications for a three-plate collision model." *Tectonics*, Vol. 3, pp.781-794.

Soper, N.J. (1986). "The Newer Granite problem: a geotectonic view." *Geological Magazine*, Vol. 123, pp.227-236.

Spear, F.S. (1994). "Metamorphic phase equilibria and pressure-temperature-time paths." *Mineralogical Society of America. Monograph*.

Steiger, R.H. and Jäger, E. (1977). "Subcommission on geochronology: Convention on the use of decay constants in geo- and cosmochronology." *Earth and Planetary Science Letters*, Vol. 36, pp359-362.

Suzouki, T. and Epstein, S. (1976). "Hydrogen isotope fractionation between OH-bearing minerals and water." *Geochimica et Cosmochimica Acta*, Vol. 40, pp.1229-1240.

Tanner, P.W.G. and Shackleton, R.M. (1979). "Structure and stratigraphy of the Dalradian rocks of the Bennabeola area, Connemara, Eire." In: Harris A. L., Holland C. H. and Leake B. E. (eds.), "Caledonides of the British Isles - Reviewed." Geological Society, London, Special Publications, 8, pp.243-256.

Tanner, P.W.G., Dempster, T.J. and Rogers, G. (1997). "New constraints upon the structural and isotopic age of the Dalradian rocks of Connemara, wesern Ireland." *Geological Journal*, Vol. 32, pp247-263.

Yardley, B.W.D. (1976). "Deformation and metamorphism of Dalradian rocks and the evolution of the Connemara cordillera." *Journal of the Geological Society, London*, Vol. 132, pp.521-542.

